

# THREE DIMENSIONAL FEM STUDY FOR EFFECT OF VALLEY SHAPE ON BEHAVIOUR OF EARTH AND ROCKFILL DAMS

A DISSERTATION

Submitted in partial fulfillment of the  
requirements for the award of the degree

of

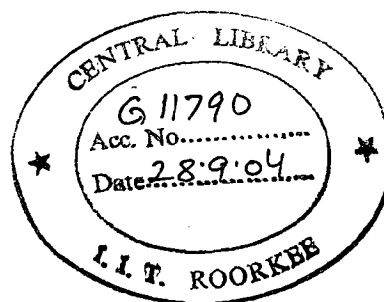
MASTER OF TECHNOLOGY

in

WATER RESOURCES DEVELOPMENT  
(CIVIL)

By

PRASETYADHIE



WATER RESOURCES DEVELOPMENT TRAINING CENTRE  
INDIAN INSTITUTE OF TECHNOLOGY ROORKEE  
ROORKEE-247 667 (INDIA)  
JUNE, 2004

## **CANDIDATE'S DECLARATION**

I hereby certify that the work which is being presented in the dissertation entitled, **“THREE DIMENSIONAL FEM STUDY FOR EFFECT OF VALLEY SHAPE ON BEHAVIOUR OF EARTH AND ROCKFILL DAMS”** in partial fulfillment of the requirement for the award of Degree of Master of Technology in WRD (CIVIL) submitted in the Water Resources Development Training Centre, Indian Institute of Technology Roorkee, Roorkee is an authentic record of my own work carried out during the period 20 July, 2003 till the date of submission under supervision of **Dr. Ram Pal Singh**, professor, WRDTC, IIT Roorkee and **Dr. B.N. Asthana**, visiting professor, WRDTC, IIT Roorkee, India.

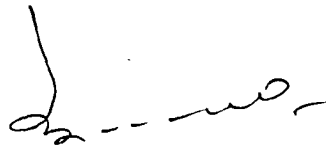
The matter embodied in this dissertation has not been submitted by me for the award of any other degree.



( **PRASETYADHIE** )

Dated : June 27, 2004

This is to certify that the above statement made by the candidate is correct to the best of our knowledge.



( **DR. B.N. ASTHANA** )

Visiting Professor  
Water Resources Development  
Training Centre  
Indian Institute of Technology  
Roorkee - India, 247667



( **DR. RAM PAL SINGH** )

Professor  
Water Resources Development  
Training Centre  
Indian Institute of Technology  
Roorkee - India, 247667

## ACKNOWLEDGEMENT

*I wish to express my very deepest thanks and gratitude to Dr. Ram Pal Singh, Professor of WRDTC, IIT Roorkee and Dr. B.N. Asthana, Visiting Professor of WRDTC, IIT Roorkee-India, for their continued and excellent guidance, inspiration and correction encouragement, which was very valuable in enhancing my knowledge and self confidence in preparing and completion of this dissertation. Working under their guidance will always remain a cherished experience in my memory.*

*I express my sincere gratitude to Dr. U.C. Chaube, Professor and Head, Water Resources Development Training Centre, for extending various facilities during the course of this work.*

*Special thanks to all the faculty members of WRDTC for providing me sufficient knowledge needed for completion of this document. To all staffs of WRDTC who in one way or another extended their support and cooperation and provided of facilities during course of preparation of this study. To all my co-trainee officers batch 47<sup>th</sup> WRD and 23<sup>rd</sup> IWM for the interaction and sharing of valuable information.*

*I wish to express my whole hearted gratitude to the Government of Indonesia especially my office PT. ISTAKA KARYA (Persero) and the sponsor for giving me this rare opportunity to study for Master of Technology in WRD in WRDTC – IIT Roorkee.*

*Ultimately, a special and sincerest thanks to my wife, Dian Mufidah, and my loving daughter, Indira Putri Arundati, for their persistent support, encouragement and prayers throughout the duration of my study at WRDTC.*

Roorkee, 28 , June, 2004

**(PRASETYADHIE)**

# CONTENTS

	Page No.
CANDIDATE'S DECLARATION	i
ACKNOWLEDGMENTS	ii
CONTENTS	iii
LIST OF TABLES	vi
LIST OF FIGURES	ix
SYNOPSIS	xvi
<b>CHAPTER 1 : INTRODUCTION</b>	<b>1</b>
1.1. GENERAL	1
1.2. IMPORTANCE OF DEFORMATION CONSIDERATION	2
1.3. AIMS AND SCOPE OF THE STUDY	4
1.4. THE ORGANISATION OF A DISSERTATION	5
<b>CHAPTER 2 : REVIEW OF LITERATURE</b>	<b>7</b>
2.1. GENERAL	7
2.2. LAYERED ANALYSIS OF EMBANKMENT DAM	7
2.3. ANALYSIS OF MAJOR DAMS	10
2.3.1. Analysis of Oroville Dam	10
2.3.2. Analysis of Duncan Dam	13
2.3.3. Analysis of Mica Dam	15
2.3.4. Analysis of Chicoasen Dam	18
2.3.5. Analysis of Dartmouth Dam	20
2.3.6. Analysis of Tehri Dam	22
2.3.7. Analysis of Dabaklamm Dam	25
2.3.8. Analysis of Bouquet Canyon Dam	27
2.3.9. Analysis of Yeguas Dam	28
2.3.10. Analysis of Tahamara Dam	28
2.4. SUMMARY	31
<b>CHAPTER 3 : METHOD OF ANALYSIS</b>	<b>54</b>
3.1. DESCRIPTION OF THE METHOD	54
3.1.1. Displacement Function	55
3.1.2. Shape Function	56
3.1.3. Strains	56
3.1.4. Stresses	59
3.1.5. Stiffness Matrix	59
3.2. NON LINEAR ANALYSIS	61



3.2.1.	Technique for Incorporating Nonlinearity	62
3.2.1.1.	Incremental Procedures	62
3.2.1.2.	Iterative Procedures	64
3.2.1.3.	Mixed Procedures	65
3.3.	SEQUENTIAL CONSTRUCTION	66
3.4.	CONSTITUTIVE LAWS	68
3.5.	STEPS OF THE ALGORITHM	73
<b>CHAPTER 4 : ABOUT THE PROGRAMES</b>		<b>80</b>
4.1.	PENTAGON3D	80
4.2.	PENTMESH	81
4.2.1.	Slice on PENTMESH	85
4.2.2.	Creation of 3D Element that Use 2D Entity	85
4.2.3.	Degenerate Elements	86
4.3.	PENPRE	87
4.4.	PENPOST	87
4.5.	STEPS IN MAKING THE MODEL	89
<b>CHAPTER 5 : RESULTS OF FEM ANALYSIS</b>		<b>96</b>
5.1.	GENERAL	96
5.2.	DISCRETIZATION OF DAM SECTION IN MESH	96
5.3.	ANALYSIS PERFORMED	97
5.4.	MATERIAL PROPERTIES	98
5.5.	SIGN CONVENTION	99
5.6.	RESULTS OF ANALYSIS	99
5.6.1.	Case I	100
5.6.2.	Case II	102
5.6.3.	Case III	104
<b>CHAPTER 6 : DISCUSSION OF RESULTS</b>		<b>118</b>
6.1.	DISCUSSION OF RESULTS OF CASE I STUDY	118
6.1.1.	Plane 1	118
6.1.1.1.	Horizontal Displacement - u	118
6.1.1.2.	Vertical Displacement - v	119
6.1.1.3.	Horizontal Normal Stress - $\sigma_x$	120
6.1.1.4.	Vertical Normal Stress - $\sigma_y$	121
6.1.2.	Plane 2	122
6.1.2.1.	Horizontal Displacement - u	122
6.1.2.2.	Vertical Displacement - v	122
6.1.2.3.	Horizontal Normal Stress - $\sigma_x$	123
6.1.2.4.	Vertical Normal Stress - $\sigma_y$	124
6.1.3.	Plane 3	124

6.1.3.1.	Horizontal Displacement - u	124
6.1.3.2.	Vertical Displacement - v	125
6.1.3.3.	Horizontal Normal Stress - $\sigma_x$	126
6.1.3.4.	Vertical Normal Stress - $\sigma_y$	126
6.2.	DISCUSSION OF RESULTS OF CASE II STUDY	127
6.2.1.	Plane 1	127
6.2.1.1.	Horizontal Displacement - u	127
6.2.1.2.	Vertical Displacement - v	128
6.2.1.3.	Horizontal Normal Stress - $\sigma_x$	129
6.2.1.4.	Vertical Normal Stress - $\sigma_y$	131
6.2.2.	Plane 2	132
6.2.2.1.	Horizontal Displacement - u	132
6.2.2.2.	Vertical Displacement - v	133
6.2.2.3.	Horizontal Normal Stress - $\sigma_x$	134
6.2.2.4.	Vertical Normal Stress - $\sigma_y$	134
6.2.3.	Plane 3	135
6.2.3.1.	Horizontal Displacement - u	135
6.2.3.2.	Vertical Displacement - v	136
6.2.3.3.	Horizontal Normal Stress - $\sigma_x$	137
6.2.3.4.	Vertical Normal Stress - $\sigma_y$	138
6.3.	DISCUSSION OF RESULTS OF CASE III STUDY	138
6.3.1.	Plane 1	138
6.3.1.1.	Horizontal Displacement - u	138
6.3.1.2.	Vertical Displacement - v	140
6.3.1.3.	Horizontal Normal Stress - $\sigma_x$	141
6.3.1.4.	Vertical Normal Stress - $\sigma_y$	142
6.3.2.	Plane 2	143
6.3.2.1.	Horizontal Displacement - u	143
6.3.2.2.	Vertical Displacement - v	144
6.3.2.3.	Horizontal Normal Stress - $\sigma_x$	145
6.3.2.4.	Vertical Normal Stress - $\sigma_y$	145
6.3.3.	Plane 3	146
6.3.3.1.	Horizontal Displacement - u	146
6.3.3.2.	Vertical Displacement - v	147
6.3.3.3.	Horizontal Normal Stress - $\sigma_x$	147
6.3.3.4.	Vertical Normal Stress - $\sigma_y$	148

**CHAPTER 7 : CONCLUSIONS** **199**

**REFERENCES** **204**

## LIST OF TABLES

No	Title	Page No.
2.1	Summary of Max. Earthquake Response under MCE Condition	24
5.1	Material Properties	99
6.1	Maximum Horizontal Displacements (cm), Plane 1, Case 1	149
6.2	Maximum Vertical Displacements (cm), Plane 1, Case 1	149
6.3	Maximum Horizontal Normal Stress (t/m <sup>2</sup> ), Plane 1, Case 1	149
6.4	Maximum Vertical Normal Stress (t/m <sup>2</sup> ), Plane 1, Case 1	149
6.5	Maximum Horizontal Displacements (cm), Plane 2, Case 1	150
6.6	Maximum Vertical Displacements (cm), Plane 2, Case 1	150
6.7	Maximum Horizontal Normal Stress (t/m <sup>2</sup> ), Plane 2, Case 1	150
6.8	Maximum Vertical Normal Stress (t/m <sup>2</sup> ), Plane 2, Case 1	150
6.9	Maximum Horizontal Displacements (cm), Plane 3, Case 1	151
6.10	Maximum Vertical Displacements (cm), Plane 3, Case 1	151
6.11	Maximum Horizontal Normal Stress (t/m <sup>2</sup> ), Plane 3, Case 1	151
6.12	Maximum Vertical Normal Stress (t/m <sup>2</sup> ), Plane 3, Case 1	151
6.13	Maximum Horizontal Displacements (cm), Plane 1, Case 2	152
6.14	Maximum Vertical Displacements (cm), Plane 1, Case 2	152
6.15	Maximum Horizontal Normal Stress (t/m <sup>2</sup> ), Plane 1, Case 2	152
6.16	Maximum Vertical Normal Stress (t/m <sup>2</sup> ), Plane 1, Case 2	152

6.17	Maximum Horizontal Displacements (cm), Plane 2, Case 2	153
6.18	Maximum Vertical Displacements (cm), Plane 2, Case 2	153
6.19	Maximum Horizontal Normal Stress (t/m <sup>2</sup> ), Plane 2, Case 2	153
6.20	Maximum Vertical Normal Stress (t/m <sup>2</sup> ), Plane 2, Case 2	153
6.21	Maximum Horizontal Displacements (cm), Plane 3, Case 2	154
6.22	Maximum Vertical Displacements (cm), Plane 3, Case 2	154
6.23	Maximum Horizontal Normal Stress (t/m <sup>2</sup> ), Plane 3, Case 2	154
6.24	Maximum Vertical Normal Stress (t/m <sup>2</sup> ), Plane 3, Case 2	154
6.25	Maximum Horizontal Displacements (cm), Plane 1, Case 3	155
6.26	Relative Horizontal Displacement (cm), Plane 1, Case 3	155
6.27	Maximum Vertical Displacements (cm), Plane 1, Case 3	155
6.28	Maximum Horizontal Normal Stress (t/m <sup>2</sup> ), Plane 1, Case 3	156
6.29	Maximum Vertical Normal Stress (t/m <sup>2</sup> ), Plane 1, Case 3	156
6.30	Maximum Horizontal Displacements (cm), Plane 2, Case 3	156
6.31	Relative Horizontal Displacement (cm), Plane 2, Case 3	157
6.32	Maximum Vertical Displacements (cm), Plane 2, Case 3	157
6.33	Maximum Horizontal Normal Stress (t/m <sup>2</sup> ), Plane 2, Case 3	157
6.34	Maximum Vertical Normal Stress (t/m <sup>2</sup> ), Plane 2, Case 3	158
6.35	Maximum Horizontal Displacements (cm), Plane 3, Case 3	158

6.36	Relative Horizontal Displacement (cm), Plane 3, Case 3	158
6.37	Maximum Vertical Displacements (cm), Plane 3, Case 3	159
6.38	Maximum Horizontal Normal Stress (t/m <sup>2</sup> ), Plane 3, Case 3	159
6.39	Maximum Vertical Normal Stress (t/m <sup>2</sup> ), Plane 3, Case 3	159

## LIST OF FIGURES

No	Title	Page No.
2.1	Displacement due to Dead Weight in Standard Dam	35
2.2	Displacement in Standard Dam: 7 & 14 Lift Construction	35
2.3(a)	Rigid Shoulder Study - Effect of Number of Layers on Settlement	35
(b)	Rigid Shoulder Study - Effect of $f$ , 6 Layers Analyses	36
(c)	Settlement on Beliche Dam Centre Line	36
2.4	Effects of Reservoir Filling on a Zoned Dam	36
2.5	Horizontal Displacement due to Reservoir Filling	37
2.6	Vertical Displacement due to Reservoir Filling	37
2.7	Calculated Horizontal Movements at 3 Stages of Reservoir Filling, Oroville Dam	37
2.8	3D FE Model of Oroville dam	37
2.9	Computed Amplification Functions for Crest Midpoint of Oroville dam	38
2.10	Acceleration Response Spectra for Motions at Crest Midpoint of Oroville dam	38
2.11(a)	Typical Cross Section of Duncan Dam	38
(b)	Longitudinal Section of Duncan Dam and Foundation showing Construction Sequence and Location of Cracks	39
2.12	The Cracking Sequence	39
2.13	Horizontal Displacement along Main Transverse Section at Elev.2150 due to Further Fill Placement (Linear Analysis)	39
2.14	Major Principal Stresses along Vertical Column of Core	40
2.15	First Modification of Chicoasen dam, Vertical and Central Impervious Core	40
2.16	Zoning of Material and Mechanical Characteristic, 3-D analysis, Case 2	41
2.17(a)	Longitudinal Max. Cross Section, Case 3	41
(b)	Transverse Cross Section along Dam Axis, Case 3	42
2.18	Modified Max. Cross Section of the Chicoasen dam	42

2.19(a)	Settlement Profile at Elev.370	43
(b)	Horizontal Movement Profile at Elev.370	43
2.20	Cross Section of Tehri Dam	
(a)	2D dam section at B-11 with max. core	44
(b)	Contours of Plastic Strain at End of Earthquake for the Two Section	44
2.22	Dabaklamm Dam	45
2.23	FEM Calculation of the Physical Model	45
2.24(a)	Comparison of Horizontal & Vertical Stress	46
(b)	Comparison of Settlement	46
2.25	Calculation of Dead Weight	47
2.26	FE Model of Bouquet Canyon Dam	47
2.27	Resonance Curves at Station B of Bouquet Canyon Dam	47
2.28	Vibration Shapes along the Crest of Bouquet Canyon Dam	48
2.29	Main Cross Section of Yeguas Dam	48
2.30	FE Mesh	49
2.31	Comparison of Settlement at End of Construction	49
2.32	Comparison Settlement at 136 days after End of Constr.	50
2.33(a)	Typical Cross Section of Tahamara Dam	50
(b)	Dam Body Model Used for Analysis	50
2.34	Distribution of differential compression and cumulative settlement due to consolidation from completion of embankment to start of reservoir filling	51
2.35	Consolidation of settlement due to secondary consolidation from start of reservoir filling to December 1995	51
2.36	Calculation of settlement due to reservoir Loading	52
2.37	Calculation of settlement due to infiltration	52
2.38	Results of calculation of settlement due to change in reservoir filling	53
2.39	Comparison between calculated and measured differential settlement	53

2.40	Comparison between calculated and measured cumulative settlement	53
2.41	Percentage of causes of crest level settlement	54
3.1	3-D Finite Element Showing Node Number	77
3.2	Non Linear Curve	77
3.3	Basic Incremental Procedure	78
3.4	Iterative Procedure	78
3.5	Step Iterative Procedure	78
3.6	Mixed Procedure	79
3.7	Hyperbolic Stress-Strain Curve	79
4.1	The PENTMESH Screen	91
4.2	Concept of Slice	91
4.3	Quad4	91
4.4	Quad8	91
4.5	Frame, Truss, Spring	91
4.6	AddElementLayer Menu	92
4.7	Creation of 3D 8-node solid element	92
4.8	The Various Shapes of Degenerated Elements	92
4.9	Degenerate Hexa Element Menu	93
4.10	The Surface Number of Element	93
4.11	AddElementLayer Box	93
4.12	The Dialog Box of Degenerated Hexa	94
4.13	PENTPRE Screen	94
4.14	PENTPRE Boundary Condition	94
4.15	PENPOST Screen	95
5.1	Section of 100 m High Earth and Rockfill Dam	106
5.2	Finite Element Idealisation of the Dam	
(a)	Longitudinal Section along Central Core	106
(b)	Maximum Transverse Section of the Dam	106
5.3		
(a)	One Stage of Construction Dam and One Stage Full Reservoir Filling	106



(b)	One Stage of Construction Dam and Four Stages Reservoir Filling	107
(c)	Seven Stages of Construction Dam and Four Stages Full Reservoir Filling	107
5.4	Sign Convention	107
5.5	3-D Horizontal Movement, End of Construction, Single Lift	108
5.6	3-D Horizontal Movement, End of Construction, Seven Lifts	108
5.7	3-D Vertical Movement, End of Construction, Single Lift	109
5.8	3-D Vertical Movement, End of Construction, Seven Lifts	109
5.9	3-D Horizontal Normal Stress, End of Construction, Single Lift	110
5.10	3-D Horizontal Normal Stress, End of Construction, Seven Lifts	110
5.11	3-D Vertical Normal Stress, End of Construction, Single Lift	111
5.12	3-D Vertical Normal Stress, End of Construction, Seven Lifts	111
5.13	3-D Horizontal Movement, Full Reservoir Filling, One Stage Full Reservoir	112
5.14	3-D Horizontal Movement, Full Reservoir Filling, Four Stages Full Reservoir	112
5.15	3-D Vertical Movement, Full Reservoir Filling, One Stage Full Reservoir	113
5.16	3-D Vertical Movement, Full Reservoir Filling, Four Stages Full Reservoir	113
5.17	3-D Horizontal Normal Stress, Full Reservoir Filling, One Stage Full Reservoir	114
5.18	3-D Horizontal Normal Stress, Full Reservoir Filling, Four Stages Full Reservoir	114
5.19	3-D Vertical Normal Stress, Full Reservoir Filling, One Stage Full Reservoir	115
5.20	3-D Vertical Normal Stress, Full Reservoir Filling, Four Stages Full Reservoir	115
5.21	3-D Horizontal Movement, Full Reservoir Filling, 7 Lifts Construction 4 Stages Reservoir Filling	116

5.22	3-D Vertical Movement, Full Reservoir Filling, 7 Lifts Construction 4 Stages Reservoir Filling	116
5.23	3-D Horizontal Normal Stress, Full Reservoir Filling, 7 Lifts Construction 4 Stages Reservoir Filling	117
5.24	3-D Vertical Normal Stress, Full Reservoir Filling, 7 Lifts Construction 4 Stages Reservoir Filling	117
6.1	Horizontal Displ. - $u$ along Height at Different Location over Plane 1, Case 1	160
6.2	Vertical Displ. - $u$ along Height at Different Location over Plane 1, Case 1	161
6.3	Horizontal Normal Stress $\sigma_x$ along Height at Different Location over Plane 1, Case 1	162
6.4	Vertical Normal Stress $\sigma_y$ along Height at Different Location over Plane 1, Case 1	163
6.5	Horizontal Displ. - $u$ along Height at Different Location over Plane 2, Case 1	164
6.6	Vertical Displ. - $u$ along Height at Different Location over Plane 2, Case 1	165
6.7	Horizontal Normal Stress $\sigma_x$ along Height at Different Location over Plane 2, Case 1	166
6.8	Vertical Normal Stress $\sigma_y$ along Height at Different Location over Plane 2, Case 1	167
6.9	Horizontal Displ. - $u$ along Height at Different Location over Plane 3, Case 1	168
6.10	Vertical Displ. - $u$ along Height at Different Location over Plane 3, Case 1	169
6.11	Horizontal Normal Stress $\sigma_x$ along Height at Different Location over Plane 3, Case 1	170
6.12	Vertical Normal Stress $\sigma_y$ along Height at Different Location over Plane 3, Case 1	171
6.13	Horizontal Displ. - $u$ along Height at Different Location over Plane 1, Case 2	172
6.14	Vertical Displ. - $u$ along Height at Different Location over Plane 1, Case 2	173
6.15	Horizontal Normal Stress $\sigma_x$ along Height at Different Location over Plane 1, Case 2	174
6.16	Vertical Normal Stress $\sigma_y$ along Height at Different Location over Plane 1, Case 2	175

6.17	Horizontal Displ. - $u$ along Height at Different Location over Plane 2, Case 2	176
6.18	Vertical Displ. - $u$ along Height at Different Location over Plane 2, Case 2	177
6.19	Horizontal Normal Stress $\sigma_x$ along Height at Different Location over Plane 2, Case 2	178
6.20	Vertical Normal Stress $\sigma_y$ along Height at Different Location over Plane 2, Case 2	179
6.21	Horizontal Displ. - $u$ along Height at Different Location over Plane 3, Case 2	180
6.22	Vertical Displ. - $u$ along Height at Different Location over Plane 3, Case 2	181
6.23	Horizontal Normal Stress $\sigma_x$ along Height at Different Location over Plane 3, Case 2	182
6.24	Vertical Normal Stress $\sigma_y$ along Height at Different Location over Plane 3, Case 2	183
6.25	Horizontal Displ. - $u$ along Height at Different Location over Plane 1, Case 3	184
6.26	Relative Horizontal Displ. to End of Construction over Plane 1, Case 3	185
6.27	Vertical Displ. - $u$ along Height at Different Location over Plane 1, Case 3	186
6.28	Horizontal Normal Stress $\sigma_x$ along Height at Different Location over Plane 1, Case 3	187
6.29	Vertical Normal Stress $\sigma_y$ along Height at Different Location over Plane 1, Case 3	188
6.30	Horizontal Displ. - $u$ along Height at Different Location over Plane 2, Case 3	189
6.31	Relative Horizontal Displ. to End of Construction over Plane 2, Case 3	190
6.32	Vertical Displ. - $u$ along Height at Different Location over Plane 2, Case 3	191
6.33	Horizontal Normal Stress $\sigma_x$ along Height at Different Location over Plane 2, Case 3	192
6.34	Vertical Normal Stress $\sigma_y$ along Height at Different Location over Plane 2, Case 3	193
6.35	Horizontal Displ. - $u$ along Height at Different Location over Plane 3, Case 3	194

6.36	Relative Horizontal Displ. to End of Construction over Plane 3, Case 3	195
6.37	Vertical Displ. - u along Height at Different Location over Plane 3, Case 3	196
6.38	Horizontal Normal Stress $\sigma_x$ along Height at Different Location over Plane 3, Case 3	197
6.39	Vertical Normal Stress $\sigma_y$ along Height at Different Location over Plane 3, Case 3	198

## SYNOPSIS

The objective of this study is to carry out the following.

1. To determine the effect of number of lifts for end of construction.
2. To determine the effect of the reservoir filling have being done in single stage and four stages.
3. To study the effect of seven lifts at end of construction with four stages reservoir filling

A 100 m high dam with a vertical core has been used in this study. The dam has been considered to be located in a narrow valley with valley wall slope of 1H:1V with 50 m base width. The materials of the various zones (shell, filter and core) of the dam are assumed to exhibit non linear behaviour. The hyperbolic model has been adopted to model the stress strain behaviour of the materials. The behaviour has been studied at three different cross section and five interfaces at different elevation on each cross section.

The dam has been discretised into 560 numbers of 8 noded brick elements, and consists of 748 nodes, each node having 3 degrees of freedom, thus having 2244 degrees of freedom. The foundations and the abutments for all the analyses have been taken as rigid. The finite element bases package 'PENTAGON3D' is used to analyze the deformations and stresses.

The major findings of the present study are as follows:

➤ **Effect of number of lifts for end of construction**

Horizontal displacement in single lift is found slightly less than the same obtained by seven lifts with a similar in pattern.

The location of vertical displacement is found at the mid height of the dam for seven lifts construction while at the top of the dam for single lift construction.

Single and seven lifts analysis indicate some tension on the crest of the dam near the abutment (Plane 3) extending to some portion of upstream and downstream faces of the dam

Due to the valley effect, the magnitude of stress and deformation in Plane 2 and Plane 3 are founded to be reducing compare to the central section (Plane 1)

➤ **Effect of reservoir filling have being done in single stage and four stages**

The vertical displacement and the stress distribution on single stage full reservoir filling are found higher than the same obtained by four stages reservoir filling while it found slightly less in horizontal displacement.

The stresses due to reservoir filling are affected in the upstream shell and there is only a small impact on the other zones. The stresses distribution due to single stage full reservoir filling is found more than the same obtained by four stages reservoir filling.

The magnitude of stress and deformation also found in decreasing towards the abutments

➤ **Effect of seven lifts at end of construction with four stages of reservoir filling**

The horizontal movement of upstream shell in the upstream direction at first and second filling of reservoir is attributed to the effects of softening of the upstream shell material. The horizontal movement in the downstream

direction at later filling stages is the effect of water load on the core.

It is observed that the increase in the magnitude of the stress and deformation due to reservoir filling on the upstream shell is more prominent than on the core zone.

# CHAPTER 1

## INTRODUCTION

### 1.1. GENERAL

In its simple and oldest form the embankment dam was constructed with low-permeability soils to a normally homogeneous profile. It was then increasingly recognized that, in principle, larger embankment dams required two components, an impervious water-retaining element or core of very low permeability soil and supporting shoulders of coarser earthfill (or of rockfill), to provide structural stability. Given the advancements in techniques of design and soil testing, the possibility of sliding failure can be almost completely eliminated. Adequate knowledge and experience is now available to enable the designer to devise effective measures to protect the dam, provided these are correctly implemented and maintained. The matter of great concern to an earth dam engineer today is the possible development of a leak through an actual or incipient crack in the dam. With increasing use of narrower gorges with steeper sides and ever-increasing dam heights, the need for safeguarding against cracks has become ever greater. Cracks occur in regions of tensile strain as a result of deformations caused by the dead load of structure, filling of the reservoir or seismic action.

Many earth and rockfill dams have been observed to have undergone large settlements and horizontal movements and cracking on reservoir filling. The dams have experienced wide variety of movements, both in the upstream direction and the



downstream direction. These complex movements need to be studied under the combined effect of two counter acting effects of reservoir filling namely (1) the water loads on the dam and (2) the softening and weakening of the fill material due to wetting (Nobari and Duncan, 1972). Correct assessment of movements in dam are called for better understanding the behaviour of the dam and to safe guard against cracks, hydraulic fracturing, etc. related failure at design stage itself.

The main complexity arises from the multiphase nature of soil and rocks. Further complications result from factor such as residual stresses, discontinuities resulting from joints and fissures. Finite element method is one of the tools which of late, have been found to be of immense utility for analysing such complex systems. It is, therefore, natural for the engineer concerned with such important structures as dams to turn to this numerical process for the answer to the questions posed at the analysis and design stages.

## **1.2. IMPORTANCE OF DEFORMATION CONSIDERATION**

The stability of an earth dam during construction or normal operation is conventionally examined using equilibrium methods of stability analysis. These procedures indicate the factor of safety of the dam with respect to instability, but they provide no information regarding the deformation of the dam. In recent years, there has been a growing realization of the need to determine the deformation of a dam during construction or operation. These deformations may be of interest for a number of reasons:

1. Excessive settlements can lead to loss of freeboard and danger of overtopping.
2. Excessive spreading of an embankment may lead to the formation of longitudinal cracks which adversely affect its stability. Such cracks have been observed in many embankment built on clay foundations.
3. Differential settlements between sections along the axis of a dam may lead to development of transverse cracks through the embankment which could allow passage of water and progressive failure by erosion and piping.
4. Differential settlements between the core and the shell of a zoned embankment can lead to reduction in the stresses in the core, and may result in hydraulic fracturing if the stresses at any elevation are reduced to values less than the pressure of the water at the same elevation (Seed, Duncan and Idriss, 1975).
5. Deformation pattern of the upstream face particularly under the water load of the reservoir is necessary for the proper design of the concrete facing of a concrete faced rockfill dam. A crack on the concrete face may lead to seeping of water through it thereby softening of fill material and an unexpected deformation of the fill material may lead to further failure of concrete face.
6. Conduits through or under embankment suffer from stretching to one portion and compression to other portion due to deformation of the dam. It may lead to cracking and concentration of tension in the conduit and hence the deformations of the embankment need to be known as well as

the magnitude of such deformation for the safe design of underlying conduits.

7. On wide rivers concrete gravity spillways are often built in the main river channel with earth dam embankment on each end. The connections are usually made simply by extending the concrete dam into the earth dam, and wrapping the embankment slopes around the end of the concrete dam on both sides. The embankment dam is generally compacted directly against the concrete dam with heavy rollers; therefore high embankment settlement would not be anticipated. In some cases the dams are fairly high at the junctions, creating a situation with potential for differential settlement cracking (Sherard, 1973).

### **1.3. AIMS AND SCOPE OF THE STUDY**

A study has been carried out to analyse the behaviour of embankment dam during construction as well as reservoir filling stages. Three dimensional incremental non linear analysis simulating construction sequence of the dam, has been done for a dam situated in a narrow valley for end of construction stage and incorporating the softening behaviour of fill material during reservoir filling so as to predict and estimate the movements of earth and rockfill dam. This study is limited to the effect of reservoir filling in stages incorporated with the sequential construction of the dam. To achieve this objective following analyses have been carried out:

1. The effect of sequential construction when the dam is assumed to be constructed in seven lifts over single lift at end of construction

2. The effect of reservoir filling being done in different stages while the dam is assumed to be constructed in single lift
3. The effect of reservoir filling is done in four stages and the dam is assumed to be constructed in seven lifts. Relative horizontal displacements with end of construction as datum have been studied to analyse the movements due to reservoir filling.

A 100 m high earth and rockfill dam with a vertical core has been selected for the study. The valley walls are inclined at approximately 1H:1V with base width of 50 m. Non linear hyperbolic stress-strain relationship has been used for all the dam materials.

#### **1.4. THE ORGANISATION OF DISSERTATION**

The study is presented in seven chapters. The contents of each chapter are briefly indicated below.

- |           |   |
|-----------|---|
| Chapter 1 | Introduction of the problem scope and objective of study are given.   |
| Chapter 2 | Review of literature has been given in this chapter   |
| Chapter 3 | The finite element method and the method incorporating non-linearity of stress-strain relationship have been described in this chapter. |
| Chapter 4 | A brief description of the PENTAGON3D program software of finite element for performing 3-D non linear sequential                       |

analysis of the dam has been given in this chapter.

Chapter 5 Gives the results and analysis.

Chapter 6 Gives the discussion of results.

Chapter 7 Gives the conclusions and suggestions for further study.

## CHAPTER 2

### REVIEW OF LITERATURE

#### 2.1. GENERAL

Measurements made in many earth and rockfill dams have shown that large settlements, horizontal movements and cracking are frequently caused by reservoir filling. The movement of embankment due to first filling of reservoir is the most complicated as measured and observed in a number of dams. The magnitude, rate and direction of displacement at a specific point within a dam may change during different phases of construction of the dam and operation of the reservoir.

The studies about reservoir filling and using of three dimensional analysis of finite element method in a few dams due to this condition are described below.

#### 2.2. LAYERED ANALYSIS OF EMBANKMENT DAM

Embankments are built up in relatively thin horizontal layers. Consequently, there will be a large number of layers during the construction of a large dam. The limitations of computer modelling require relatively thick layers to be used in the idealization. In the past, to provide an insight into the errors involved, the closed form solution of the incremental analysis was usually compared to the finite element 'layered' analysis using a one dimensional model which represents either a soil column or a fill of large lateral extent. In the next approach of the conventional stress deformation, the structure is assumed to be completed in single stage and the gravity load is applied instantaneously as an external load to the complete

structure. This conventional solution treats the gravity effects as an external load applied to the finished structure and valid if the state of the stresses in the structure is statically determinate at all stage of construction process, but in actual condition most embankments are constructed in layers by incremental process and the load is accumulated gradually during construction thus invalidates the assumption of one stage layer analysis.

Goodman and Brown (1963) were the first to consider the difference between incremental construction and instantaneous loading in stress analysis of embankments. They focussed on the stresses and displacement in structures which is caused by the dead weight applied on the placing of material in layer. As an example, the case of an embankment built up in horizontal layers is considered and the stress results lead to a rational description of the rotational instability of slopes. The elastic analysis developed indicates the dependence on the construction sequence of the stress distribution in statically indeterminate structures. It predicts the curved failure surfaces observed in embankments and provides an explanation for the appearance of cracks on the top surface of steep cuts.

Later Clough and Woodward (1967) applied this concept of incremental construction to the analysis of earth dam by finite element method. They evaluated the effect of incremental construction, the standard embankment was first analyzed considering it to be constructed in single lift, and was then reanalyzed with the incremental construction process using 10 lifts. The stress distribution determined in the two cases indicated similar pattern. The displacements were, in contrast,

found to be considerably affected by construction process. The horizontal displacements were seen to be quite similar in both cases but the vertical displacement for single lift case was seen to be the largest at the top due the fact that they are merely the integrated strains developed over the full height. The incremental analysis, however, shows zero vertical displacement at the top, because after the top layers was placed, no further strains were developed. The maximum vertical displacement in this case occurs near mid height as the region is affected by all the strains occurring below this level, as shown in Fig.2.1. The important question remains, however, as to the number of lifts required in order to obtain good accuracy in the solution. For comparison purposes, an analysis was made of the standard embankment considering 7 lifts and 14 lifts. Vertical displacements computed at the 15 ft level and at 60 ft level are plotted in Fig.2.2 for both cases. Both sets of data points fall on the same curve for both elevations. Thus it is clear that seven lift analysis provides an adequate representation of the construction procedure.

Naylor and Mattar (1988) studied about the effect of stiffness reduction factor ( $f$ ) to reduce the layer analysis. They made a comparison in two cases, first case with linear elastic ( $f=4$ ) and K-G model ( $f=3$ ). The difference was insignificant and the second case described the effect of varying  $f$  and the number of layers being kept constant at six, shown in Fig.2.3(a-b). The modelling of the construction of Beliche dam, Brazil, was investigated with this effect. K-G model,  $f$  equal to 3 with 2, 3 and 6 layers was used in the modelling. The very small difference of displacement from the



result was observed. Even with only two layers the central displacement only differs slightly from that in the six layer analysis. The study concluded that the value of stiffness reduction factor from 3 to 5 with non linear analysis could reduce the layered analysis upto 4 to 6 layers; it will normally be sufficient in any embankment dam analysis.

## **2.3. ANALYSIS OF MAJOR DAMS**

### **2.3.1. Analysis of Oroville Dam**

Nobari and Duncan (1972) used finite element method to describe the movement of the dam due to reservoir filling. The stresses in the part of the dam wetted by the reservoir are changed very significantly by effect of buoyancy and water loading. The movements in Oroville dam were calculated using the finite element procedure and were compared with those measured during reservoir filling. The Oroville dam is 235 m high with a moderately inclined central core and thick shells of rockfill compacted to 100% relative density on either side of core.

The effect of reservoir filling on a zoned dam is illustrated in Fig.2.4. These effects which result directly from the water loading are in following:

1. The water load on the core causes downstream and downward movements.
2. The water load on the upstream foundation causes upstream and downward movements.
3. The buoyant uplift forces in the upstream shell cause upward movements within this zone.
4. The effect due to softening and weakening caused by wetting of the upstream shell material.

The study of the movements of the Oroville dam was described as below. The movements first in the upstream direction and later in the downstream direction during continuous rise of the reservoir can be explained in terms of the counteracting effects of softening of the upstream shell and the water load on the core. The upstream movements caused by softening are greatest during the first stage of reservoir filling because the amount of compression due to wetting is greatest when overburden pressure is large. The downstream movement caused by water loads, on the other hand, are greatest during the later stages of reservoir filling, because the water load on the core increases as the square of the depth of the impounded water. Therefore, movements resulting from softening due to wetting dominate during the early stages of reservoir filling and movements resulting from the water load dominate during the later stages, with the result that the dam moves first upstream and then downstream.

Nobari and Duncan developed the finite element procedure which may be used to calculate movements and stress changes in dams during reservoir filling, taking into account the effects of softening of the shell material due to wetting, as well as the effect of water loads. Contours of the calculated horizontal movements are shown in Fig.2.5. The movements are in the downstream direction throughout most of the dam, with exception of the toe of the upstream slope. Contours of the calculated vertical settlements are shown in Fig.2.6. Throughout most of the embankment the calculated settlements due to reservoir filling were between zero and 0.5 ft. At the upstream toe of the dam and at the downstream edge of the crest, the calculations

indicated a small amount of heave. Within the upstream shell the settlements are dominated by compression of shell material due to wetting and the tendency for expansion of shell as the effective stresses are reduced by submergence. These two counteracting effects result in settlement which is largest near midheight of the dam. In addition, it may be noted that the downward movement of material within most of the upstream shell results in a displacement of material in the upstream direction and a small amount of heave near the upstream toe.

The movements of the core calculated in this procedure are shown in Fig.2.7. The undeflected position of the core before reservoir filling is represented by vertical line and subsequent horizontal movements are indicated to the left and right.

Mejia, Seed and Lysmer (1982) presented a description of finite element techniques for the dynamic response analysis of earth and rockfill dams in three dimensions. The method has been used to compute the dynamic response of Oroville dam for Oroville earthquake in August 1975 and to evaluate the dynamic material properties of the dam. Eight node isoparametric brick elements with three degrees of freedom per node are used in the model of the actual embankment. It is assumed that the walls of the canyon are rigid and therefore all points in these boundaries move in phase and with the same displacement amplitudes. The validity of this assumption depends on (1) the relative stiffness of the material comprising the canyon walls and the dam, (2) the geometry of the canyon, (3) the size of the dam and (4) the frequency range of the motion being applied to the canyon. The corresponding 3D finite element model is shown in Fig.2.8. This model of half the dam has 591 elements, 543

free nodal points and 8 section in the cross valley direction. The average ratio of shear modulus to shear strength for cohesive soil has been used to evaluate the low strain moduli of the core material. The computed amplification functions at the midpoint of the crest of the dam for the selected shell of the function of strain level and relative density,  $K_{2max}$ , values are shown in Fig.2.9. These amplification functions give, for the spectrum of frequencies of harmonic excitation, the ratio between the amplitude of absolute acceleration at the crest midpoint and the amplitude of acceleration at the rigid boundaries of the model. A simpler comparison between computed and recorded response of the dam can be made in terms of the acceleration response spectra for the crest motions, shown in Fig.2.10.

Considering that the natural period of the dam and the response at the crest for the levels of strain induced by the Oroville earthquake computed with a  $K_{2max}=170$  offer the best match to the corresponding recorded parameters, it can be concluded that this value of  $K_{2max}$  is representative of the in-situ dynamic properties of the Oroville shell material. The reasonable agreement between both this value and the laboratory measured values would seem to indicate the potential applicability of the method for use in design studies.

### **2.3.2. Analysis of Duncan Dam**

Eisenstein, Krishnayya and Morgenstern (1972) analysed the history of cracking sequence at Duncan dam in Canada with finite element procedure which taking into account of incremental loading, non linear stress-strain relations and three

dimensionality. Duncan dam, built in 1964-1967 on the Duncan River in British Columbia, Canada, is an earthfill dam of about 36 m height and 762 m length with an upstream sloping core. The dam has been built across a valley underlain by buried canyon about 378 m deep which is filled with sediment. The stratigraphy of the foundation is rather irregular with the upper layer possessing considerable compressibility. A typical cross section of the dam and longitudinal section are shown in Fig.2.11.

The designers of the dam anticipated large amount of settlement and designed the dam to accommodate these. While the predicted and observed settlements agreed in their magnitudes the observed distribution pattern differed from the predicted one. The maximum settlement which was expected beneath the middle of the dam finally appeared to be close to the left abutment. This nonuniformity exaggerated the differential movements and as a result transverse cracks appeared in an area located at the upstream side of the dam close to the left abutment. All the cracks did not all appear simultaneously and at the same level of filling. The cracking sequence is illustrated in Fig.2.12.

The dam has been analysed by a 3-D finite element program using hexahedral isoparametric elements with 8 nodes. The analysis has been performed incrementally and follows the actual sequence of filling. The elastic parameters have been derived from stress-strain relationship obtained from triaxial compression tests on the core and shell materials. The curves were introduced directly into the computer point by point and the tangent material stiffness parameters were interpolated from them according to the particular level of deviator and minor

principal stresses. The volumetric strain data were truncated to preclude any dilatancy.

The results of the area computed to be in tension agreed well with the position of the cracks observed on the dam. The results from incremental analysis were consistent with both location of the cracks and their propagation during construction. Hence it can be inferred that finite element analysis can provide substantial information about stress and deformation and regarding the location and extent of cracks in earth dams.

### **2.3.3. Analysis of Mica Dam**

Eisenstein and Simmons (1975) investigated the construction settlements and stresses of Mica dam in British Columbia, Canada by three dimensional finite element analyses. The 243 m high earthfill structure in a skewed and steep valley has been extensively instrumented and observations are taken regularly. The dam's axis is slightly curved upstream to add arching action as a measure against cracking.

A 3-D finite element program FENA3D was used in this study using eight noded isoparametric hexahedral elements and has options for linear as well as non linear stress-strain relationship for incremental analysis. The mesh consisted of 254 elements and 276 nodes and the number of lifts taken were five with the first lift modelling the river overburden excavation and the remaining four lifts representing each of the four construction seasons (1969-1972).

As the study was comparative in nature, following types of analyses were performed:

#### 1. Two-dimensional Linear Analysis

The mesh between Sta.22+50 and 25+50 was isolated in plane strain by fixing all nodes on or between these sections against cross-valley movement. Five lifts were used to simulate filling and linear elastic parameters represented the seven different materials in the embankment.

#### 2. Three-dimensional Linear Analysis

The full mesh was used, assuming rigid boundaries and embankment filling in five lifts, with the same linear elastic parameter as in 2-D analysis.

#### 3. Three-dimensional Linear Analysis with Bedrock Movements

Excavation of river burden material for the core trench caused bedrock to heave upward a maximum of about 15 cm. The heaved zone when subsequently loaded by the fill experienced settlements larger than elsewhere. The measured vertical movements (heave or settlement) were used as known displacements at appropriate boundary nodes. Since the bedrock movements were related to the weight of fill, the boundary displacements were applied incrementally with corresponding lifts of the dam.

#### 4. Three-dimensional Multi-linear Analysis

Using the non linear approach, the deformation moduli of individual elements were allowed to change with the stress level reached after each lift. This analysis also included the bedrock movements.

The computed displacements of Mica dam showed good agreement with field measurement. The plane strain settlements were for most points somewhat larger than the corresponding 3-D results, the maximum difference amounting to less than 20%.

However, since the difference was not constant within the profile investigated it could be due to the coarse mesh. Horizontal movements were very small and no meaningful comparison could be made with the computed values. Of a considerable importance were the horizontal displacements computed by the 3-D analysis for the main transverse section 22+50 which was also the plane strain section used in 2-D analysis. The results, shown in Fig.2.13, indicate that the maximum longitudinal displacement was 4 cm as opposed to a maximum vertical displacement (within the same section) of 82 cm. On average, there was about an order of magnitude difference between the two directions of displacement. The 3-D and 2-D plane strain stresses for the main transverse section in the zoned dam were very similar indicating that cross valley arching did not play an important role in the stress transfer.

In order to separate the effects of non-homogeneity of the zoned profile and of the arching across the narrow valley, a 3-D analysis of an equivalent homogeneous embankment was performed. For this type of analysis a modulus value was sought which would yield overall displacement results matching approximately the overall field behaviour. The major principal stress along a vertical in the core is shown in Fig.2.14 for different analyses. It is seen that for the homogeneous dam, there is a stress transfer of about 30% from the core portion to the shell portion, while for the zoned dam the stress transfer is of the order of about 70% near the base. At higher elevations where the geometric effects would be minimal, the stress transfer was constant at about 10% and 40% respectively for the homogeneous and zoned embankment.



The study concluded that the 3-D finite element analysis despite the coarseness of the mesh has successfully reproduced aspects of the field behaviour of Mica dam. Comparison of 3-D and 2-D analysis indicated that even with a structure so markedly 3-D as Mica dam the main transverse section can be studied using the plane strain model without a significant loss of accuracy. Thus increased detail and the sophistication of stress-strain response which can be incorporated into 2-D analyses appear to be more rewarding than efforts spent on 3-D modelling. Also, the need for 3-D analysis remains when studying the cracking potential of a dam. Such potential usually is highest near abutments where a 2-D analysis can shed no light at all. Considerable but thoughtful simplification of material behaviour can be made and still produce adequate information for design and monitoring purposes.

#### **2.3.4. Analysis of Chicoasen Dam**

Marsal and Moreno (1979) reported of the changing of the dam design due to analyse of the stress-strain computation with finite element method at Chicoasen dam, Mexico. Chicoasen dam is an earth and rockfill embankment, 210 m high over river bed with maximum height over the bed rock of 264 m.

The first stress-deformation studies were made for the original design of the dam, which had an inclined, central impervious core (case 1), as shown on Fig.2.15. The finite element method was used and non linear elastic analyses were confined to the case of plane strain. Therefore, two main cross sections were considered, (1) the maximum cross section of the dam, in a plane parallel to the river and (2) the transverse

cross section along the dam axis. Results disclosed a strong arching induced by the walls of the canyon and also significant interaction between the compacted zones of the shells and the core. The consequence of both effects was a substantial reduction in the vertical stresses. At this stage of the studies, the lower gorge of the canyon was not included in the analysis. Furthermore, these studies suggested 3-D analyses, to take into account the influence of the canyon walls and the acceptable alluvial materials left in the river, on the distribution of the stresses inside the embankment.

The 3-D finite element analysis was undertaken assuming linear elastic behaviour of the embankment materials. The mechanical characteristic and zoning of the cross section were developed in five layers (case 2), shown on Fig.2.16. The analysis showed that the vertical stresses within the core are greater than the adjacent pervious zones, particularly in the lower third of the embankment, and they substantially decrease towards the abutments. The maximum values of  $\sigma_z$  are about 25 kg/cm<sup>2</sup> which are of the same order of magnitude as the hydraulic head.

Based on those results, it was proposed to change the zoning materials within the embankments as illustrated by Fig.2.17 (case 3). Two zones of dumped rockfill adjacent to the transition materials were included and, in addition, a strip 4 m wide of soft clayey soil was provided along the abutments. Results for case 3 similar to those previously commented (case 2). Total vertical stresses ( $\sigma_z$ ) reached to values up to 30 kg/cm<sup>2</sup> near the bottom of the canyon, or about 1.5 times the

hydraulic head at that elevation. However,  $\sigma_z$  values close to the banks are smaller than the corresponding water pressure, thus disclosing zones of potential fracturing; this is particularly critical on the left abutment and also a principal stress ratio in the upper central zone of core was equal to 3 or greater, which implies that the clayey material may be subject to large deformations..

Additional computations were made for a curved embankment (radius of crest equal to 800 m). Comparison of the stress states developed in this case with those of the straight crest structure did not reveal any significant influence of the curvature, except on the upper 30 to 40 m of the dam. The analysis was repeated considering a non linear elastic behaviour of the embankment materials. The distribution of total stresses within the dam was similar to that given by linear elastic analysis. Important differences, however, were detected in the magnitude of the deformations calculated with the two above mentioned assumptions (linearity and non linearity).

On the basis of the stress-strain analyses briefly described, it was decided to build adjacent to the transition, two strips 10 m wide, made of uniform rockfill with nominal grain sizes comprised between 15 and 25 cm. The final modified cross section is shown in Fig.2.18.

### **2.3.5. Analysis of Dartmouth Dam**

Adikari, Donald and Parkin (1982) had studied about Dartmouth dam, a 180 m high rockfill with a central clay core and well instrumented, located in North-Eastern Victoria, Australia. A non linear finite element analysis simulating its

construction behaviour was carried out, taking into account the water load prevailing at the end of construction.

The finite element mesh to represent the maximum cross section of the dam has been formed of four-node linear isoparametric quadrilateral. The mesh has been built up in 10 equal layers, to simulate construction in 10 lifts, and the nodal points have been chosen to coincide with instrument location as far as practicable. The mesh has not been continued into foundation as it was found to be effectively rigid and of no significance to deformation within the dam. At the end of construction the reservoir water was 60% full and therefore it was necessary to incorporate 6 steps of incremental reservoir filling into analysis. The water load acts on the upstream face of the core and filling is assumed to be rapid.

Agreement of the result of predicted and measured values of displacement are generally satisfactory, as shown in Fig.2.19. The highest stress occurs in the filter zone but the core stresses are lower, the maximum being about 50% of the maximum stress in the filter zone. The stiffer filter zones have resulted in significant interaction effects and a reduction in vertical stresses in the core at all elevations. The prediction of construction pore pressure in core has taken into account the difference in laboratory pore pressure response of material placed (between elev. +400 and +430) from that of the rest of the core material. Negative pore pressure were recorded at that location since November 1977 until positive reading were obtained in March 1979, and have remained positive but only a few metres head. The behaviour of the material at this location

indicates that the load transfer could have been a significant contributory cause for negative pressures.

Some difference between measured and predicted behaviour would appear to be unavoidable. Possible sources of error may be found in the approximations in forming the constitutive law, the use of triaxial data in a plane strain problem and in the inadequate representation of real variations in material properties, including anisotropy due to rolling and variations in placement moisture content.

### **2.3.6. Analysis of Tehri Dam**

Singh, Gupta and Saini (1985) have presented a 3-D finite element analysis of the Tehri dam to study the effect of providing curvature to the axis under different loading condition, viz. end of construction stage and reservoir full condition stage. Tehri dam is 260.5 m high earth and rockfill dam with a central moderately inclined core with upstream and downstream transition zones. The gorge at the dam site is narrow with slopes at 1.1H:1V. In the study, the construction in one lift is assumed and full reservoir load is also applied in one stage. The valley shape is assumed to be V-shaped and the linear material behaviour was used for the analysis with the straight and curved axis (radius equal to 800 m). The computer program used 20 noded isoparametric brick element.

The water load has been accounted for as below:

1. Water load on core
2. Buoyancy effect in the shell
3. Additional weight of core zone due to saturation

The results show that there is no significant change in the stresses and displacements in the dam straight and curved axis for both loading combinations. It is observed that at the vertical normal compressive stresses got reduced in most part of upstream shell and increased in downstream shell for reservoir full condition. The horizontal stresses at end of construction get reduced all over the section with the filling of reservoir. The cross valley horizontal stresses in the reservoir filling condition are reduced in the upstream shell but in the core the stresses are increased. All over the upstream face of the core, the stresses are less than the reservoir water pressure indicating potential for hydraulic fracturing. The minor principal stress for the reservoir full over the central section and longitudinal section across the valley have shown that even though the cross section of the dam does not appear in any appreciable tension, there is a large tensile zone in the shell extending from one abutment to another. To predict cracking, therefore, a 3-D analysis is necessary as crack can not be predicted by 2-D analysis and to study the indication of the occurrence of hydraulic fracturing in the dam.

Paul, D.K. (2002) has studied about the seismic safety of the Tehri dam. The dam was later tested for various levels of shaking as per different earthquake strong motions that were evolved by experts progressively in due consideration to all possible worst case scenarios in Himalayan environs. He presented a test to a Maximum Credible Earthquake (MCE) producing Peak Ground Acceleration (PGA) 0.5g at the dam site which includes a sequential non linear static analysis using the

Mohr-Coulomb material model for the rockfill and the clay core materials.

Two section corresponding to (i) Section-1, which has the maximum core height and (ii) Section-2 having maximum downstream slope but short upstream slope have been taken for analysis, as shown in Fig.2.20. The sections clearly show that dam is very much restrained by the hills and therefore for analysis, the effective height of the dam is significantly reduced. 2D finite element plain strain idealisation mapped with eight noded isoparametric is used for the analysis. The nodes at the base of the dam are assumed to be fixed. The water pressure at full reservoir condition is taken as edge load on the U/S portion of the clay core.

Since both the sections are part of the same dam and should be vibrating with the same frequencies. The earthquake response is evaluated considering the same fundamental frequency for the two sections. Table 2.1 gives the maximum horizontal/vertical accelerations and displacements at the dam crest. Figure 2.21 shows the contours of plastic strain at the end of earthquake. It is observed that the plastic strains occur mainly near U/S and D/S slope of the dam.

Tab.2.1. Summary of Maximum Earthquake Response under MCE Condition

Response Parameters	Section-1	Section-2
Max. horz. Acceleration at dam crest	1.136g	0.978g
Max. vert. Acceleration at dam crest	0.703g	0.434g
Max. horz. Displ. at dam crest (cm)	40.25	36.69
Max. vert. Displ. at dam crest (cm)	25.87	14.78
Max. plastic strain	0.08	0.08

Quantitatively, the dam is found to undergo plastic deformations mostly near the U/S and D/S slopes, which are taken care of by providing a sumptuous riprap composed of blasted rock. The top portion of the fill dam is being built with the

same material to withstand severe accelerations. Under MCE, the dam could have limited local damage, would not, by itself could be termed as failure as it could be restored as special repairs and remedial actions as is the international practise.

### **2.3.7. Analysis of Dabaklamm Dam**

Schober and Hupfauf (1991) have studied about the behaviour of embankment dams in narrow valley with Dabaklamm dam in Austria as a study case. An effort is therefore made to use an approximation to determine the 3-D effects using finite element method. The Dabaklamm dam is a central core dam with 220 m height, as shown in Fig.2.22. The foundation of shell zone on the upstream side rests on the compressible overburden of fluvial sediments. The 1.5 ratio of crest length to dam height indicates a narrow valley situation. The behavior in narrow valley is dependent on several influential factors, whereby valley shape stands in the foreground. Furthermore, the deformability and shear resistance of the fill material, the zoning of the dam section, the roughness of the valley flanks and the bearing behaviour of the foundation are of considerable significance.

Using a physical model of barite sand, both deformation and stress conditions were measured during and after filling. Fig.2.23 shows several results for a flank friction angle of  $37^\circ$ . The points at which stresses were measured are also marked on the FE-net on Fig.2.23(a). Fig.2.24 shows a comparison of the vertical and horizontal stresses measured in the model with calculated values for various of the flanks. Fig.2.25 shows the amount of settlement which was measured at 4 different levels as



compared to the calculated values. The investigation of the main cross section of the dam was shown in Fig.2.25. As expected, the compressibility of the overburden has great influence in dead weight load case. Movement toward the upstream side occur which also extend to the downstream side through the upper third core (Fig.2.25(c)). Particularly in the core, this led to zones of greater material utilization (Fig.2.25(b)). Another result which deserves particular mention is that the compressible overburden affects the rise in vertical stresses in the upstream half of the core as a result of saddling (Fig.2.25(a)).

In summary, the following conclusions can be drawn on the basis of the test result:

- The parametric studies which were carried out showed that even extreme assumptions have only minor influence on the bearing behavior in the 3D case. This stable behavior is a result of the dominant influence of the geometrical marginal conditions such as valley shape and type of dam, as well as the unchanged parameters such as water pressure, unit weights and shear resistance.
- The contact areas between the earth core and the valley flanks should be as rough as possible. This would mean that disadvantageous displacement along the valley flanks could largely be avoided and that the core would not be isolated in its behavior from these of flanking dam shells.
- To increase the level of stress in the lower half of the dam, the flanks should have as concave a shape as possible.

### 2.3.8. Analysis of Bouquet Canyon Dam

Ohmachi (1991) has developed a simplified method for the 3D dynamic analysis of elastic dams with homogeneous sections in which a prismatic finite element is used to discretize a dam in the longitudinal direction. The method can account for any dam configuration subjected to motions in the upstream-downstream direction. The Bouquet Canyon dam in US was investigated by this method to calculate the restraining effects of canyon wall. The dam is approximately 60 m high, 363 m long along the crest. Both the upstream and downstream surfaces have a slope of 3:1. The majority of the dam consists of a compacted fill of sandy clay.

Fig.2.26 shows a profile along the dam axis, together with the finite element model. Resonance curves at the station B are shown in Fig.2.27. The broken line shows the observation and others show computed results based on the assumption of three types of shear modulus distribution. Note that the observed resonance peak are in good agreement with the computed one resulting from the model whose shear modulus increase as  $2/3$  power of depth. Mode shapes along the crest are shown in Fig.2.28. The simulated results are in good agreement with the observed. The first and second numbers in the parentheses in the figure represent the node number along the vertical and horizontal axes, respectively. For instance, the mode (1,2) is the first mode along the depth, and the second mode along the crest length. Thus, many modes having a similar vertical mode shape exist within a narrow range of frequency. It concluded that variation of dynamic displacement resulting from the canyon restraint gives rise to shear strain. The strain may be

influential in earthquake stability of the impervious core of a dam built in a narrow canyon.

### **2.3.9. Analysis of Yeguas Dam**

Justo, et.al. (2000) observed the settlement of Yeguas dam in France for during and after construction with 3D finite element in FORTRAN language. Yeguas dam has a height of 87 m and a central earth core, the main cross section of the dam is shown in Fig.2.29 with five main zones.

The mesh of the dam was dividing by 10 zones of homogeneous material with hexahedron elements, shown in Fig.2.30. The result of calculation is shown in Fig.2.31 for end of construction. And for the reservoir filling, they used Nobari and Duncan (1972) principles to accommodate the algorithm in the model, laws for the decrease of the modulus with time have been established. The result of calculation was shown in Fig.2.32. It is note that the observed settlement are in good agreement with the computed one.

### **2.3.10. Analysis of Tahamara Dam**

Inoue, et.al.(2000) studied the mechanism of long term settlement of rockfill dam after reservoir filling with the Tahamara dam in Japan as a sample case. Tahamara dam is a zoned rockfill dam with a central earth core with height of 116 m and a crest length of 570 m, shown in Fig.2.33(a). The following five causes were assumed for post construction long term settlement of the dam:

1. Settlement due to consolidation during the period between completion of embankment and start of reservoir filling. In the

period between the completion and the start of reservoir filling, no additional loads are applied and only the dissipation of pore water pressure developed in the core during embankment construction continues.

2. Settlement due to secondary consolidation. Even after the dissipation of pore water pressure, long term secondary consolidation occurs under a constant embankment load.

3. Settlement due to reservoir loading. Reservoir load acts on the dam body after reservoir filling. They are applied on the upstream face of the core zone during initial filling.

4. Settlement due to infiltration during reservoir filling. Saturation of unsaturated soil generally leads to the loss of surface tension at contacts between soil particles due to water entry into pores and to the movement of soil particles due to decrease of shear resistance between particle contacts.

5. Settlement due to substantial drawdown of reservoir level. Each time reservoir level is lowered substantially, the settlement is increased. In other words, substantial drawdown of reservoir level causes unrecoverable settlement in an area in the core zone where the water level lowers.

Of the above five causes above, 1 through 3 were modeled by numerical analysis. For 4, infiltration settlement of the actual dam body was calculated based on the results of existing laboratory infiltration tests. For 5, quantification was carried out from the results of cyclic drained shear tests of core materials based on the mechanism assumed from analysis of measured behavior. Numerical analysis of causes 1 through 3 was made using plane strain finite element method. As a constitutive rule of embankment material, an elasto-viscoplastic model was

adopted. The model used for the analysis is shown in Fig.2.33(b); at each step of construction an additional element was incorporated. During reservoir filling, water pressure was applied to the upstream face of the core zone, as a distributed load.

Shown in Fig.2.34 are the results of calculation by elasto-viscoplastic coupled analysis of settlement in the core during the period between the completion of embankment and the start of reservoir filling and demonstrating fair agreement to the actual measurement. Fig.2.35 shows the result of calculation of the settlement due to secondary consolidation in the period between the start of reservoir filling and December 1995. Fig.2.36 shows a distribution of vertical displacement in the core when a distributed load equivalent to such water pressure was applied on the upstream of the core. Since reservoir loading acts mainly downstream, displacement of the core is predominantly in the horizontal direction. Fig.2.37 shows the results of settlement due to infiltration. Infiltration compression concentrated at high levels in the core zone. This was because the effect of post embankment consolidation is reduced by the decrease of the density due to compaction at this level and also with the reduction of loading. Fig.2.38 shows the result of settlement due to change in reservoir level. They are based only on the settlements obtained by analysis of several elements in the vicinity of a Crossarm. Since the volumetric strain was in proportional to the exponent of shear stress ratio, settlement concentrated at high levels in the core.

Fig.2.39 compares a combined total of differential settlement obtained for different causes from 1 to 5 and actual

measurement. As a result of calculation, differential compression was largest at top, medium and bottom levels in the core, agreeing to the actual measurement. Fig.2.40 provides a comparison between the measured settlement and analytical cumulative settlement, the combined total of differential settlement. The curve of distribution of cumulative settlement has several inflection points. It was suggested that the mechanism of long term settlement after the start of reservoir filling is not simple and that settlement is a product of complex combination of factors including material properties, construction condition and post construction loading condition. Fig.2.41 shows percentages of causes of crest level settlement. For the Tahamara dam, the causes are ranked in the descending order from dissipation of pore water pressure to secondary consolidation, infiltration settlement, drawdown of reservoir level and reservoir filling loading.

#### **2.4. SUMMARY**

The following summary can be drawn from the literature review described in this chapter:

1. For problem involving complex material properties and boundary conditions, the engineer resorts to numerical methods that provide approximate, but acceptable, solutions. Finite element method was one of the best tools in this area which is the approach shares many of features common to the previous numerical approximations and it possess certain characteristic that take advantage of the special facilities offered by the high speed computers.

2. The literatures show that finite element method could be used to evaluate the effect of incremental construction as compared with single step loading on the stresses and deformations developed in embankments. Seven stages of construction could be sufficient to analyse the incremental embankment construction. The horizontal displacement were seen to be quit similar in both cases but the vertical displacement in single lift was seen to be largest at the top while in seven lifts was seen at the mid height of the dam.
3. Non linear hyperbolic stress strain model by Kondner and developed later by Kulhawy, Duncan and Chang was widely used to be a constitutive model in analysing the stresses and deformations in dams.
4. The movements observed during reservoir filling were first in upstream direction and later in downstream direction. These complex movements may be understood as the combined effect of two counteracting effects of reservoir filling; (1) the water loads on the dam and (2) the softening and weakening of the fill material due to wetting.
5. 2D analysis provides an accurate representation of condition in centrally located transverse sections of long dams of uniform cross sections. However, 2D analysis may not provide a suitable representation of the transverse section for dam in steep valleys, because of cross valley stress transfer. Thus 3D analysis could be needed to evaluate stresses and deformation in steep valley.
6. In 3-D analysis, the effect of inclined core, the arching of the dam and the effect of material properties on the dam

situated in narrow valley could take into account to evaluate the dams' behaviour.

7. In reservoir filling study, the saturation of unsaturated soil generally leads to the loss of surface tension at contact between soil particles due to water entry into cores. The stiffer filter zones have resulted in significant interaction effects to distribute the stresses thus eliminate the zones of potential fracturing.



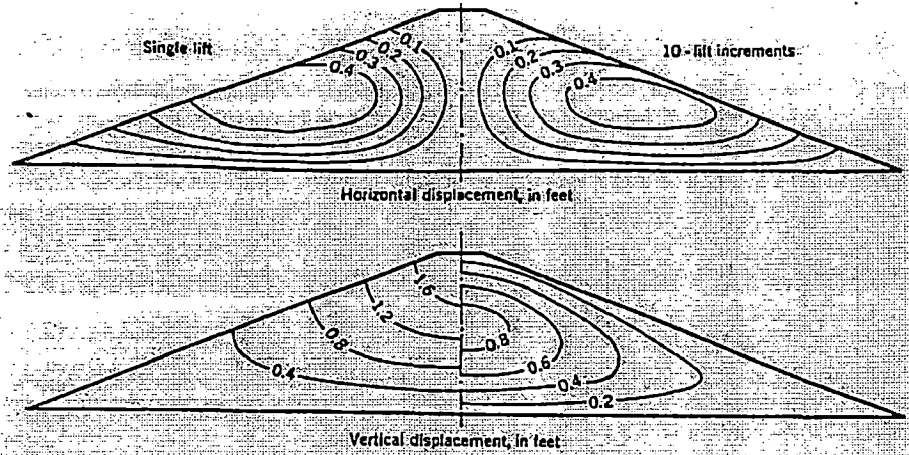


Fig.2.1. Displacement due to Dead Weight in Standard Dam

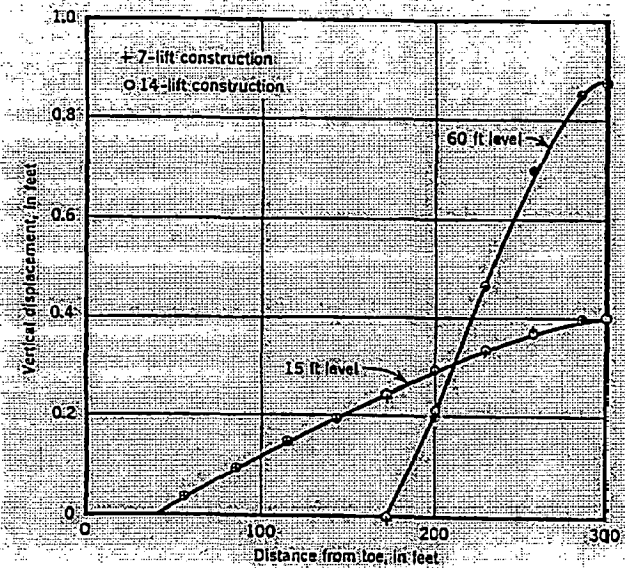
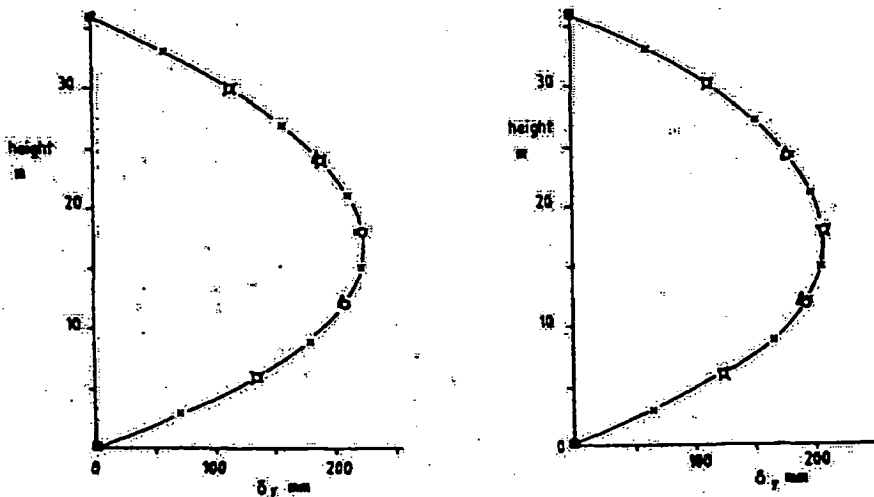


Fig.2.2. Displacements in Standard Dam: 7 & 14 Lift Construction



(a) Linear elastic ( $k=4$ )

(b) K-G model ( $k=3$ )

Legend  $\Delta$  3 layers  
 $\circ$  6 layers  
 $\times$  12 layers

Fig.2.3(a). Rigid Shoulder Study - Effect of Number of Layers on Settlement

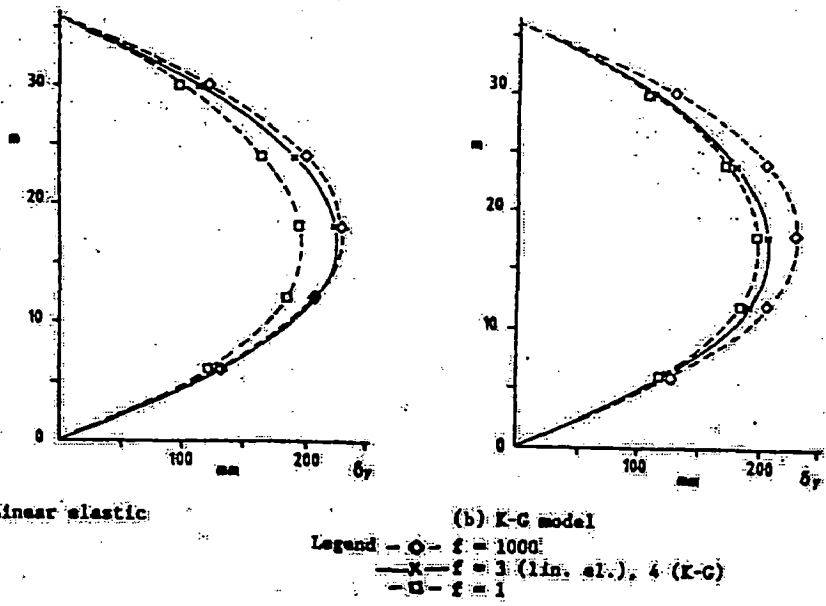


Fig.2.3(b). Rigid Shoulder Study - Effect of  $f$ , 6 Layers Analyses

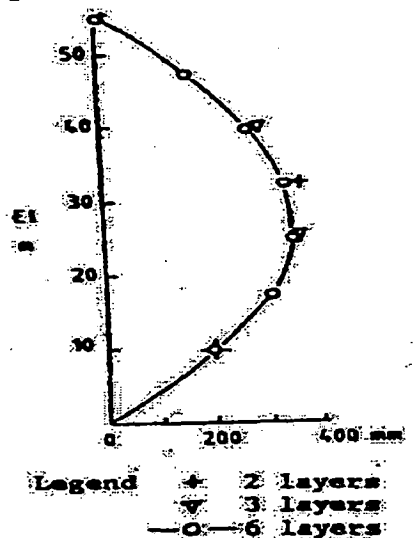


Fig.2.3(c). Settlement on Beliche dam Centre Line

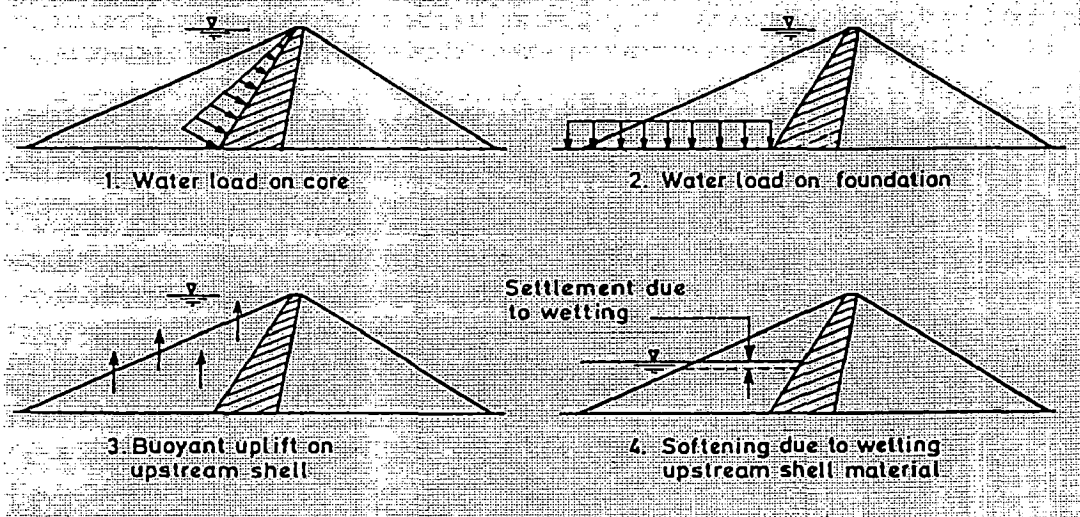
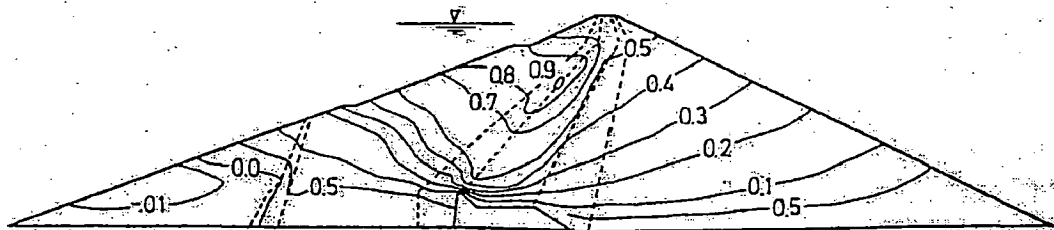
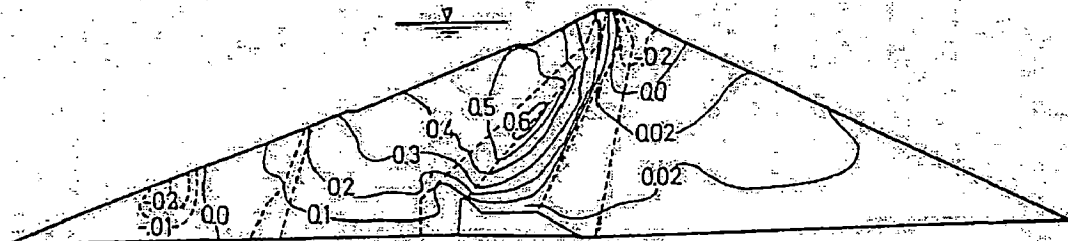


Fig.2.4. Effects of Reservoir Filling on a Zoned Dam



Displacement contours are in feet, downstream— is positive

Fig.2.5. Horizontal Displacement due to Reservoir Filling



Settlement contours are in feet, settlement is positive.

Fig.2.6. Vertical Displacement due to Reservoir Filling

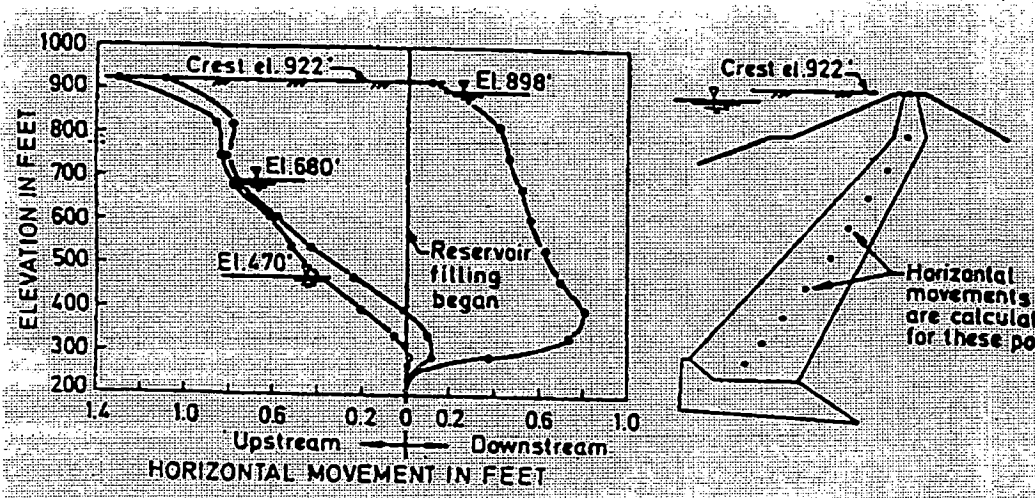


Fig.2.7. Calculated Horizontal Movements at 3 Stages of Reservoir Filling, Oroville dam

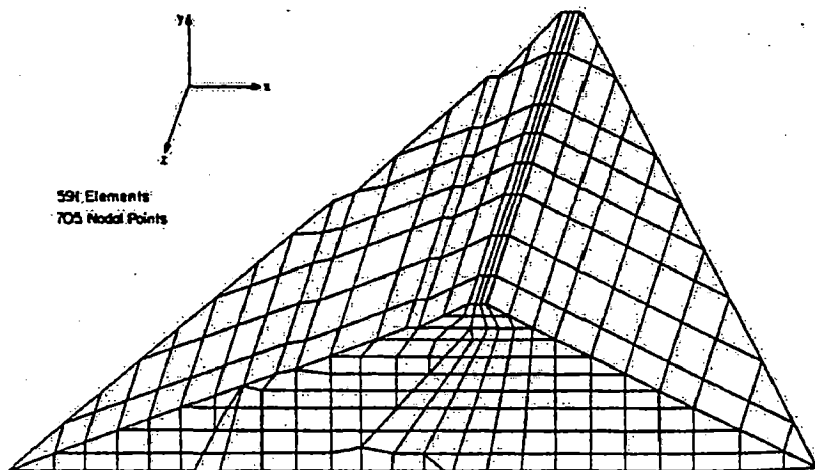


Fig.2.8. 3D FE Model of Oroville dam

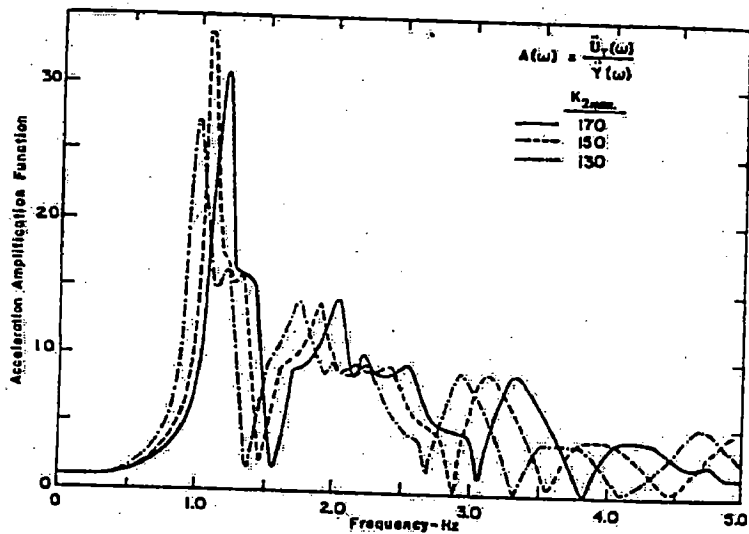


Fig.2.9. Computed Amplification Functions for Crest Midpoint of Oroville dam

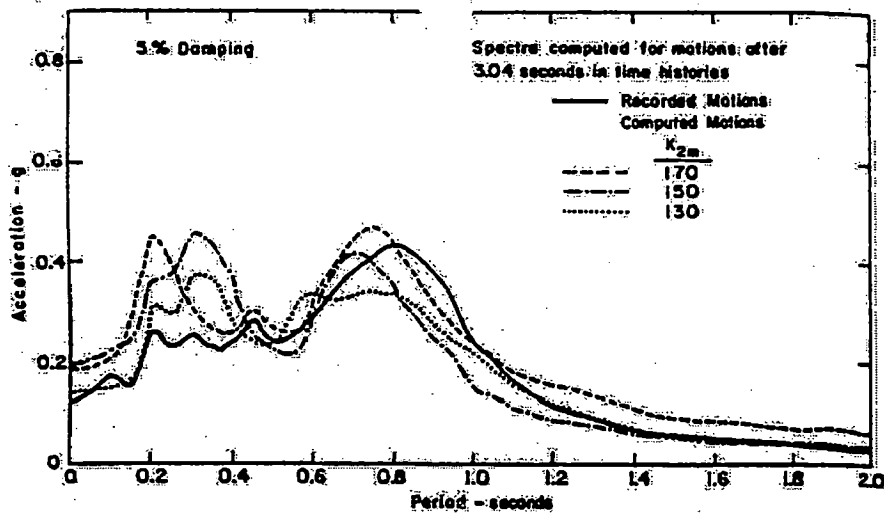


Fig.2.10. Acceleration Response Spectra for Motions at Crest Midpoint of Oroville dam

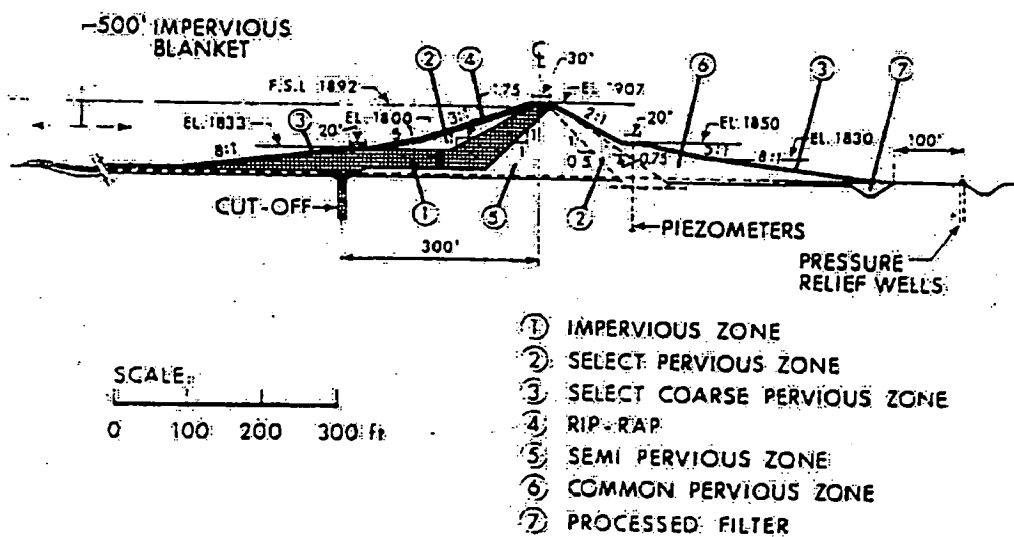


Fig.2.11(a) Typical Cross Section of Duncan dam

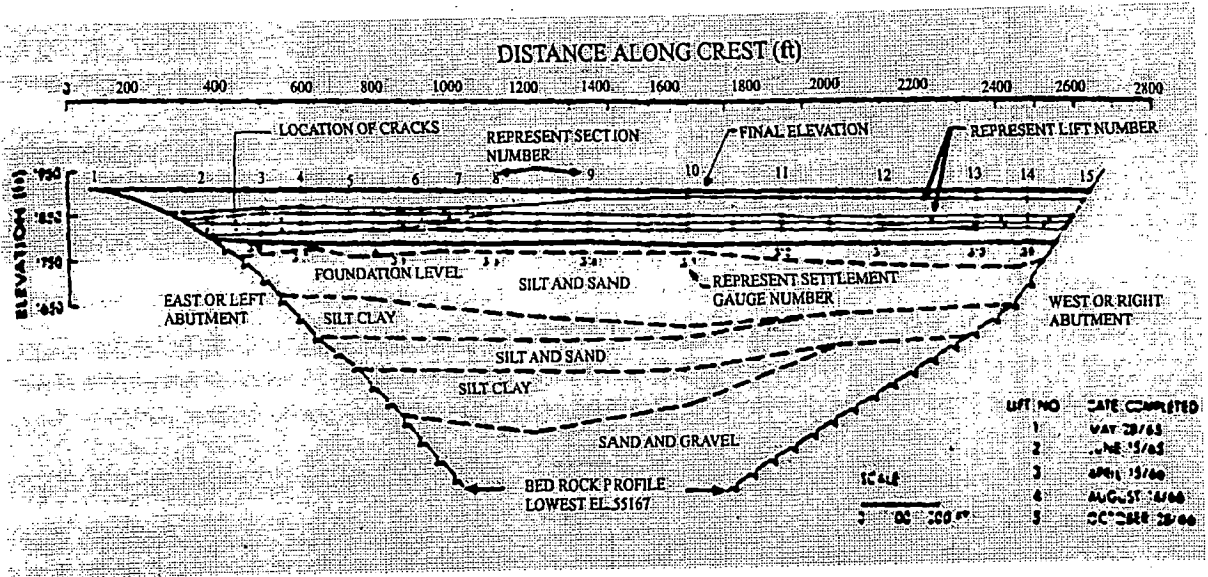


Fig.2.11(b) Longitudinal Section of Duncan dam and Foundation showing Construction Sequence and Location of Cracks

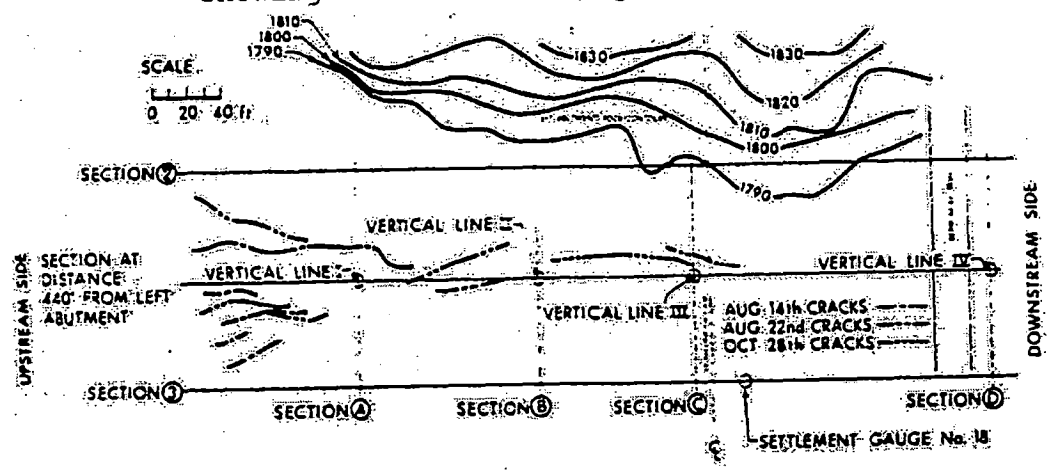


Fig.2.12. The Cracking Sequence

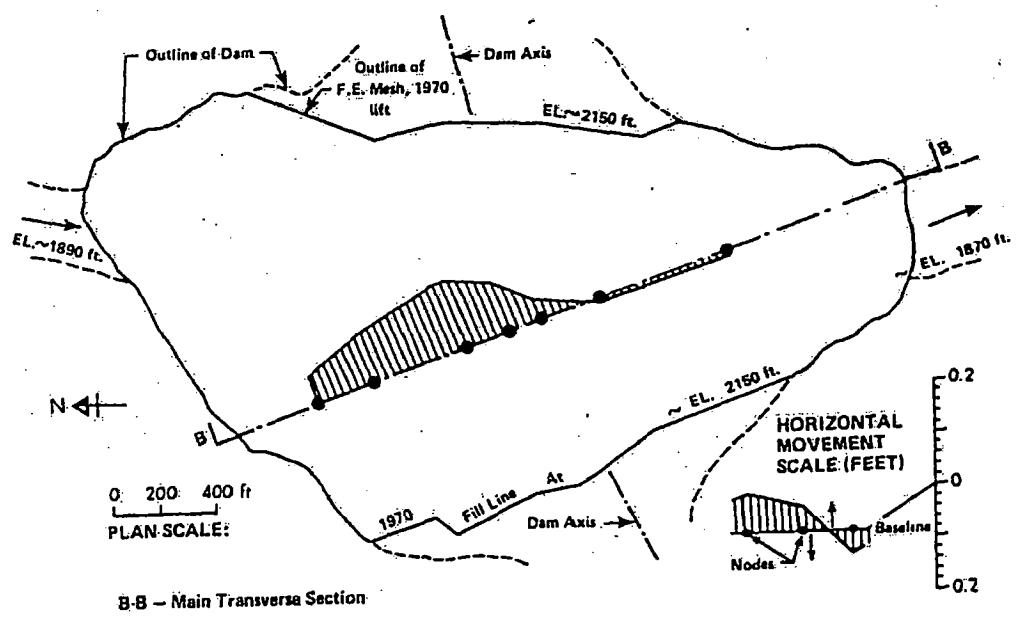


Fig.2.13. Horizontal Displacement along Main Transverse Section at Elev.2150 due to Further Fill Placement (Linear Analysis)

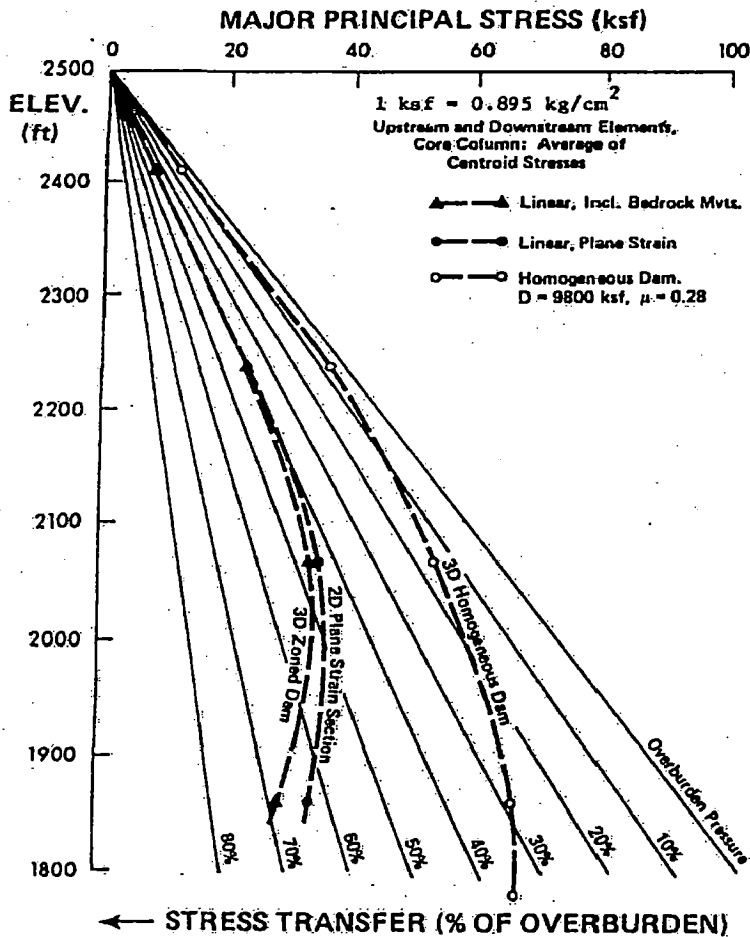


Fig.2.14. Major Principal Stresses along Vertical Column of Core

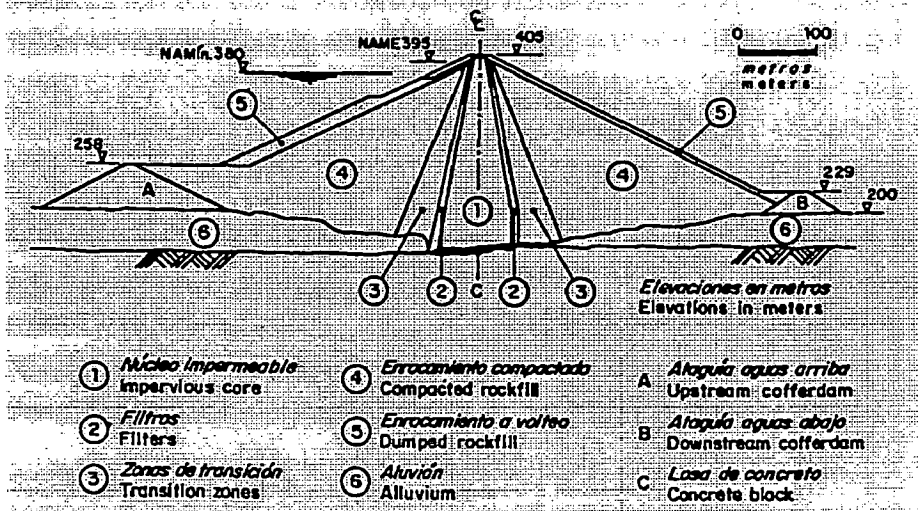


Fig.2.15. First Modification of Chicoasen dam, Vertical and Central Impervious Core

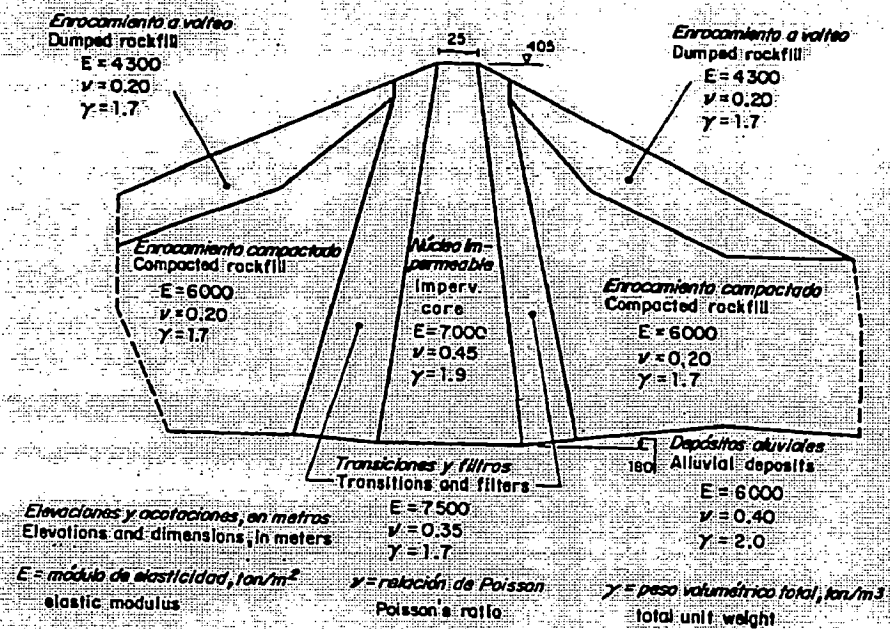


Fig.2.16. Zoning of Material and Mechanical Characteristic, 3-D analysis, Case 2

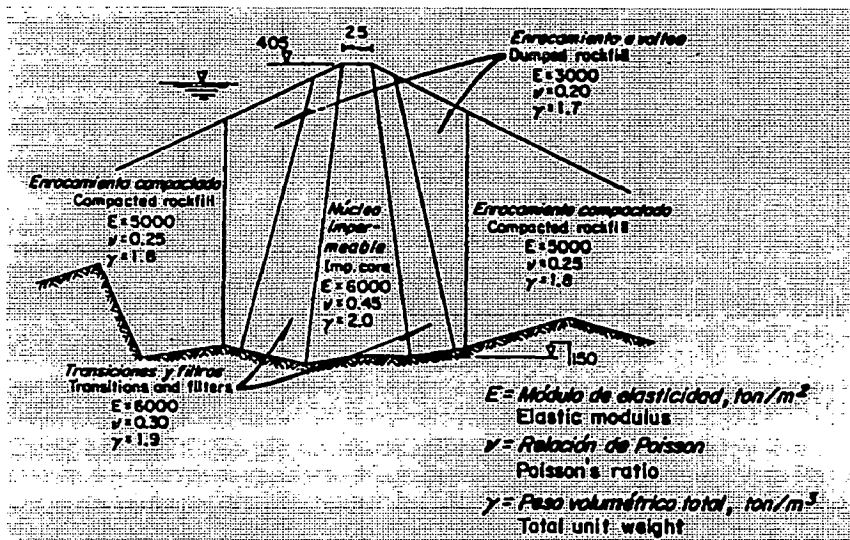
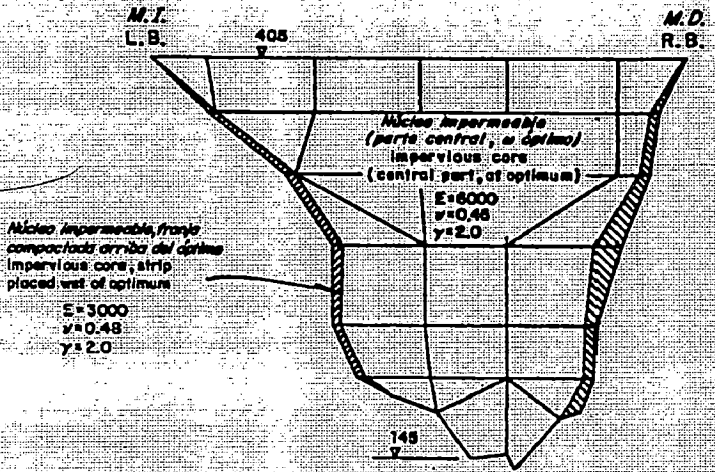


Fig.2.17(a) Longitudinal Max. Cross Section, Case 3



b) Sección transversal a lo largo del eje de la presa  
 Transverse cross-section along the dam axis

Fig.2.17(b) Transverse Cross Section along Dam Axis, Case 3

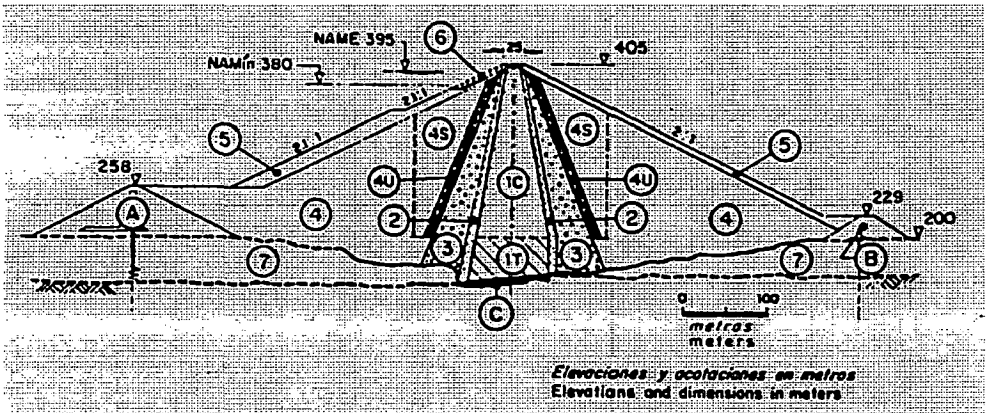


Fig.2.18. Modified Max. Cross Section of the Chicoasen dam

- A. Upstream cofferdam
- B. Downstream cofferdam
- C. Concrete block
- 1 Impervious Core
- 2 Filters
- 3 Transition Zones
- 4 Compacted Rockfill (well graded)
- 5 Dumped Rockfill
- 6 Selected Rockfill
- 7 Alluvium



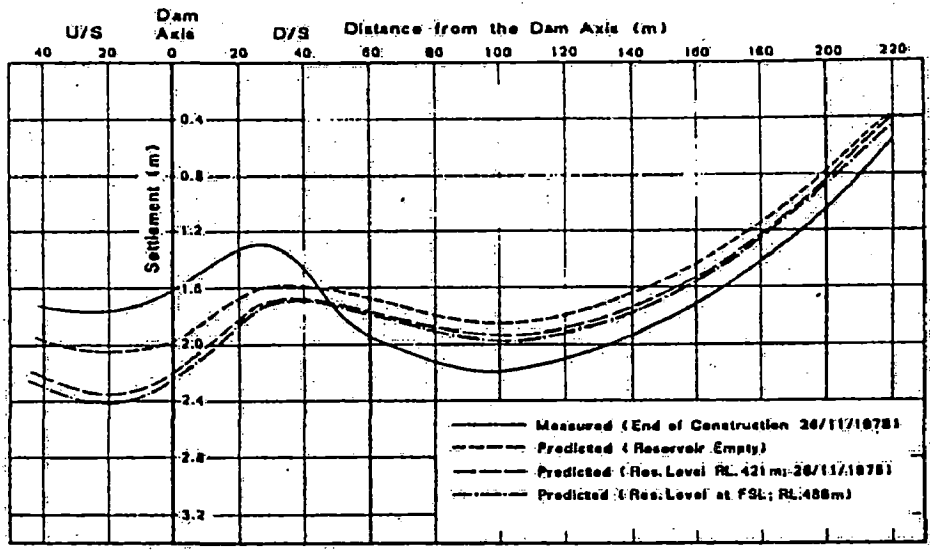


Fig.2.19(a) Settlement Profile at Elev.370

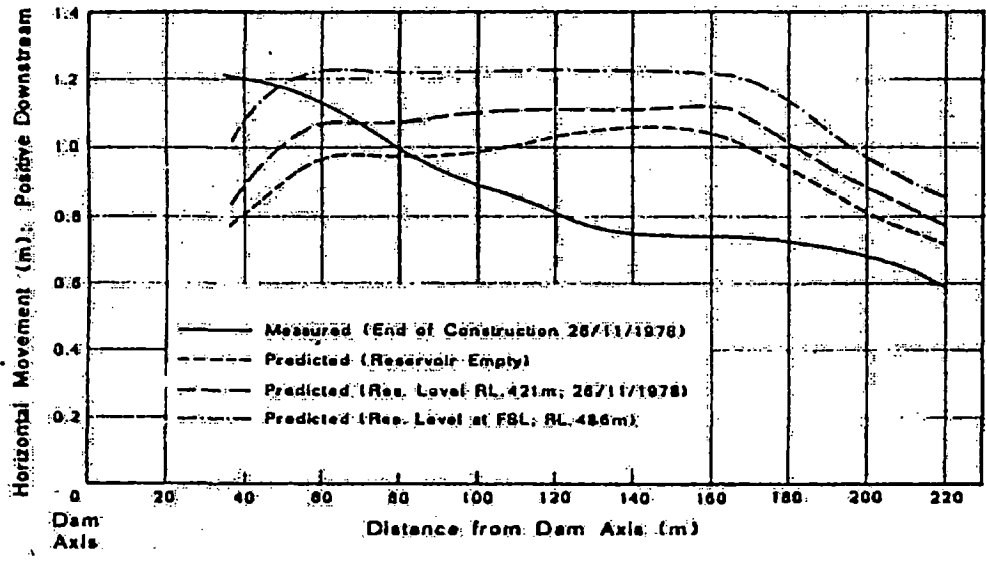


Fig.2.19(b) Horizontal Movement Profile at Elev.370

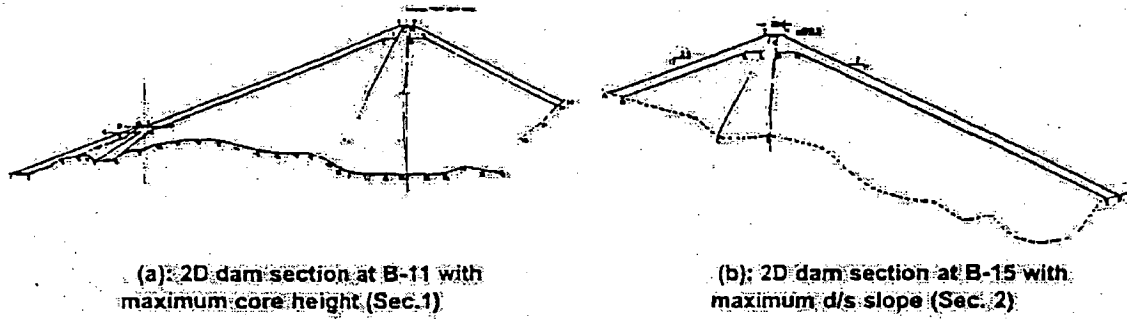


Fig.2.20. Cross Section of Tehri Dam

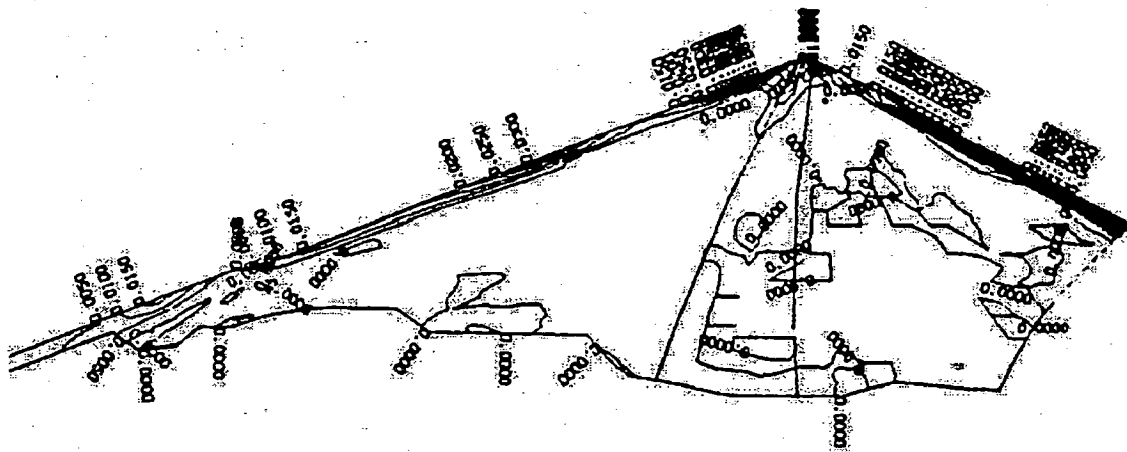


Fig.2.21. Contours of Plastic Strain at End of Earthquake for the Two Section

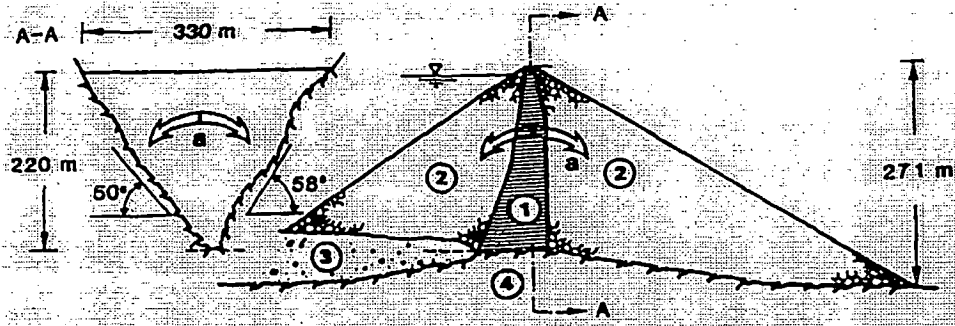


Fig.2.22. Dabaklamm Dam

- 1. Earth Core
- 2. Shell Zones
- 3. Overburden
- 4. Bedrock
- a. Arching effect

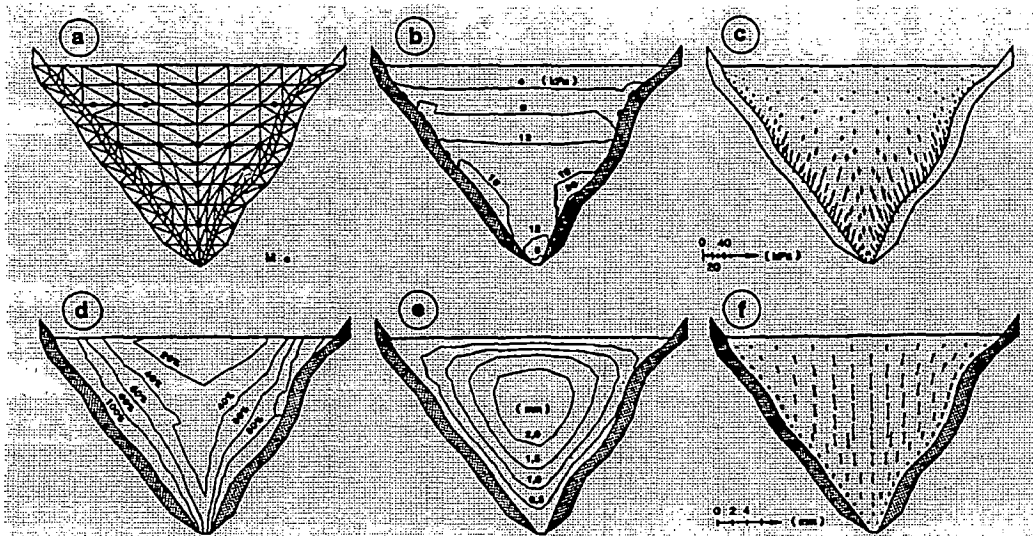


Fig.2.23. FEM Calculation of the Physical Model

- a. FEM net, 1000 points mstrmnt.
- b.  $\sigma_y$  Isolines
- c. Main Stress Axis
- d. Isolines of Material Utilization Factor
- e. Settlement Isolines
- f. Vectors of Deformation

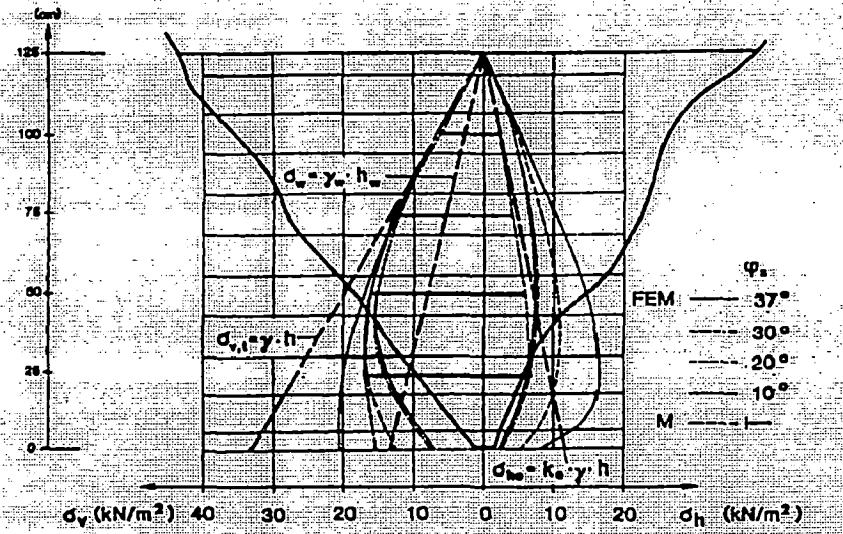


Fig.2.24(a). Comparison of Horizontal & Vertical Stress

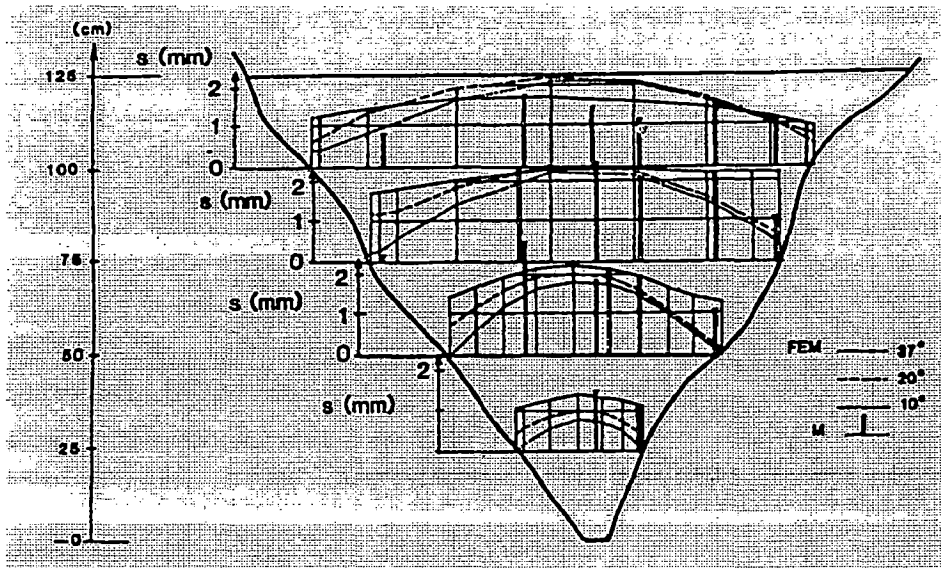


Fig.2.24(b). Comparison of Settlement

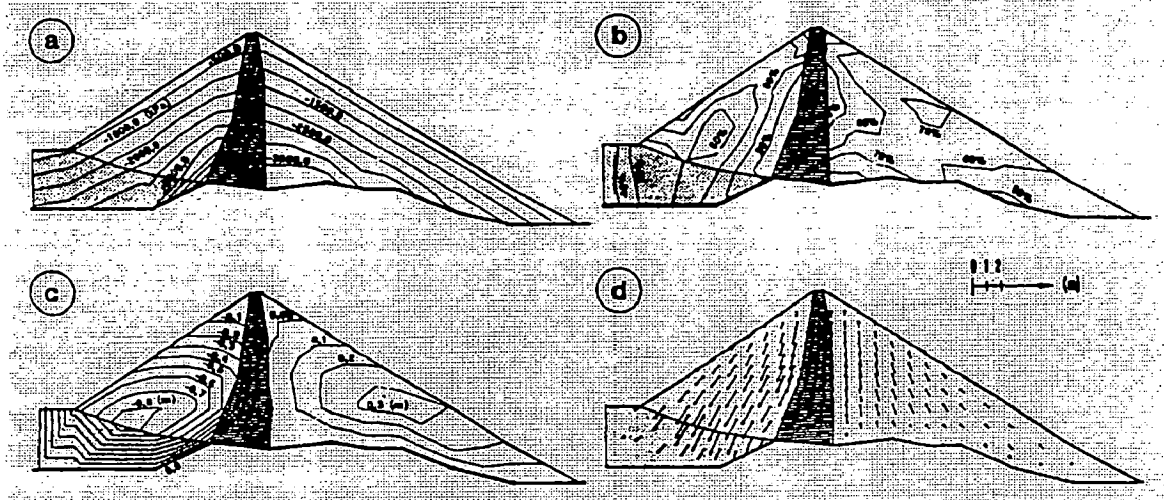


Fig. 2.25. Calculation of Dead Weight

- a.  $\sigma$  Isolines
- b. Material Utilization Fac. Isolines
- c. Horz. Displ. Isolines
- d. Vector of Deformation

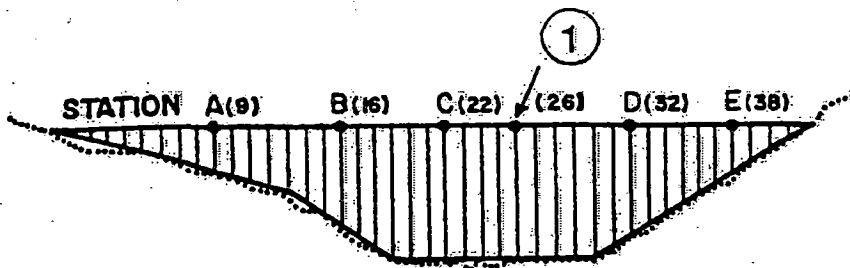


Fig. 2.26. FE Model of Bouquet Canyon Dam

1 - Shaking Machine

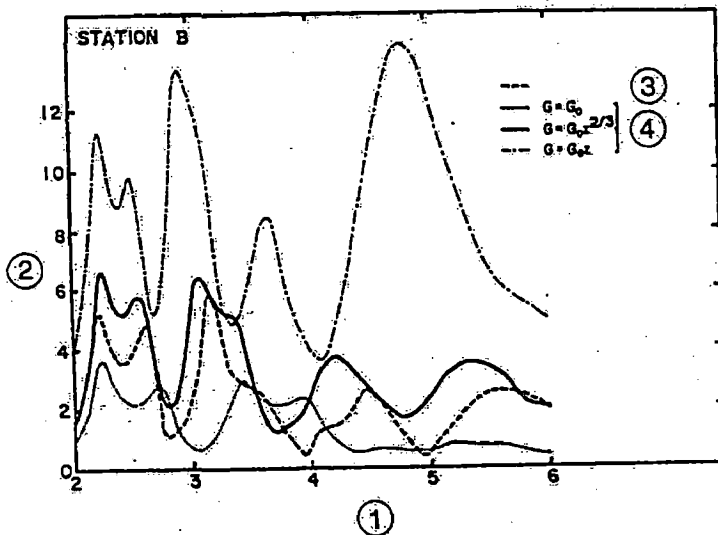
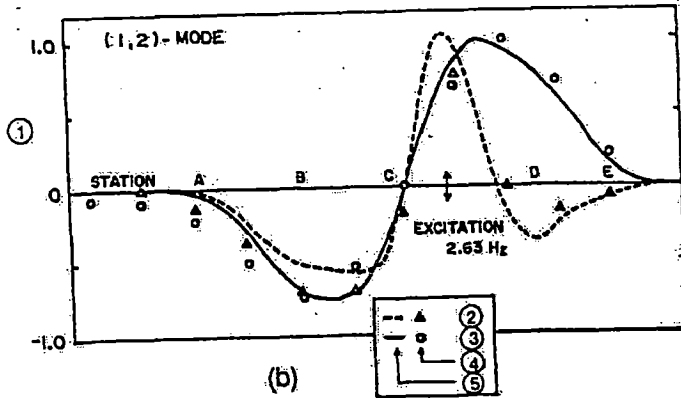
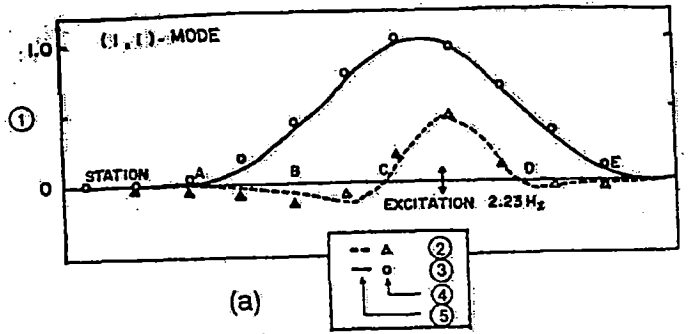


Fig. 2.27. Resonance Curves at Station B of Bouquet Canyon Dam

- 1 - Frequency (Hz)
- 2 - Displacement Amplitude
- 3 - Observed
- 4 - Computed



- ① Normalized Displacement
- ② In-phase with Excitation
- ③ At 90° Phase to Excitation
- ④ Observed
- ⑤ Computed

- ① Déplacement normalisé
- ② En phase avec l'excitation
- ③ Décalé de 90° par rapport à l'excitation
- ④ Observée
- ⑤ Calculée

Fig.2.28. Vibration Shapes along the Crest of Bouquet Canyon Dam

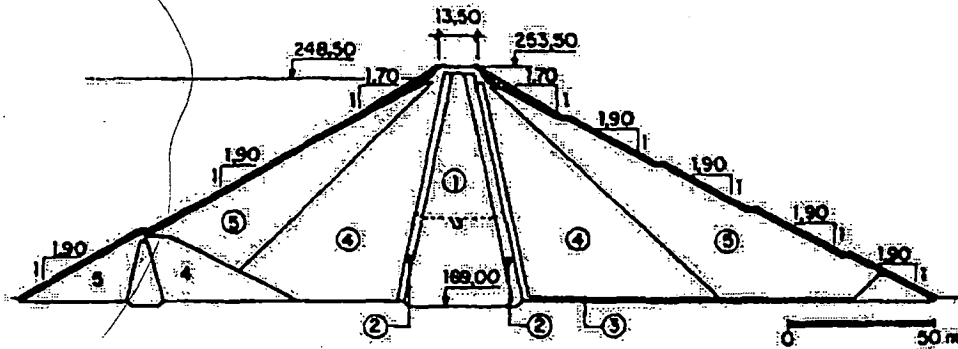


Fig.2.29. Main Cross Section of Yeguas Dam

- 1 - Clay Core
- 2 - Filter
- 3 - Drain
- 4 - Conglomerate Transition
- 5 - Slate Rockfill

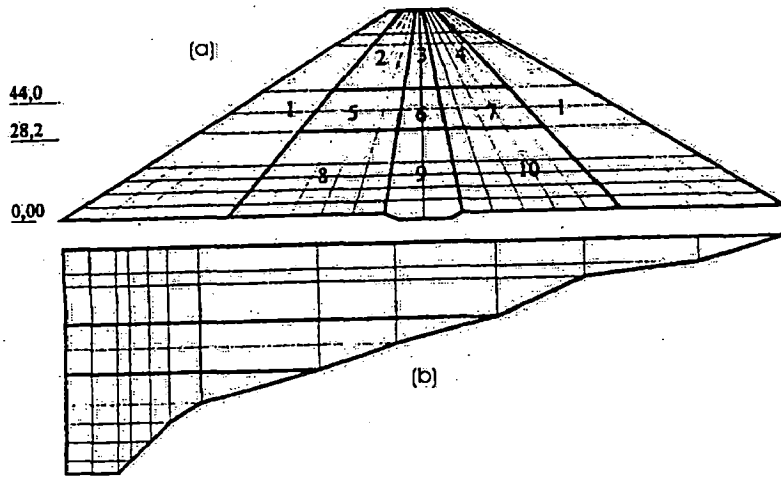


Fig.2.30. FE Mesh

- (a) Cross Section Showing the 10 Zones of Homogeneous Properties  
 (b) Left half Section

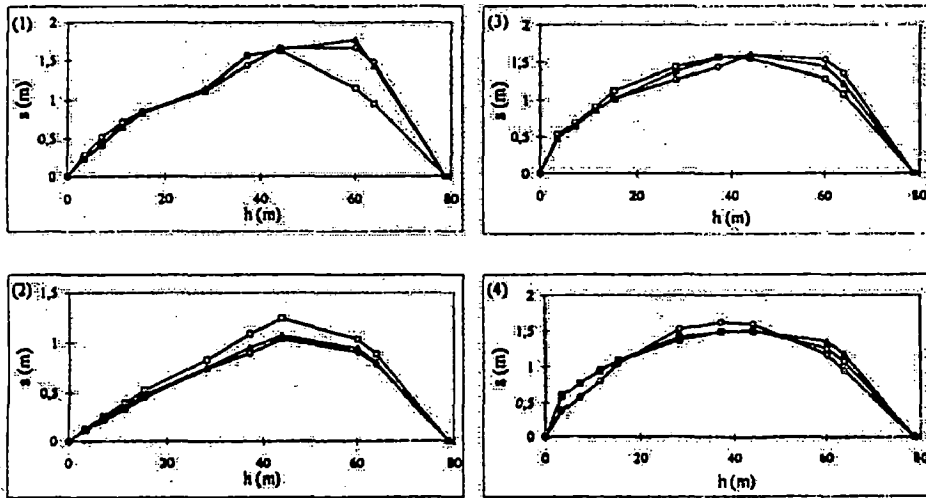


Fig.2.31. Comparison of Settlement at End of Construction

- 1 - Upstream Transition                      □ - Computation  
 2 - Downstream Transition                  ∇ - Measured  
 3 - Upstream Core  
 4 - Downstream Core

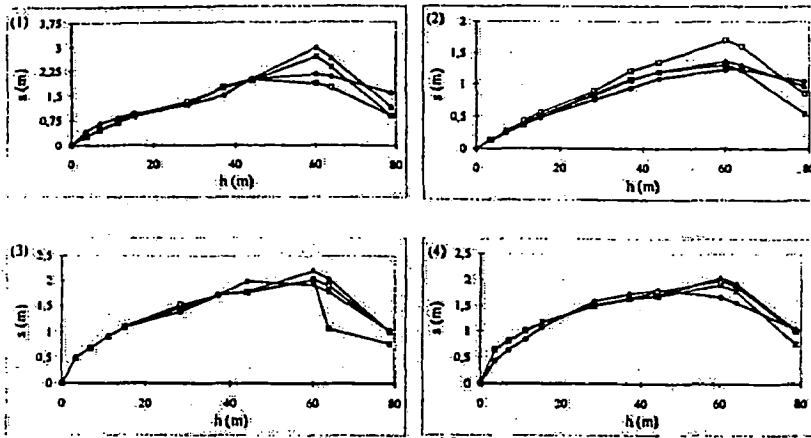


Fig.2.32. Comparison Settlement at 136 days after End of Constr.

- |                           |                 |
|---------------------------|-----------------|
| 1 - Upstream Transition   | □ - Computation |
| 2 - Downstream Transition | ▽ - Measured    |
| 3 - Upstream Core         |                 |
| 4 - Downstream Core       |                 |

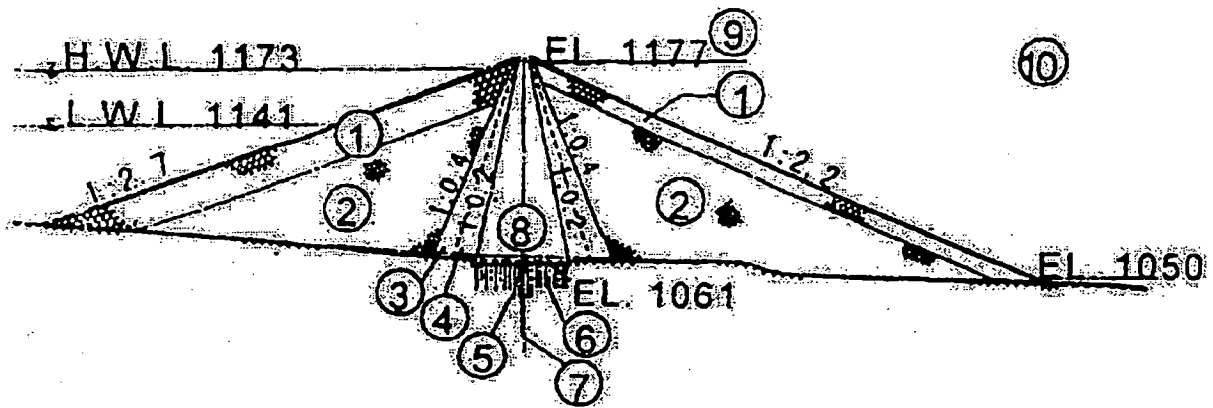


Fig.2.33(a). Typical Cross Section of Tahamara Dam

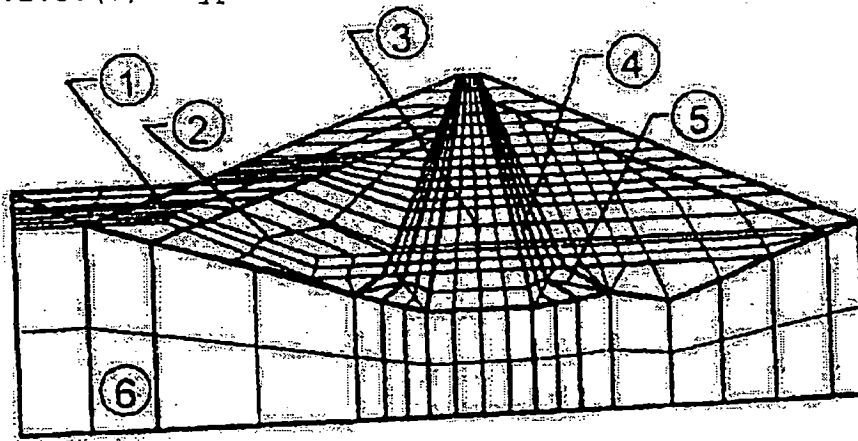


Fig.2.33(b). Dam Body Model Used for Analysis

- |                 |                     |
|-----------------|---------------------|
| 1 - Outer Shell | 4 - Fine Filter     |
| 2 - Inner Shell | 5 - Coarse Filter   |
| 3 - Core        | 6 - Foundation Rock |



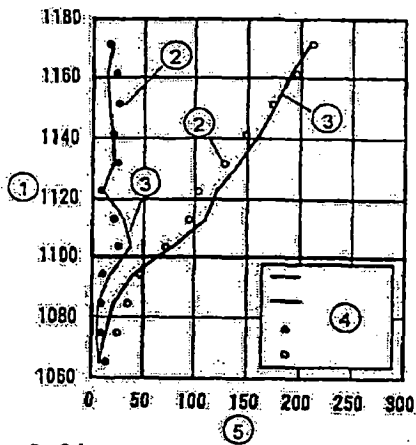


Fig. 2.34.

Distributions of differential compression and cumulative settlement due to consolidation from completion of embankment to start of reservoir filling

- |   |  |
|---|--|
| 1 Elevation (m)   | 1 Cote (m)   |
| 2 Actual measurement                                    | 2 Valeur mesurée                                     |
| 3 Calculated value                                      | 3 Valeur calculée                                    |
| 4 — Differential compression (calculated value)         | 4 — Compression différentielle (valeur calculée)     |
| — Cumulative settlement (calculated value)              | — Tassement cumulé (valeur calculée)                 |
| • Differential compression (actual measurement)         | • Compression différentielle (valeur mesurée)        |
| ○ Cumulative settlement (actual measurement)            | ○ Tassement cumulé (valeur mesurée)                  |
| 5 Differential compression / Cumulative settlement (mm) | 5 Compression différentielle / Tassement cumulé (mm) |

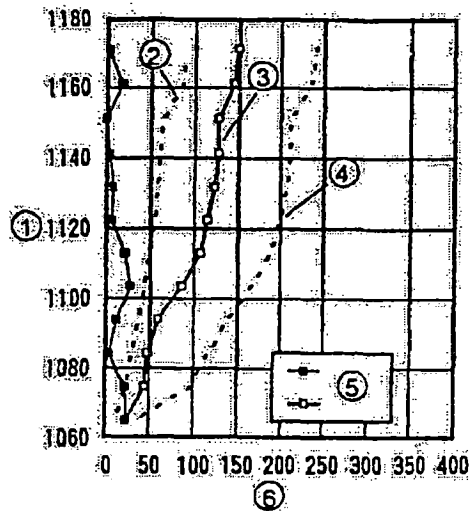
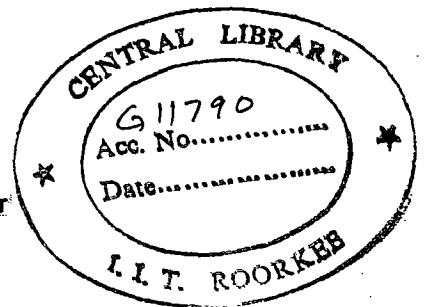


Fig. 2.35.

Calculation of settlement due to secondary consolidation from start of reservoir filling to December 1995

- |   |  |
|---|--|
| 1 Elevation (m)   | 1 Cote (m)   |
| 2 Lower limit   | 2 Limite inférieure                                  |
| 3 Mean value  | 3 Valeur moyenne                                     |
| 4 Upper limit   | 4 Limite supérieure                                  |
| 5 — Differential compression                            | 5 — Compression différentielle                       |
| ○ Cumulative settlement                                 | ○ Tassement cumulé                                   |
| 6 Differential compression / Cumulative settlement (mm) | 6 Compression différentielle / Tassement cumulé (mm) |



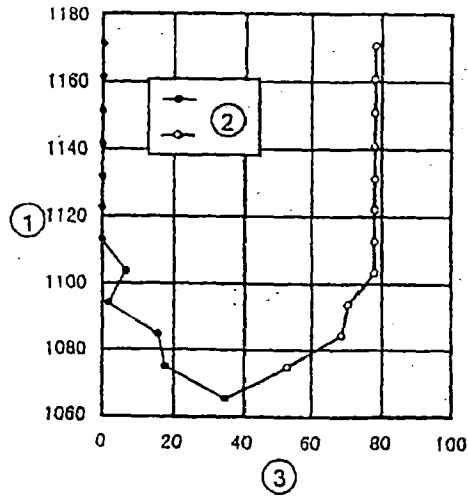


Fig. 2.36.

Calculation of settlement due to reservoir loading

- |   |  |   |   |
|---|--|---|---|
| 1 | Elevation (m)  | 1 | Cote (m)  |
| 2 | —●— Differential compression                             | 2 | —●— Compression différentielle                        |
|   | —○— Cumulative settlement                                |   | —○— Tassement cumulé                                  |
| 3 | Differential compression /<br>Cumulative settlement (mm) | 3 | Compression différentielle /<br>Tassement cumulé (mm) |

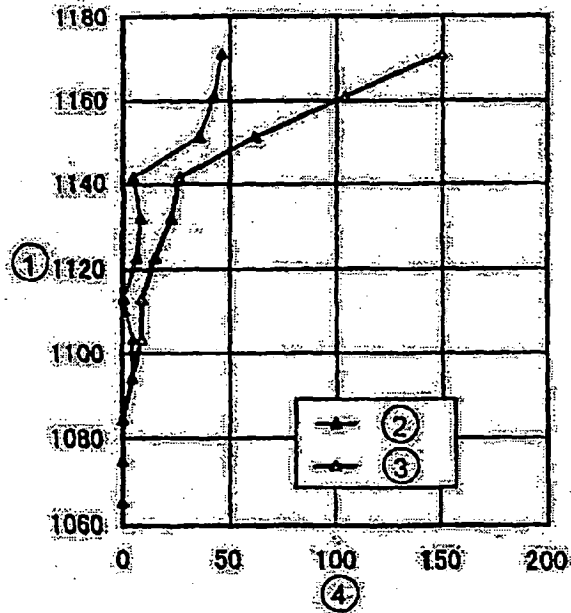


Fig. 2.37.

Calculation of settlement due to infiltration

- |   |  |   |   |
|---|--|---|---|
| 1 | Elevation (m)  | 1 | Cote (m)  |
| 2 | Differential compression                                 | 2 | Compression différentielle                            |
| 3 | Cumulative settlement                                    | 3 | Tassement cumulé                                      |
| 4 | Differential compression /<br>Cumulative settlement (mm) | 4 | Compression différentielle /<br>Tassement cumulé (mm) |

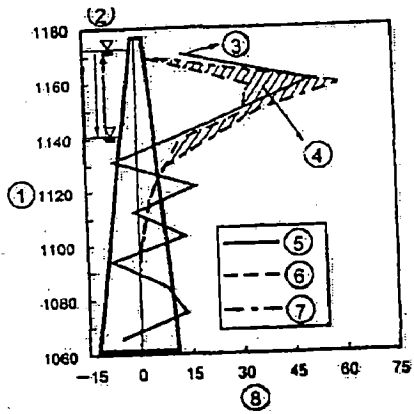


Fig.2.38. Results of calculation of settlement due to change in reservoir filling

- 1 - Elevation (m)
- 2 - Cumulative drawdown in 1<sup>st</sup> to 10<sup>th</sup> phases
- 3 - Actual measurement
- 4 - Range of calculated value
- 5 - Incremental compression due to reservoir level drawdown
- 6 - Minimum calculated value
- 7 - Maximum calculated value
- 8 - Incremental diff. compression

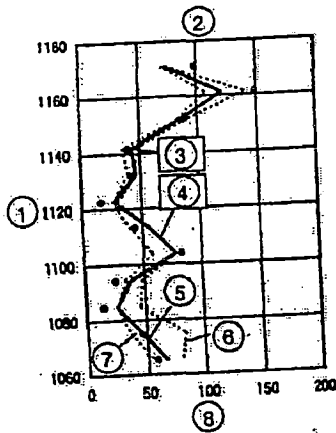


Fig.2.39. Comparison between calculated and measured differential settlement

- 1 - Elevation (m)
- 2 - From Oct, 1981 to Dec, 1995
- 3 - Measurement
- 4 - Calculation
- 5 - Mean value
- 6 - Upper limit
- 7 - Lower limit
- 8 - Differential compression (mm)

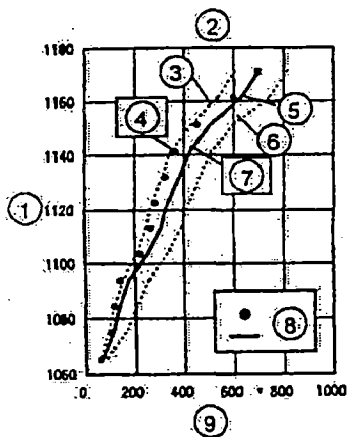


Fig.2.40. Comparison between calculated and measured cumulative settlement

- 1 - Elevation (m)
- 2 - From Oct, 1981 to Dec, 1995
- 3 - Lower limit
- 4 - Measurement
- 5 - Mean value
- 6 - Upper limit
- 7 - Calculation
- 8 - Cumulative settlement:  $\bullet$  actual measurement,  $\square$  calculated value
- 9 - Cumulative settlement (mm)

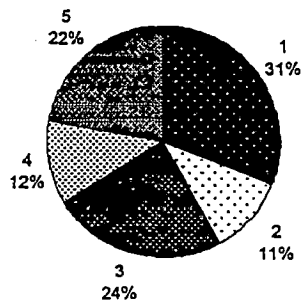


Fig.2.41. Percentage of causes of crest level settlement

- 1 - Consolidation settlement
- 2 - Reservoir Loading
- 3 - Secondary consolidation
- 4 - Drawdown of reservoir level
- 5 - Infiltration settlement

## CHAPTER 3

### METHOD OF ANALYSIS

The finite element method was introduced to the geotechnical engineering when Clough and Woodward (1967) demonstrated its usefulness for analysis of stresses and movements in earth dams. Geotechnical engineers had long been aware of the limited usefulness of linear elastic analysis of soil and rock masses, and it was immediately apparent that the ability to analyse nonlinear behaviour gave the finite element method great potential for use in geotechnical engineering problems. The method has other unique capabilities as well; these include the fact that it can be used for problem involving nonhomogeneous materials, complex boundary conditions, sequential loading and so on.

#### 3.1. DESCRIPTION OF THE METHOD

The analysis of the structures by the finite element method is an idealization of an actual elastic continuum as an assemblage of discrete element interconnected at their nodal points (Singh, 1991).

The various steps followed in a finite element analysis are:

- (i) Subdivision of the continuum into finite element of suitable configuration
- (ii) Evaluation of element properties
- (iii) Assembly of element properties to obtain the global stiffness matrix and load vector

- (iv) Solution of resulting linear simultaneous equation for the primary unknowns after introducing the boundary conditions
- (v) Determination of secondary unknown quantities such as stresses and strain

### 3.1.1. Displacement Function

An 8 noded isoparametric finite element is shown in Fig.3.1. For a typical finite element 'e', defined by nodes i, j, m etc, the displacement {f} within the element are expressed as:

$$\{f\} = [N] \{\delta\}^e \quad \dots\dots(3.1)$$

where  $[N] = [N_i \ N_j \ N_m \ \dots \ ]$

and  $\{\delta\}^e = \{\delta_i \ \delta_j \ \delta_m \ \dots \ \delta_n\}^T \quad \dots\dots(3.2)$

The components of [N] are in general functions of position and {δ}<sup>e</sup> represents a listing of nodal displacements for a particular element.

For the three dimensional element

$$\{f\} = \begin{Bmatrix} u \\ v \\ w \end{Bmatrix} \quad \dots\dots(3.3)$$

represent the displacement in x, y and z directions at a point within the element and

$$\{\delta_i\} = \begin{Bmatrix} u_i \\ v_i \\ w_i \end{Bmatrix} \quad \dots\dots(3.4)$$

are the corresponding displacements of node i.

[N<sub>i</sub>] is equal to [IN<sub>i</sub>'] where Ni' is the shape function of node i and I is an identity matrix.

### 3.1.2. Shape Functions

The shape functions for an 8 noded isoparametric hexahedral element used in this study are given by the following.

At corner nodes (nodes nos. 1,2,3,4,5,6,7,8)

$$N_i = \frac{1}{8} (1 + \xi_0)(1 + \eta_0)(1 + \zeta_0) \quad \dots\dots (3.5)$$

$$\xi_i = \pm 1, \eta_i = \pm 1, \zeta_i = \pm 1$$

$$\text{where } \left. \begin{array}{l} \xi_0 = \xi \xi_i \\ \eta_0 = \eta \eta_i \\ \zeta_0 = \zeta \zeta_i \end{array} \right\} \quad \dots\dots (3.6)$$

$\xi_i, \eta_i, \zeta_i$  are the local coordinates of the  $i^{\text{th}}$  node and  $\xi, \eta, \zeta$  are the local coordinates of the point concerned.

### 3.1.3. Strains

With displacement known at all points within the element, the strains at any point can be determined. Six strain components are relevant in three dimensional analyses and the strain vector can be expressed as:

$$\{\epsilon\} = \begin{Bmatrix} \epsilon_x \\ \epsilon_y \\ \epsilon_z \\ \gamma_{xy} \\ \gamma_{yz} \\ \gamma_{zx} \end{Bmatrix} = \begin{Bmatrix} \frac{\partial u}{\partial x} \\ \frac{\partial v}{\partial y} \\ \frac{\partial w}{\partial z} \\ \frac{\partial u}{\partial y} + \frac{\partial v}{\partial x} \\ \frac{\partial v}{\partial z} + \frac{\partial w}{\partial y} \\ \frac{\partial w}{\partial x} + \frac{\partial u}{\partial z} \end{Bmatrix} \quad \dots\dots (3.7)$$

this can be further written as:

$$\{\epsilon\} = [B]\{\delta\}^e = [B_1 \ B_2 \ B_m \ \dots]\{\delta\}^e \quad \dots\dots (3.8)$$

in which [B] is the strain displacement matrix.

$[B_i]$  is given by

$$[B_i] = \begin{bmatrix} \frac{\partial N_i}{\partial x} & 0 & 0 \\ 0 & \frac{\partial N_i}{\partial y} & 0 \\ 0 & 0 & \frac{\partial N_i}{\partial z} \\ \frac{\partial N_i}{\partial y} & \frac{\partial N_i}{\partial x} & 0 \\ 0 & \frac{\partial N_i}{\partial z} & \frac{\partial N_i}{\partial y} \\ \frac{\partial N_i}{\partial z} & 0 & \frac{\partial N_i}{\partial x} \end{bmatrix} \quad \dots (3.9)$$

with other sub matrices obtained in a similar manner simply by interchanges of subscripts.

For isoparametric elements

$$\left. \begin{aligned} x &= \sum N_i x_i, & y &= \sum N_i y_i, & z &= \sum N_i z_i \\ u &= \sum N_i u_i, & v &= \sum N_i v_i, & w &= \sum N_i w_i \end{aligned} \right\} \quad \dots (3.10)$$

the summation being over total number of nodes in an element.

Because the displacement model is formulated in terms of the natural coordinates  $\xi, \eta$  and  $\zeta$ , it is necessary to relate Eq.(3.9) to the derivatives with respect to these local coordinates.

The natural coordinates  $\xi, \eta$  and  $\zeta$  are functions of global coordinates  $x, y, z$ . Using the chain rule of partial differentiation, we can write:

$$\frac{\partial N_i}{\partial \xi} = \frac{\partial N_i}{\partial x} \frac{\partial x}{\partial \xi} + \frac{\partial N_i}{\partial y} \frac{\partial y}{\partial \xi} + \frac{\partial N_i}{\partial z} \frac{\partial z}{\partial \xi} \quad \dots (3.11)$$

Performing the same differentiation with respect to the other two coordinates and writing in matrix form



$$\begin{Bmatrix} \frac{\partial N'_i}{\partial \xi} \\ \frac{\partial N'_i}{\partial \eta} \\ \frac{\partial N'_i}{\partial \zeta} \end{Bmatrix} = [J] \begin{Bmatrix} \frac{\partial N'_i}{\partial x} \\ \frac{\partial N'_i}{\partial y} \\ \frac{\partial N'_i}{\partial z} \end{Bmatrix} \quad \dots\dots (3.12)$$

where [J] is given by

$$[J] = \begin{bmatrix} \frac{\partial x}{\partial \xi} & \frac{\partial y}{\partial \xi} & \frac{\partial z}{\partial \xi} \\ \frac{\partial x}{\partial \eta} & \frac{\partial y}{\partial \eta} & \frac{\partial z}{\partial \eta} \\ \frac{\partial x}{\partial \zeta} & \frac{\partial y}{\partial \zeta} & \frac{\partial z}{\partial \zeta} \end{bmatrix} \quad \dots\dots (3.13)$$

The matrix [J] is called the Jacobian matrix. The global derivatives can be found by inverting [J] as follows:

$$\begin{Bmatrix} \frac{\partial}{\partial x} \\ \frac{\partial}{\partial y} \\ \frac{\partial}{\partial z} \end{Bmatrix} = [J]^{-1} \begin{Bmatrix} \frac{\partial}{\partial \xi} \\ \frac{\partial}{\partial \eta} \\ \frac{\partial}{\partial \zeta} \end{Bmatrix} \quad \dots\dots (3.14)$$

Substituting Eq.(3.10) into Eq.(3.13), the Jacobian is given by

$$[J] = \begin{bmatrix} \sum x_i \frac{\partial N'_i}{\partial \xi} & \sum y_i \frac{\partial N'_i}{\partial \xi} & \sum z_i \frac{\partial N'_i}{\partial \xi} \\ \sum x_i \frac{\partial N'_i}{\partial \eta} & \sum y_i \frac{\partial N'_i}{\partial \eta} & \sum z_i \frac{\partial N'_i}{\partial \eta} \\ \sum x_i \frac{\partial N'_i}{\partial \zeta} & \sum y_i \frac{\partial N'_i}{\partial \zeta} & \sum z_i \frac{\partial N'_i}{\partial \zeta} \end{bmatrix} \quad \dots\dots (3.15a)$$

$$\text{or } [J] = \begin{bmatrix} \frac{\partial N'_1}{\partial \xi} & \frac{\partial N'_2}{\partial \xi} & \frac{\partial N'_3}{\partial \xi} & \dots & \frac{\partial N'_n}{\partial \xi} \\ \frac{\partial N'_1}{\partial \eta} & \frac{\partial N'_2}{\partial \eta} & \frac{\partial N'_3}{\partial \eta} & \dots & \frac{\partial N'_n}{\partial \eta} \\ \frac{\partial N'_1}{\partial \zeta} & \frac{\partial N'_2}{\partial \zeta} & \frac{\partial N'_3}{\partial \zeta} & \dots & \frac{\partial N'_n}{\partial \zeta} \end{bmatrix} \begin{bmatrix} x_1 & y_1 & z_1 \\ x_2 & y_2 & z_2 \\ x_3 & y_3 & z_3 \\ \vdots & \vdots & \vdots \\ x_n & y_n & z_n \end{bmatrix} \quad \dots\dots (3.15b)$$

### 3.1.4. Stresses

The stresses are related to the strains as:

$$\{\sigma\} = [D](\{\varepsilon\} - \{\varepsilon_0\}) + \{\sigma_0\} \quad \dots\dots(3.16)$$

where [D] is an elasticity matrix containing the appropriate material properties,  $\{\varepsilon_0\}$  is the initial strain vector,  $\{\sigma\}$  is the stress vector  $\{\sigma_x, \sigma_y, \sigma_z, \tau_{xy}, \tau_{yz}, \sigma_{xz}\}^T$  and  $\{\sigma_0\}$  is the initial stress vector.

For an elastic, isotropic material the elasticity matrix is given by:

$$[D] = \frac{E}{(1+\nu)(1-2\nu)} \begin{bmatrix} 1-\nu & \nu & \nu & 0 & 0 & 0 \\ & 1-\nu & \nu & 0 & 0 & 0 \\ & & 1-\nu & 0 & 0 & 0 \\ & & & \frac{(1-2\nu)}{2} & 0 & 0 \\ \text{Symetric} & & & & \frac{(1-2\nu)}{2} & 0 \\ & & & & & \frac{(1-2\nu)}{2} \end{bmatrix} \quad (3.17)$$

where E is the Young's modulus of elasticity and  $\nu$  the Poisson's ratio of the material of the element.

### 3.1.5. Stiffness Matrix

The stiffness matrix of the element is given by the following relation

$$\{F\}^e = [K]^e \{\delta\}^e \quad \dots\dots(3.18)$$

where  $\{F\}^e$  is the element nodal load vector and  $[K]^e$ , the element stiffness matrix given by:

$$[K]^e = \int_V [B]^T [D] [B] dV \quad \dots\dots(3.19)$$

where V refers to the volume of the element.

The equivalent nodal forces are obtained as:

(i) Forces due to body forces  $\{b_x \ b_y \ b_z\}^T$  per unit volume are given by:

$$\{F^e\}_b = \int_v [N]^T \{b\} dV \quad \dots\dots(3.20a)$$

(ii) Forces due to pressure distribution  $\{p_x \ p_y \ p_z\}^T$  per unit area are given by:

$$\{F^e\}_b = \int_v [N]^T \{p\} dA \quad \dots\dots(3.20b)$$

For the complete structure, relation of the form given below is obtained

$$[K] \{\delta\} = \{F\} \quad \dots\dots(3.21)$$

where  $\{\delta\}$  is the vector of global displacement,  $\{F\}$  the load vector and  $[K]$  the stiffness matrix.

The global stiffness matrix  $[K]$  is obtained by directly adding the individual stiffness coefficients in the global stiffness matrix. Similarly the global load vector for the system is also obtained by adding individual element loads at the appropriate locations in the global vector.

The mathematical statement of the assembly procedure is:

$$\left. \begin{aligned} [K] &= \sum_{e=1}^E [K]^e \\ [F] &= \sum_{e=1}^E \{F\}^e \end{aligned} \right\} \quad \dots\dots(3.22)$$

where  $E$  is the total number of elements.

To transform the variable and the region with respect to which the integration is made, the relationship

$$dx \ dy \ dz = \det [J] \ d\xi \ d\eta \ d\zeta \quad \text{is used.}$$

Writing explicitly

$$\int dx \ dy \ dz = \int_{-1}^1 \int_{-1}^1 \int_{-1}^1 \det[J] \ d\xi \ d\eta \ d\zeta \quad \dots\dots(3.23)$$

A 2x2x2 integration has been used for the three dimensional analysis. Similar relationships can be derived for 2-D parabolic isoparametric elements.

### 3.2. NON LINEAR ANALYSIS

Nonlinear structural behavior arises from a number of causes, which can be grouped into these principal categories:

#### a) Changing Status (Including Contact)

Many common structural features exhibit nonlinear behavior that is *status-dependent*. For example, a tension-only cable is either slack or taut; a roller support is either in contact or not in contact. Status changes might be directly related to load (as in the case of the cable), or they might be determined by some external cause.

Situations in which *contact* occurs are common to many different nonlinear applications. Contact forms a distinctive and important subset to the category of changing-status nonlinearities.

#### b) Geometric Nonlinearities

If a structure experiences large deformations, its changing geometric configuration can cause the structure to respond nonlinearly. Geometric nonlinearity is characterized by large displacements and/or rotations.

#### c) Material Nonlinearities

Nonlinear stress-strain relationships are a common cause of nonlinear structural behavior. Many factors can influence a material's stress-strain properties, including load history (as in elastoplastic response), environmental conditions

(such as temperature), and the amount of time that a load is applied (as in creep response).

The nature of soils and rocks, however, is highly complex and requires different considerations from the materials used in structures. Deformation behavior of soils is influenced by a number of factors, such as the physical structures, porosity, density, stress history or loading characteristic. These factors render the stress deformation behavior highly complex and non linear.

Since the matrix [D] containing E and  $\nu$  depends upon the stresses and thus displacements, it follows that matrix [K] is a function of  $\{\delta\}$  and  $\{F\}$ , as  $\{\delta\}$  depends upon  $\{F\}$ . [K], therefore, can be presented by

$$[K] = [K(\{\delta\}, \{F\})] \quad \dots\dots (3.24)$$

The symbolic non linear relationship between  $\{F\}$  and  $\{\delta\}$  is shown in Fig.3.2(a). Figure 3.2(b) shows the non linear stress-strain curve corresponding to the load  $\{F\}$  and displacements. It is on the basis of this stress-strain or constitutive law that the variable matrix  $\{D(\{\delta\})\}$  for the non linear analysis is determined.

### 3.2.1. Techniques For Incorporating Nonlinearity

The solution of non linear problem by the finite element method is usually attempted by one of three basic technique viz. (a) incremental or step wise procedures (b) iterative or Newton methods and (c) step-iterative or mixed procedures.

#### 3.2.1.1. Incremental Procedures

The basis of the incremental or step wise procedure is the subdivision of the load into many small partial loads or

increments. Usually these load increments are of equal magnitude, but in general they need not be equal. The load is applied one increment at a time and during the application of each increment the equation is assumed to be linear. A fixed value of  $[K]$  is thus assumed throughout each load increment but  $[K]$  take different values during different increments.

The solution for each step of loading is obtained as an increment of the displacement  $\{\Delta\delta\}$ , which is added up to give the total displacement at any stage of the loading, and the incremental process is repeated until the total load has been reached.

Essentially, the incremental procedure approximates the non linear problem as a series of linear problems, that is, the nonlinearity is treated as piecewise linear.

The total load  $\{F\}$  is given by

$$\{F\} = \{F_0\} + \sum_{i=1}^M \{\Delta F_i\} \quad \dots\dots (3.25)$$

where  $\{F_0\}$  is the initial load vector and  $M$  is the total number of increments and  $\{\Delta F_i\}$  is the incremental load vector in the  $i^{\text{th}}$  increment. Hence after the application of the  $i^{\text{th}}$  increment, the load is given by

$$\{F_i\} = \{F_0\} + \sum_{j=1}^i \{\Delta F_j\} \quad \dots\dots (3.26)$$

Similarly after the  $i^{\text{th}}$  iteration, the displacement is given by

$$\{\delta_i\} = \{\delta_0\} + \sum_{j=1}^i \{\Delta\delta_j\} \quad \dots\dots (3.27)$$

where  $\{\delta_0\}$  represents initial displacement.

Usually  $\{F_0\}$  and  $\{\delta_0\}$  are null vectors because the solution is started from the undeformed state of the body. However, any initial equilibrium state of  $\{F_0\}$  and  $\{\delta_0\}$  can be specified.

To compute the increment of displacements, a fixed value of stiffness is used which is evaluated at the end of the previous increment. Therefore,

$$[K_{i-1}] \{\Delta\delta_i\} = \{\Delta F_i\} \text{ for } i=1,2,3,\dots,M \quad \dots\dots(3.28)$$

where the subscripts refer to the incremental stage and  $[K_0]$  is the initial value of the stiffness.  $[K_0]$  is computed from material constant derived from the given stress-strain curves at the start of the loading.

The incremental procedure is schematically indicated in Fig.3.3. Usually, in the incremental procedure the tangent moduli ( $E_t$ ) are used to formulate  $[D\{\sigma\}]$  and to compute the stiffness  $[K]$ . The matrix  $[K]$  is often referred to as the tangent stiffness matrix.

The accuracy of the incremental procedure can be improved by taking smaller increments of the load, say by adopting half of the load increment. However, since a new incremental stiffness matrix  $[K_{i-1}]$  must be computed for each step, the accuracy, it is evident, is purchased at the cost of additional computational effort.

### 3.2.1.2. Iterative Procedures

The iterative procedure involves a sequence of calculations in which the structure is fully loaded in each iteration. Because some approximate, constant value of the stiffness is used in each step, the equilibrium is not necessarily satisfied. After each iteration, the portion of the total load that is not balanced is calculated and used in the next step to compute an additional increment of the displacements. The process is repeated until equilibrium is

approximated to some acceptable degree. Essentially, the iterative procedure consists of successive corrections to a solution until equilibrium under the load  $\{F\}$  is satisfied.

For the  $i^{\text{th}}$  cycle of iteration process, the necessary load is determined by

$$\{F_i\} = \{F\} - \{F_{e,i-1}\} \quad \dots\dots (3.29)$$

where  $\{F_{e,i-1}\}$  is the load equilibrated after the previous step. An increment to the displacement is computed during the  $i^{\text{th}}$  step by using the relation.

$$[K_{i-1}] \{\Delta\delta_i\} = \{F_i\} \quad \dots\dots (3.30)$$

where the subscript,  $i$ , denotes a cycle of iteration. The total displacement after the  $i^{\text{th}}$  iteration is computed using the relationship of Eq. (3.27).

Finally,  $\{F_{e,i}\}$  is calculated as the load necessary to maintain the displacement  $\{\delta_i\}$ . The procedure is repeated until the increments of displacement or the unbalanced forces become zero, that is,  $\{\Delta\delta_i\}$  or  $\{F_i\}$  become null according to some preselected criterion.

Instead of computing a different stiffness for each iteration, a modified iterative technique is also employed which utilizes only the initial stiffness  $[K_0]$ . Obviously, the modified procedure necessitates a greater number of iterations. However, there is a substantial saving of computation because it is not necessary to invert a new stiffness at each cycle. The iterative procedures are illustrated schematically in Fig.3.4.

### 3.2.1.3. Mixed Procedures

The step iteration or mixed procedure utilizes a combination of the incremental and iterative schemes. In this



method, the load is applied incrementally, but after each increment successive iterations are performed. This method yields higher accuracy at the price of more computational efforts. The scheme of procedure is illustrated in Fig.3.5.

Because the mixed method combines the advantages of both the incremental and iterative procedures and tends to minimize the disadvantage of each, step iteration is being utilized increasingly. The additional computational effort is justified by the fact that the iterative part of the procedure permits one to assess the quality of the approximate equilibrium at each stage.

Another version of the mixed method known as the procedure of successive approximation which is schematically represented in Fig.3.6. The problem is analysed repeatedly adjusting the modulus values assigned to each element each time, until the calculated values of stress and strain are consistent with the desired non linear relationship. Since at each iteration a new value of  $[K]$  has to be calculated and the number of iterations may be, in some cases large, the numbers of the iterations are specified not to exceed a given number.

### **3.3. SEQUENTIAL CONSTRUCTION**

Engineering structures are usually constructed in a definite sequence of operations. A conventional linear analysis of such structures is performed by assuming that the entire construction takes place in a single operations. The stresses and deformation are computed by considering loads on completed structures. However, for the non linear problem typical in soil and foundation engineering, the behavior at a particular stage

of loading is dependent upon the state of stress and stress history. Thus the stresses in the final configuration are dependent upon the sequence of intermediate configurations and loading (Desai and Abel, 1987). Most embankments are constructed in layers by incremental process and the load is accumulated gradually during construction which invalidates the assumption of instantaneous application of the entire gravity load in one stage. For realistic analyses of both stresses and movements in complex conditions, the sequence analysis provides a rational procedure of considerable engineering value.

In the sequential analysis, the structure is first divided into horizontal slices, known as lifts or layers corresponding to the construction scheme. The analysis is then carried out in succession for stresses and displacements corresponding to different stages of construction. Thus, first of all, the analysis is carried out for the first lift for its own load, i.e. the structure is supposed to comprise one lift only and the stiffness is formulated for the elements of this lift only. These stresses and deformation are stored, and the second lift is added to the structure. Now the structure is supposed to be made up of two layers and stiffness is generated for the elements of these two layers but the gravity forces considered are due to the dead weight of the second layer only, whereas the first layer is considered weightless. The stresses and deformations due to this incremental load are calculated for the whole structure and are added up to the previously stored value. This process is repeated till the analysis is complete for the whole structure.

### 3.4. CONSTITUTIVE LAWS

It has been repeatedly shown that the most influential factor in the finite element analysis of embankment dams is the modelling of the stress-strain behaviour of the fill by an appropriate constitutive law. However, in spite of the diversity of the stress-strain relationship being used, reasonable agreement has usually been found when the results of finite element analyses (typically movements) have been compared with field observations. This is not surprising bearing in mind the fact that most of the analyses were done after the field measurement had been made.

The most widely used function for simulation of stress-strain curves in finite element analysis was formulated by Duncan and Chang (1970) using Kondner's (1963) finding that the plots of stress v/s strain in a triaxial compression test is very nearly a hyperbola. The procedure uses Mohr Coulomb failure criterion and develops relationships for the tangent modulus and Poisson's ratio which may be expressed in terms of total or effective stresses.

Kondner's approximated the equations of stress-strain curves for both clays and sands by the following hyperbolic relation:

$$\sigma_1 - \sigma_3 = \frac{\varepsilon_1}{a + b\varepsilon_1} \quad \text{.....(3.31)}$$

where  $\sigma_1$  = major principal stress

$\sigma_3$  = minor principal stress;

$\varepsilon_1$  = major principal strain; and,

a, b = constants whose values are determined by fitting experimental data

It is shown at Fig.3.7. that

$$a = \frac{1}{E_i} \quad \dots (3.32)$$

and

$$b = \frac{1}{(\sigma_1 - \sigma_3)_{ULT}} \quad \dots (3.33)$$

where

$E_i$  = initial tangent modulus

$(\sigma_1 - \sigma_3)_{ULT}$  = the asymptotic value of the principal stress difference at infinite strain

Assuming  $\sigma_3$  constant, the tangent modulus  $E_t$  is given by

$$E_t = \frac{\partial(\sigma_1 - \sigma_3)}{\partial \varepsilon_1} = \frac{a}{(a + b\varepsilon_1)^2} \quad \dots (3.34)$$

where Eq.(3.31) has been substituted for the principal stress difference. Using Eq.(3.31),  $\varepsilon_1$  can be eliminated from Eq.(3.34) to give

$$E_t = \frac{1}{a} [1 - b(\sigma_1 - \sigma_3)]^2 \quad \dots (3.35)$$

Duncan and Chang noted that each of the constant a and b should be dependent on the minor principal (confining) effective stress  $\sigma_3$ . More precisely, they suggested that  $E_i$  vary in the following manner:

$$E_i = \frac{1}{a} = K \cdot P_{atm} \left( \frac{\sigma_3}{P_{atm}} \right)^n \quad \dots (3.36)$$

where K = a dimensionless modulus number

$P_{atm}$  = the atmospheric pressure

N = a dimensionless modulus exponent which determines the rate of variation of  $E_1$  with  $\sigma_3$

Duncan and Chang further suggested that

$$(\sigma_1 - \sigma_3)_f = R_f (\sigma_1 - \sigma_3)_{ULT} \quad \dots (3.37)$$

$R_f$  = a failure ratio

$(\sigma_1 - \sigma_3)_{ULT}$  = the asymptotic value of the principal stress difference

$(\sigma_1 - \sigma_3)_f$  = the principal stress difference at failure

The principal stress difference at failure is related to the minor principal (confining) stress through the Mohr-Coulomb failure criterion:

$$(\sigma_1 - \sigma_3)_f = \frac{2(c \cdot \cos \phi + \sigma_3 \sin \phi)}{1 - \sin \phi} \quad \dots (3.38)$$

where  $c$  = the cohesion intercept

$\phi$  = the friction angle

It follows that:

$$b = \frac{1}{(\sigma_1 - \sigma_3)_{ULT}} = \frac{R_f}{(\sigma_1 - \sigma_3)_f} = \frac{R_f(1 - \sin \phi)}{2(c \cos \phi + \sigma_3 \sin \phi)} \quad \dots (3.39)$$

Substituting Eq. (3.36) and (3.39) into Eq. (3.35) gives

$$E_t = \left[ 1 - \frac{R_f(1 - \sin \phi)(\sigma_1 - \sigma_3)}{2(c \cdot \cos \phi + \sigma_3 \sin \phi)} \right]^2 K P_{atm} \left( \frac{\sigma_3}{P_{atm}} \right)^n \quad \dots (3.40)$$

Based on the results of a number of loading-unloading-reloading tests on sands, Duncan and Chang proposed the following relationship for the variation of the initial elastic modulus:

$$E_{ur} = K_{ur} P_{atm} \left( \frac{\sigma_3}{P_{atm}} \right)^n \quad \dots (3.41)$$

where  $E_{ur}$  = the loading-reloading modulus

$K_{ur}$  = the corresponding modulus number

Thus, for histories involving loading, unloading and re-loading, the same value ( $E_{ur}$ ) of the elastic modulus is used - admittedly a simplification of the actual state of affairs. In Duncan and Chang's paper the second elastic constant, Poisson's ratio, was assumed to be constant. This assumption was subsequently modified by Kulhawy and Duncan.

While maintaining the same expressions for  $E_i$ ,  $E_t$  and  $E_{ur}$  as presented by Duncan and Chang, Kulhawy and Duncan (1972) proposed the following relation between the axial strain  $\epsilon_a$  and the radial strain  $\epsilon_r$ :

$$\epsilon_a = \frac{\epsilon_r}{f + d\epsilon_r} \quad \dots\dots(3.42)$$

where  $f$  = the value of tangent Poisson's ratio at zero strain  
or the initial tangent Poisson's ratio,  $\nu_i$

$d$  = a parameter expressing the rate of change  $\nu_i$  with strain

They found that the value of  $\nu_i$  generally decreased with increasing confining pressure,  $\sigma_3$ , in the form:

$$\nu_i = G - F \log\left(\frac{\sigma_3}{P_{atm}}\right) \quad \dots\dots(3.43)$$

where  $G$  = the value of  $\nu_i$  at one atmosphere

$F$  = the rate of change of  $\nu_i$  with  $\sigma_3$

Utilizing the preceding equation and the basic definition of the tangent Poisson's ratio:

$$\nu_t = \frac{\partial \epsilon_r}{\partial \epsilon_a} \quad \dots\dots(3.44)$$

it can be shown that the resulting expression for the tangent Poisson's ratio is:

$$\nu_t = \frac{G - F \log\left(\frac{\sigma_3}{P_{atm}}\right)}{(1 - d\varepsilon_a)^2} \quad \dots\dots(3.45)$$

From Eq.(3.31) it follows that the major principal strain is given by

$$\varepsilon_1 = \frac{a(\sigma_1 - \sigma_3)}{1 - b(\sigma_1 - \sigma_3)} \quad \dots\dots(3.46)$$

Assuming that  $\varepsilon_1 = \varepsilon_a$ , and using Eq.(3.36) and (3.39) leads to

$$\varepsilon_a = \frac{(\sigma_1 - \sigma_3)}{K P_{atm} \left(\frac{\sigma_3}{P_{atm}}\right)^n \left[1 - \frac{R_f(\sigma_1 - \sigma_3)(1 - \sin \phi)}{2c \cos \phi + 2\sigma_3 \sin \phi}\right]} \quad \dots\dots(3.47)$$

Equation (3.45), with  $\varepsilon_a$  given by Eq.(3.47), is thus used to compute the tangent Poisson's ratio.

The modification was made in order to avoid a serious problem which was observed in a number of analyses. The problem occurred for regions where the confining pressure  $\sigma_3$  was sufficiently low to yield a low modulus, but not low enough to yield a high Poisson's ratio  $\nu$ . The result was that the soil in these regions experienced large decreases in volume, it effectively disappeared. Thus, conservation of mass was violated. To prevent this problem, an alternative expression is available for  $\nu$ . It is assumed that the soil possesses a constant bulk modulus  $B$ ; the incremental value of  $\nu$  is then calculated from the expression:

$$\nu_i = 0.5 \left(1 - \frac{E_i}{3B}\right) \quad \dots\dots(3.48)$$

The meaning of the parameters  $K$ ,  $K_{ur}$ ,  $\nu$ ,  $\phi$ ,  $c$  and  $R_f$  is the same as for the other versions of the hyperbolic model. The

quantities  $K_b$  and  $m$  are used to make the bulk modulus  $B$  a function of confining pressure  $\sigma_3$ :

$$B = K_b P_{atm} \left( \frac{\sigma_3}{P_{atm}} \right)^m \quad \dots\dots (3.49)$$

where  $K_b$  = the dimensionless "bulk modulus number" (equal to the value of  $B/P_{atm}$  at  $\sigma_3 = P_{atm}$ )

$m$  = the dimensionless "bulk modulus exponent"

Using Eq.(3.49) for the bulk modulus, Poisson's ratio is computed from Eq.(3.48).

### 3.5. STEPS OF THE ALGORITHM

Incremental construction analysis as proposed by Clough and Woodward (1967) has been modified to analyze the dam behavior for the construction stage by Sharma (1975) and Singh (1985), which is used in this study. For the water loading and effect of softening the approach as adopted by Nobari and Duncan has been adopted.

The various steps in the solution algorithm are:

1. Take first layer
2. Calculate the elastic constant based on the anticipated values of stress.  $\sigma_1 = \gamma h$  and  $\sigma_3 = K_0 \sigma_1$ , where  $h$  is the average height of the fill in the layer and a constant value of 0.50 for  $K_0$ , the coefficient of earth pressure at rest, has been adopted for all zones of the dam
3. The gravity loads of the new layer only ( $\Delta F^i$ ) are calculated. These are added to the loads of the previous layer to get the total loads  $\{F^i\} = \{F^{i-1}\} + \{\Delta F^i\}$



4. The stiffness matrix  $[K]$  of the structure upto the end of current layer is calculated
5. The incremental displacements  $\{\Delta\delta\}$ , the incremental strains  $\{\Delta\varepsilon\}$  and incremental stresses  $\{\Delta\sigma\}$  are calculated

$$\{\Delta\delta\} = [K]^{-1}\{\Delta F^i\}$$

$$\{\Delta\varepsilon\} = [B]^T\{\Delta\delta\}$$

$$\{\Delta\sigma\} = [D]\{\Delta\varepsilon\}$$

The  $[D]$  matrix used here is calculated according to the proposed stress-strain model at the existing stress level, prior to this iteration

6. The stress-strain matrix is found out at the stress state obtained by adding the incremental stresses in step 5 to those at the beginning of the iteration
7. Incremental stresses  $\{D_s\}$  are recalculated with the new value of  $[D]$
8. The total stresses are found out by adding the incremental stresses of step 7 to the stresses at the beginning of the iteration
9. The equilibrium load vector is calculated by

$$\{F_e\} = \int_v [B]^T \{\sigma\} dv$$

and residual load vector  $\{\psi\}$  by

$$\{\psi\} = \{F^i\} - \{F_e\}$$

10.  $\{\Delta F_j\}$  is set equal to  $\{\psi\}$ , where  $j$  is the iteration number and the superscript refers to the layer number
11. Calculate the norms of the residual load by the relation

$$|\{\psi\}| = (\{\psi\}^T \{\psi\})^{1/2}$$

and compare it with the norm of total loads applied, find convergence factor:

$$\text{Convergence factor} = \frac{\text{Norm of residual loads}}{\text{Norm of applied loads}}$$

12. If the ratio of norm residual to that of total applied load is within specified tolerance factor, the stresses, strains, displacements and principal stresses are stored and the next step is skipped otherwise the next step is followed
13. If the ratio of norm of residual with the norm of applied force is not within the specified tolerance limit, convergence ratio is calculated

$$\text{Convergence ratio} = \frac{\text{Conv. factor in the current iteration}}{\text{Conv. factor in the prev. iteration}}$$

If the convergence ratio less than 1.5 go to step 4, otherwise go to step 5

14. Take next layer, if left and proceed from step 2 if the analysis is for construction stage. If the analysis is to be done for reservoir filling also go to next step if any stage is left. Stop if no layer/stage is left
15. Calculate the additional gravity loads for the elements in the current layer only leaving the elements in the previous layer. The additional gravity loads will be upward in case of upstream shell and transition due to buoyancy and downward in the core due to the saturation of the core material. These will be no additional gravity load in elements downstream of core
16. Calculate the water pressure load on the upstream face of core for elements upto the end of current layer. For elements in current layer it will be calculated on the basis

of water pressure head at the nodes while for elements in the previously filled stages the water pressure head will be equal to the height of current reservoir rise

17. Calculate the water load acting on top each layer based on the pressure head equal to the height of reservoir rise in that stage
18. Calculate softening load for elements upstream of core lying in the current layer only
19. Add the loads in step 15 to 18 to get  $\{F_i\}$  for further calculations
20. The stiffness matrices is calculated for the entire load
21. Go to step 5

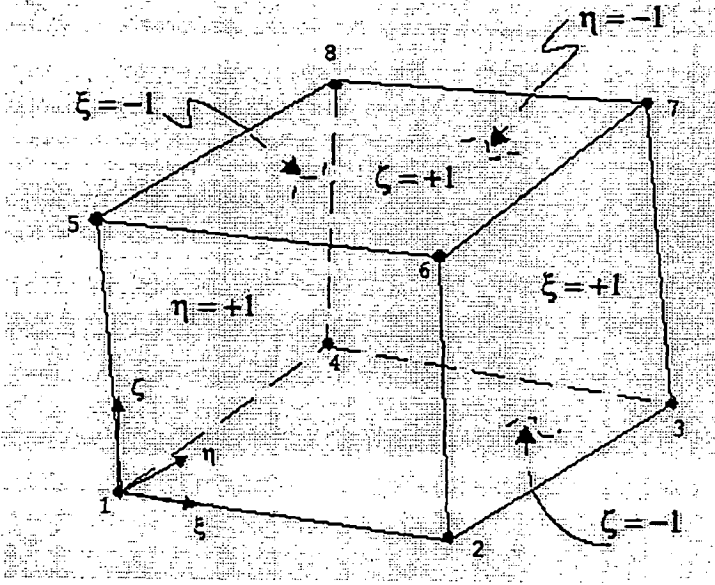
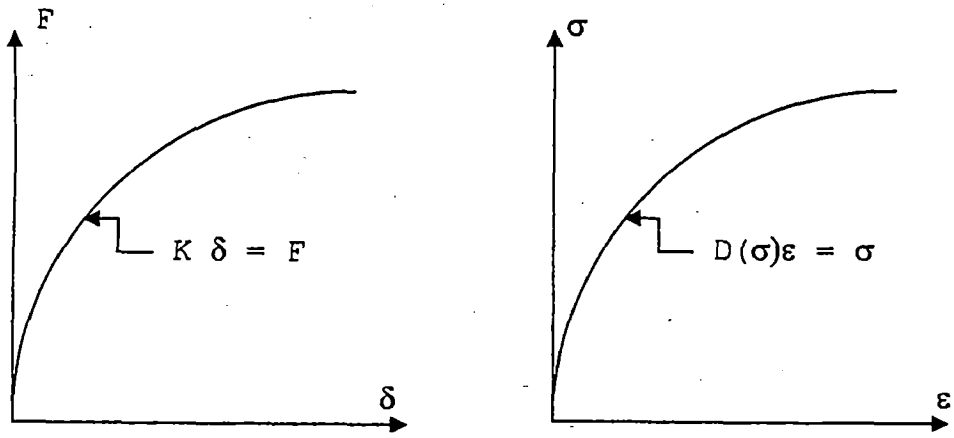


Fig.3.1. 3-D Finite Element Showing Node Numbers



(a) Load Displacement (b) Stress-Strain Curve  
 Fig.3.2. Non Linear Curve

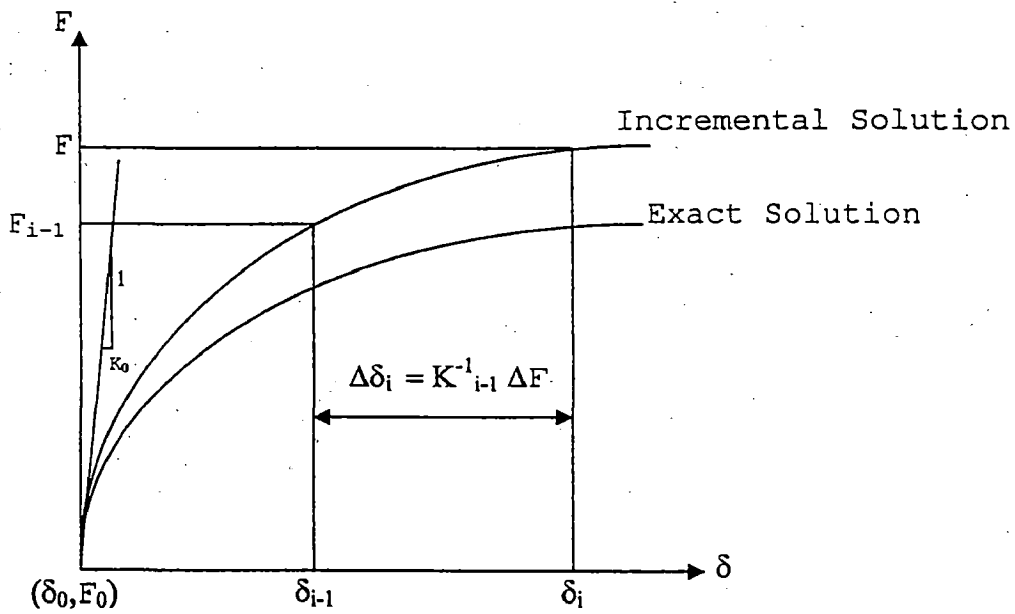
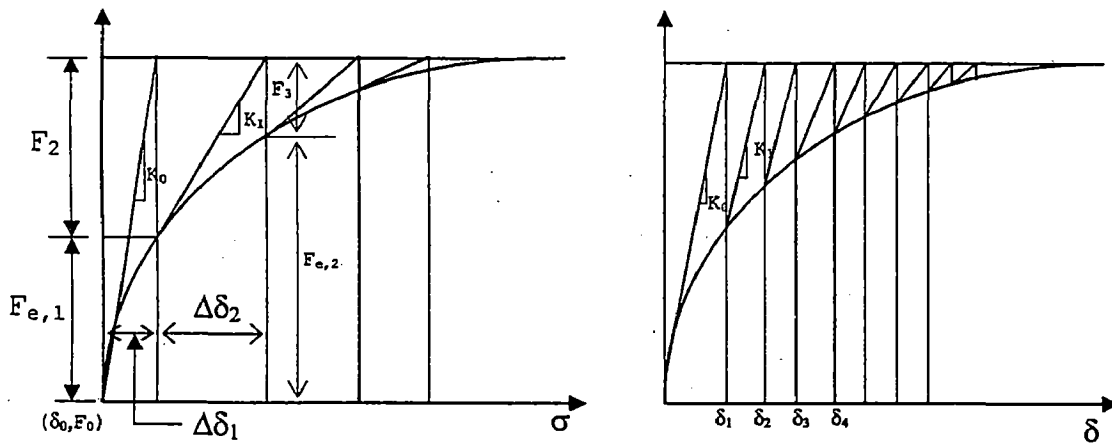


Fig.3.3. Basic Incremental Procedure



(a) Tangent Stiffness Procedure (b) Modified Procedure  
Fig.3.4. Iterative Procedure

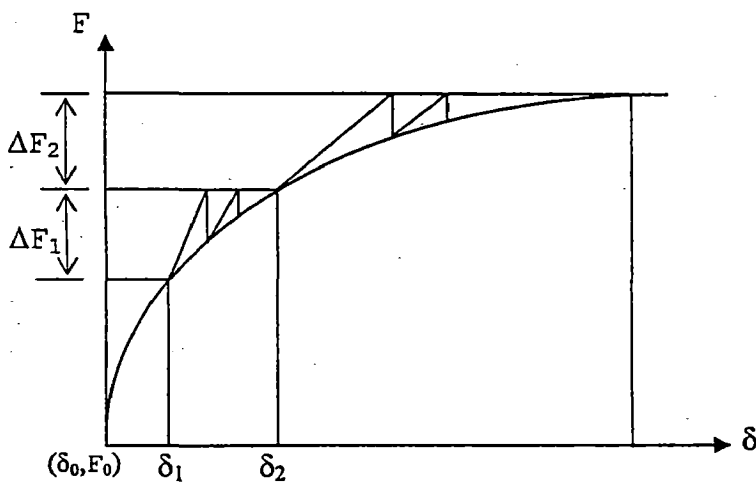


Fig.3.5. Step Iterative Procedure

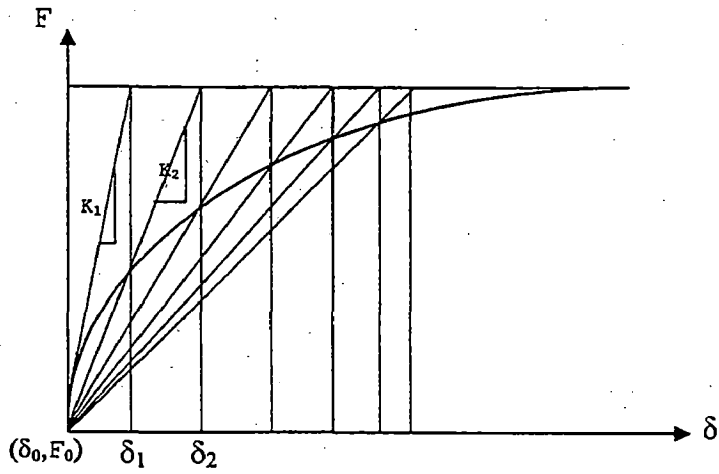


Fig.3.6. Mixed Procedure

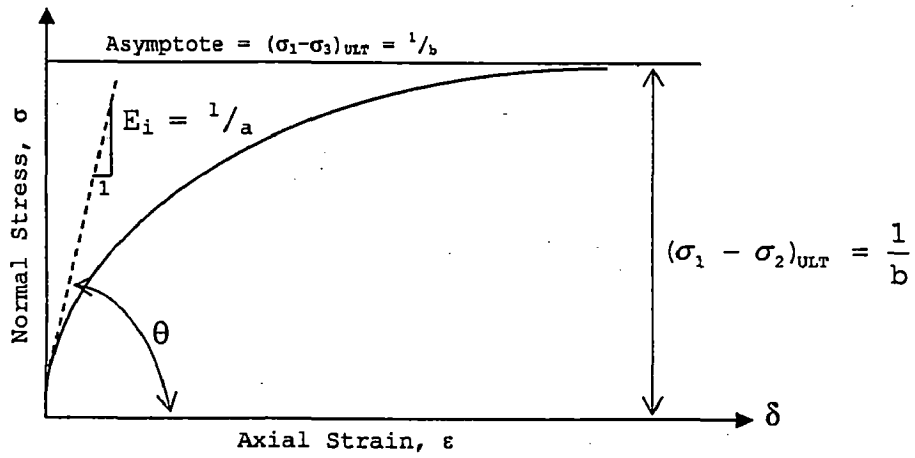


Fig.3.7. Hyperbolic Stress-Strain Curve

## CHAPTER 4

### ABOUT THE PROGRAMMES

#### 4.1. PENTAGON3D

PENTAGON3D finite element analysis software, which is developed by Emerald Soft P.E. South Korean, enables users to perform the following tasks:

1. Build computer models of geotechnical structures
2. Apply operating loads or other design performance conditions
3. Study physical responses, such as deformation level and stress distributions

The PENTAGON3D program has a comprehensive Graphical User Interface (GUI) that gives users easy, interactive access to program functions, commands, documentation, and reference material. The users use the GUI for virtually all interactive PENTAGON3D work. The GUI provides an interface between users and the PENTAGON3D program, which commands drive internally. Each GUI function - a series of picks resulting in an action - ultimately produces one or more PENTAGON3D commands that the program executes and records on the input history file. An intuitive menu system helps users navigate through the PENTAGON3D program.

The PENTAGON3D program is organized into three basic levels:

1. PENTMESH
2. PENPRE
3. PENPOST

The PENTMESH level acts as a gateway into and out of the PENTAGON3D program. It is also used for certain global program controls such as build the model, input and clearing the database, loading or stages, and solve the FEM data with the main processor, Frontdbx. When users first enter the program, they are at the PENTMESH level. At the PENPRE level, the model including data input from PENTMESH level are verifying. The boundary condition and the sequence of construction could be easily checked to find out the errors. The PENPOST is the level to evaluate the results of a solution.

The program, which is permitted to be used for limited version only by the developer, is feasible to cope with 700 elements of 8-noded isoparametric hexahedral and 1500 nodes. The program has been executed on PC PENTIUM III - 1000 MHz.

#### **4.2. PENTMESH**

PENTMESH is the preprocess program of PENTAGON3D system. These provide the full graphical user interface to complete the analysis model including the geometry, the material properties, the boundary conditions and the construction stages etc. The screen on PENTMESH, shows at Fig.4.1, is categorized with two groups in the main menus. The one group is mainly used to form and to display the entities in the workspace. The entities mean the nodes and the elements. The elements are composed with the quadratic, the frame, the truss, and the spring element types. The menus are: (1) Edit Menu (2) Model Menu (3) Mode2 Menu (4) Delete/Select Menu (5) Display Menu (6) Set Menu (7) MeshGen Menu (8) Layer Menu and (9) Misc Menu. The other menu group is



mainly used to do the works except forming the entities, they are: (1) File Menu (2) View Menu (3) FEM Menu and (4) Help Menu.

A short description about the functions of the various menus following:

1. Edit Menu: The menu for copy and paste the points and the elements

2. Model Menu: This menu specifies the mouse mode to a certain mode (or state). Once users choose a mode, the mode is effective until another mode is selected. The menu contains: Zoom Mode, Select Points, Deselect Points, Relive Points, Add Points, Move Points, Select Elements (Within Box), Deselect Elements, Pan and Distance between Two Points

3. Mode2 Menu: This menu specifies the elements used on the model and generate the meshing on the geometrical plane. The menu contains: Add Quad3 Elements, Add Quad4 Element, Add Truss2 Elements, Add Spring Elements, Add Frame2 Elements, Find Nodal Coordinate, Add Points from 2 Points, Add Points from 3 Points, Add Points from 3 Points Arc, Point L0 - Point S0 - Point L1 - Point S1, Add Quad6 Elements, Add Quad8 Elements and Moving Line Node

4. Delete/Select Menu: The menu is used to delete the points and elements, which are selected. The menu contains: Select All Active Points, Select All Active Elements, Deselect All Points, Deselect All Elements, Delete Selected Points and Delete Selected Elements.

5. Display Menu: The Display Menu controls the screen display by the view scaling and the view translation. With the various menu lists, users can choose the preferred view by selecting the viewing items, refreshing the window, displaying entire model,

displaying the reduced model, displaying previous screen scale, and translating the model. The menu contains: Display Toggle, Redraw, Redraw All, Zoom Out, Previous View, View Up, View Down, View Left and View Right.

6. Set Menu: The Set Menu specifies the various settings for the modelling environment. The menu contains: Analysis Range, Coordinate Resolution, Entity Toggle, Entity Capacity, Entity Scale, Entity Color, Print Offset/Scale, Background Color, Save Time Interval, Options, Grid Size for Node Numbering, and Set Star Number of Entities for Save Process.

7. MeshGen Menu: In MeshGen Menu, there are sub-menus to create the finite element geometry. Users can generate elements and nodes, mirror the mesh, copy the mesh, move the mesh, rotate the mesh and so on. The menu contains: Generate Quad4, Generate Truss2, Generate Spring, Generate Frame2, Mirror Elements, Add a Point, Add (Generate) Points, Copy Points, Move a Point, Move Points, Move Points onto a Circle, Rotate Points, Rotate Seq. No, Change Element Type, Smoothing, Generate Points From Background, Undo, Convert to Quad6 Quad8, and Renumber.

8. Layer Menu: In the Layer Menu, the layers are defined for the 3D mesh generation and boundary condition, the construction and loading conditions and so on. The number of input layers for each Layer menu is limited to 300 and that of sublayers is limited to 1500. The layer is defined for the selected nodes or elements. The sublayer is created when some nodes or elements are selected. The menu contains: Coordinate Layer, Boundary Layer, Add Element Layer, Change Element Layer, Remove Element Layer, Calc Residual Force Layer, Prescribed Disp Layer, Gravity Force Layer, Surface Force Layer, Point Load Layer, Residual

Force Layer, Prestress Layer, Prescribed Head Layer, Review Bound Layer, Point Flux Layer, Surface Flux Layer and Temperature Layer.

9. Misc Menu: In this menu, users can change the material number, boundary type, degenerate elements or other function which used to modify the element model. The menu contains: Material No, Mechanical Boundary, Arc Layer, Degenerated Hexa Layer, Node Sublayer List, Element Sublayer List, Remove Unused Sublayer List, Load Function for Time History Analysis, Ground Motion Function for Ground Motion Analysis and Current Coordinate <--->Slice Coordinate.

10. File Menu: The menu used for clears all the database of current project from memory, open the file, save the file or others function which is connected to arranged the file. The menu contains: New, Open, Save, Save As, Import, Print, Print Preview, Print Setup and Exit.

11. View Menu: In the View Menu, users can set the toolbar and the status bar to be displayed in the PENTMESH window. And users can view the model and the result in 3D in PENPRE and PENPOST respectively. The PENPRE and the PENPOST are executed by clicking the menu then another window will pop-up. The menu contains: Toolbar, Status Bar, 3-D Preview By PENPRE, 3-D Result By PENPOST, 3-D Preview by PENPRE without recreation FEM Data, 3-D Result by PENPOST without recreation FEM Data.

12. FEM Menu: This menu used to complete the FEM data such as analysis control, material properties or stages configuration. The menu contains: Project ID, Analysis Type, Analysis Control, Material Property, Stage Configuration, Verify Stage/Layer, Set Work Space Property, Save FEM data, Analyze by Frontdbx with

recreation FEM Data and Analyze by Frontdbx without recreation FEM Data.

#### **4.2.1. Slice on PENTMESH**

The real three-dimensional entities (elements and nodes) are created and specified in Layer Menu. The real three-dimensional entities are described and prescribed by combining the two-dimensional entities with the concepts of slices. Here, the two-dimensional entities are just the ones which view on the PENTMESH work space which represents the two dimensional X-Y plane. And the slice represents the remaining Z axis, after creating the multiple X-Y planes along to the minus(-) Z axis direction Each X-Y plane is called the Slice, the Slice 0 means the first X-Y plane ,the largest z coordinate, and the Slice 1 means the second X-Y plane ,the next largest z coordinate, etc. The Slices are created in the Layer - Coordinate Layer Menu, in which the slices are created with assigning the z coordinate at each slice, as shown in Fig.4.2.

In view of the node connection, there are three element forms in PENTMESH work space, because the element is combined by linking the nodes. They are: (1) Quad4: consist of 4 node's links, Fig.4.3. (2) Quad8: consists of 8 node's links, Fig.4.4. and (3) Frame, Truss, Spring: consists of 2 node's link, Fig.4.5. Therefore, the elements can be created after nodes are created.

#### **4.2.2. Creation of 3D Element that Use 2D Entity**

Addition of three-dimensional element in PENTMESH is accomplished in 'Layer - Add Element Layer Menu, Fig.4.6. The necessary two-dimensional entity and three-dimensional shape for

each type of added three-dimensional elements are the following. The example below is the case for adding 3D elements in one slice from 2D entity. If several slices are selected, 3D elements are added in the each selected slices. This study creates 3D 8-node solid elements using 2D Quad4 element. Select 'Slice 3' in 'Applied Slice' column in the prior figure (Fig.4.6), then 3D 8-node solid elements are created between slice 3 and 4, illustrated on Fig.4.7.

#### 4.2.2. Degenerate Elements

This model is used to degenerate elements due to the shape of the elements on the slope valley of the abutments. Figure 4.8 shows the various shapes of degenerate elements by PENTMESH. In Figure 4.8, No.1 is a normal Solid (Quad8) element. No.2 to No.5 are degenerated by each surface.

Users should specify it in "Misc - Degenerated Hexa Layer" menu in advance of degenerated elements, then the dialog box is pop up (Fig.4.9). Front Slice Surface No. represents of surface number of divided element part, Fig.4.10. Front Slice No represents front element slice number of where the degenerate elements exists. When the degenerated exist among Add Element Layer list, 'Degenerated' check box should be checked such as Fig.4.11. If the degenerated element does not exist in the 'Applied Slices', users should not check on the 'Degenerated' button, reversely, but if the degenerated elements exist in more than one slices among the selected 'Applied Slices', users should check on the 'Degenerated' button. A this time, the dialog box of Fig.4.12 pop up. In this dialog box, users should choose the applied position of added elements. Front position means the element which is surface contact to front slice. Rear

position means the element which is in corner contact to front slice.

#### **4.3. PENPRE**

PENPRE can be used to check the input data before being analyzed by the FEA solver, Frontdbx. By using PENPRE, various input information can be displayed such as the model evolution along construction stages, the boundary conditions and the loading conditions. The graphics of PENPRE is programmed by OpenGL, the 3D graphic library; the model can be rendered with beautiful color and lights, and also can be cut, rotated, and even mirrored simply. The screen on PENPRE, shows at Fig.4.13, displays the first stage of construction. The next step for check of the sequence of construction, users can select Control - Go to the Specified Stage Menu to check the stages. Users can check the element status or material color in this level according to the stage of construction. For check of the boundary conditions, users can select Set - Display Entity Menu to see the type of boundary and the direction, shown on Fig.4.14.

#### **4.4. PENPOST**

PENPOST is the level in which users could analysis the solution from the solver Frontdbx. In PENPOST, as users open the input file name, the corresponding post-processing result file (\*.pos) is opened automatically. The role of input file for PENPOST is to provide the information such as the geometry, the boundary condition, the loading condition and the save condition, shown on Fig.4.15. The role of result file (\*.pos) is

to provide PENPOST with the analysis result only. PENPOST can display the FEA results in texts, contours and vectors. Some items are displayed in global coordinate systems and other items in local coordinate system.

A short description about the functions of the various menus following:

1. File Menu: In this menu the FEM data could be opened and saved. The menu contains: Open, Open Environment, Save Environment, Save as Environment and Exit.
2. Set Menu: Users could set the entity related items and the environmental variables, such as rendering light the object, select color of element, material or boundary. The menu contains: Information, Display Entities, Element Status and Font Size.
3. Constraint Menu: This menu is used to restrict the coordinate and the entity number for specific purpose. The menu contains: Display Range and Display Entity.
4. View Menu: This menu is used for adjusting the screen menu for specific object such as zooming, mirror or rotates the object. The menu contains: Select View, Set View Parameter, Redraw, Previous Zoom, Zoom In, Rotate U, V, W axis and Mirror.
4. Control Menu: Users can specify the stages that require to be checked. The menu contains: Next Stage, Previous Stage, Go to Specified Stage, Next Time/Mode, Previous Time/Mode, Start Animation and Stop Animation.
5. Function Menu: In this menu users can view the Eigen values, get the results in text format and save the result in the text file. The menu contains: Eigen Value, Graph, Save the Result History and Save Image to File

#### 4.5. STEPS IN MAKING THE MODEL

PENTAGON3D is the program that uses 2D entities with layer to make 3D entities. The following steps are used in making the model at the PENTMESH level:

1. Set of the Coordinate Range
2. Input Nodes with Add a Point Menu
3. Generate Nodes with Add Point Menu
4. Create 2D four node quadratic elements
5. 2D node renumbering
6. Assign the material number to the 2D elements
7. Assign the 2D boundary
8. Set of the material properties for each material numbering in FEM - Material Property Menu. In this stage the 15 material properties for each material are given in the following order:  
Young modulus of elasticity, Poisson's ratio, Unit weight, Cohesion, Friction angle, K0-X, K0-Y, K0-Z, n(Ei exponent), Kb (Bulk number), m (Kb exponent), Pa (the atmospheric pressure), Rf (Failure ratio), K (the modulus number) and Kur (the corresponding modulus number)
9. Set of the stage configuration for the construction system and the analysis in FEM - Stage Configuration Menu. The sequence of construction was detailed in this level
10. Set of 3D coordinate from 2D nodes with Coordinate Layer Menu. Coordinate Layer Menu used for users in making slice of a 3D model from 2D model.
11. Degenerate elements such as described at previous paragraphs.



12. Add the 3D elements from 2D elements with Add Element Layer Menu. Add Element Layer connected with the stage configuration which is used for determines the sequence of element was built accordance to the stages.
13. Set of the 3D mechanical boundary condition from 2D nodes with Boundary Layer Menu. Boundary Layer used for establishes the boundary type in each node, users should determine for fixed, free or rotational type in x, y, z direction.
14. Add the body force with Gravity Force Layer. All element defines in the model should be identified with the gravity force.
15. Change the material properties due to wetting conditions with Change Element Layer Menu. Users should determine the wet elements due to reservoir filling and replace the material properties according to this condition.
16. Add the surface pressure with Surface Force Layer Menu. In this stage users should determine the node which is connected with the water pressure load.
17. Set of Analysis Control in FEM - Analysis Control Menu. The program solves the set of simultaneous linear equation with frontal solver method and the convergence criterion was fixed in this level.
18. Verify 3D FEM data with PENPRE level
19. Run solver process, Frontdbx
20. Check the result at PENPOST level.

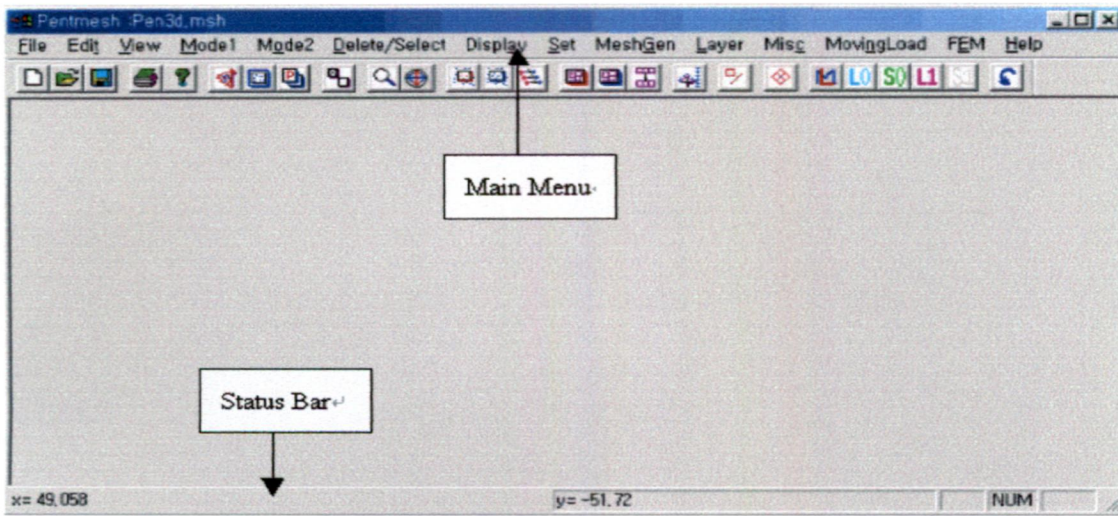


Fig.4.1. The PENTMESH Screen

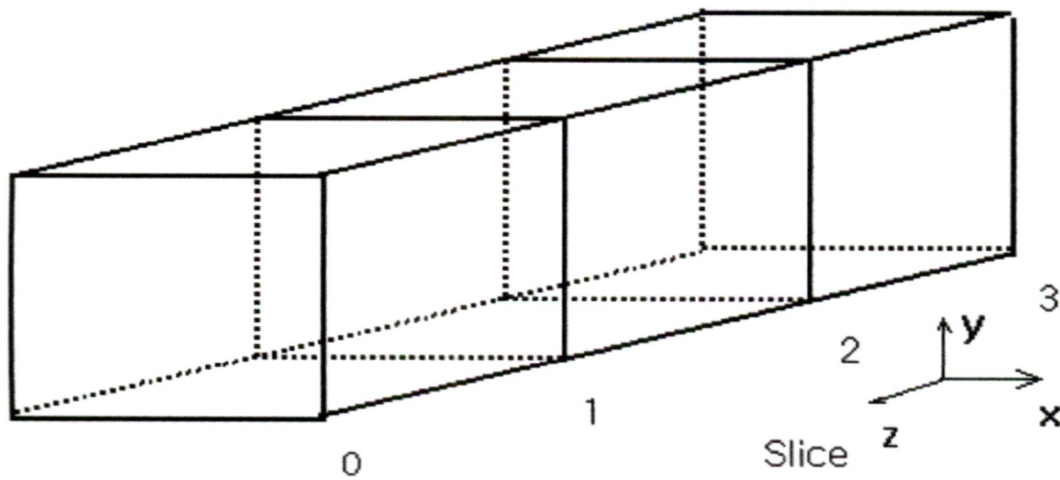


Fig.4.2. Concept of Slice

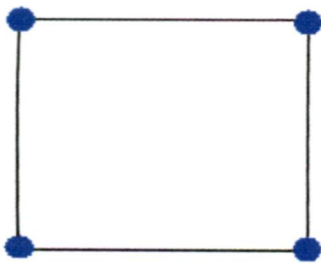


Fig.4.3. Quad4

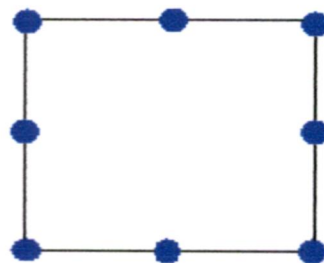


Fig.4.4. Quad8



Fig.4.5. Frame, Truss, Spring

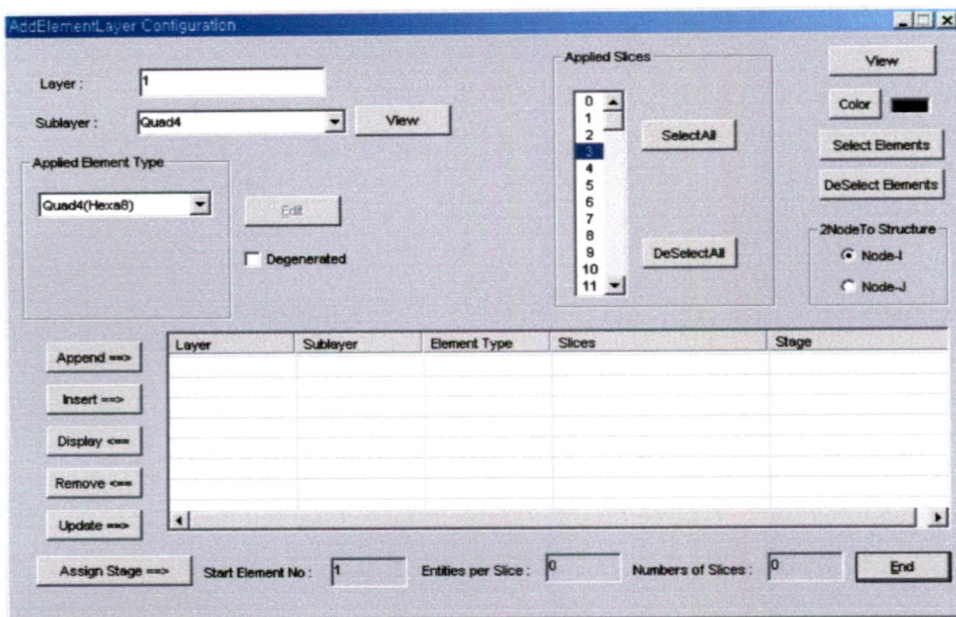


Fig.4.6. AddElementLayer Menu

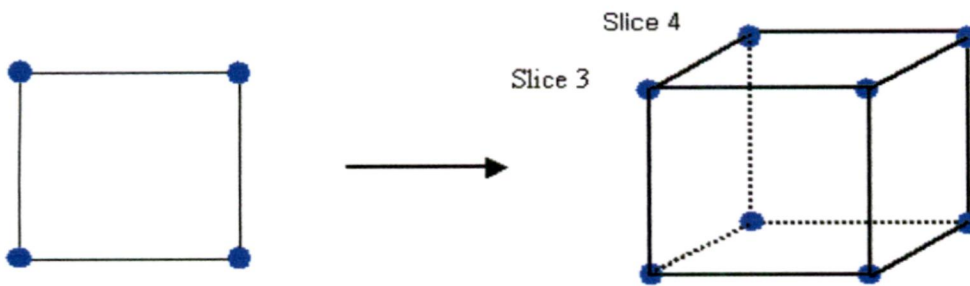


Fig.4.7. Creation of 3D 8-node solid element.

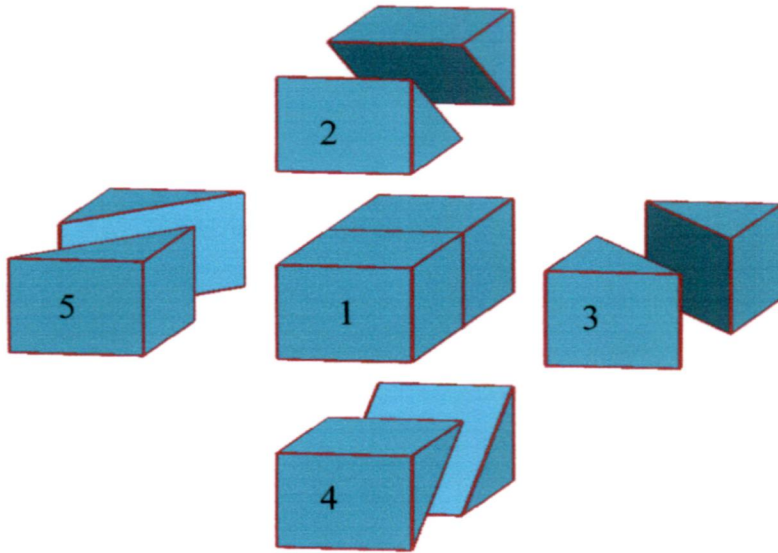


Fig.4.8. The Various Shapes of Degenerated Elements



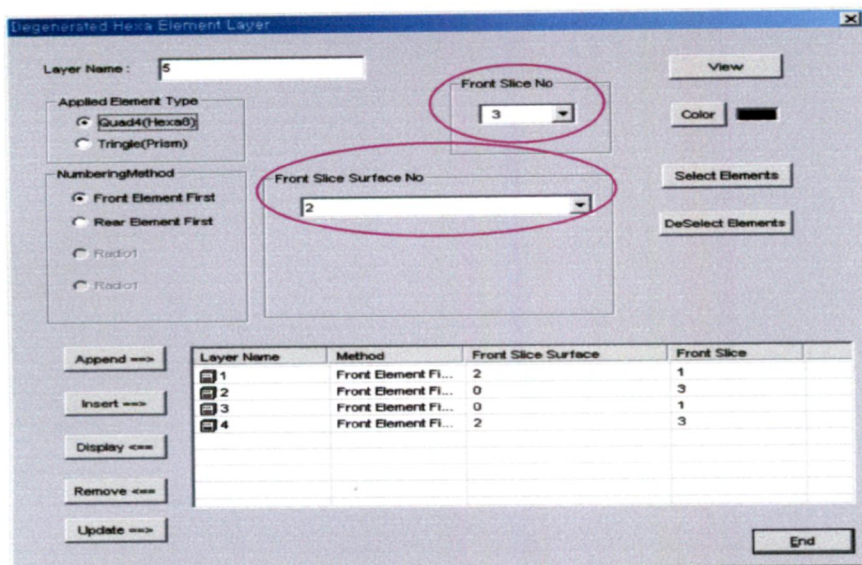


Fig.4.9. Degenerate Hexa Element Menu

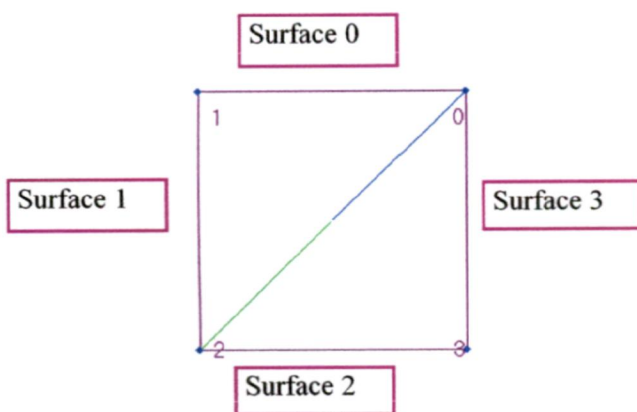


Fig.4.10. The Surface Number of Element

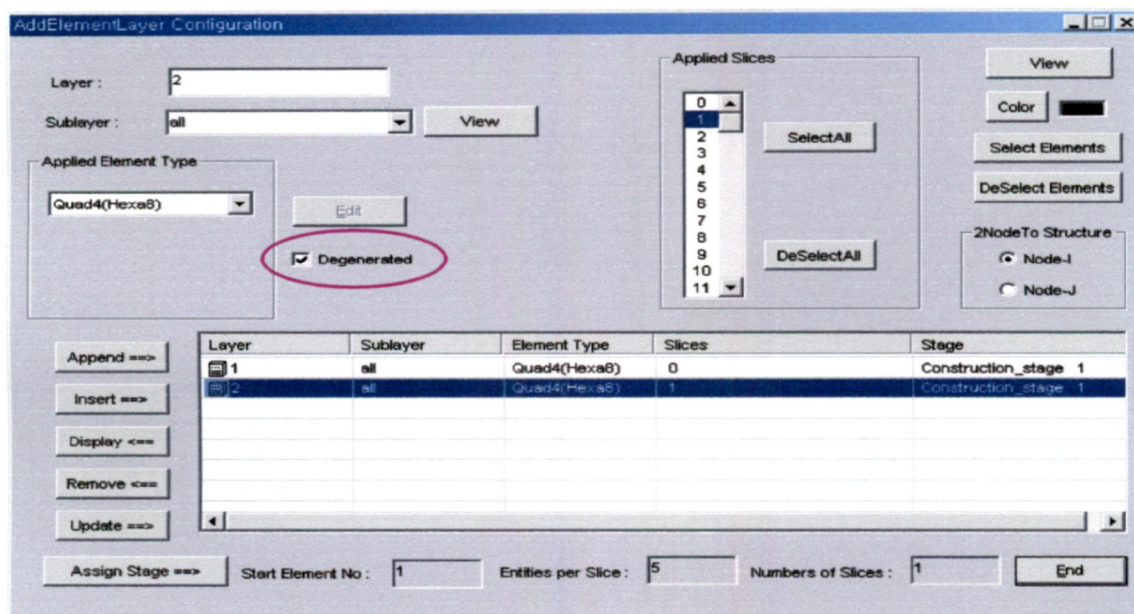


Fig.4.11. AddElementLayer Box



Fig.4.12. The Dialog Box of Degenerated Hexa

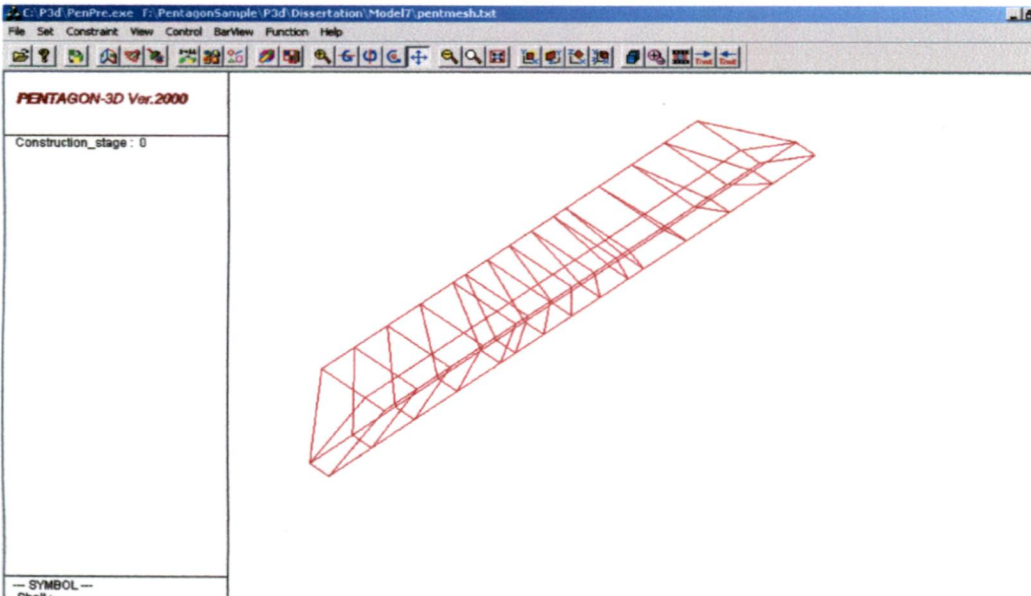


Fig.4.13. PENTPRE Screen

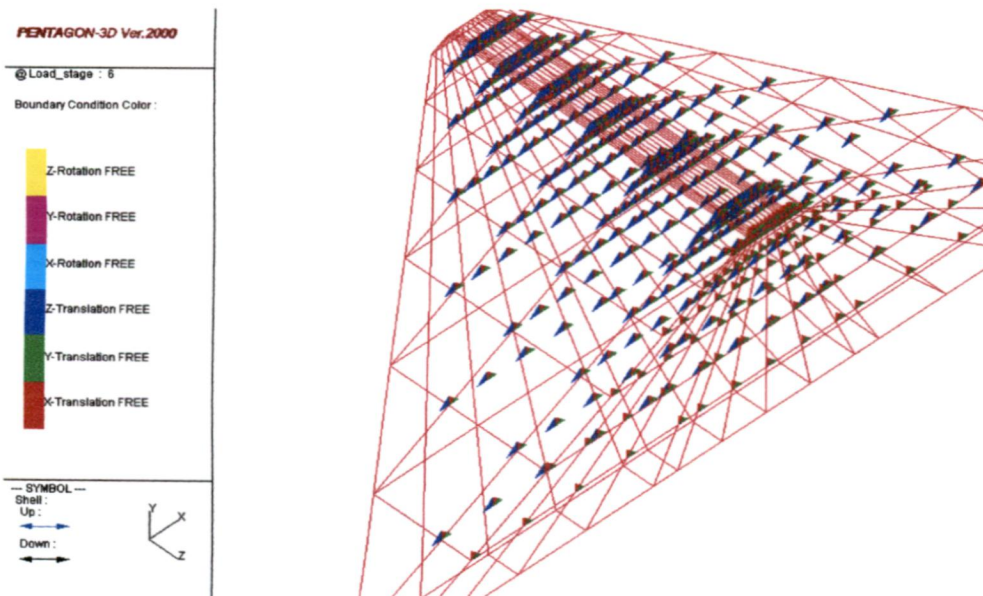


Fig.4.14. PENTPRE Boundary Condition

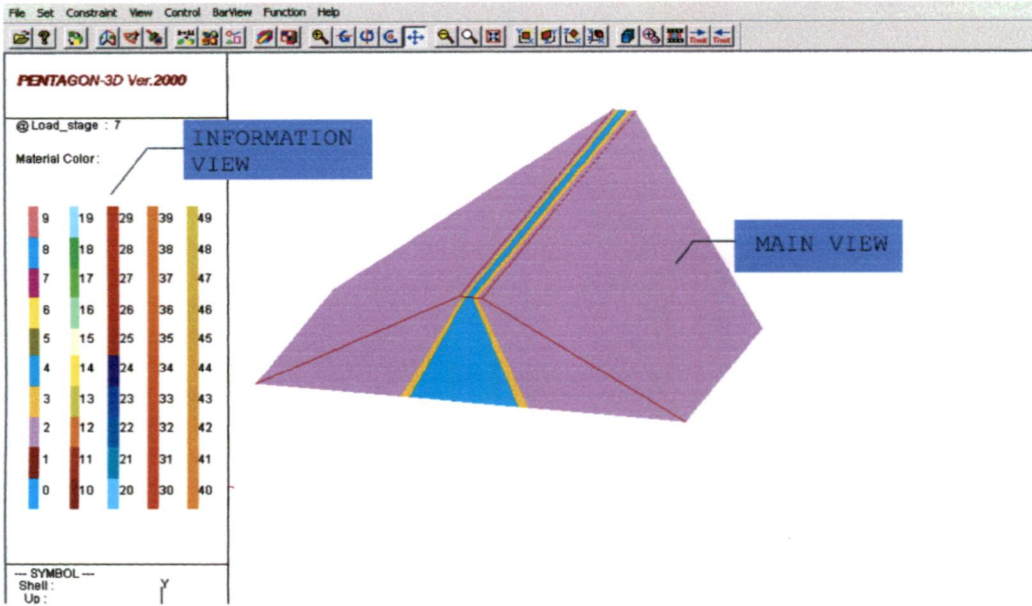


Fig.4.15. PENPOST Screen



## CHAPTER 5

### RESULTS OF FEM ANALYSIS

#### 5.1. GENERAL

A 100 m high earth and rockfill dam with valley wall slope of 1H:1V has been taken for the analyses purpose and the section is shown in Fig.5.1. The dam is considered to be located in V-shaped valley with fixed bottom width of 50 m. The dam has a central core and zones of filter between core and shell. The slopes of upstream and downstream core faces are 0.5H:1V and 0.4H:1V respectively. The upstream and downstream slopes of the dam are 1.8H:1V. Free board is kept as 5 m. The dam foundation is taken to be rigid and as such, the movements at base, in both horizontal and vertical direction, are taken to be restrained. The dams usually are situated in irregular shapes of valley and to reduce the size of the problem, the valley profile has been assumed symmetrical about the centre line of the valley and, therefore, only a half of the dam has been considered in the analysis.

#### 5.2. DISCRETIZATION OF DAM SECTION IN MESH

The mesh is idealized as shown in Fig.5.2. The dam has been discretised into 560 numbers of 8 noded brick elements, each node having 3 degrees of freedom. The mesh consists of 748 nodes, thus having 2244 degrees of freedom. Since the valley is symmetrical in the z-direction all the nodes on the central section have been assigned zero movement values in that direction. To simulate sequential construction, the dam is assumed to be raised in 7 layers with the height 24 m, 20 m, 18

m, 14 m, 11 m, 8 m and 5 m respectively and to be filled in 4 stages with height 24 m, 44 m, 76 m and 95 m respectively, shown in Fig.5.3(c). The numbers of elements in the 7 stages of construction are 32, 48, 64, 80, 96, 112 and 128 respectively. The element numbering has been done from left to right and from top to bottom layer.

### 5.3. ANALYSES PERFORMED

Non linear 3-D analysis have been carried out to compare the effects of dam being constructed in single or several lifts and also the reservoir filling being accomplished in one or more stages. The study has been made for the following cases:

1. Case I: Effect of number of lifts for end of construction stage:
  - The dam is completed upto the entire height in one single lift
  - The dam is completed in seven lifts of stages
2. Case II: Effect of the reservoir filling being done in different stages. The dam is completed in one lift and the reservoir is then filled in:
  - Single stage, as shown in Fig.5.3(a)
  - Four stages, as shown in Fig.5.3(b)
3. Case III: Combined effect of construction stages and reservoir filling:
  - Dam constructed in seven lifts
  - Reservoir is filled in four stages, as shown in Fig.5.3(c)



The displacements of  $u$  and  $v$  in  $x$  and  $y$  direction and the normal stresses  $\sigma_x$  and  $\sigma_y$  in  $x$  and  $y$  direction were studied for various causes along the height and at constant elevations over the transverse section of the dam. The details regarding maximum displacements and stresses are highlighted after critically examining the results obtained.

The behaviour has been studied at three different cross sections, Plane 1 to 3 as shown in Fig.5.2(a). The study at plane 1 enables to analyse the dam at maximum height. The study at plane 2 and 3 are representative of the behavior on sections towards the abutment.

The displacements and stresses were studied at five interfaces henceforth called verticals; one each in upstream and downstream shell, one each in upstream and downstream interface of filter and core and one in the centre line of core. Figure 5.2(b) elaborates the interfaces chosen for the study. The distribution pattern along horizontal planes has been studied at ground level and at elevations 24 m, 44 m, 62 m, 76 m, 87 m, 95 m and 100 m above ground level.

#### **5.4. MATERIAL PROPERTIES**

The properties of the material used in the analysis are given in Table 5.1. These properties are the same as used by Szostak-Chrzanowski et.al. (2001) for analysis of West dam, Diamond Valley Lake Project, US.

Table 5.1. Material Properties

No	Parameters	Shell	Filter	Core
1	Unit Weight $\gamma$ , kN/m <sup>3</sup>	20.00	20.54	22.12
2	Cohesion C, kN/m <sup>2</sup>	-	-	60.00
3	Friction angle $\phi$ , deg	45.00	47.00	38.00
4	Modulus Number K	500.00	560.00	500.00
5	Modulus exponent n	0.50	0.48	0.55
6	Bulk Modulus Num. Kb	300.00	330.00	210.00
7	Bulk Mod. Exp. m	0.35	0.33	0.40
8	Failure Ratio	0.70	0.65	0.65
9	Young Mod. E, kN/m <sup>2</sup>	50,000.00	90,000.00	42,000.00

### 5.5. SIGN CONVENTION

The following sign convention has been followed in this study.

The positive x-direction is from upstream to downstream along the river, positive y-direction is from downward to upward along the height of the dam and positive z-direction from the abutment to the central section along the dam axis as indicated in Fig.5.4.

The displacements u and v are positive in the positive x and y directions respectively.

The normal stresses  $\sigma_x$  in the transverse direction and  $\sigma_y$  in the vertical direction are positive if tensile and negative if compressive.

### 5.6. RESULTS OF ANALYSIS

In this chapter the stress and displacement contours of the maximum height dam section for the three cases defined in Para 5.3 are presented and discussed. The pattern of contours of the stresses and displacement at other sections and verticals will be similar nature. These are discussed in more detail in the next chapter.

### 5.6.1. CASE I

The displacements and stresses by 3-D non linear single lift and non linear sequential seven stages analysis of the dam at end of construction are presented in this case. Zero displacement at the base and along the abutments of the dam has been considered as the boundary condition.

#### **Horizontal Displacements:**

The contours of horizontal displacement -  $u$  over the transverse section by 3-D non linear single lift and seven lifts analysis are shown in Fig.5.5 and 5.6. The variation of the displacement in each zone is shown in the legend in the figure. The maximum movement is attained at two locations such as the face of upstream and downstream shell having magnitudes of 0.0467 m and 0.0471 m respectively by single lift analysis and at the mid height of upstream and downstream shell having magnitude of 0.0462 m and 0.0481 m respectively by seven lifts analysis. The pattern of the distribution of horizontal displacement -  $u$  observed in the two cases is similar and the magnitude also does not differ significantly. The movement in both cases also similar with in the upstream shell move toward upstream direction and in the downstream shell move toward downstream direction.

#### **Vertical Displacements:**

The contours of vertical displacement -  $v$  over the transverse section by 3-D non linear single lift and seven lifts analysis are shown in Fig.5.7 and 5.8. The maximum movement is attained at the top of the dam having a magnitude of 0.2905 m by single lift and at two third of the height of the dam with a

### 5.6.2. CASE II

The parameter such as displacements and stresses studied; by 3-D non linear single lift construction of the dam with one stage of full reservoir filling and four stages of reservoir filling is presented here.

#### **Horizontal Displacements:**

The contours of horizontal displacement -  $u$  over the transverse section by 3-D non linear single lift construction of the dam with one stage of full reservoir filling and four stages of reservoir filling analysis are shown in Fig.5.13 and 5.14. The dam is observed to move in downstream direction from the entire of upstream filter towards downstream shell. The maximum movement is attained at two locations, 0.0642 m in the upstream face of the shell move towards upstream direction and 0.0575 m in the downstream face of the shell move towards downstream direction for one stage of full reservoir filling analysis and at the mid height of the face of the upstream shell and the crest of the face of downstream shell with a magnitude of 0.0522 m move towards upstream direction and 0.0699 m move towards downstream direction respectively for four stage reservoir filling analysis.

#### **Vertical Displacements:**

The contours of vertical displacement -  $v$  over the transverse section by 3-D non linear single lift construction of the dam with one stage of full reservoir filling and four stages of reservoir filling analysis are shown in Fig.5.15 and 5.16. The maximum settlement is attained at the upstream face of the shell zones near the abutments having a magnitude of 0.3852 m

and 0.3767 m for single stage and four stage of full reservoir filling respectively. This upper part of the core also experience considerable settlement (0.28 m) in both cases. However the downstream shell is not affected.

#### **Horizontal Normal Stress:**

The contours of horizontal normal stress ( $\sigma_x$ ) over the transverse section by 3-D non linear single lift construction of the dam with one stage of full reservoir filling and four stages of reservoir filling analysis are shown in Fig.5.17 and 5.18. The maximum horizontal normal stress is attained at the base of upstream and downstream shell having magnitude of -34.382 t/m<sup>2</sup> and -35.327 t/m<sup>2</sup> by one stage full and four stages full reservoir filling respectively. At the base of the core, the horizontal normal stress is of the order of -25 t/m<sup>2</sup> in both cases and it decreasing with the height. The location of maximum tension having a magnitude of 2.1 t/m<sup>2</sup> to 3.8 t/m<sup>2</sup> has been found at the crest of the dam near the abutments for both cases. It is seen to spread on upstream and downstream faces of the dam.

#### **Vertical Normal Stress:**

The contours of vertical normal stress ( $\sigma_y$ ) over the transverse section by 3-D non linear single lift construction of the dam with one stage of full reservoir filling and four stages of reservoir filling analysis are shown in Fig.5.19 and 5.20. The zone of maximum vertical normal stress is attained at the base of upstream shell and core having a magnitude of -97.134 t/m<sup>2</sup> by one stage full reservoir filling and -89.697 t/m<sup>2</sup> by four stages reservoir filling analysis. The stresses decrease

with the height reducing to a value about  $-20 \text{ t/m}^2$  near the crest of the dam. A tensile zone of magnitude around  $2.5 \text{ t/m}^2$  has been observed in both cases at the crest of upstream and downstream face of the dam. So at the interface of core with upstream and downstream shell, there is reversal of stress.

### **5.6.3. CASE III**

The results of the analysis for displacements and stresses by 3-D non linear seven lifts of construction of the dam with four stages of reservoir filling is presented in this chapter.

#### **Horizontal Displacements:**

The contours of horizontal displacement -  $u$  over the transverse section by 3-D non linear seven lifts construction of the dam with four stages of reservoir filling is shown in Fig.5.21. The dam is observed to move in downstream direction with only lower part of upstream shell tending to move in upstream direction. The maximum movement for downstream direction is attained at the mid height of upstream face of the core having a magnitude of  $0.0848 \text{ m}$ . The movement in upstream direction is attained at the one fourth height of the upstream shell near the face of the dam having magnitude of  $0.0478 \text{ m}$ .

#### **Vertical Displacements:**

The contours of vertical displacement -  $v$  over the transverse section by 3-D non linear seven lifts construction of the dam with four stages of reservoir filling is shown in Fig.5.22. The maximum movement is attained at about the mid height in the core at the upstream and downstream face having a

magnitude of 0.3112 m. The upstream and downstream shell experience little settlement.

**Horizontal Normal Stress:**

The contours of horizontal normal stress ( $\sigma_x$ ) over the transverse section by 3-D non linear seven lift construction of the dam with four stages of reservoir filling analysis is shown in Fig.5.23. The maximum horizontal normal stress is attained at the base of downstream face of the core having magnitude of -35.304 t/m<sup>2</sup>. It is observed from the figure that the zone of compression is concentrated in the base of the dam and the core portion and also in the downstream shell. It keeps on decreasing towards the upstream and downstream face of the dam. The zone of maximum tension occurs at the upstream and downstream face close to the abutments having a maximum magnitude upto 7.956 t/m<sup>2</sup>.

**Vertical Normal Stress:**

The contours of vertical normal stress ( $\sigma_y$ ) over the transverse section by 3-D non linear seven lifts construction of the dam with four stages of reservoir filling analysis is shown in Fig.5.24. The maximum vertical normal stress is attained at the base of the core and downstream shell zone having a magnitude of -99.689 t/m<sup>2</sup>. It is seen reducing symmetrically with increase in elevation. A tensile zone of magnitude upto 2.3 t/m<sup>2</sup> has been observed in the whole area of upstream and downstream face of the dam.

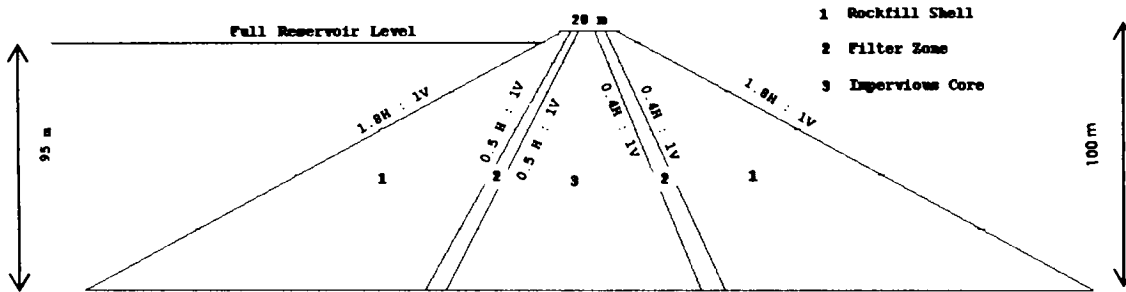


Fig.5.1. Section of 100 m High Earth and Rockfill Dam

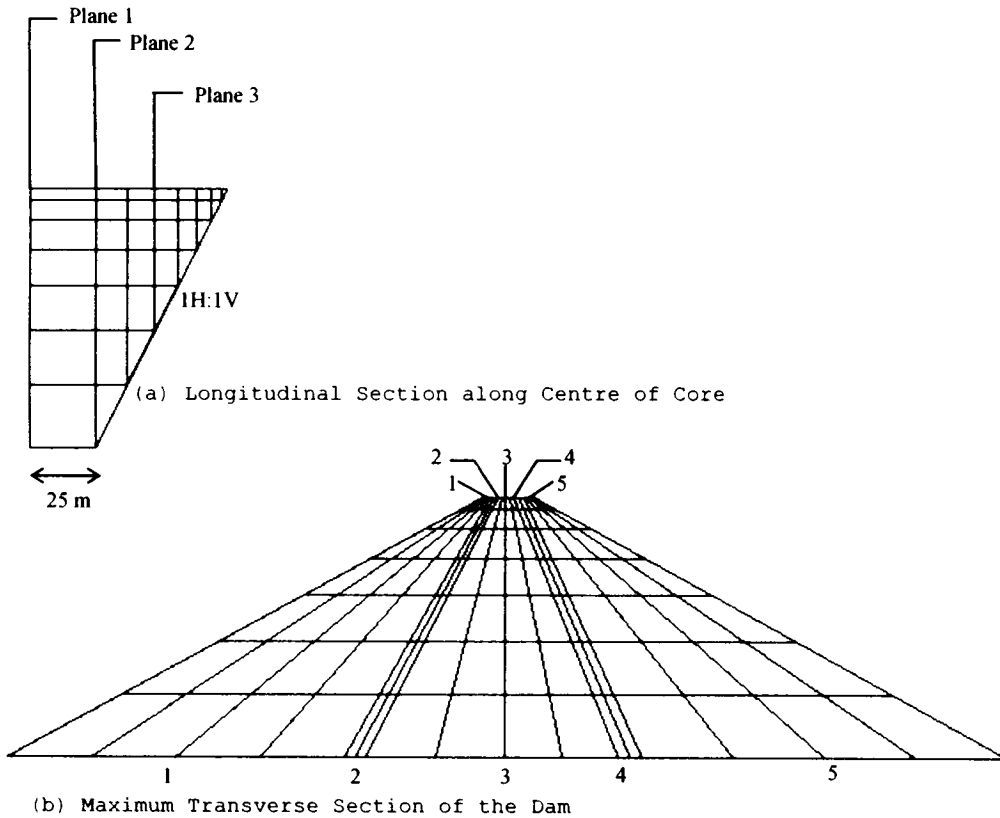


Fig.5.2. Finite Element Idealisation of the Dam

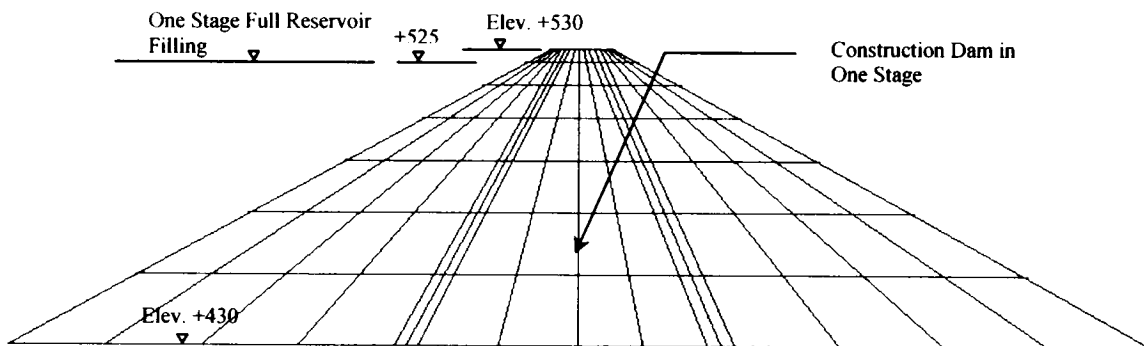


Fig.5.3(a). One Stage of Construction Dam and One Stage Full Reservoir Filling



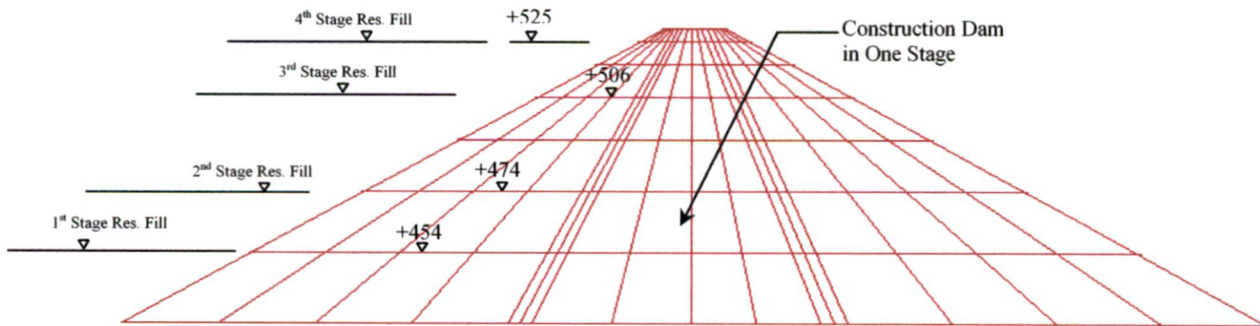


Fig.5.3(b). One Stage of Construction Dam and Four Stages Reservoir Filling

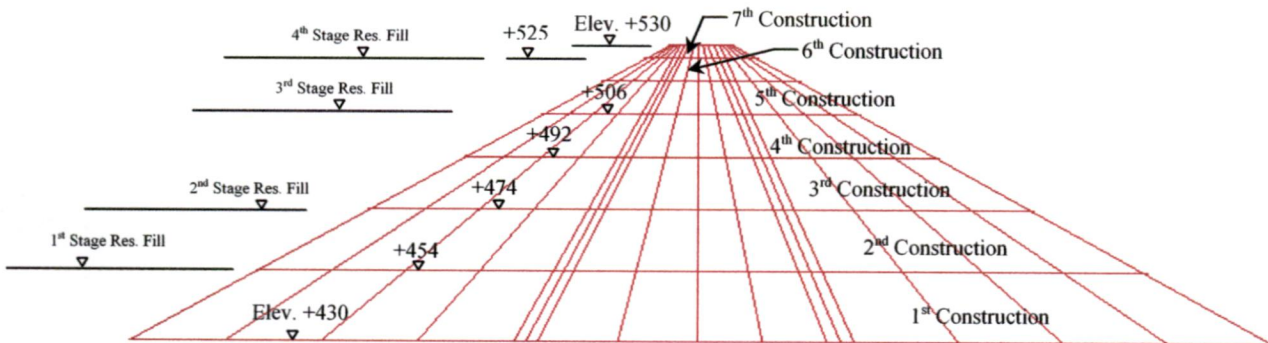


Fig.5.3(c). Seven Stages of Construction Dam and Four Stages Reservoir Filling

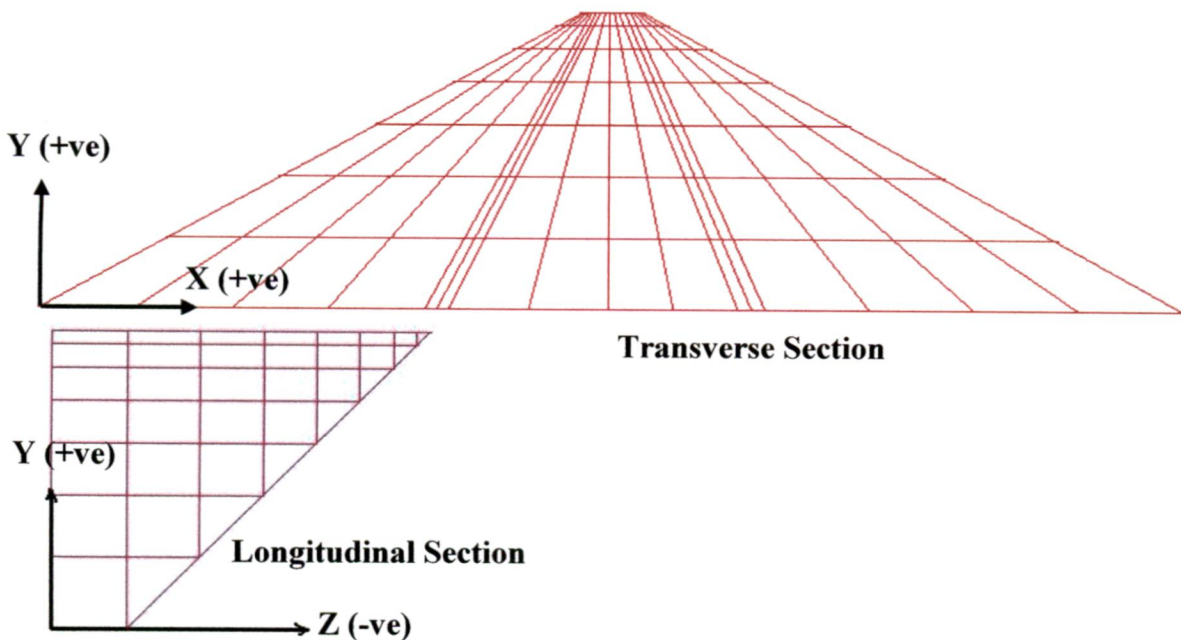


Fig.5.4. Sign Convention

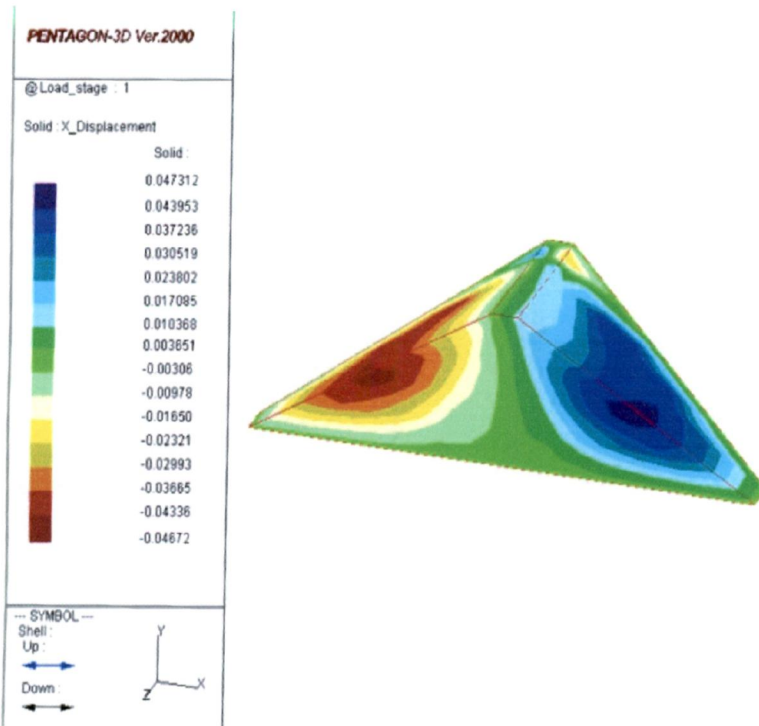


Fig.5.5. 3-D Horizontal Movement, End of Construction, Single Lift

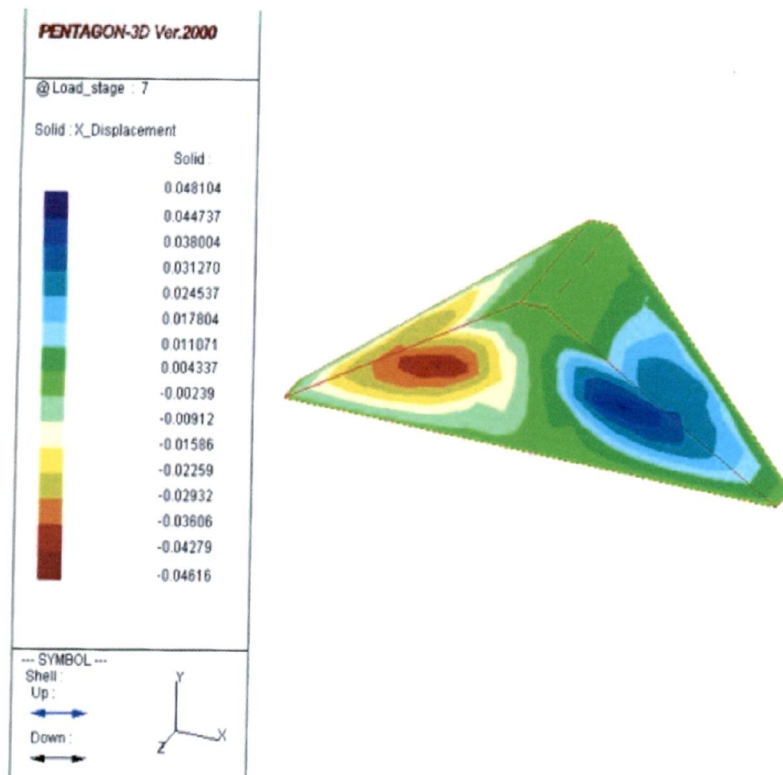


Fig.5.6. 3-D Horizontal Movement, End of Construction, Seven Lifts

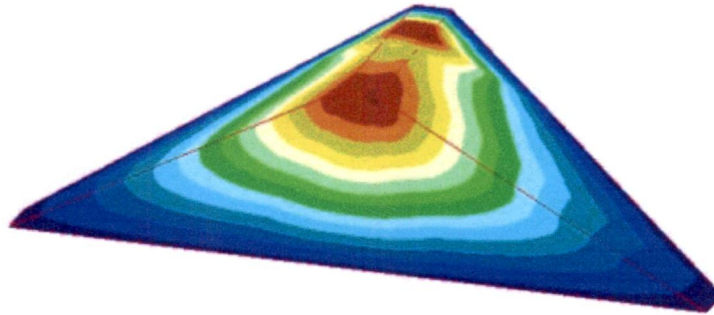
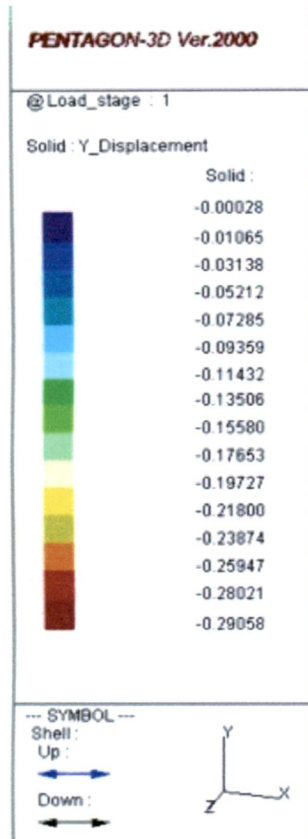


Fig.5.7. 3-D Vertical Movement, End of Construction, Single Lift

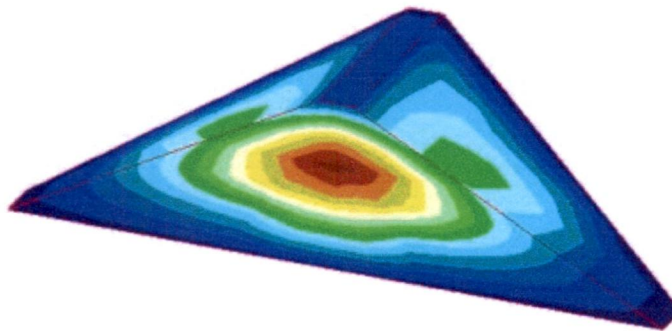
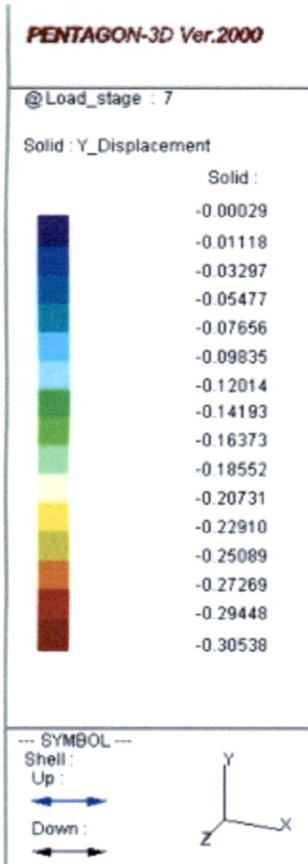


Fig.5.8. 3-D Vertical Movement, End of Construction, Seven Lifts

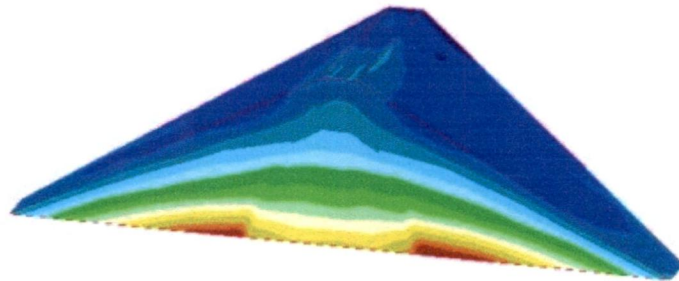
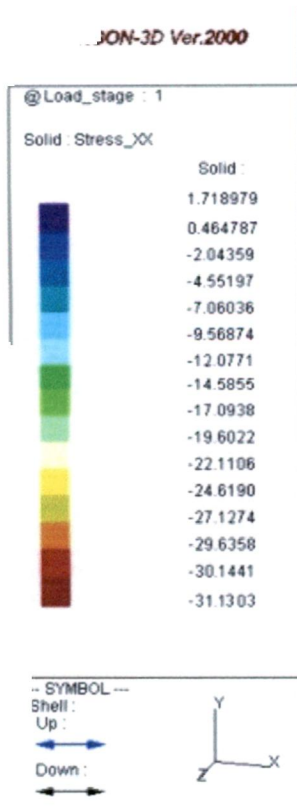


Fig.5.9. 3-D Horizontal Normal Stress, End of Construction, single Lift

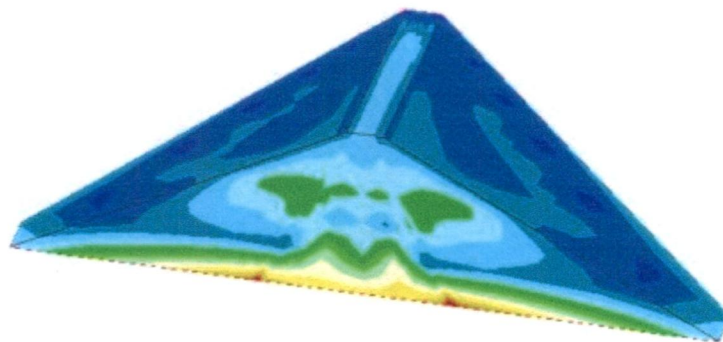
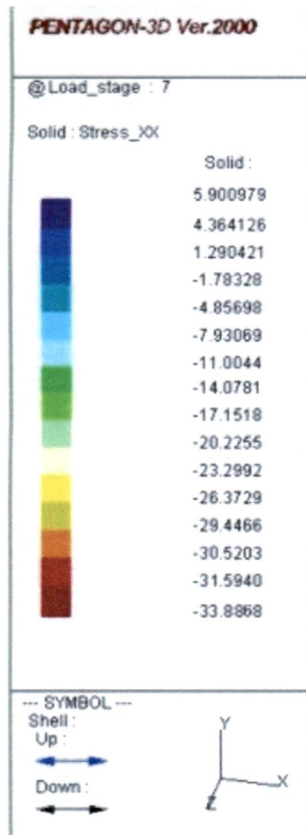


Fig.5.10. 3-D Horizontal Normal Stress, End of Construction, Seven Lifts

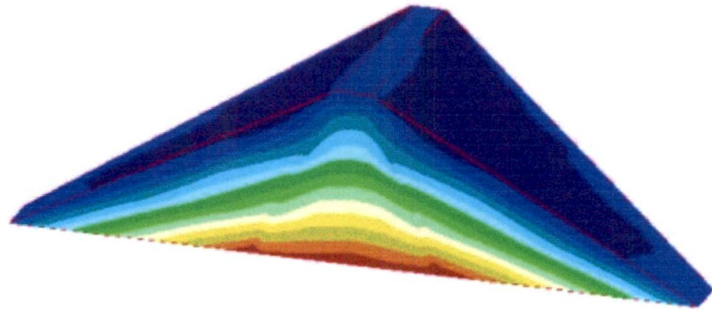
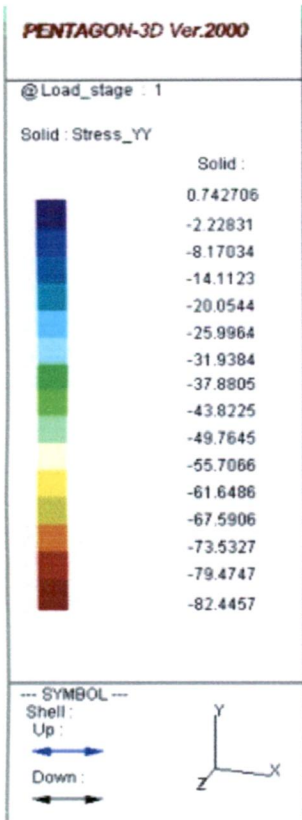


Fig.5.11. 3-D Vertical Normal Stress, End of Construction, Single Lift

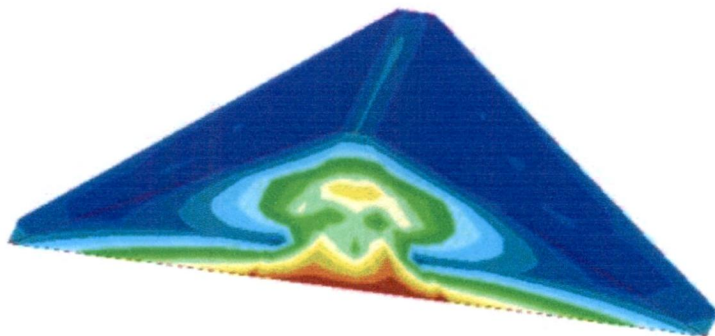
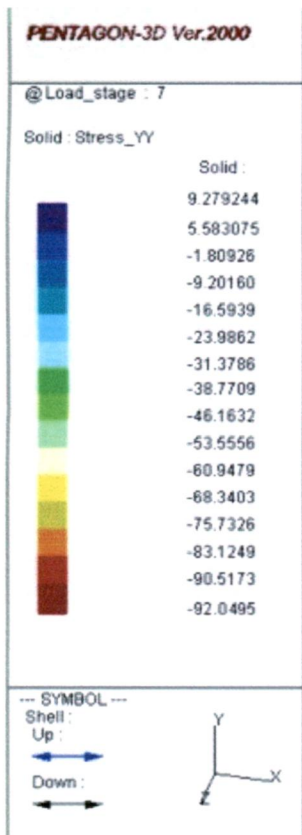


Fig.5.12. 3-D Vertical Normal Stress, End of Construction, Seven Lifts



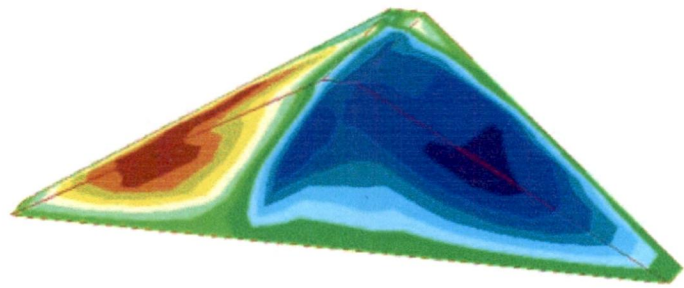
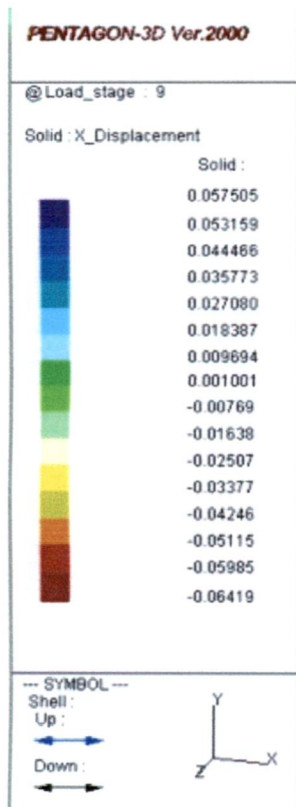


Fig.5.13. 3-D Horizontal Movement, Full Reservoir Filling, One Stage Full Reservoir

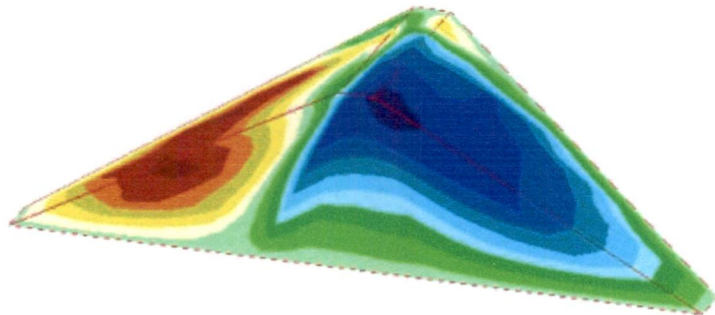
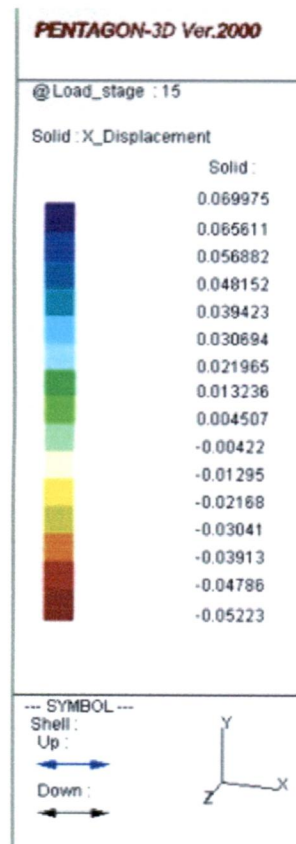


Fig.5.14. 3-D Horizontal Movement, Full Reservoir Filling, Four Stages Full Reservoir

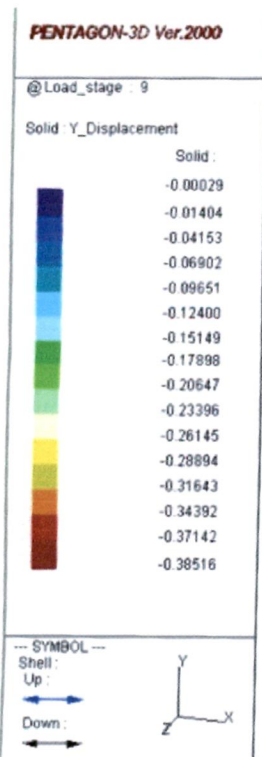


Fig.5.15. 3-D Vertical Movement, Full Reservoir Filling, One Stage Full Reservoir

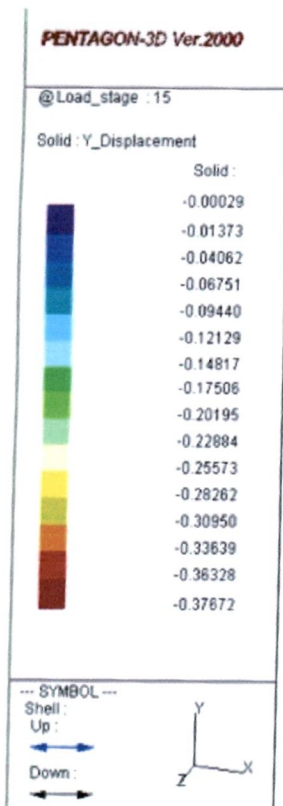


Fig.5.16. 3-D Vertical Movement, Full Reservoir Filling, Four Stages Full Reservoir

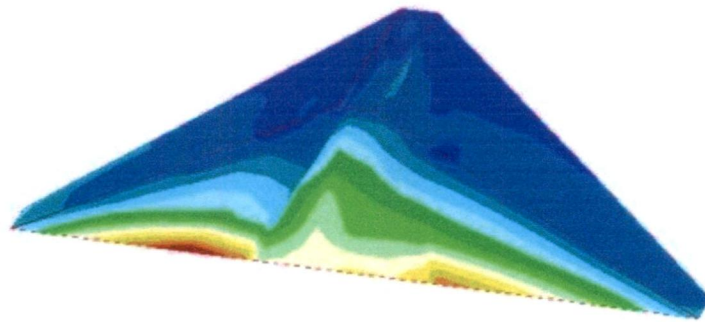
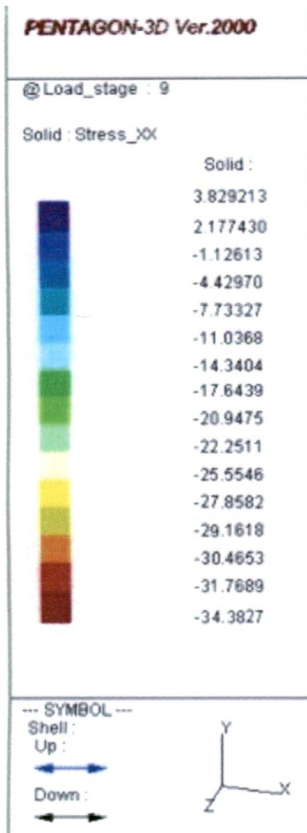


Fig.5.17. 3-D Horizontal Normal Stress, Full Reservoir Filling, One Stage Full Reservoir

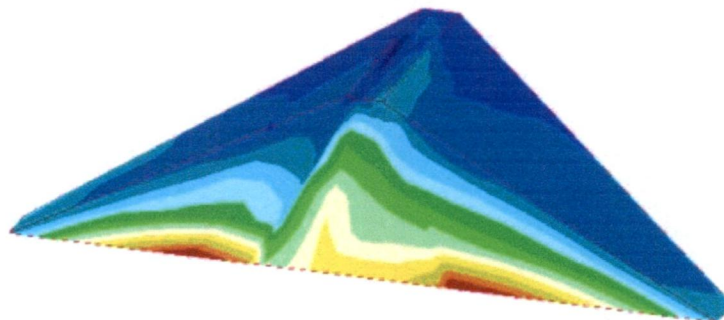
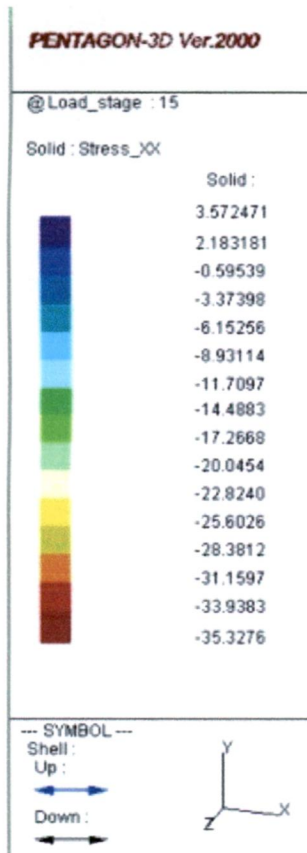


Fig.5.18. 3-D Horizontal Normal Stress, Full Reservoir Filling, Four Stages Full Reservoir



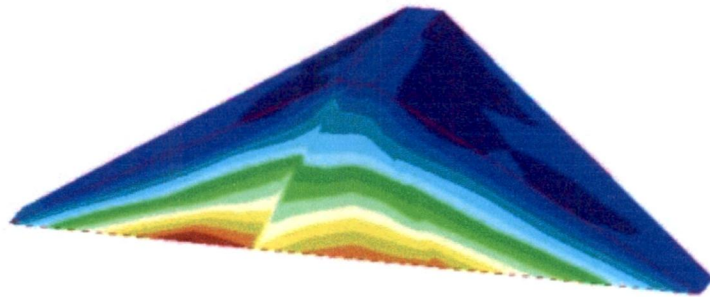
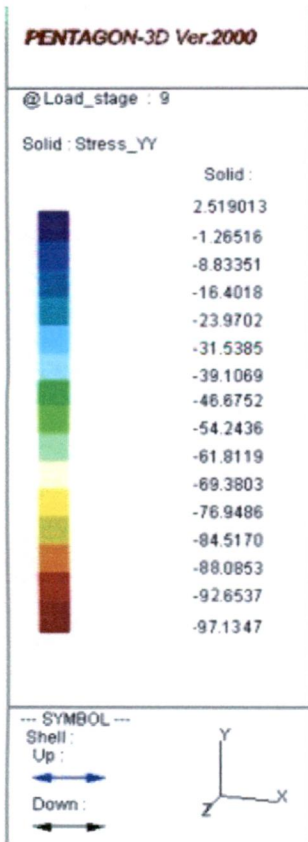


Fig.5.19. 3-D Vertical Normal Stress, Full Reservoir Filling, One Stage Full Reservoir

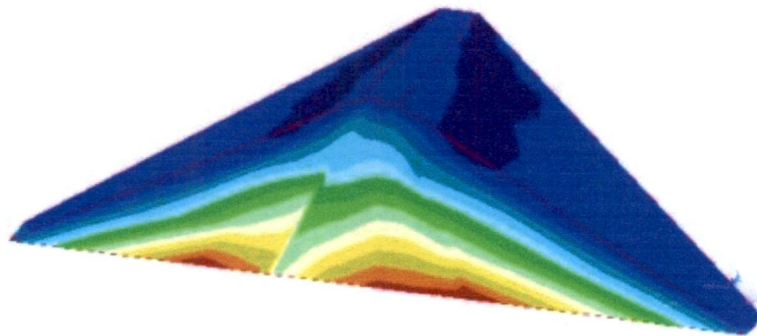
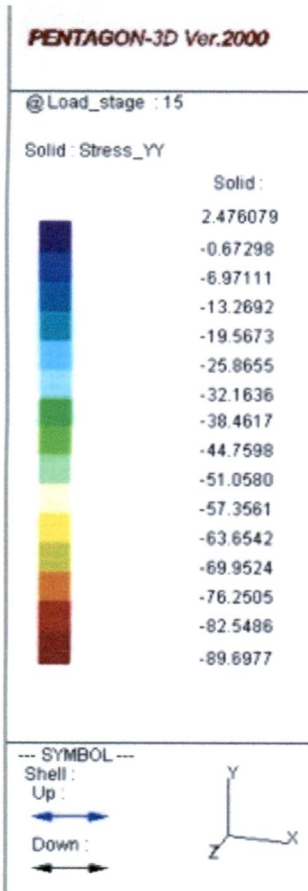


Fig.5.20. 3-D Vertical Normal Stress, Full Reservoir Filling, Four Stages Full Reservoir

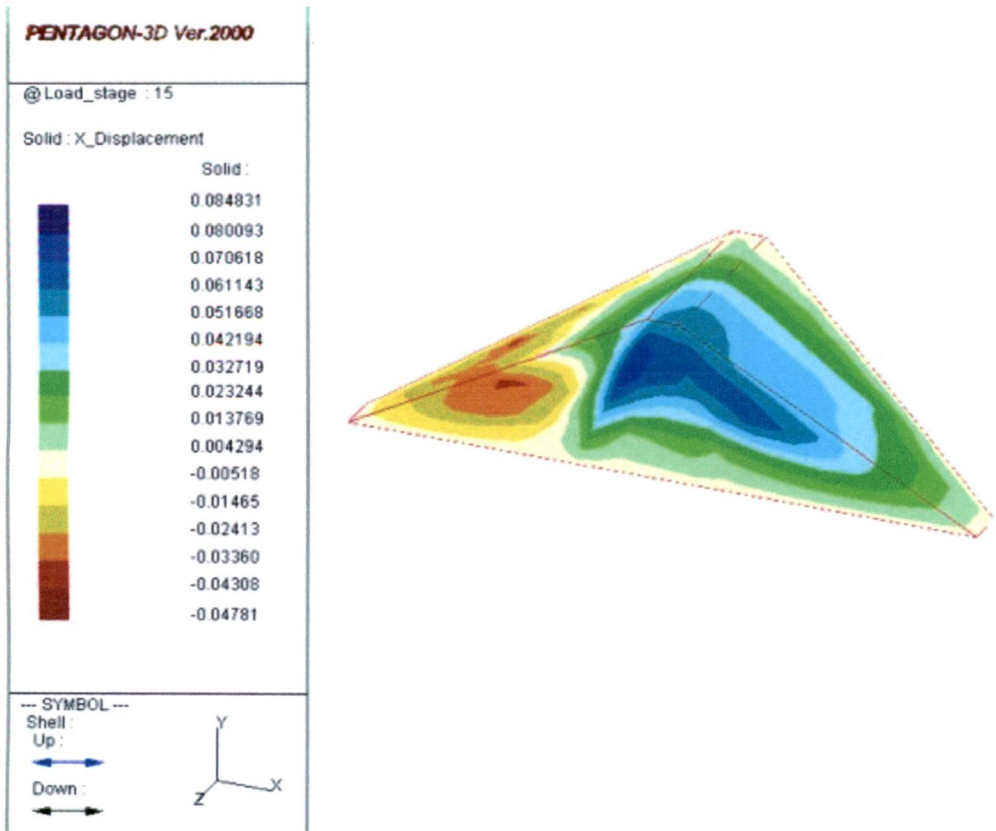


Fig.5.21. 3-D Horizontal Movement, Full Reservoir Filling, Seven Lifts Construction Four Stages Reservoir Filling

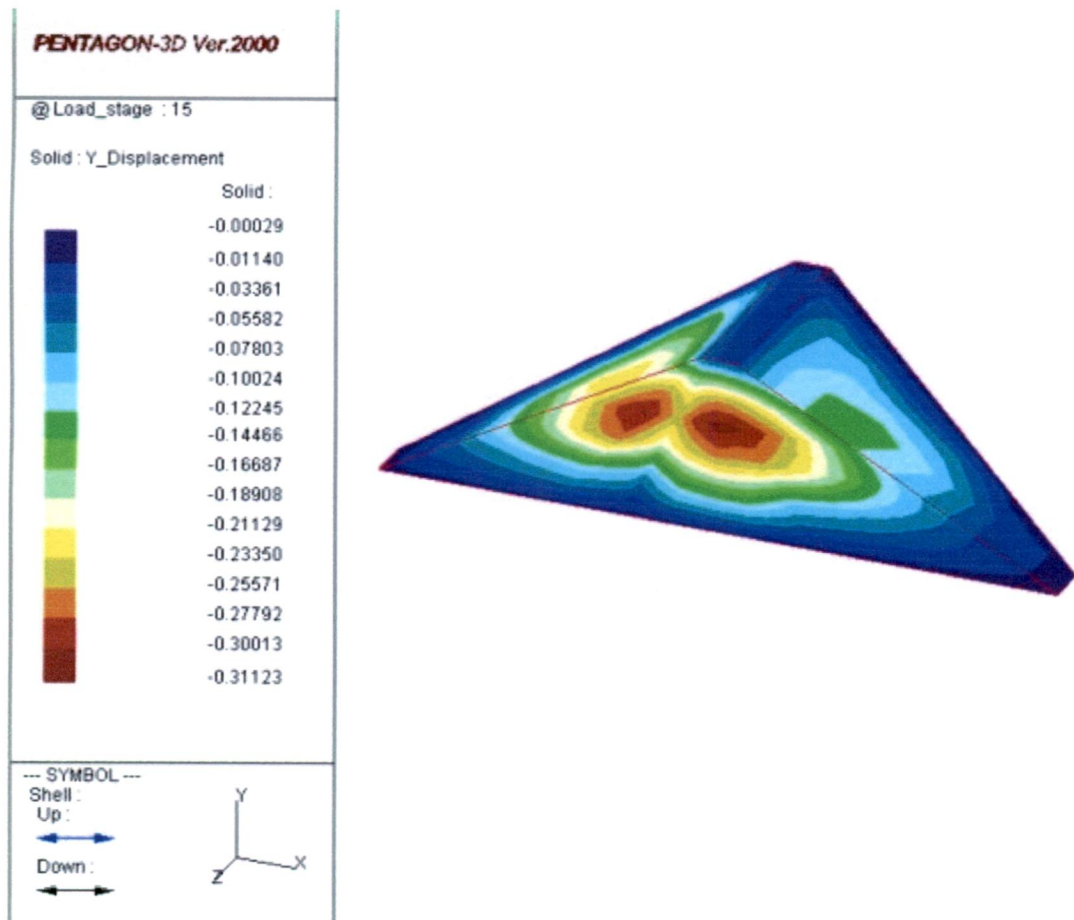


Fig.5.22. 3-D Vertical Movement, Full Reservoir Filling, Seven Lifts Construction Four Stages Reservoir Filling

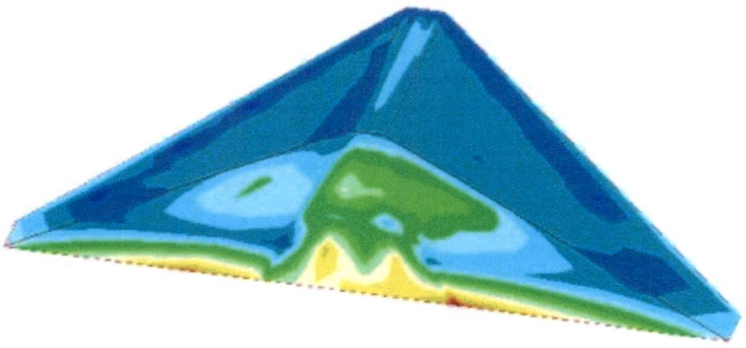
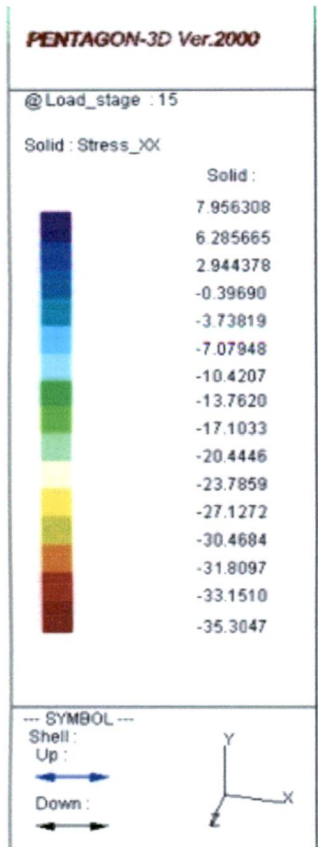


Fig.5.23. 3-D Horizontal Normal Stress, Full Reservoir Filling, Seven Lifts Construction Four Stages Reservoir Filling

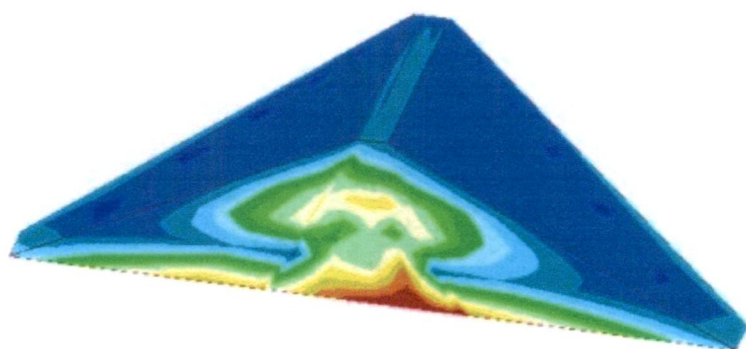
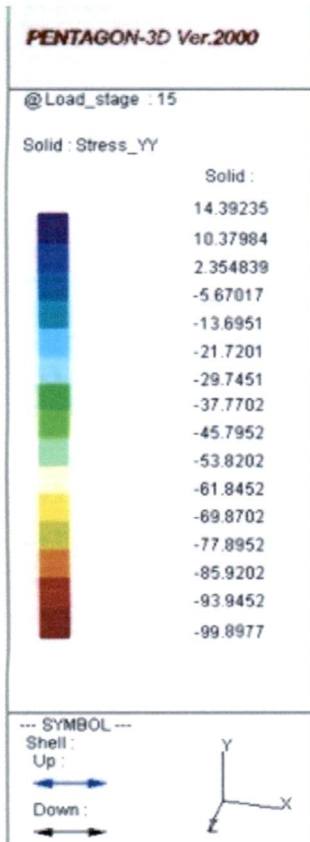


Fig.5.24. 3-D Vertical Normal Stress, Full Reservoir Filling, Seven Lifts Construction Four Stages Reservoir Filling

## CHAPTER 6

### DISCUSSION OF RESULTS

The contours for displacements and stresses for maximum height section as obtained by FEM analysis for the three cases are given in Chapter 5. The results at various sections and verticals for the three cases are discussed below.

#### 6.1. DISCUSSION OF RESULTS OF CASE I STUDY

The displacements and stresses in respect of Case I are discussed over Plane 1, Plane 2 and Plane 3 in following paragraph.

##### 6.1.1. Plane 1 (Maximum Height Section)

##### 6.1.1.1. Horizontal Displacements - u

1. The contours of horizontal displacements by single lift and seven lifts, shown in Fig.5.5 and 5.6 and described in Para 5.6.1., show that the displacements are almost symmetrical for both upstream and downstream faces of the dam. The displacement of this two faces is opposite to each other.
2. Figure 6.1 shows the variation of horizontal displacement along the height of Plane 1 for single lift and seven lifts over five interfaces. The pattern is similar for both analyses. It is seen from the figure that the values of horizontal displacements are maximum at mid height in the upstream and downstream shells and it is negligible in the core in both cases.
3. It is observed that the horizontal displacement in the top 20 m height does not take place in case of seven lifts case unlike the single lift case.

4. The maximum horizontal displacements values for single lift and seven lifts for five different interfaces are also tabulated in Tab.6.1. The upstream and downstream shell has the highest value of 4.01 cm for single lift analysis and around 4.61 cm for seven lift analysis. Finding reveals that the magnitude in seven lifts case is slightly higher than the magnitude in single lifts.

#### 6.1.1.2. Vertical Displacements - v

1. Figure 5.7 and 5.8 shows the contours of vertical displacement by single lift and seven lifts analysis at end of construction. It is seen from the figures that the maximum displacement is found at the top of the dam for single lift analysis and at the mid height of the dam for seven lifts analysis.
2. Figure 6.2 shows the variation of vertical displacement along the height of Plane 1 for single lift and seven lifts over five interfaces. It is seen from the figure that the magnitude of vertical displacement by single lift analysis keeps on increasing upto the top of the dam while the magnitude in the seven lifts analysis keeps on increasing up to mid height from the base of the dam and then decrease towards the crest of the dam.
3. The maximum vertical displacement (settlement) values for single lift and seven lifts analysis for five different interfaces are also tabulated in Tab.6.2. It is observed that the magnitude of maximum displacement at all the five interfaces for single lift case are practically same ranging between 27.4-28.4 cm on the top of the dam while for seven

lifts analysis the highest magnitude of 30.54 cm, is found at the centre line of core (vertical 3).

#### 6.1.1.3. Horizontal Normal Stress - $\sigma_x$

1. The contours of horizontal normal stress by single lift and seven lifts at end of construction are shown in Fig.5.9 and 5.10 respectively. The stress distribution for single lift analysis shows the maximum stress at the base under the shell zones at the interface with core. It is seen reducing towards shell interfaces and also in the upwards with minimum at the crest where it becomes tensile. The distribution for seven lifts analysis shows maximum stresses at the base of the core reducing with the height. Thus in this case the core is more stresses. The zone of tensile stresses on shell surface has also reduced in this case.
2. Figure 6.3 shows the variation of horizontal normal stress along the height of Plane 1 for single lift and seven lifts over five interfaces. It is seen from the figure that the pattern of the curve of  $\sigma_x$  by single lift analysis is almost similar with seven lift analyses. The maximum stress for all the five interfaces is found at the base of the dam and it decreased towards the top of the dam. The stresses at the crest in all five interfaces is found compressive.
3. The maximum horizontal normal stress for single lift and seven lifts analysis for five different interfaces are tabulated in Tab.6.3. The maximum values of  $\sigma_x$  are -31.13 t/m<sup>2</sup> and -33.88 t/m<sup>2</sup> for single lift and seven lifts analyses respectively were found at the base of downstream face of the core (vertical 4).

#### 6.1.1.4. Vertical Normal Stress - $\sigma_y$

1. The contours of horizontal normal stress by single lift and seven lifts at end of construction are shown in Fig.5.11 and 5.12 respectively. It is seen from the figure that the stresses are very low at the dam faces for both analysis; increases gradually towards the interior of the shell for single lift analysis while the low stresses still found at the lower one third of the height at the shell zones for seven lifts analysis.
2. From the contours plot, the maximum stresses are observed at the base of the dam and in or at the upstream and downstream face of the core. A tension zone is seen at the top of the dam and extending towards upstream and downstream face of the dam.
3. Figure 6.4 shows the variation of vertical normal stress along the height of Plane 1 for single lift and seven lifts over five interfaces. It is seen from the figure that the pattern of the curve of  $\sigma_y$  by single lift analysis is almost similar to seven lift analyses in the shell zones but has lesser values than seven lifts analysis in the core portion. The maximum stress for five interfaces is found at the base of the dam and seen decreasing towards the top of the dam.
4. The maximum vertical normal stress for single lift and seven lifts analysis for five different interfaces are tabulated in Tab.6.4. The maximum values of  $\sigma_y$  are -82.44 t/m<sup>2</sup> and -92.05 t/m<sup>2</sup> for single lift and seven lifts analyses respectively were found at the base of downstream face of the core (vertical 4).

### **6.1.2. Plane 2 (Maximum Height Section Adjacent to Valley Slope)**

#### **6.1.2.1. Horizontal Displacements - u**

1. Figure 6.5 shows the variation of horizontal displacement along the height of Plane 2 for single lift and seven lifts over five interfaces. The pattern is almost similar for both analyses. It is seen from the figure that the values of horizontal displacements are maximum in the shell and negligible in the core. The pattern is similar to that in Plane 1.
2. The maximum horizontal displacements values for single lift and seven lifts for five different interfaces are tabulated in Tab.6.5. The upstream and downstream shell has the highest value with 3.77 cm for single lift analysis and around 4.81 cm for seven lift analysis. The magnitude of seven lifts is higher than the magnitude of single lift case and it is noted that the displacement values on Plane 2 are slightly reduced from the values of Plane 1.

#### **6.1.2.2. Vertical Displacements - v**

1. Figure 6.6 shows the variation of vertical displacement (settlement) along the height of Plane 2 for single lift and seven lifts over five interfaces. It is seen from the figure that the magnitude of vertical displacement by single lift analysis keeps on increasing upto the top of the dam while the magnitude in the seven lifts analysis keeps on increasing up to 60 m height from the base of the dam and then decrease towards the crest of the dam. The pattern is similar to that obtained fro Plane 1.



2. The maximum vertical displacement values for single lift and seven lifts analysis for five different interfaces are tabulated in Tab.6.6. It is observed that the magnitude of maximum displacement at five interfaces for single lift is 26.98 cm on the top of the dam while for seven lifts analysis the highest maximum magnitude, 30.17 cm, is found at centre line of core (vertical 3). It is noted that the values on Plane 2 are practically same as for Plane 1.

#### 6.1.2.3. Horizontal Normal Stress - $\sigma_x$

1. Figure 6.7 shows the variation of horizontal normal stress along the height of Plane 2 for single lift and seven lifts over five interfaces. It is seen from the figure that the pattern of the curve of  $\sigma_x$  by single lift analysis is almost similar with seven lift analyses at all the verticals except in the upstream and downstream face of the core where the single lift case has shown higher stresses in the middle third height than the seven lift analysis. The maximum stress for all the five interfaces is found at the base of the dam reducing sharply in bottom 20 m height and there after reducing gradually to a small value at the top of the dam.
2. The maximum horizontal single lift and seven lifts analysis for five different interfaces are tabulated in Tab.6.7. The maximum values of  $\sigma_x$  are -30.65 t/m<sup>2</sup> and -33.04 t/m<sup>2</sup> were found at the vertical centre of the core and the base of downstream face of the core (vertical 4) for single lift and seven lifts analyses respectively. It is noted that the

values on Plane 2 are slightly less than the values obtained for Plane 1.

#### **6.1.2.4. Vertical Normal Stress - $\sigma_y$**

1. Figure 6.8 shows the variation of vertical normal stress along the height of Plane 2 for single lift and seven lifts over five interfaces. It is seen from the figure that the pattern of the curve of  $\sigma_y$  by single lift analysis is almost similar with seven lift analyses in both the shell zone. It is also similar at the upstream and downstream face of the core. At the vertical through the core the vertical normal stress in seven lifts analysis is higher than the single lift analysis. The maximum values for five interfaces is found at the base of the dam which sharply decreased upto 20 m height and thereafter reduced gradually to a small value at the top of the dam.
2. The maximum vertical normal stress for single lift and seven lifts analyses for five different interfaces are tabulated in Tab.6.8. The maximum values of  $\sigma_y$  are -81.36 t/m<sup>2</sup> and -89.82 t/m<sup>2</sup> for single lift and seven lifts analyses respectively. These are found at the base of centre of the core (vertical 3). It is noted that the values on Plane 2 are slightly less than the values of Plane 1.

#### **6.1.3. Plane 3 (A Section in the Middle of Valley Shape)**

##### **6.1.3.1. Horizontal Displacements - u**

1. Figure 6.9 shows the variation of horizontal displacement along the height of Plane 3 for single lift and seven lifts over five interfaces. The pattern of displacement for single lift is similar to seven lifts analysis and also similar to

- that at Plane 1 and 2. It is seen from the figure that the values of horizontal displacements is maximum in both the shell zones at the mid height and is negligible in the core.
2. The maximum horizontal displacements values for single lift and seven lifts for five different interfaces are tabulated in Tab.6.9. The upstream and downstream shell has the highest value of 3.50 cm for single lift analysis and around 2.55 cm for seven lift analysis. The magnitude in case of seven lifts is less than the magnitude of single lift and it is noted that the values on Plane 3 are substantially less than those of Plane 1 because of the reduced height.

#### **6.1.3.2. Vertical Displacements - v**

1. Figure 6.10 shows the variation of vertical displacement along the height of Plane 3 for single lift and seven lifts analysis over five interfaces. It is seen from the figure that the vertical displacement by single lift analysis is maximum at the top starting from zero at the base at all the vertical interfaces. In case of seven lifts analysis the vertical displacement increasing from the base to the maximum at the mid height and then reduced to zero at the top. This pattern was also observed in case Plane 1 and 2.
2. The maximum vertical displacements values for single lift and seven lifts analyses for five different interfaces are tabulated in Tab.6.10. It is observed that the highest magnitude of maximum displacement for single lift is 22.97 cm on the top of the dam while for seven lifts analysis the highest maximum magnitude, 17.57 cm, is found at centre line of core (vertical 3). It is noted that the values on Plane 3 are reduced at about 57-77% of the values of Plane 1.

### 6.1.3.3. Horizontal Normal Stress - $\sigma_x$

1. Figure 6.11 shows the variation of horizontal normal stress along the height of Plane 3 for single lift and seven lifts over five interfaces. It is seen from the figure that the pattern of the curve of  $\sigma_x$  by single lift analysis is close to the tensile zone from the top of the dam down to the mid height of the abutment and slightly increases towards the compression zone. In case of seven lifts analysis, the tensile stress appears at the mid height of the abutment and increase to the compression stress towards the base of the abutment. The maximum value of compression stress is obtained at the base of abutments for all interfaces.
2. The maximum horizontal normal stress for single lift and seven lifts analysis for five different interfaces are tabulated in Tab.6.11. The maximum values of  $\sigma_x$  are -19.07 t/m<sup>2</sup> and -19.09 t/m<sup>2</sup> were found at the centre of the core and the base of downstream face of the core (vertical 4) for single lift and seven lifts analyses respectively. It is noted that the values on Plane 3 are reduced about 21-26% from the values of Plane 1.

### 6.1.3.4. Vertical Normal Stress - $\sigma_y$

1. Figure 6.12 shows the variation of vertical normal stress along the height of Plane 3 for single lift and seven lifts over five interfaces. It is seen from the figure that the stress pattern of  $\sigma_y$  by single lift analysis is increase towards the base of the abutments while the stress pattern of seven lift analysis tend to move to the tensile zone at about one third height from the base of the abutments and

rapidly increase to the compression zone at the base of the abutments.

2. The maximum vertical normal stress for single lift and seven lifts analysis for five different interfaces are tabulated in Tab.6.12. The maximum values of  $\sigma_y$  are  $-72.84 \text{ t/m}^2$  and  $-71.84 \text{ t/m}^2$  for single lift and seven lifts analyses respectively were found at the base of centre of the core (vertical 3). It is noted that the values on Plane 3 are reduced about 36-42% from the values of Plane 1.

## 6.2. DISCUSSION OF RESULTS OF CASE II STUDY

The displacements and stresses in Plane 1, Plane 2 and Plane 3 for Case II are discussed in following paragraphs.

### 6.2.1. Plane 1

#### 6.2.1.1. Horizontal Displacements - u

1. Figure 5.13 and 5.14 shows the contours of horizontal displacements by single stage and four stages reservoir filling respectively. It is seen from the figure that the displacement from the upstream face of the core and small part of upstream shell tend to move towards downstream direction while the upstream shell zone tends to move in upstream direction in both case of reservoir filling.
2. The maximum displacement for one stage full reservoir filling is observed at the mid height of downstream shell zone and for four stages the maximum displacement is observed at the top of downstream shell zone near the core. The magnitude of horizontal displacement of downstream shell for four stages reservoir filling is more than one stage full reservoir analysis.

3. Figure 6.13 shows the variation of horizontal displacement along the height of Plane 1 for one stage and four stages of reservoir filling over five interfaces. The displacements are in the downstream direction for four interfaces except for the upstream shell (vertical 1) which shows displacement in the upstream direction. This confirms the trend shown by the contours. It is seen from the figure that the magnitude of horizontal displacements for four stages of reservoir filling is higher than one stage full reservoir filling.
4. The maximum horizontal displacements values for one stage and four stages of reservoir filling for five different interfaces are tabulated in Tab.6.13. The maximum displacement in the upstream shell is 4.25 cm towards upstream direction at one third height from the base and 5.39 cm towards downstream direction at vertical 5 at one third height from the top for one stage full reservoir filling. The maximum displacement at four stages reservoir filling in the upstream direction in the upstream shell is 3.86 cm and it is 6.99 cm towards downstream direction in downstream shell. The location of the maximum displacement is the same as for one stage filling.

#### **6.2.1.2. Vertical Displacements - v**

1. Figure 5.15 and 5.16 shows the contours of vertical displacement by one stage and four stages reservoir filling analysis with one lift construction of the dam. It is seen from the figures that the maximum vertical displacement (settlement) is found in the upstream shell near the top of the dam for both cases. The magnitude of one stage full

reservoir is slightly more than four stages reservoir filling.

2. Figure 6.14 shows the variation of vertical displacement along the height of Plane 1 for one stage and four stage of reservoir filling over five interfaces respectively. It is seen from the figure that one stage reservoir filling has higher values of settlement than four stages reservoir filling. The magnitude of vertical displacement for both cases keeps on increasing from the base to the maximum at the top of the dam.
3. The maximum vertical displacements values for one stage and four stages of reservoir filling analysis for five different interfaces are tabulated in Tab.6.14. It is observed that the magnitude of maximum displacement at five interfaces for one stage full reservoir filling is 34.07 cm in the upstream shell zone at the top whereas for four stages analysis the highest magnitude is 34.75 cm, which is also found at the upstream shell (vertical 1). The entire core at the top in 15 m depth has a settlement at about 30 cm.

#### **6.2.1.3. Horizontal Normal Stress - $\sigma_x$**

1. The contours of horizontal normal stress by one stage and four stages reservoir filling are shown in Fig.5.17 and 5.18 respectively. The stress distribution for both the analyses is found to be similar. The stress distribution on the upstream shell is observed to decrease towards the upstream face of the core and then tends to increase in the core zone and thereafter it tends to decrease in downstream shell.

2. It is observed from those figures that the maximum value occurs in the base of the dam at the upstream and downstream face of the core extending towards the mid of shell zone. The tension zone has appeared near the abutment, extending to some portion of the upstream and downstream face of the dam. The magnitude of the tensile stress is found varying from 2.1 to 3.8 t/m<sup>2</sup>.
3. Figure 6.15 shows the variation of horizontal normal stress along the height of Plane 1 for one stage and four stages of reservoir filling over five interfaces. It is seen from the figure that the pattern of the curve of  $\sigma_x$  by both analyses is found similar. The stresses with one stage full reservoir are generally higher than four stages filling analysis in the lower half height of the dam and in the upper half the stresses in the two cases are practically same on all interfaces except vertical 5 (downstream shell) in the entire height of the dam, where the stresses in the two cases are same
4. At all interfaces except vertical 2 (upstream face of the core) the reservoir filling has increased the stress developed at the end of construction stage. At vertical 2 the end of construction stress are found to be reduced due to reservoir filling.
5. The maximum horizontal normal stress for one stage and four stages of reservoir filling analysis for five different interfaces are tabulated in Tab.6.15. The maximum values of  $\sigma_x$  are -34.38 t/m<sup>2</sup> and -35.33 t/m<sup>2</sup> for one stage and four stages reservoir filling analyses respectively at the base



of dam on downstream face of the core (vertical 4). The stresses in the shell zones are less than those in the core. These stresses reduce with the height and are minimum at the dam top.

#### 6.2.1.4. Vertical Normal Stress - $\sigma_y$

1. The contours of vertical normal stress by one stage and four stages of reservoir filling are shown in Fig.5.19 and 5.20 respectively. The stress distribution for both analyses is found to be similar. There is an abrupt change in stress pattern at the interface of upstream shell and core in both cases upto one third height above the base beyond that there is regular decreasing trend in rest two third heights in stress. It is seen from the figure that the stresses are very low at the dam faces for both cases of analysis. However, the maximum compressive stress is at the base under the upstream shell, downstream half of core base and the downstream shell.
2. A tension zone has appeared at the top of the dam and it has extended towards upstream and downstream faces of the dam in both cases.
3. Figure 6.16 shows the variation of vertical normal stress along the height of Plane 1 for one stage and four stages of reservoir filling over five interfaces. It is seen from the figure that the pattern of the curve of  $\sigma_y$  by one stage analysis has higher magnitude than four stages of reservoir filling at all the interfaces except the downstream shell when these are the same in both cases. The maximum for all

five interfaces is found at the base of the dam and found decreasing towards the top of the dam.

4. In all interfaces except vertical 5 (downstream shell) the filling of reservoir has increased the stresses of the end of construction stage. However the impact is more significant in upstream shell and upstream face of core.
5. The maximum vertical normal stress for one stage and four stages of reservoir filling analysis for five different interfaces are tabulated in Tab.6.16. The maximum values of  $\sigma_y$  are  $-97.13 \text{ t/m}^2$  and  $-89.69 \text{ t/m}^2$  for one stage and four stages reservoir filling analyses respectively were found at the base of upstream face of the core (vertical 2).

#### **6.2.2. Plane 2**

##### **6.2.2.1. Horizontal Displacements - u**

1. Figure 6.17 shows the variation of horizontal displacement along the height of Plane 2 for one stage and four stages of reservoir filling over five interfaces. The pattern is almost similar with the pattern of Plane 1 for both analyses. It is seen from the figure that the values of horizontal displacements for four stages of reservoir filling is higher than one stage full reservoir filling in the upper half of the dam height.
2. The maximum horizontal displacements values for one stage and four stages of reservoir filling for five different interfaces are tabulated in Tab.6.17. It is noted that for one stage full reservoir filling the upstream shell move towards upstream direction by 4.26 cm at the mid height and moves in the downstream in top 10 m height and the

downstream shell moves towards downstream direction by 5.46 cm. The deflection is maximum at mid height but the deflection remaining practically same in the upper half dam height. For four stages analysis, the movements are of the similar pattern. With one stage analysis with maximum value of displacement is 3.80 cm in upstream direction in upstream shell and 6.56 cm in downstream direction in downstream shell. It is seen that the displacement in Plane 2 are slightly less than the values of Plane 1.

#### 6.2.2.2. Vertical Displacements - v

1. Figure 6.18 shows the variation of vertical displacement along the height of Plane 2 for one stage and four stage of reservoir filling over five interfaces respectively. It is seen from the figure that the pattern of the curve is similar to Plane 1. One stage full reservoir filling has higher displacement values than four stages reservoir filling.
2. The maximum vertical displacements values for one stage and four stages analysis for five different interfaces are tabulated in Tab.6.18. It is observed that the magnitude of maximum displacement of the dam top at five interfaces for one stage full reservoir filling is 32.93 cm in the upstream shell zone while for four stages analysis maximum displacement is 34.36 cm, in the upstream shell (vertical 1). It is noted that the values on Plane 2 are slightly less than the values on Plane 1.

### 6.2.2.3. Horizontal Normal Stress - $\sigma_x$

1. Figure 6.19 shows the variation of horizontal normal stress along the height of Plane 2 for one stage and four stages of reservoir filling over five interfaces. It is seen from the figure that the pattern of the curve of  $\sigma_x$  is similar for both analysis. The maximum stress for five interfaces is found at the base of the dam. It abruptly decreases in lower 20% dam height above the base. Thereafter it remains constant upto another 20% height and then gradually decrease upto dam top.
2. The maximum horizontal normal stress for one stage and four stages of reservoir filling analysis for five different interfaces are tabulated in Tab.6.19. The maximum values of  $\sigma_x$  are -33.49 t/m<sup>2</sup> and -31.34 t/m<sup>2</sup> and found at the centre of the core (vertical 3) for single lift and seven lifts analyses respectively. It is noted that the values on Plane 2 are slightly less than the values of Plane 1 through the pattern is same.
3. The reservoir filling is seen to increase the stress of end of construction stage at all interfaces except the downstream shell.

### 6.2.2.4. Vertical Normal Stress - $\sigma_y$

1. Figure 6.20 shows the variation of vertical normal stress along the height of Plane 2 for one stage and four stages of reservoir filling over five interfaces. It is seen from the figure that the pattern of the curve of  $\sigma_y$  by one stage analysis has higher magnitude than four stages of reservoir filling at all the interfaces except the downstream shell.

- The maximum stress for five interfaces is found at the base of the dam. It sharply decreased in lower 20% height of the dam, then increased upto some height and thereafter gradually decreased upto top of the dam. The pattern is similar to the pattern of Plane 1.
2. The maximum vertical normal stress for one stage and four stages of reservoir filling analysis for five different interfaces are tabulated in Tab.6.20. The maximum values of  $\sigma_y$  are  $-93.91 \text{ t/m}^2$  and  $-88.94 \text{ t/m}^2$  for one stage and four stages reservoir filling analyses respectively, and are found at the base of upstream face of the core and centre line of the core respectively. It is noted that the values on Plane 2 are slightly less than the values on Plane 1.

### **6.2.3. Plane 3**

#### **6.2.3.1. Horizontal Displacements - u**

1. Figure 6.21 shows the variation of horizontal displacement along the height of Plane 3 for one stage and four stages of reservoir filling over five interfaces. The pattern is almost similar with the pattern of Plane 1 for both analyses but the magnitude is small. It is seen from the figure that the values of horizontal displacements for four stages of reservoir filling is also higher than one stage full reservoir filling.
2. The maximum horizontal displacements values for one stage and four stages of reservoir filling for five different interfaces are tabulated in Tab.6.21. It is noted that for one stage full reservoir filling the upstream shell move towards upstream direction by a maximum value of 4.95 cm and

this displacement occurs at the mid height. The downstream shell moves towards downstream direction by a maximum values of 4.90 cm. The horizontal displacement in the core and downstream shell is practically constant in the upper half height of the dam. For four stages analysis, the movements are in the similar pattern with one stage analysis with value of 4.14 cm at upstream direction in upstream shell and 5.47 cm at downstream direction in downstream shell. It is also noted that the values on Plane 3 are reduced to about 77-85% from the values of Plane 1 because of the reduced height.

3. Reservoir filling has increased the end of construction stage displacement in all the interfaces except the upstream shell when reservoir filling has little impact on horizontal displacement.

#### 6.2.3.2. Vertical Displacements - v

1. Figure 6.22 shows the variation of vertical displacement along the height of Plane 3 for one stage and four stage of reservoir filling over five interfaces respectively. It is seen from the figure that the pattern of the curve is similar with the Plane 1 and Plane 2. One stage full reservoir filling has higher values than four stages reservoir filling.
2. The maximum vertical displacements values for one stage and four stages analysis for five different interfaces are tabulated in Tab.6.22. It is observed that the magnitude of maximum displacement at five interfaces for one stage full reservoir filling is 27.82 cm at the upstream shell zone while for four stages analysis the highest magnitude is

29.85 cm, found in the upstream shell (vertical 1) in the top portion of the dam. It is noted that the values on Plane 3 are reduced to about 69-85% from the values of Plane 1.

3. The impact of reservoir filling on vertical displacement is observed only in upstream shell. The other interfaces do not show significant impact.

#### 6.2.3.3. Horizontal Normal Stress - $\sigma_x$

1. Figure 6.23 shows the variation of horizontal normal stress along the height of Plane 3 for one stage and four stages of reservoir filling over five interfaces. It is seen from the figure that the pattern of the curve of  $\sigma_x$  is similar for both analysis, with the maximum for all five interfaces at the base of the dam and decreasing towards the top of the dam. It also observed that from the crest of the dam down upto 20 m, the stresses distribution are close to tend to tension.
2. The maximum horizontal normal stress for one stage and four stages of reservoir filling analysis for five different interfaces are tabulated in Tab.6.23. The maximum values of  $\sigma_x$  are -20.23 t/m<sup>2</sup> and -20.58 t/m<sup>2</sup> were found at the centre of the core (vertical 3) for single lift and seven lifts analyses respectively. It is noted that the values on Plane 3 are reduced to about 50-58% from the values of Plane 1.
3. The reservoir filling by both methods is seen to have little effect on the end of construction stage stresses at this plane.

#### 6.2.3.4. Vertical Normal Stress - $\sigma_y$

1. Figure 6.24 shows the variation of vertical normal stress along the height of Plane 3 for one stage and four stages of reservoir filling over five interfaces. It is seen from the figure that  $\sigma_y$  by one stage analysis has only slightly higher magnitude than four stages of reservoir filling, with the maximum for five interfaces at the base of the dam and decreasing towards the top of the dam.
2. The maximum vertical normal stress for one stage and four stages of reservoir filling analysis for five different interfaces are tabulated in Tab.6.24. The maximum values of  $\sigma_y$  are  $-77.89 \text{ t/m}^2$  and  $-75.34 \text{ t/m}^2$  for one stage and four stages reservoir filling analyses respectively were found at the centre line of the core. It is noted that the values on Plane 3 are reduced to about 77-86% from the values of Plane 1.
3. Reservoir filling is seen to have practically no effect on the end of construction stage stresses at this plane.

### 6.3. DISCUSSION OF RESULTS OF CASE III STUDY

The displacements and stress in respect of Case III results are discussed over Plane 1, Plane 2 and Plane 3. The effect of seven lifts at end of construction has already been discussed in Case I. In this study focus is on the reservoir filling effect.

#### 6.3.1. Plane 1

##### 6.3.1.1. Horizontal Displacements - $u$

The horizontal displacements in respect of Case III results of FEM analysis are discussed below. To study the effect of each



stage of reservoir filling on the dam body, the horizontal displacements of the dam from stage 1 to 4 relative to the displacement at end of construction as the datum have been plotted.

1. The contours of horizontal displacements by reservoir filling in four stages, as shown in Fig.5.21, shows that the maximum movement is at the upstream face of the core and the movements are in the downstream direction most part of the dam except the upstream shell which tends to move towards upstream direction.
2. Figure 6.25 shows the variation of horizontal displacement along the height of Plane 1 after end of construction in seven lifts and four stages reservoir filling over five interfaces. It is seen from the figure that upto second stage of filling the movement for five verticals tend to move slight in upstream direction with respect to end of construction movement following the trend of end of construction movement. During third and fourth stage of filling the verticals tend to move in downstream direction.
3. The maximum horizontal displacements values on this case for five different interfaces are tabulated in Tab.6.25. It is noted from the table that the maximum displacement at first stage is 4.56 cm in upstream direction on vertical 1 and 4.58 cm in downstream direction on vertical 5. After fourth stage the displacement is 3.18 cm in upstream direction on vertical 1 and 7.98 cm in downstream direction on vertical 2. It is indicated that the water load has pushed the dam towards downstream from first to fourth stage and reduced the upstream movement of the upstream shell. The rest of the

dam (core and downstream shell) moved towards downstream direction from first to fourth stage.

4. Figure 6.26 and Tab.6.26 shows the relative horizontal movement at five interfaces for each stage of reservoir filling taking the displacement at end of construction as the datum. It is observed from the figure that the first and second stage of reservoir filling have moved the dam body slightly towards upstream direction (0.16 cm) but after the third and fourth stage of reservoir filling the entire dam body has to move in downstream direction (maximum displacement is 10 cm). The relative horizontal movements suggest that upto second stage of reservoir filling the softening of upstream shell and filter is predominant causing upstream movement. After third and fourth stage of reservoir filling, the water load on the core dominates to move the dam body towards downstream movement direction.

#### **6.3.1.2. Vertical Displacements - v**

1. The contours of vertical displacements by full reservoir filling in four stages, as shown in Fig.5.22, shows that the maximum displacements occur in two portion, the upstream shell and the core. It is indicated that the water due to reservoir filling through the upstream shell exert pressure on core causing vertical displacement in core and downstream shell.
2. Figure 6.27 shows the variation of vertical displacement along the height of Plane 1 after end of construction in seven lifts and four stages reservoir filling over five interfaces. It is seen from the figure that the change of the displacement due to reservoir filling was more in the

upstream shell, while only slight difference was observed on the core zone towards the downstream shell.

3. The maximum horizontal displacements values on this case for five different interfaces are tabulated in Tab.6.27. It is noted from the table that the maximum displacement is occurring in the centre of the core for four stages of reservoir filling with the maximum magnitude of 31.12 cm at full reservoir filling. From the table, the change of the displacement on the upstream shell from end of construction to full reservoir is 19.93 cm to 28.96 cm compared to the centre of the core, 30.54 cm to 31.12 cm. It is to note that the upstream shell displacement increased by about 40% as compared to 2% increase in the centre line of the core.

#### 6.3.1.3. Horizontal Normal Stress - $\sigma_x$

1. The contours of horizontal normal stress by seven lifts on construction and four stages reservoir filling is shown in Fig.5.23. It is seen from the figure that the core and downstream shell zone get compressed after full reservoir filling. The maximum magnitude of compressive stress occurs at the bottom of downstream face of the core. The stresses in the dam body decreases with increase in dam height.
2. It is observed from that figure that the tension zone has appeared at the upstream and downstream face of the dam close to the abutments with the magnitude varying from 3 to 7 t/m<sup>2</sup>.
3. Figure 6.28 shows the variation of horizontal normal stress along the height of Plane 1 for this case over five interfaces. It is seen from the figure that the stress

increases with decrease in height from dam crest to one third of dam height from the base then it sharply increases with decrease in height and the maxima occurs at the base.

4. The maximum horizontal normal stress for seven lifts and four stages of reservoir filling analysis for five different interfaces are tabulated in Tab.6.28. The maximum values of  $\sigma_x$  is  $-35.30 \text{ t/m}^2$  for fourth stage reservoir filling which is found at the base of downstream face of the core (vertical 4). From the table, the change of the stresses on the upstream shell from end of construction to full reservoir is  $-21.26 \text{ t/m}^2$  to  $-25.08 \text{ t/m}^2$  compared to the downstream face of the core,  $-33.88 \text{ t/m}^2$  to  $-35.30 \text{ t/m}^2$ .

#### **6.3.1.3. Vertical Normal Stress - $\sigma_y$**

1. The contours of vertical normal stress by seven lifts and four stages of reservoir filling are shown in Fig.5.24. It is observed that the stress distribution concentrated in the core zones after full reservoir filling spread towards upstream and downstream shell at mid height of the dam and decreases upto the face of the dam.
2. From the contours plot, the maximum stress is observed at the base of the downstream face of the core. A tension zone has appeared in the upstream and downstream face of the dam.
3. Figure 6.29 shows the variation of vertical normal stress along the height of Plane 1 after seven lifts and four stages of reservoir filling over five interfaces. The stresses because of reservoir filling have been found to be affected significantly in lower one third portion of dam section. The distribution is nearly hydrostatic from top of

the dam upto one third of the dam height and below it the stress increases rapidly to reach the maxima at the base of the dam.

4. The maximum vertical normal stress for seven lifts and four stages of reservoir filling analysis for five different interfaces are tabulated in Tab.6.29. The maximum value of  $\sigma_x$  is  $-99.69 \text{ t/m}^2$  for fourth stage reservoir filling. From the table, the change of the stresses on the upstream shell from end of construction to full reservoir is  $-44.26 \text{ t/m}^2$  to  $-62.45 \text{ t/m}^2$  compared to the downstream face of the core,  $-92.05 \text{ t/m}^2$  to  $-99.68 \text{ t/m}^2$ . It is clear that the upstream shell gets more affected due to reservoir filling as compared to the core zone.

### 6.3.2. Plane 2

#### 6.3.2.1. Horizontal Displacements - u

1. Figure 6.30 shows the variation of horizontal displacement along the height of Plane 2 after seven lifts and four stages of reservoir filling over five interfaces. The pattern is almost similar with the pattern of Plane 1 for this analysis. It is observed from the figure that the first and second stage of reservoir filling moves the dam body slightly towards upstream direction but after the third and fourth stage of reservoir filling the entire dam body moves in downstream direction.
2. The maximum horizontal displacements values after seven lifts and four stages of reservoir filling for five different interfaces are tabulated in Tab.6.30. It is observed from the table that the maximum displacement at

first stage is 4.74 cm in upstream direction on vertical 1 and 4.79 cm in downstream direction on vertical 5. After fourth stage the upstream movement is reduced to 3.43 cm on vertical 1 at mid height of dam and it is 8.48 cm in downstream direction on vertical 2. The magnitude of displacement on Plane 2 is slightly less than the values on Plane 1.

3. Figure 6.31 shows the relative horizontal at five interfaces for each stage of reservoir filling and take the displacement at end of construction as the datum and the pattern is almost similar with the pattern of Plane 1.
4. Table 6.31 describes the relative horizontal movements of each stage of reservoir filling with end of construction as a datum. The dam moves to upstream direction from the end of construction stage after first filling for five interfaces with a maximum displacement of 0.22 cm on upstream face of the core. After fourth stage (full reservoir), the movement is in downstream direction from the end of construction stage for all the five interfaces with maximum magnitude of 9.98 cm on upstream face of the core

#### **6.3.2.2. Vertical Displacement - v**

1. Figure 6.32 shows the variation of vertical displacement along the height of Plane 2 after seven lifts and four stage of reservoir filling over five interfaces respectively. It is seen from the figure that the pattern of displacement is similar to the Plane 1.
2. The maximum vertical displacements values after seven lifts and four stages analysis for five different interfaces are tabulated in Tab.6.32. It is noted from the table that the

maximum magnitude is 30.97 cm on centre of the core. The change of the displacement on the upstream shell from end of construction to full reservoir is 19.72 cm to 29.32 cm compare to the centre of the core, 30.17 cm to 30.97 cm; it is note that the upstream shell is more affected than the core. It is noted that the values on Plane 2 are slightly less than the values on Plane 1.

#### **6.3.2.3. Horizontal Normal Stress - $\sigma_x$**

1. Figure 6.33 shows the variation of horizontal normal stress along the height of Plane 2 for this case over five interfaces. It is seen from the figure that the pattern of the curve is similar to the Plane 1.
2. The maximum horizontal normal stress for seven lifts and four stages of reservoir filling analysis for five different interfaces are tabulated in Tab.6.33. The maximum values of  $\sigma_x$  is -33.82 t/m<sup>2</sup> for fourth stage reservoir filling which is found at the base of downstream face of the core (vertical 4). It is noted that the values on Plane 2 are slightly less than the values on Plane 1.

#### **6.3.2.4. Vertical Normal Stress - $\sigma_y$**

1. Figure 6.34 shows the variation of vertical normal stress along the height of Plane 2 after seven lifts and four stages of reservoir filling over five interfaces. The pattern of the stresses show that the stresses increase rapidly at one third of the dam height and have the maximum magnitude at the base of the dam.
2. The maximum vertical normal stress for seven lifts and four stages of reservoir filling analysis for five different

interfaces are tabulated in Tab.6.34. The maximum values of  $\sigma_x$  is -99.45 t/m<sup>2</sup> for fourth stage reservoir filling. It is noted that the values on Plane 2 are slightly less than the values on Plane 1.

### 6.3.3. Plane 3

#### 6.3.3.1. Horizontal Displacement - u

1. Figure 6.35 shows the variation of horizontal displacement along the height of Plane 3 after seven lifts and four stages of reservoir filling over five interfaces. The pattern is almost similar with the pattern of Plane 1 for this analysis.
2. The maximum horizontal displacements values after seven lifts and four stages of reservoir filling for five different interfaces are tabulated in Tab.6.35. It is observed from the table that the maximum displacement after first stage is 2.49 cm in upstream direction on vertical 1 and 2.55 cm in downstream direction on vertical 5. After fourth stage it slightly reduced to 2.47 cm in upstream direction on vertical 1 and increased to 5.58 cm in downstream direction on vertical 2. The magnitudes of movement on Plane 3 have decreased to about 55-69% from Plane 1.
3. Figure 6.36 shows the relative horizontal at five interfaces for each stage of reservoir filling and take the displacement at end of construction as the datum and the pattern is almost similar with the pattern of Plane 1.
4. Table 6.36 describe the relative horizontal movements of each stage of reservoir filling from end of construction as



a datum. The dam move to upstream direction from the end of construction stage after first filling for five interfaces with maximum magnitude of only 0.04 cm on upstream face of the core after fourth stage (full reservoir). However the movement is in downstream direction from the end of construction stage for all the five interfaces with maximum magnitude of 6.06 cm on upstream face of the core.

#### **6.3.3.2. Vertical Displacement - v**

1. Figure 6.37 shows the variation of vertical displacement along the height of Plane 3 after seven lifts and four stage of reservoir filling over five interfaces respectively. It is seen from the figure that the pattern of the curve is similar with the Plane 1.
2. The maximum vertical displacements values after seven lifts and four stages analysis for five different interfaces are tabulated in Tab.6.37. It is noted from the table that the maximum magnitude is 19.08 cm in the upstream shell. The change of the displacement in the upstream shell from end of construction to full reservoir is 13.50 cm to 19.08 cm and in the core it is 17.57 cm to 18.05 cm. It shows that the upstream shell is more affected by reservoir filling rather than the core. It is noted that the values on Plane 3 are about 57-66% of the values on Plane 1.

#### **6.3.3.3. Horizontal Normal Stress - $\sigma_x$**

1. Figure 6.38 shows the variation of horizontal normal stress along the height of Plane 3 for this case over five interfaces. It is seen from the figure that there is some

tension zone (2 t/m<sup>2</sup>) at about mid height of the dam. The compression stresses are maximum at the base.

2. The maximum horizontal normal stress after seven lifts and four stages of reservoir filling analysis for five different interfaces are tabulated in Tab.6.38. The maximum values of  $\sigma_x$  is -20.52 t/m<sup>2</sup> for fourth stage reservoir filling which is found at the base of downstream shell (vertical 5). It is noted that the values on Plane 3 are reduced to 54-76% of the values of Plane 1.

#### **6.3.3.4. Vertical Normal Stress - $\sigma_y$**

1. Figure 6.39 shows the variation of vertical normal stress along the height of Plane 3 after seven lifts and four stages of reservoir filling over five interfaces. It is seen from the figure that the pattern of the stress distribution is similar to Plane 1 with minimum compressive stress at about mid height of the dam and maximum at the base of dam.
2. The maximum vertical normal stress for seven lifts and four stages of reservoir filling analysis for five different interfaces are tabulated in Tab.6.39. The maximum value of  $\sigma_x$  is -64.29 t/m<sup>2</sup> for fourth stage reservoir filling at centre of the core. It is noted that the values on Plane 3 are reduced to about 62-77% of the values of Plane 1.

Tab.6.1. Maximum Horizontal Displacements (cm), Plane 1, Case 1

Particulars	EOC One Stage	EOC Seven Stages
Vertical 1	-3.968	-4.408
Vertical 2	-1.247	-2.114
Vertical 3	-0.039	-0.010
Vertical 4	0.661	1.451
Vertical 5	4.007	4.608

Tab.6.2. Maximum Vertical Displacements (cm), Plane 1, Case 1

Particulars	EOC One Stage	EOC Seven Stages
Vertical 1	-27.660	-19.928
Vertical 2	-27.426	-27.816
Vertical 3	-27.526	-30.538
Vertical 4	-27.624	-28.792
Vertical 5	-28.378	-20.704

Tab.6.3. Maximum Horizontal Norm. Stress (t/m<sup>2</sup>), Plane 1, Case 1

Particulars	EOC One Stage	EOC Seven Stages
Vertical 1	-21.486	-21.264
Vertical 2	-30.392	-32.764
Vertical 3	-28.915	-27.207
Vertical 4	-31.130	-33.886
Vertical 5	-22.017	-21.918

Tab.6.4. Maximum Vertical Norm. Stress (t/m<sup>2</sup>), Plane 1, Case 1

Particulars	EOC One Stage	EOC Seven Stages
Vertical 1	-44.379	-44.262
Vertical 2	-80.543	-87.694
Vertical 3	-80.845	-89.441
Vertical 4	-82.466	-92.049
Vertical 5	-50.474	-50.348

Tab.6.5. Maximum Horizontal Displacements (cm), Plane 2, Case 1

Particulars	EoC One Stage	EoC Seven Stages
Vertical 1	-3.775	-4.618
Vertical 2	-1.259	-1.506
Vertical 3	-0.046	-0.083
Vertical 4	0.642	1.011
Vertical 5	3.786	4.810

Tab.6.6. Maximum Vertical Displacements (cm), Plane 2, Case 1

Particulars	EoC One Stage	EoC Seven Stages
Vertical 1	-26.297	-19.721
Vertical 2	-26.228	-27.391
Vertical 3	-26.324	-30.170
Vertical 4	-26.426	-28.384
Vertical 5	-26.980	-20.461

Tab.6.7. Maximum Horizontal Norm. Stress (t/m<sup>2</sup>), Plane 2, Case 1

Particulars	EoC One Stage	EoC Seven Stages
Vertical 1	-23.380	-24.625
Vertical 2	-29.377	-31.615
Vertical 3	-30.650	-31.679
Vertical 4	-30.249	-33.040
Vertical 5	-27.449	-28.227

Tab.6.8. Maximum Vertical Norm. Stress (t/m<sup>2</sup>), Plane 2, Case 1

Particulars	EoC One Stage	EoC Seven Stages
Vertical 1	-43.453	-52.387
Vertical 2	-77.091	-83.610
Vertical 3	-81.366	-89.818
Vertical 4	-78.299	-88.596
Vertical 5	-64.738	-68.203

Tab.6.9. Maximum Horizontal Displacements (cm), Plane 3, Case 1

Particulars	EoC One Stage	EoC Seven Stages
Vertical 1	-3.502	-2.499
Vertical 2	-1.162	-0.480
Vertical 3	0.070	-0.034
Vertical 4	0.984	1.417
Vertical 5	3.383	2.552

Tab.6.10. Maximum Vertical Displacements (cm), Plane 3, Case 1

Particulars	EoC One Stage	EoC Seven Stages
Vertical 1	-22.060	-13.510
Vertical 2	-21.498	-16.679
Vertical 3	-21.642	-17.575
Vertical 4	-21.891	-17.384
Vertical 5	-22.977	-13.955

Tab.6.11. Max. Horizontal Norm. Stress (t/m<sup>2</sup>), Plane 3, Case 1

Particulars	EoC One Stage	EoC Seven Stages
Vertical 1	-14.688	-17.890
Vertical 2	-16.697	-17.736
Vertical 3	-19.067	-17.153
Vertical 4	-17.548	-17.719
Vertical 5	-16.144	-19.092

Tab.6.12. Max. Vertical Norm. Stress (t/m<sup>2</sup>), Plane 3, Case 1

Particulars	EoC One Stage	EoC Seven Stages
Vertical 1	-39.289	-54.937
Vertical 2	-57.355	-69.386
Vertical 3	-72.836	-71.840
Vertical 4	-60.830	-70.477
Vertical 5	-43.626	-56.647

Tab. 6.13. Maximum Horizontal Displacements (cm), Plane 1, Case 2

Particulars	EoC One Stage	Full Reservoir 4 Stages	Full Reservoir 1 Stage
Vertical 1	-3.966	-3.859	-4.253
Vertical 2	-1.247	6.194	5.311
Vertical 3	-0.039	6.107	4.435
Vertical 4	0.661	6.369	4.600
Vertical 5	4.007	6.998	5.390

Tab. 6.14. Maximum Vertical Displacements (cm), Plane 1, Case 2

Particulars	EoC One Stage	Full Reservoir 4 Stages	Full Reservoir 1 Stage
Vertical 1	-27.660	-34.755	-34.069
Vertical 2	-27.426	-29.651	-30.666
Vertical 3	-27.526	-29.417	-30.384
Vertical 4	-27.624	-29.356	-30.186
Vertical 5	-28.376	-30.374	-30.648

Tab. 6.15. Max. Horizontal Norm. Stress (t/m<sup>2</sup>), Plane 1, Case 2

Particulars	EoC 1 Stage	Full Reserv. 4 Stages	Full Reserv. 1 Stages
Vertical 1	-21.496	-25.474	-29.061
Vertical 2	-30.392	-24.543	-29.421
Vertical 3	-26.915	-27.314	-29.936
Vertical 4	-31.130	-35.327	-34.382
Vertical 5	-22.017	-22.482	-22.517

Tab. 6.16. Max. Vertical Norm. Stress (t/m<sup>2</sup>), Plane 1, Case 2

Particulars	EoC 1 Stage	Full Reserv. 4 Stages	Full Reserv. 1 Stages
Vertical 1	-44.379	-59.750	-69.775
Vertical 2	-80.543	-89.698	-97.134
Vertical 3	-80.845	-85.323	-93.482
Vertical 4	-80.664	-86.150	-92.464
Vertical 5	-50.474	-51.095	-51.117

Tab.6.17. Maximum Horizontal Displacements (cm), Plane 2, Case 2

Particulars	EoC One Stage	Full Reservoir 4 Stages	Full Reservoir 1 Stage
Vertical 1	-3.775	-3.801	-4.255
Vertical 2	-1.259	5.608	4.812
Vertical 3	-0.046	5.684	4.180
Vertical 4	0.642	6.046	4.483
Vertical 5	3.786	8.557	5.463

Tab.6.18. Maximum Vertical Displacements (cm), Plane 2, Case 2

Particulars	EoC One Stage	Full Reservoir 4 Stages	Full Reservoir 1 Stage
Vertical 1	-26.297	-34.355	-32.933
Vertical 2	-26.228	-28.342	-29.308
Vertical 3	-26.324	-28.284	-29.033
Vertical 4	-26.426	-29.235	-28.892
Vertical 5	-26.980	-28.970	-29.073

Tab.6.19. Max. Horizontal Norm. Stress (t/m<sup>2</sup>), Plane 2, Case 2

Particulars	EoC 1 Stage	Full Reserv. 4 Stages	Full Reserv. 1 Stages
Vertical 1	-23.380	-28.802	-30.348
Vertical 2	-29.377	-30.503	-33.353
Vertical 3	-30.650	-31.346	-33.490
Vertical 4	-30.249	-30.865	-32.176
Vertical 5	-27.449	-27.980	-28.116

Tab.6.20. Max. Vertical Norm. Stress (t/m<sup>2</sup>), Plane 2, Case 2

Particulars	EoC 1 Stage	Full Reserv. 4 Stages	Full Reserv. 1 Stages
Vertical 1	-43.453	-61.785	-66.143
Vertical 2	-77.091	-84.852	-93.913
Vertical 3	-82.366	-88.939	-90.894
Vertical 4	-78.299	-83.028	-87.093
Vertical 5	-64.738	-65.416	-65.711

Tab.6.21. Maximum Horizontal Displacements (cm), Plane 3, Case 2

Particulars	EOC One Stage	Full Reservoir 4 Stages	Full Reservoir 1 Stage
Vertical 1	-3.502	-4.144	-4.951
Vertical 2	-1.162	3.691	3.366
Vertical 3	0.070	4.101	3.031
Vertical 4	0.984	4.609	3.743
Vertical 5	3.383	5.469	4.903

Tab.6.22. Maximum Vertical Displacements (cm), Plane 3, Case 2

Particulars	EOC One Stage	Full Reservoir 4 Stages	Full Reservoir 1 Stage
Vertical 1	-22.060	-29.847	-27.824
Vertical 2	-21.498	-20.482	-22.418
Vertical 3	-21.642	-21.239	-22.789
Vertical 4	-21.891	-21.742	-23.143
Vertical 5	-22.977	-22.908	-24.016

Tab.6.23. Max. Horizontal Norm. Stress (t/m<sup>2</sup>), Plane 3, Case 2

Particulars	EOC 1 Stage	Full Reserv. 4 Stages	Full Reserv. 1 Stages
Vertical 1	-14.688	-20.342	-19.471
Vertical 2	-16.697	-17.929	-18.844
Vertical 3	-19.067	-20.575	-20.231
Vertical 4	-17.548	-19.721	-18.923
Vertical 5	-16.144	-20.156	-16.640

Tab.6.24. Max. Vertical Norm. Stress (t/m<sup>2</sup>), Plane 3, Case 2

Particulars	EOC 1 Stage	Full Reserv. 4 Stages	Full Reserv. 1 Stages
Vertical 1	-39.289	-48.156	-45.072
Vertical 2	-57.355	-63.393	-64.202
Vertical 3	-72.836	-75.344	-77.899
Vertical 4	-60.830	-65.567	-63.271
Vertical 5	-43.626	-49.643	-43.607



Tab.6.25. Maximum Horizontal Displacements (cm), Plane 1, Case 3

Particulars	EoC Seven Stages	Stage 1 (W.L. 24 m)	Stage 2 (W.L. 44 m)	Stage 3 (W.L. 76 m)	Stage 4 (W.L. 95 m)
Vertical 1	-4.408	-4.565	-4.599	-3.795	-3.181
Vertical 2	-2.114	-2.257	-1.084	3.851	7.981
Vertical 3	-0.010	-0.143	-0.207	2.992	6.778
Vertical 4	1.451	1.393	1.524	3.330	6.339
Vertical 5	4.608	4.585	4.621	5.381	6.247

Tab.6.26. Relative Horizontal Displ. (cm), Plane 1, Case 3

Particulars	EoC Seven Stages	Stage 1 (W.L. 24 m)	Stage 2 (W.L. 44 m)	Stage 3 (W.L. 76 m)	Stage 4 (W.L. 95 m)
Vertical 1	Datum	-0.157	-0.191	0.612	1.227
Vertical 2	Datum	-0.143	1.030	5.964	10.095
Vertical 3	Datum	-0.133	-0.198	3.001	6.788
Vertical 4	Datum	-0.058	0.073	1.879	4.888
Vertical 5	Datum	-0.023	0.013	0.773	1.639

Tab.6.27. Maximum Vertical Displacements (cm), Plane 1, Case 3

Particulars	EoC Seven Stages	Stage 1 (W.L. 24 m)	Stage 2 (W.L. 44 m)	Stage 3 (W.L. 76 m)	Stage 4 (W.L. 95 m)
Vertical 1	-19.928	-20.150	-22.331	-27.836	-28.959
Vertical 2	-27.816	-27.860	-28.510	-26.880	-24.449
Vertical 3	-30.538	-30.538	-30.731	-30.981	-31.124
Vertical 4	-28.792	-28.729	-29.027	-29.456	-29.637
Vertical 5	-20.704	-20.667	-20.719	-20.942	-21.184

Tab.6.28. Max. Horizontal Norm. Stress (t/m<sup>2</sup>), Plane 1, Case 3

Particulars	EoC (W.L. 0 m)	Stage 1 (W.L. 24 m)	Stage 2 (W.L. 44 m)	Stage 3 (W.L. 76 m)	Stage 4 (W.L. 95 m)
Vertical 1	-21.264	-21.928	-23.596	-24.501	-25.079
Vertical 2	-32.764	-37.642	-33.827	-27.982	-24.975
Vertical 3	-27.207	-26.895	-27.705	-28.046	-27.852
Vertical 4	-33.886	-33.542	-33.889	-34.935	-35.304
Vertical 5	-21.918	-21.887	-21.922	-22.140	-22.326

Tab.6.29. Max. Vertical Norm. Stress (t/m<sup>2</sup>), Plane 1, Case 3

Particulars	EoC (W.L. 0 m)	Stage 1 (W.L. 24 m)	Stage 2 (W.L. 44 m)	Stage 3 (W.L. 76 m)	Stage 4 (W.L. 95 m)
Vertical 1	-44.262	-46.816	-52.443	-56.443	-62.452
Vertical 2	-87.694	-95.292	-93.229	-87.720	-90.925
Vertical 3	-89.441	-89.342	-91.968	-92.236	-95.672
Vertical 4	-92.049	-91.451	-92.046	-94.049	-99.689
Vertical 5	-50.348	-50.334	-50.370	-50.604	-53.394

Tab.6.30. Maximum Horizontal Displacements (cm), Plane 2, Case 3

Particulars	EoC Seven Stages	Stage 1 (W.L. 24 m)	Stage 2 (W.L. 44 m)	Stage 3 (W.L. 76 m)	Stage 4 (W.L. 95 m)
Vertical 1	-4.616	-4.741	-4.686	-3.940	-3.427
Vertical 2	-1.506	-1.732	-0.555	5.113	8.483
Vertical 3	-0.083	-0.250	-0.218	2.728	6.321
Vertical 4	1.011	0.925	0.960	3.164	5.583
Vertical 5	4.810	4.788	4.818	5.517	6.328

Tab.6.31. Relative Horizontal Displ. (cm), Plane 2, Case 3

Particulars	EoC Seven Stages	Stage 1 (W.L. 24 m)	Stage 2 (W.L. 44 m)	Stage 3 (W.L. 76 m)	Stage 4 (W.L. 95 m)
Vertical 1	Datum	-0.125	-0.069	0.677	1.189
Vertical 2	Datum	-0.226	0.951	6.619	9.989
Vertical 3	Datum	-0.167	-0.135	2.811	6.404
Vertical 4	Datum	-0.087	-0.052	2.153	4.571
Vertical 5	Datum	-0.023	0.007	0.707	1.518

Tab.6.32. Maximum Vertical Displacements (cm), Plane 2, Case 3

Particulars	EoC Seven Stages	Stage 1 (W.L. 24 m)	Stage 2 (W.L. 44 m)	Stage 3 (W.L. 76 m)	Stage 4 (W.L. 95 m)
Vertical 1	-19.721	-19.818	-21.902	-27.948	-29.322
Vertical 2	-27.391	-27.432	-28.119	-27.141	-24.845
Vertical 3	-30.170	-30.158	-30.591	-30.740	-30.976
Vertical 4	-28.384	-28.338	-28.617	-29.065	-29.270
Vertical 5	-20.461	-20.431	-20.472	-20.662	-20.882

Tab.6.33. Max. Horizontal Norm. Stress (t/m<sup>2</sup>), Plane 2, Case 3

Particulars	EoC (W.L. 0 m)	Stage 1 (W.L. 24 m)	Stage 2 (W.L. 44 m)	Stage 3 (W.L. 76 m)	Stage 4 (W.L. 95 m)
Vertical 1	-24.625	-25.664	-27.540	-29.088	-30.425
Vertical 2	-31.615	-32.232	-33.151	-32.854	-32.725
Vertical 3	-31.679	-31.862	-32.554	-32.756	-32.740
Vertical 4	-33.040	-32.821	-33.082	-33.667	-33.817
Vertical 5	-28.227	-28.181	-28.247	-28.514	-28.694

Tab. 6.34. Max. Vertical Norm. Stress (t/m<sup>2</sup>), Plane 2, Case 3

Particulars	EoC (W.L. 0 m)	Stage 1 (W.L. 24 m)	Stage 2 (W.L. 44 m)	Stage 3 (W.L. 76 m)	Stage 4 (W.L. 95 m)
Vertical 1	-52.387	-55.169	-59.603	-63.213	-69.914
Vertical 2	-83.610	-86.138	-89.698	-90.912	-96.819
Vertical 3	-89.818	-90.860	-93.362	-94.333	-99.452
Vertical 4	-88.596	-88.292	-88.862	-90.083	-95.084
Vertical 5	-68.203	-68.185	-68.273	-68.541	-72.202

Tab. 6.35. Maximum Horizontal Displacements (cm), Plane 3, Case 3

Particulars	EoC Seven Stages	Stage 1 (W.L. 24 m)	Stage 2 (W.L. 44 m)	Stage 3 (W.L. 76 m)	Stage 4 (W.L. 95 m)
Vertical 1	-2.499	-2.512	-2.543	-2.172	-2.474
Vertical 2	-0.480	-0.522	-0.637	1.872	5.580
Vertical 3	-0.034	-0.072	-0.170	1.277	3.597
Vertical 4	1.417	1.404	1.386	1.880	3.485
Vertical 5	2.552	2.542	2.533	2.808	3.681

Tab. 6.36. Relative Horizontal Displ. (cm), Plane 3, Case 3

Particulars	EoC Seven Stages	Stage 1 (W.L. 24 m)	Stage 2 (W.L. 44 m)	Stage 3 (W.L. 76 m)	Stage 4 (W.L. 95 m)
Vertical 1	Datum	-0.012	-0.044	0.327	0.026
Vertical 2	Datum	-0.042	-0.158	2.352	6.060
Vertical 3	Datum	-0.038	-0.136	1.311	3.631
Vertical 4	Datum	-0.013	-0.031	0.464	2.068
Vertical 5	Datum	-0.010	-0.018	0.256	1.129

Tab.6.37. Maximum Vertical Displacements (cm), Plane 3, Case 3

Particulars	EoC Seven Stages	Stage 1 (W.L. 24 m)	Stage 2 (W.L. 44 m)	Stage 3 (W.L. 76 m)	Stage 4 (W.L. 95 m)
Vertical 1	-13.510	-13.502	-13.706	-16.655	-19.086
Vertical 2	-16.679	-16.676	-16.868	-15.470	-14.426
Vertical 3	-17.575	-17.569	-17.709	-17.659	-18.051
Vertical 4	-17.384	-17.374	-17.460	-17.537	-17.772
Vertical 5	-13.955	-13.947	-13.959	-14.044	-14.172

Tab.6.38. Max. Horizontal Norm. Stress (t/m<sup>2</sup>), Plane 3, Case 3

Particulars	EoC (W.L. 0 m)	Stage 1 (W.L. 24 m)	Stage 2 (W.L. 44 m)	Stage 3 (W.L. 76 m)	Stage 4 (W.L. 95 m)
Vertical 1	-17.890	-18.062	-18.366	-18.868	-19.186
Vertical 2	-17.736	-17.861	-18.142	-18.434	-18.269
Vertical 3	-17.153	-17.224	-17.367	-18.055	-18.205
Vertical 4	-17.719	-17.784	-17.907	-18.624	-19.070
Vertical 5	-19.092	-19.222	-19.368	-19.935	-20.523

Tab.6.39. Max. Vertical Norm. Stress (t/m<sup>2</sup>), Plane 3, Case 3

Particulars	EoC (W.L. 0 m)	Stage 1 (W.L. 24 m)	Stage 2 (W.L. 44 m)	Stage 3 (W.L. 76 m)	Stage 4 (W.L. 95 m)
Vertical 1	-41.203	-43.089	-44.494	-46.684	-48.609
Vertical 2	-52.040	-54.664	-56.984	-60.394	-63.577
Vertical 3	-53.880	-56.612	-58.931	-61.444	-64.290
Vertical 4	-52.858	-55.522	-57.659	-59.569	-62.205
Vertical 5	-42.486	-44.626	-46.299	-47.579	-49.350

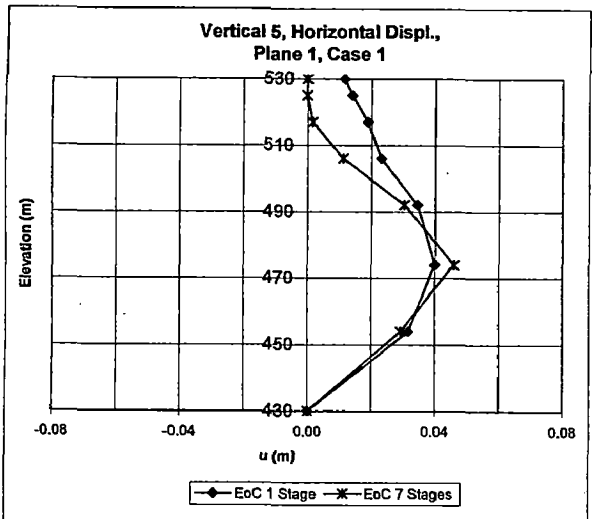
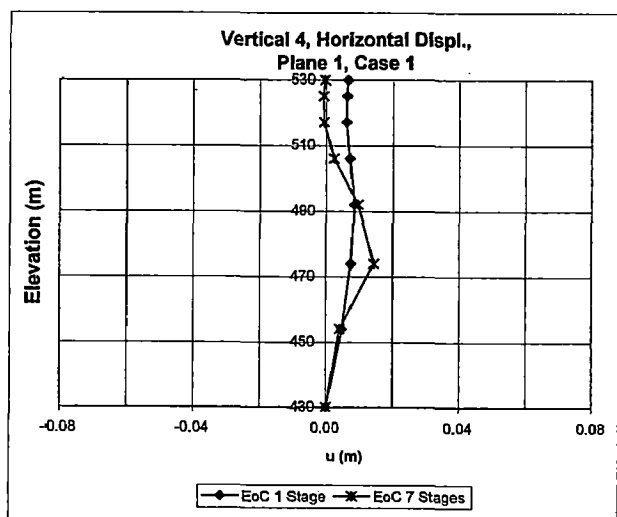
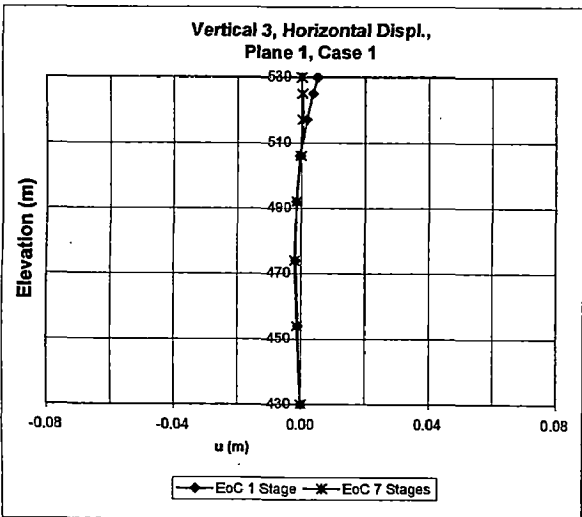
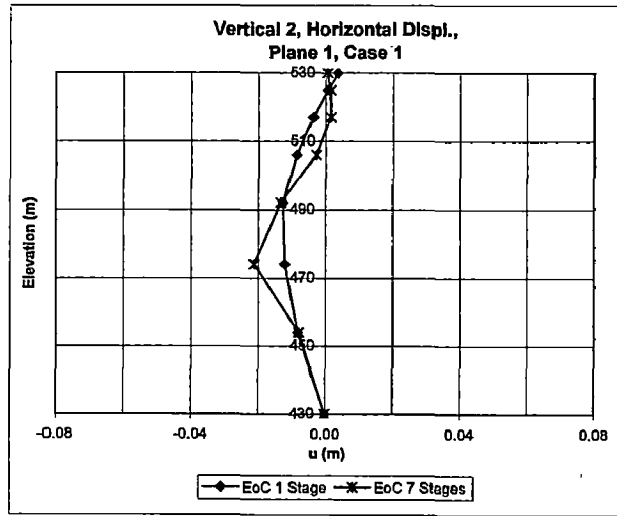
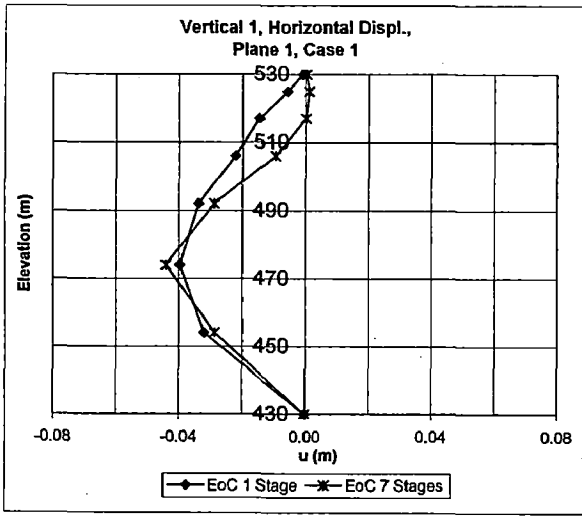


Fig.6.1. Horizontal Displ. u along Height at Different Location over Plane 1, Case 1

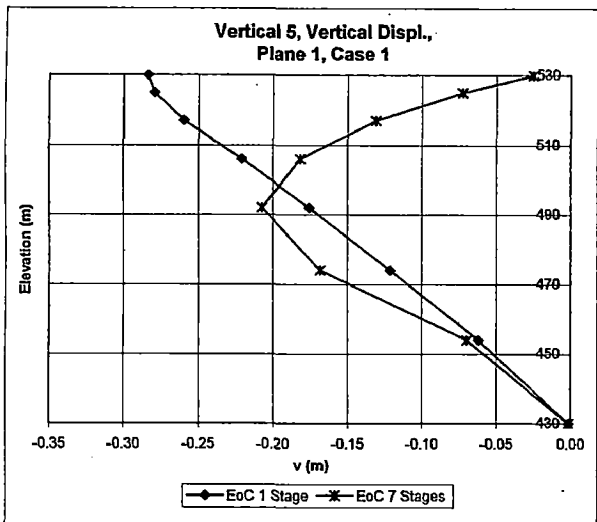
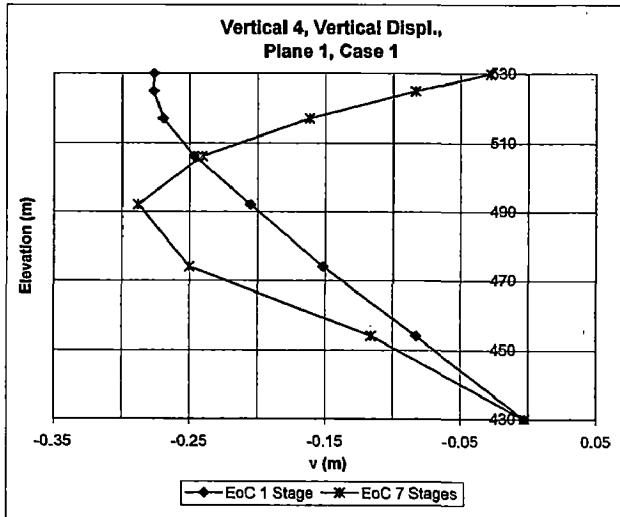
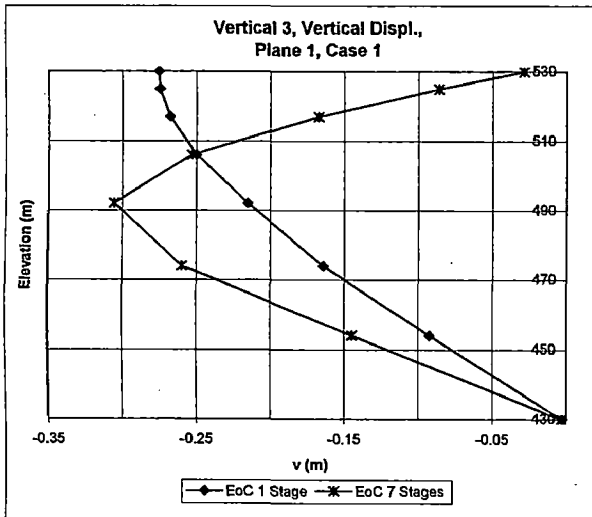
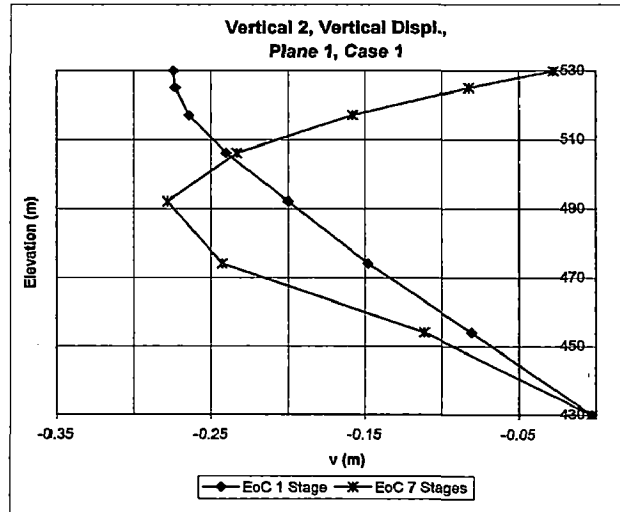
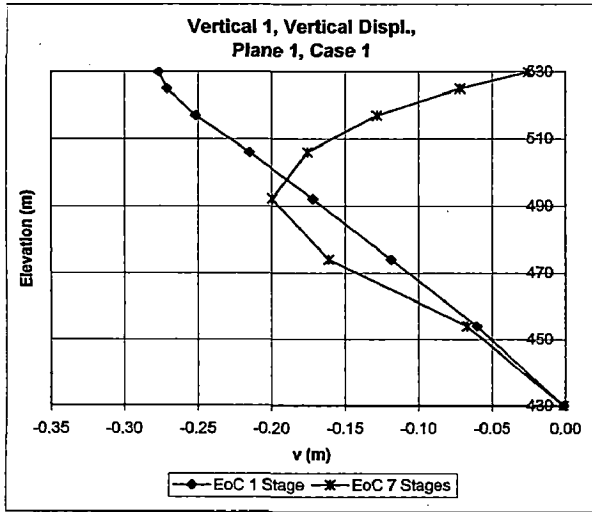


Fig.6.2. Vertical Displ. - v along Height at Different Location over Plane 1, Case 1

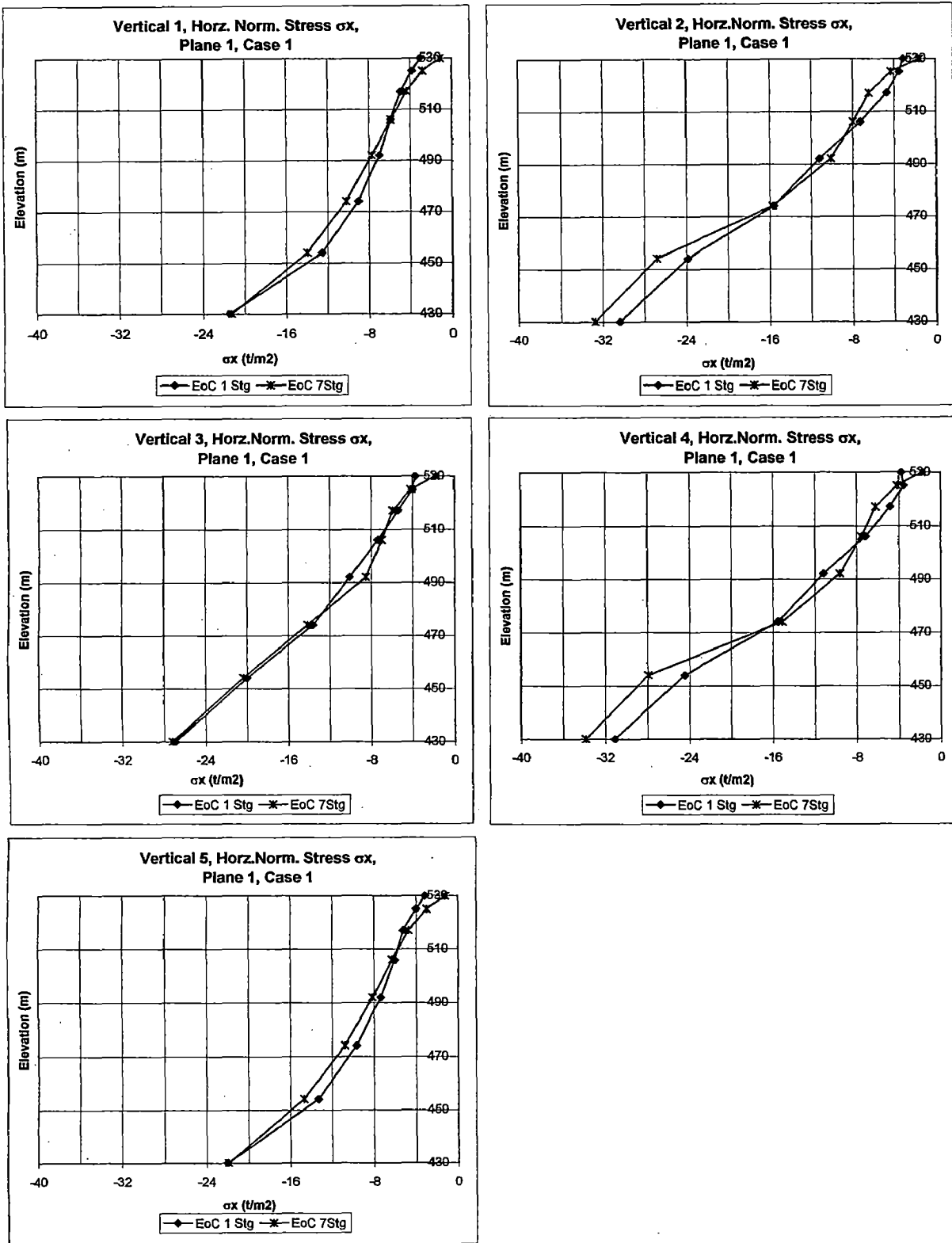


Fig.6.3. Horizontal Normal Stress  $\sigma_x$  along Height at Different Location over Plane 1, Case 1



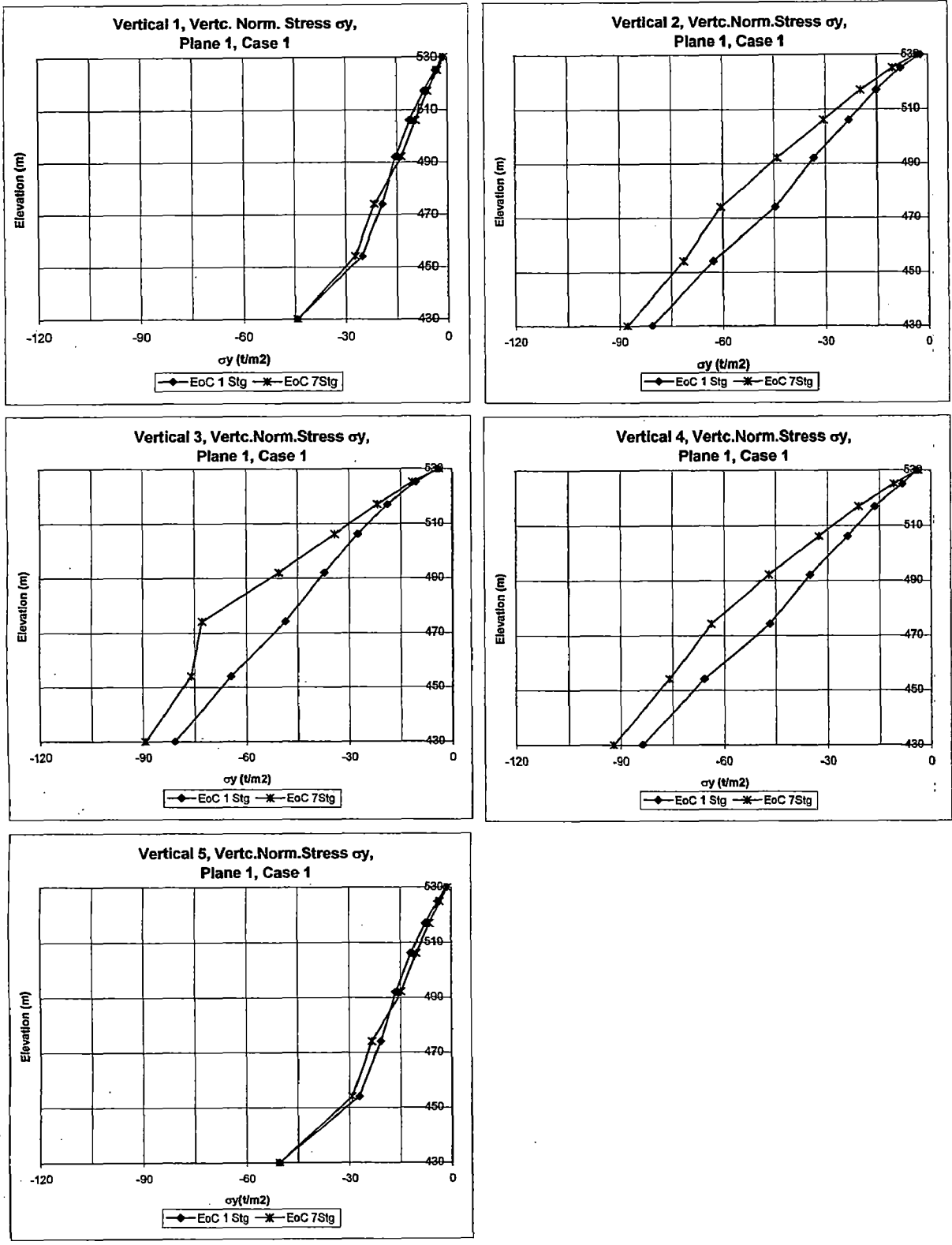


Fig.6.4. Vertical Normal Stress  $\sigma_y$  along Height at Different Location over Plane 1, Case 1

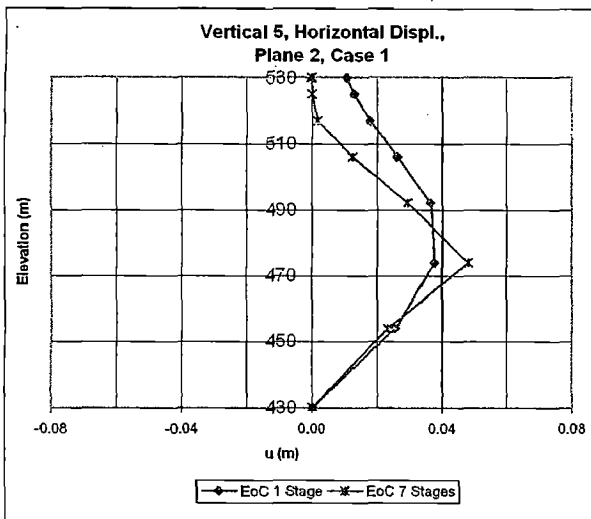
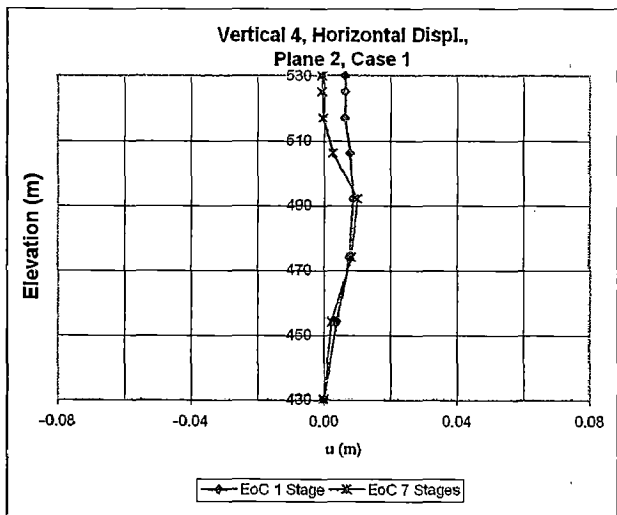
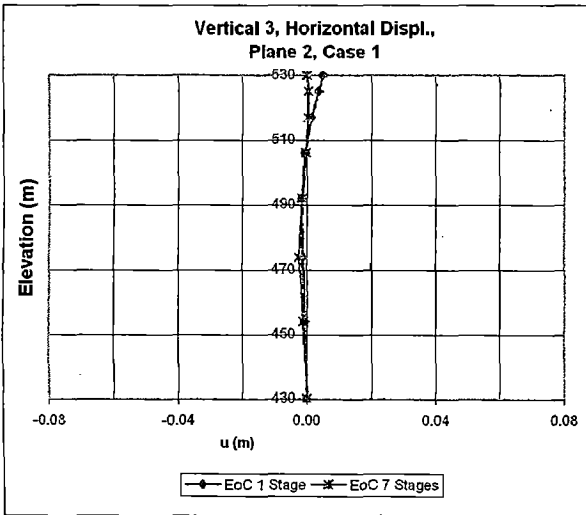
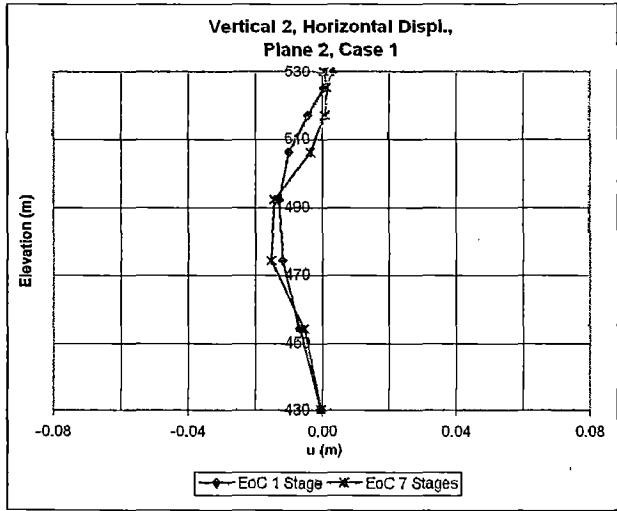
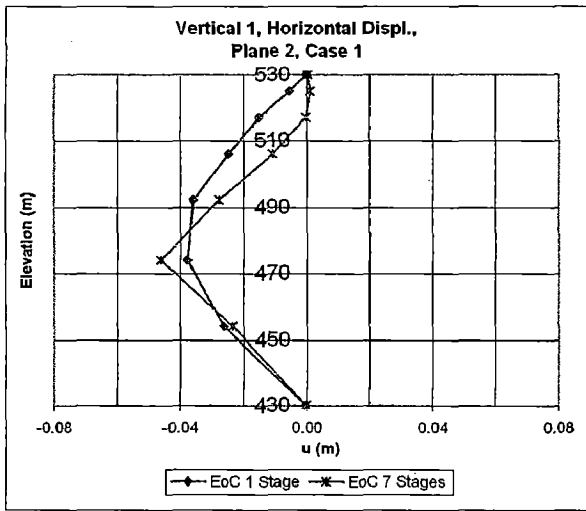


Fig.6.5. Horizontal Displ.  $u$  along Height at Different Location over Plane 2, Case 1

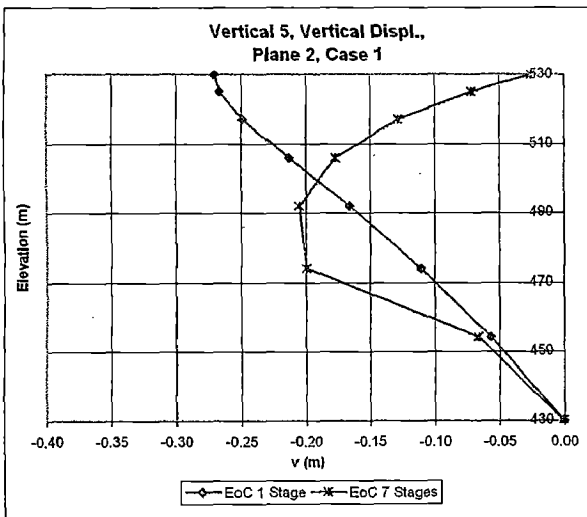
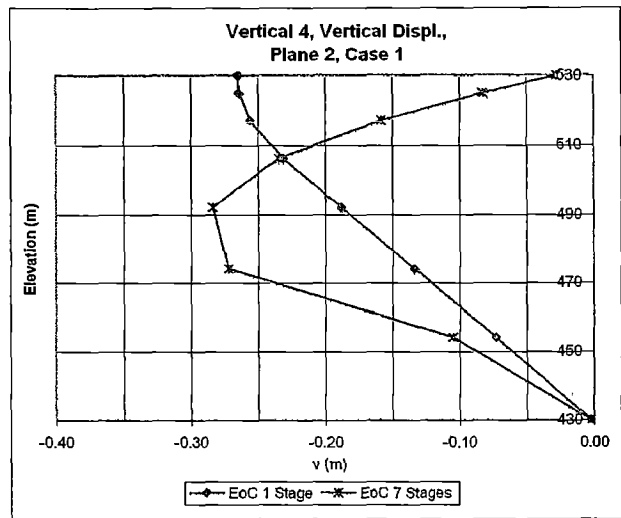
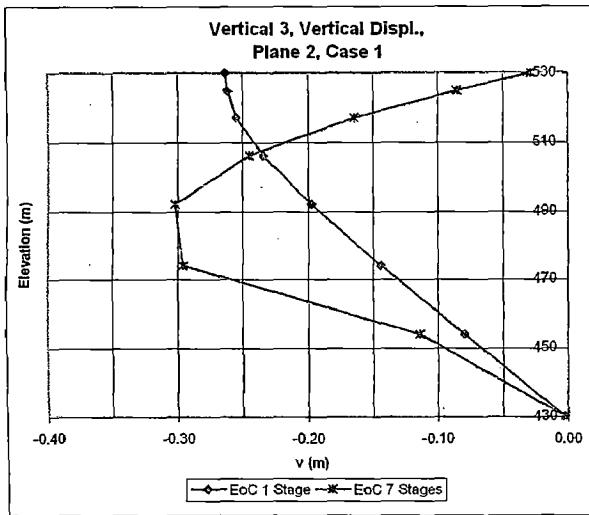
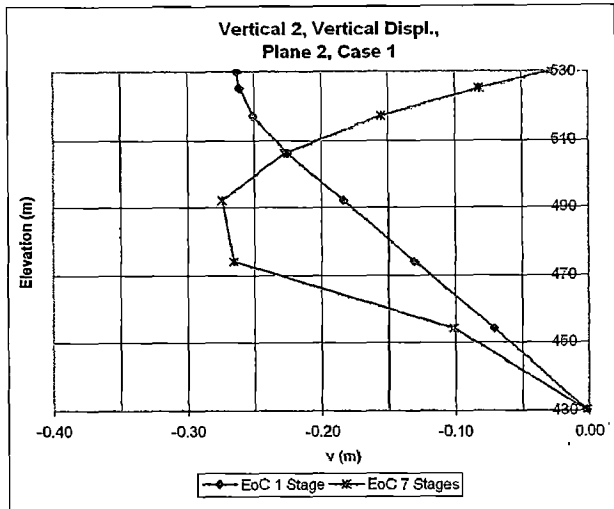
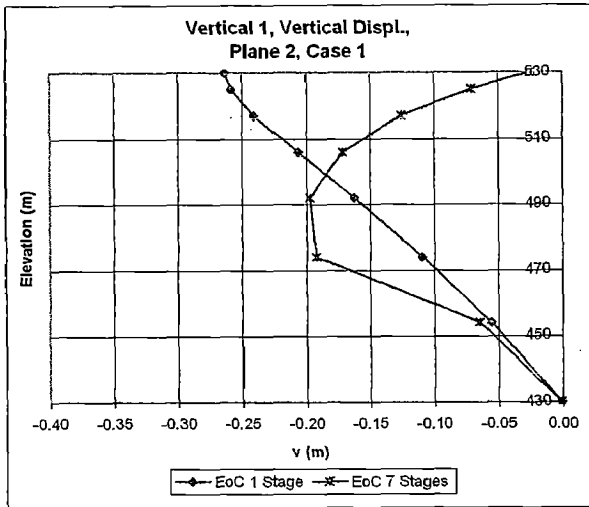


Fig.6.6. Vertical Movement - v along Height at Different Location over Plane 2, Case 1

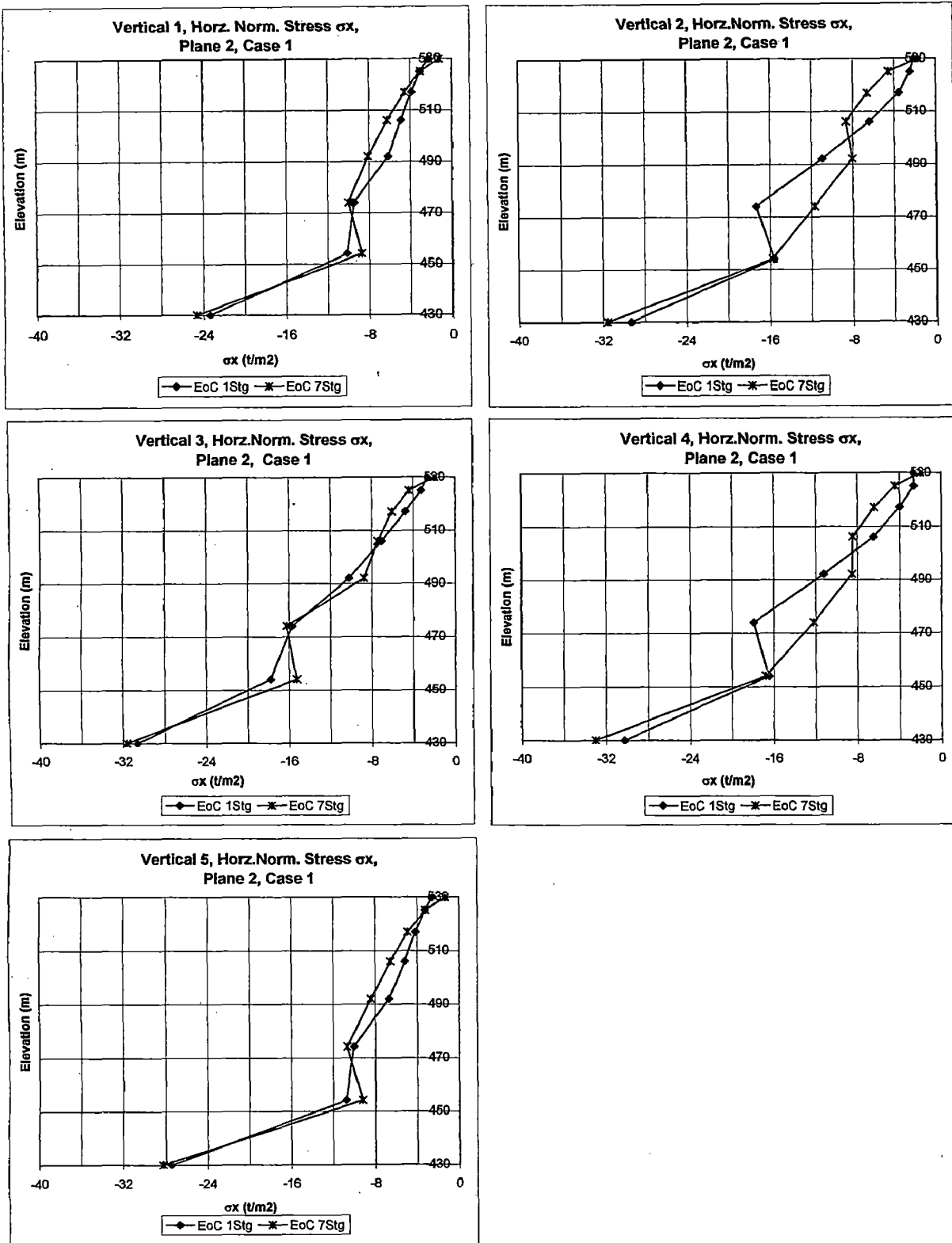


Fig.6.7 Horizontal Normal Stress  $\sigma_x$  along Height at Different Location over Plane 2, Case 1

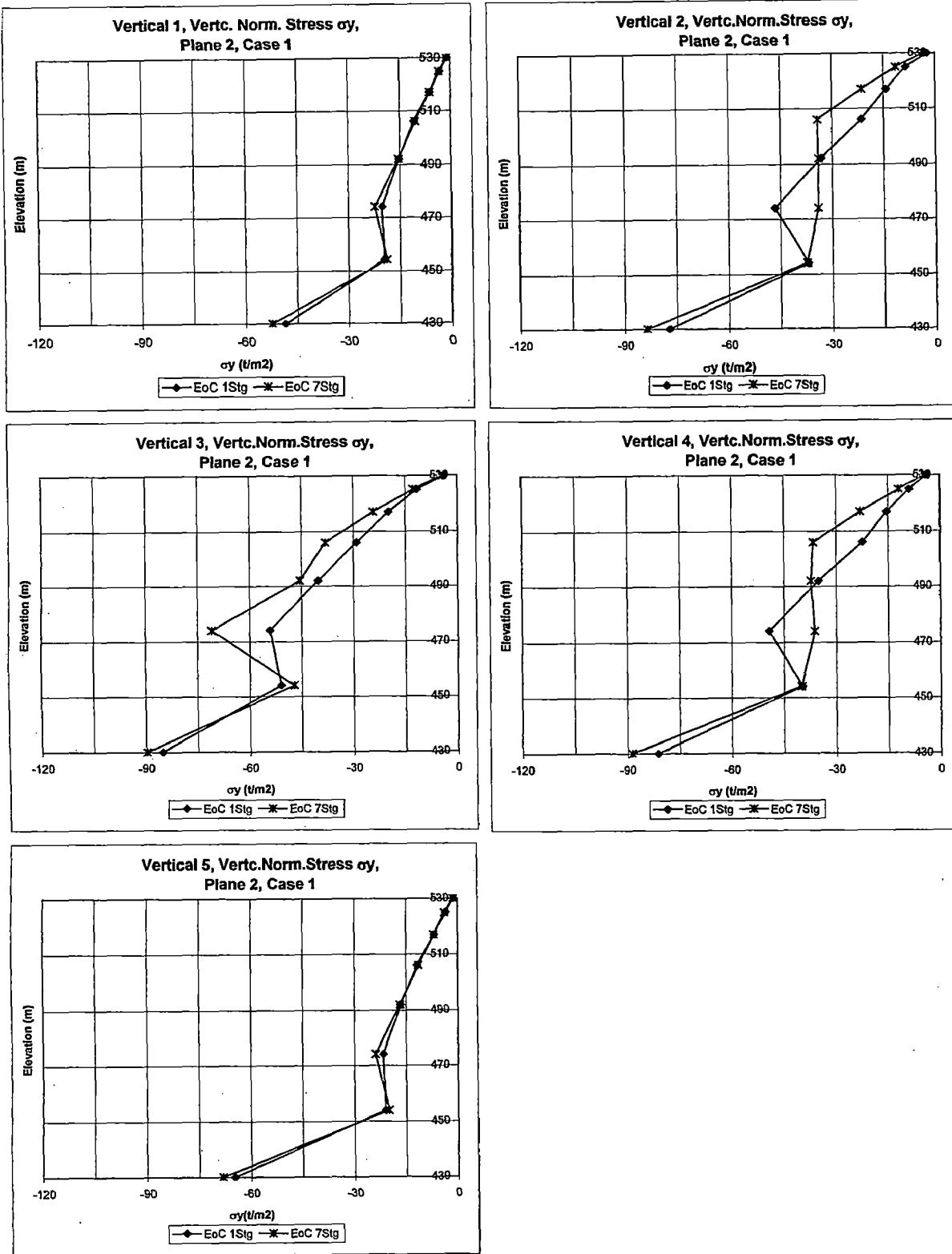


Fig.6.8. Vertical Normal Stress  $\sigma_y$  along Height at Different Location over Plane 2, Case 1

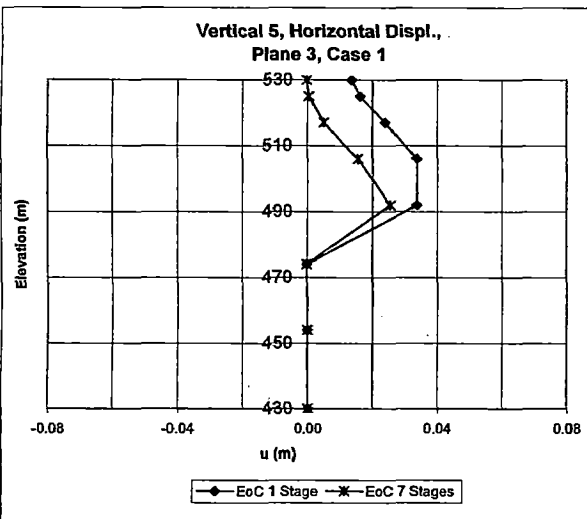
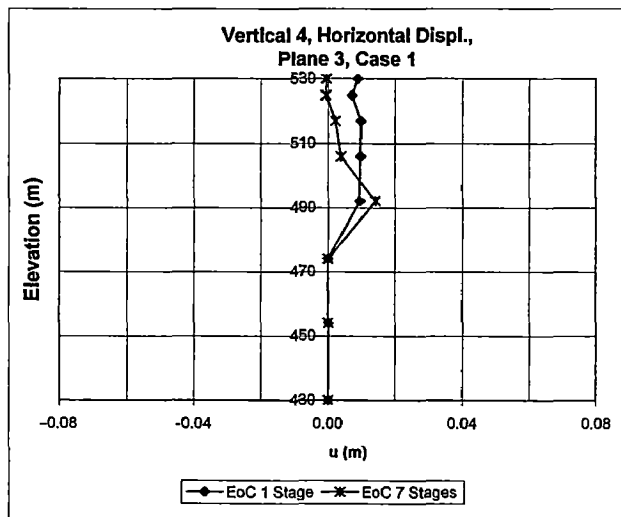
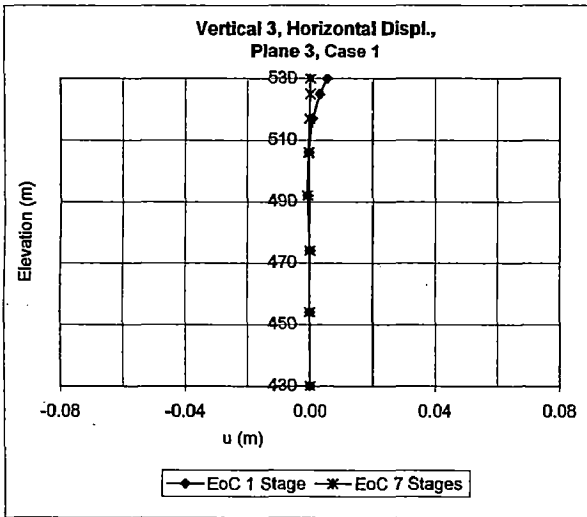
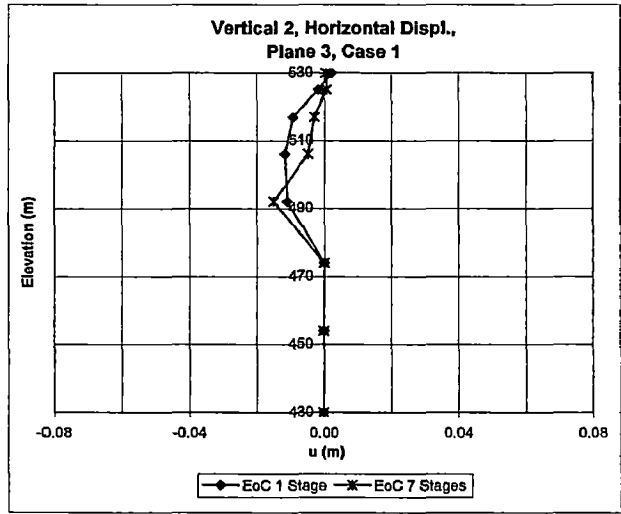
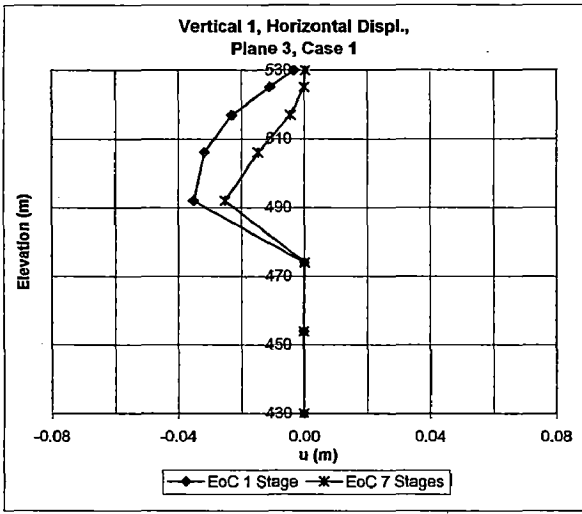


Fig.6.9. Horizontal Displ.  $u$  along Height at Different Location over Plane 3, Case 1

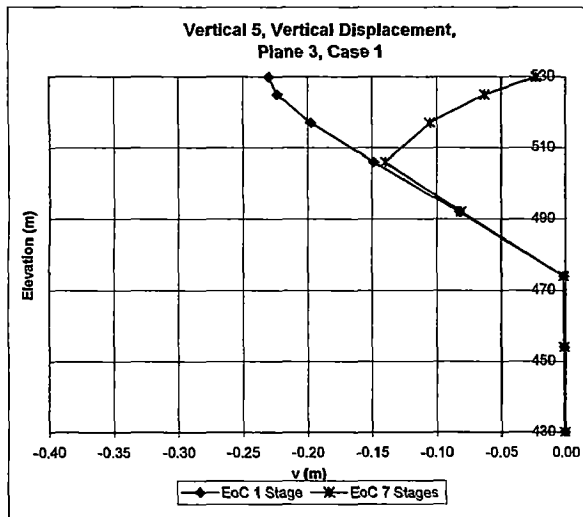
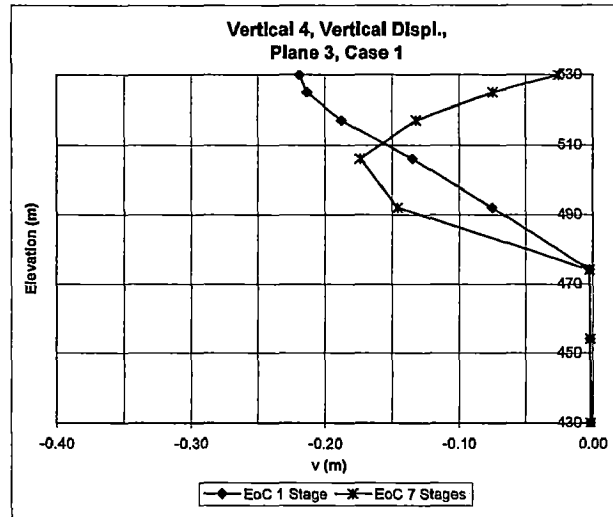
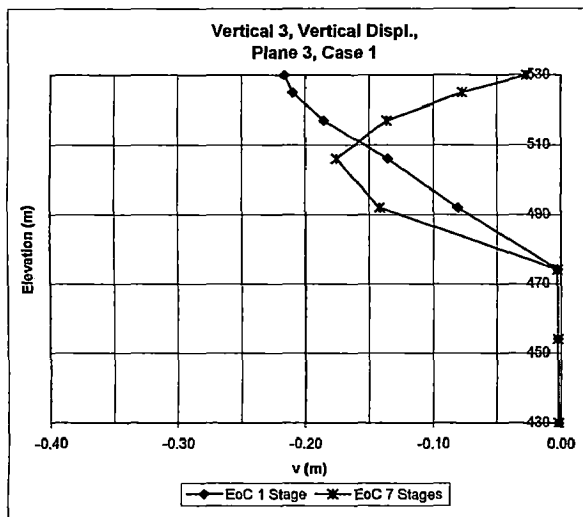
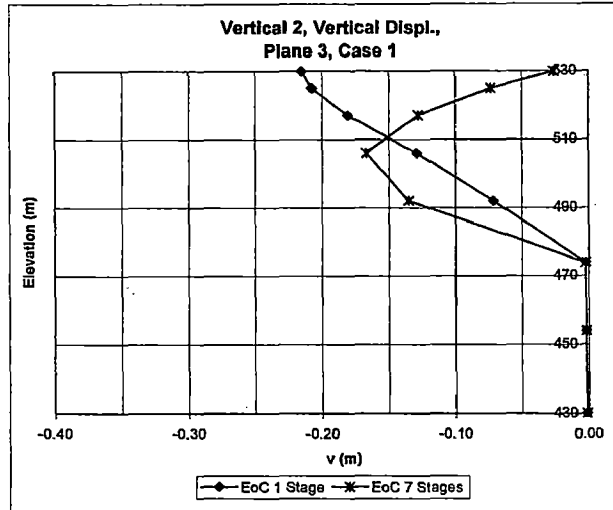
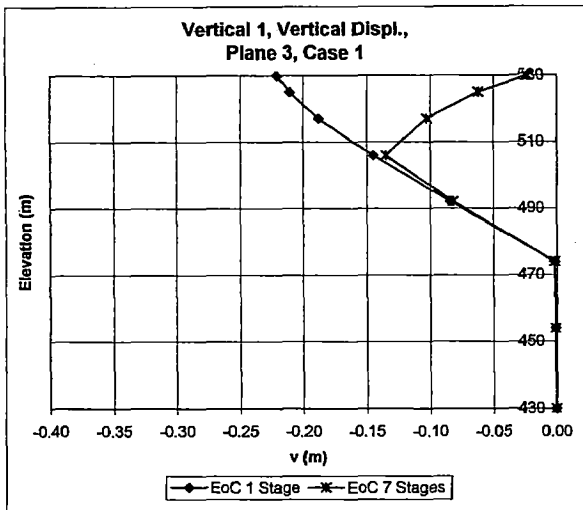


Fig.6.10. Vertical Displ. - v along Height at Different Location over Plane 3, Case 1

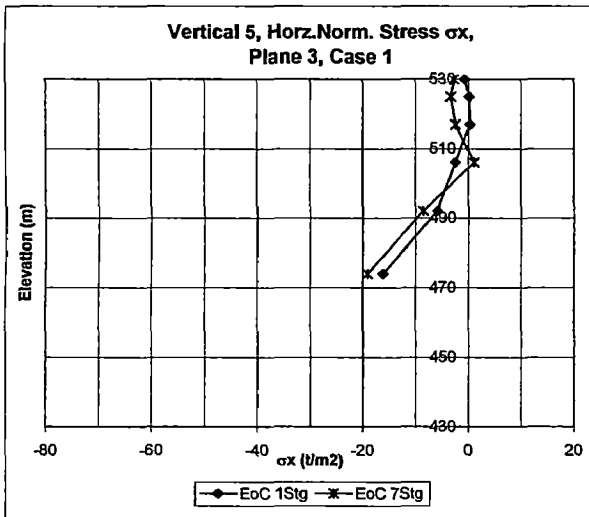
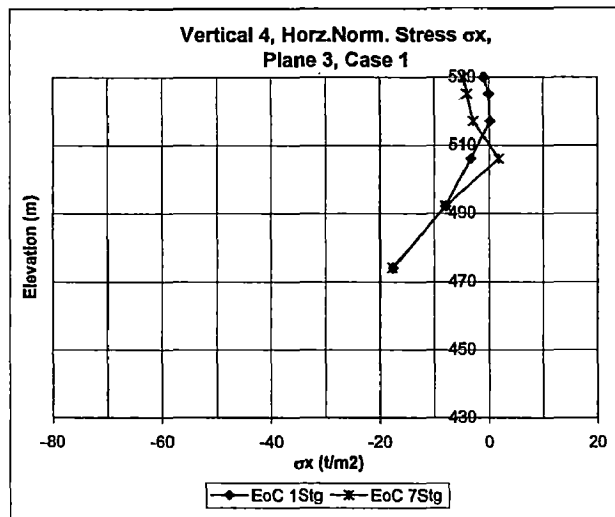
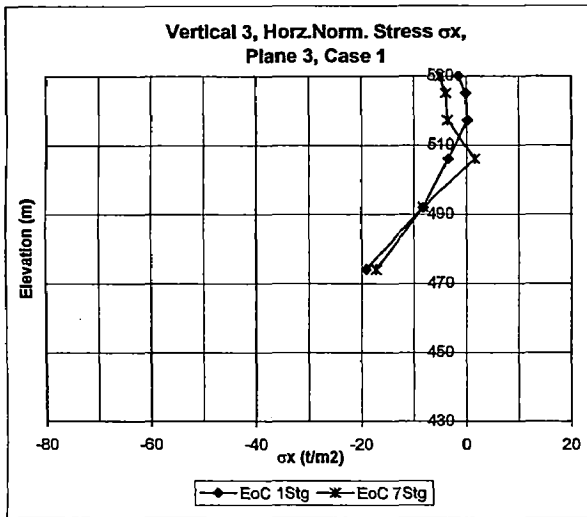
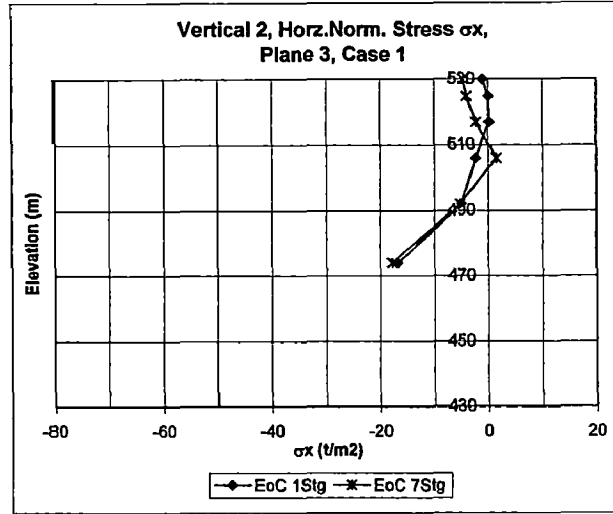
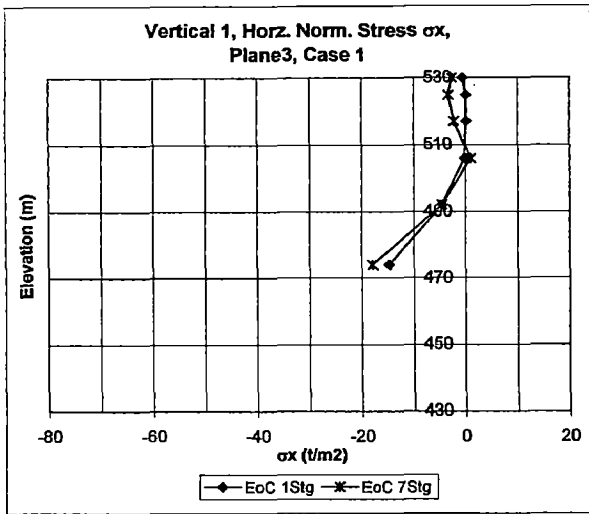


Fig.6.11. Horizontal Normal Stress  $\sigma_x$  along Height at Different Location over Plane 3, Case 1



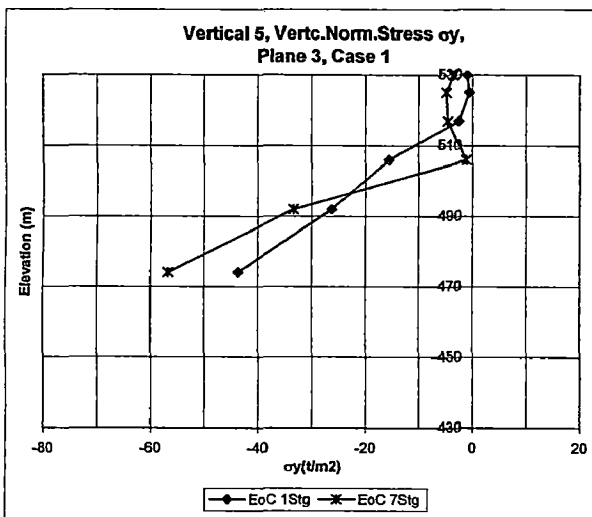
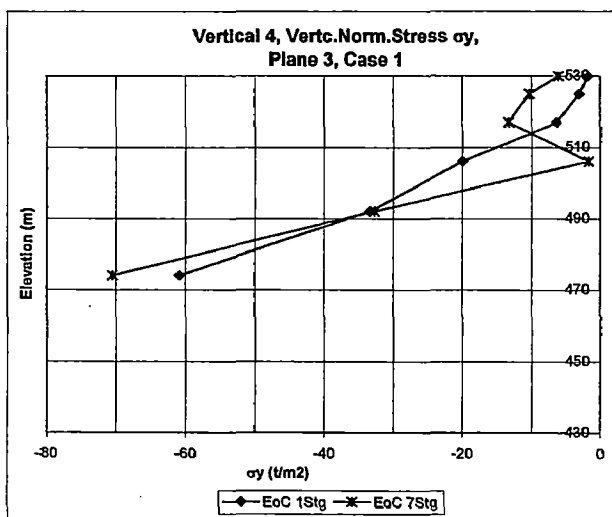
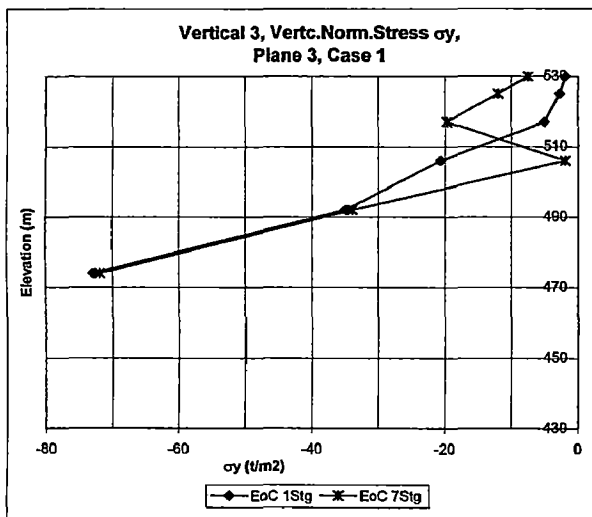
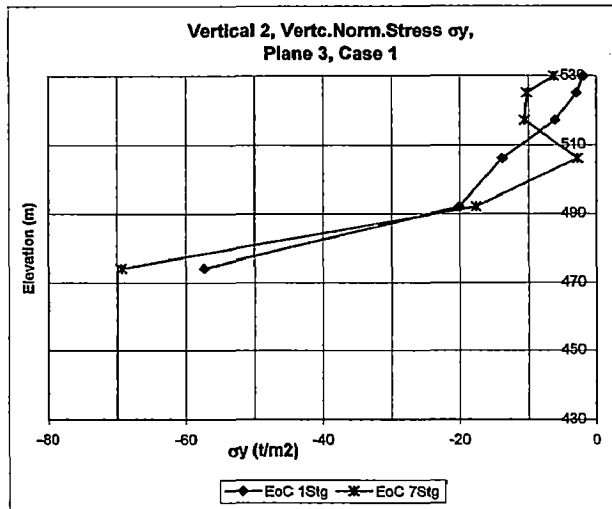
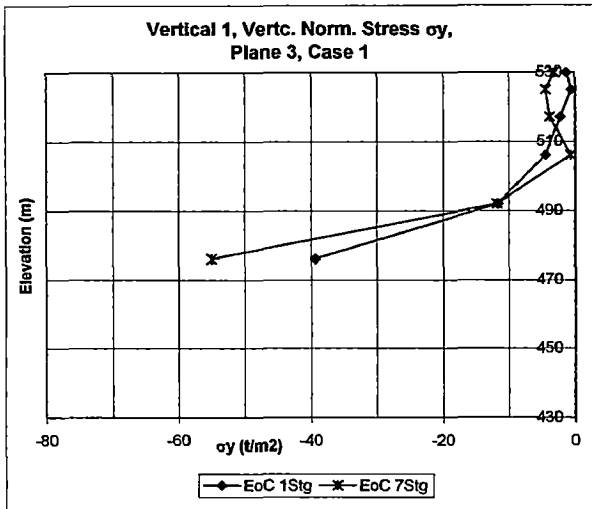


Fig.6.12. Vertical Normal Stress  $\sigma_y$  along Height at Different Location over Plane 3, Case 1

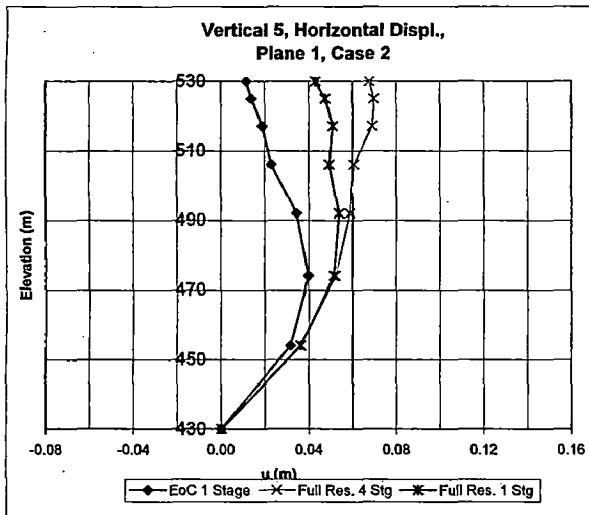
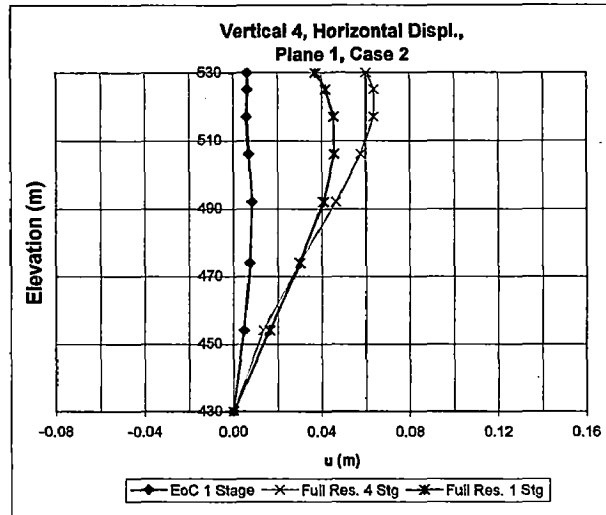
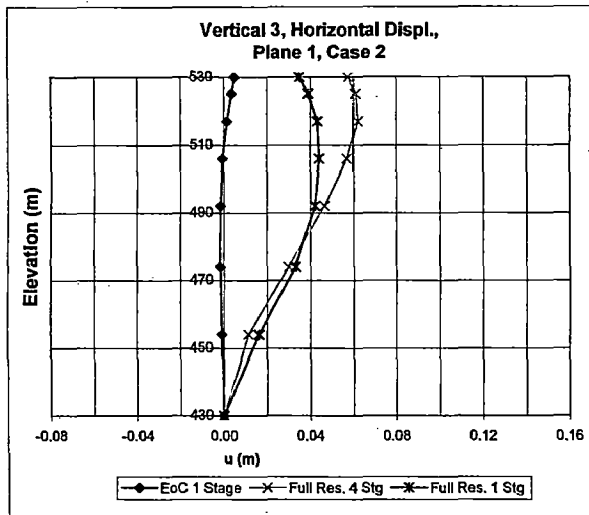
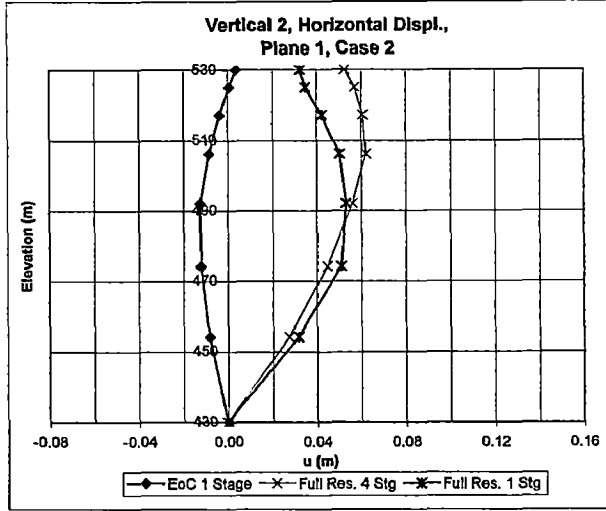
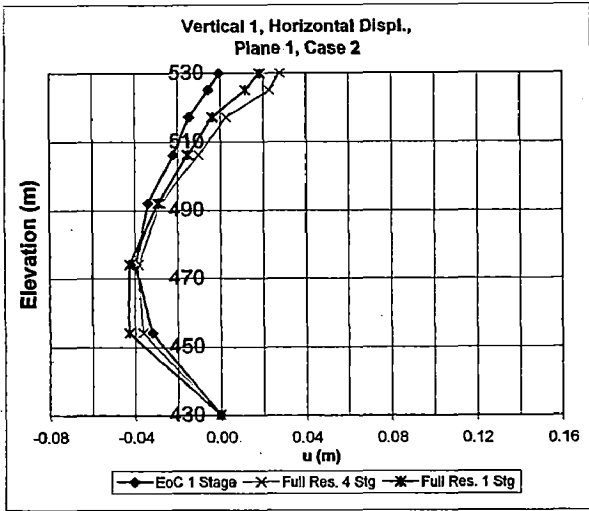


Fig.6.13. Horizontal Displ. u along Height at Different Location over Plane 1, Case 2

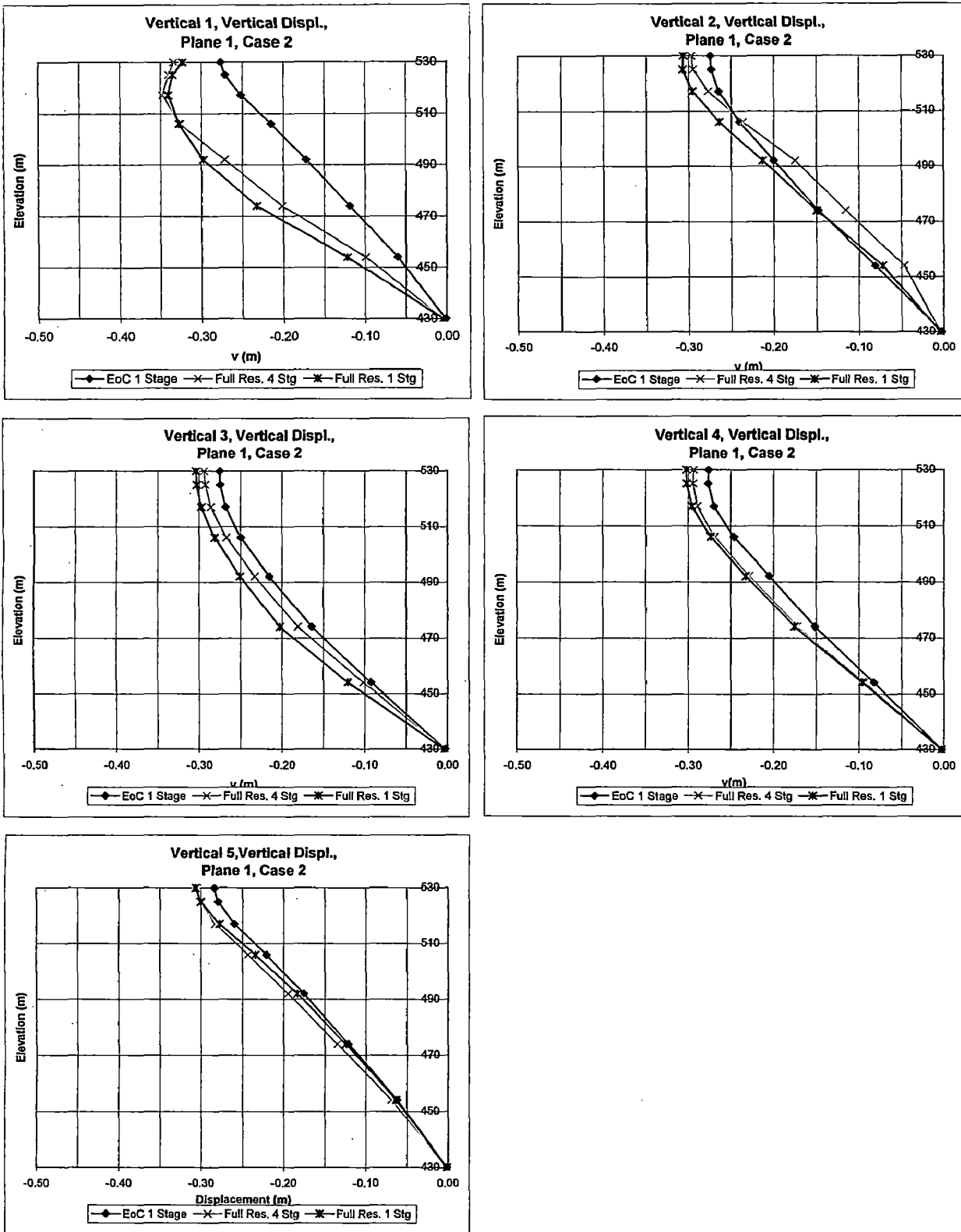
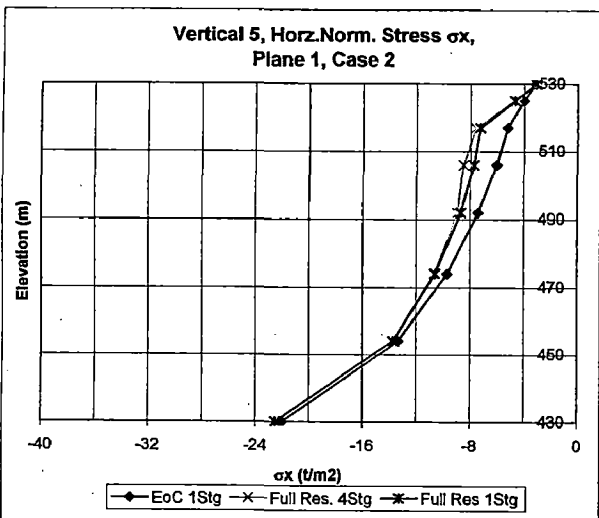
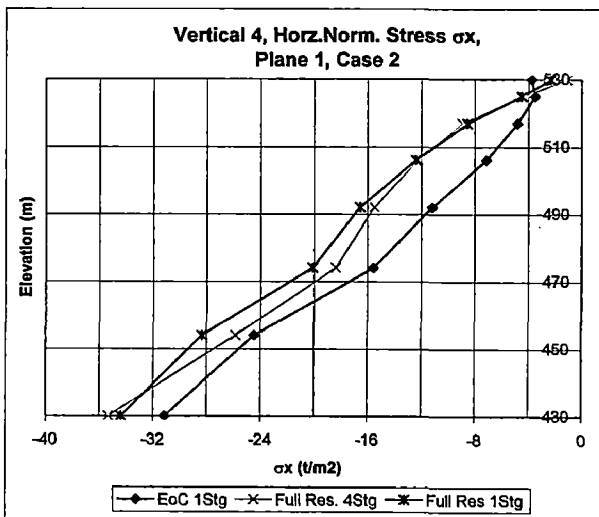
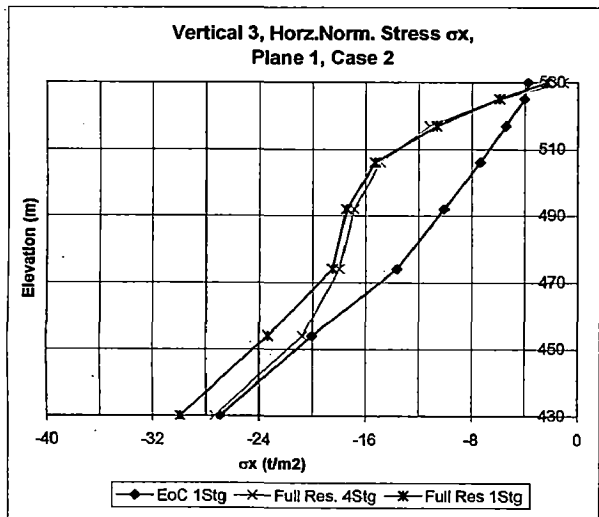
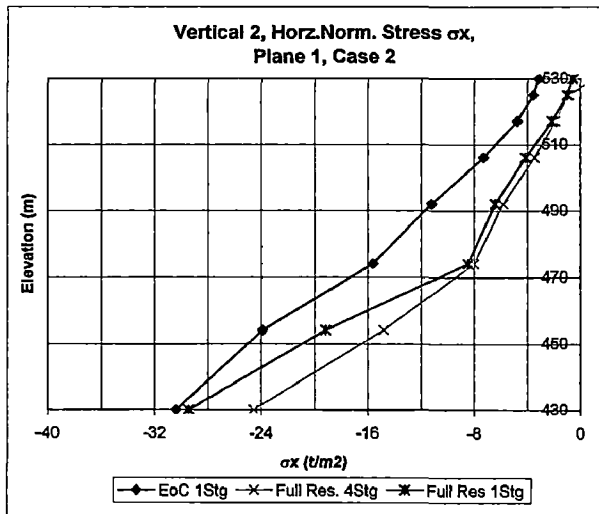
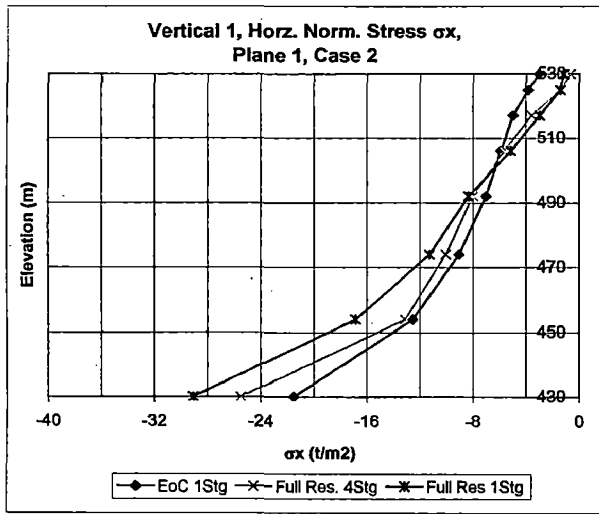


Fig.6.14. Vertical Movement - v along Height at Different Location over Plane 1, Case 2



**Fig.6.15. Horizontal Normal Stress  $\sigma_x$  along Height at Different Location over Plane 1, Case 2**

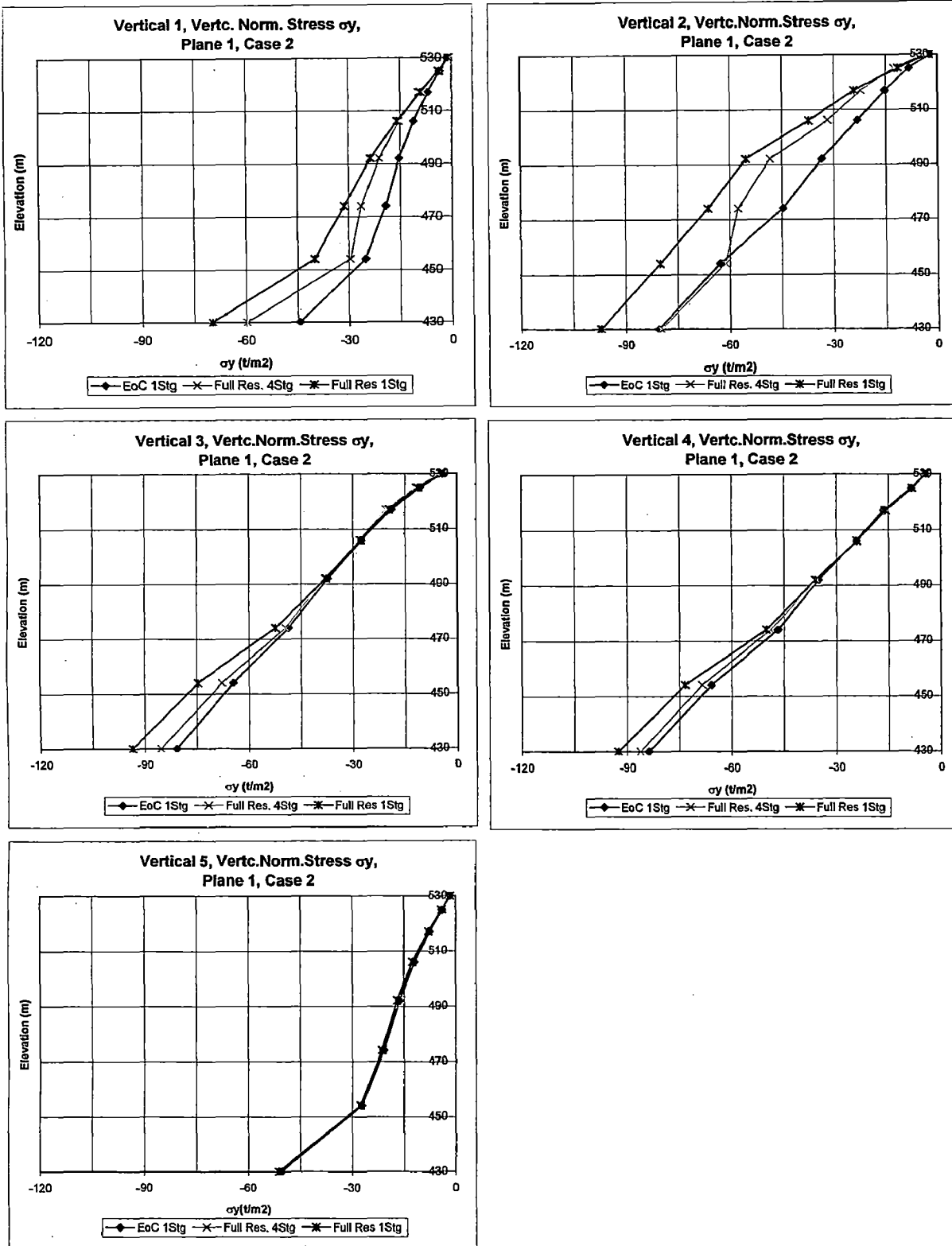


Fig.6.16. Vertical Normal Stress  $\sigma_y$  along Height at Different Location over Plane 1, Case 2

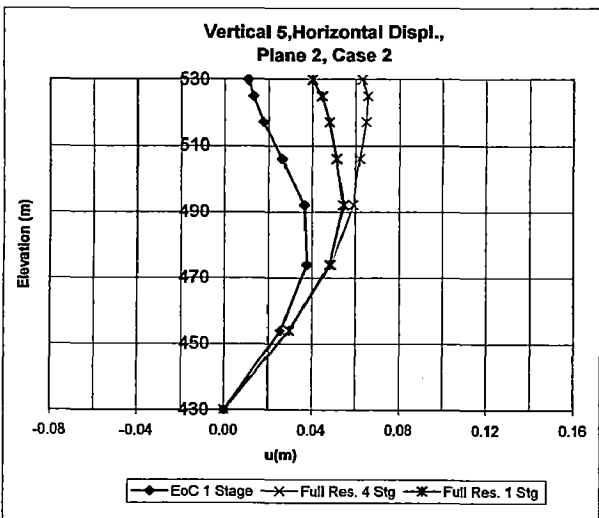
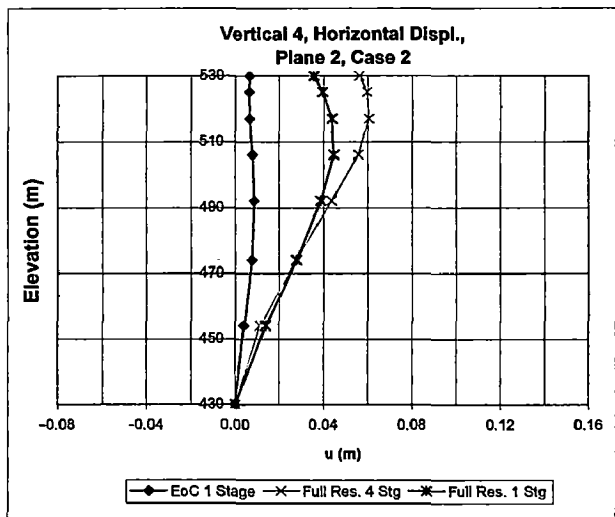
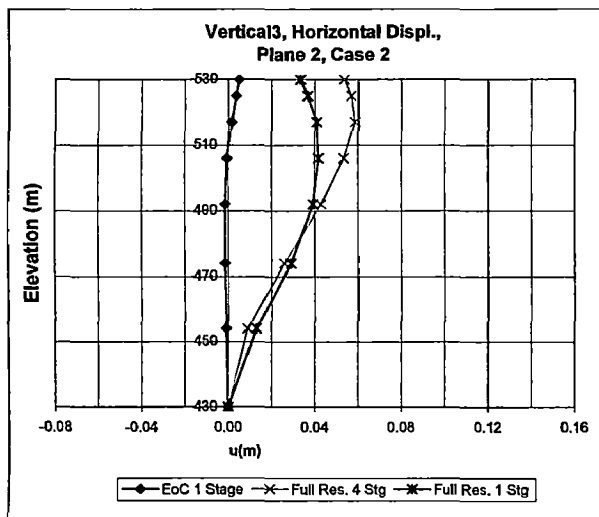
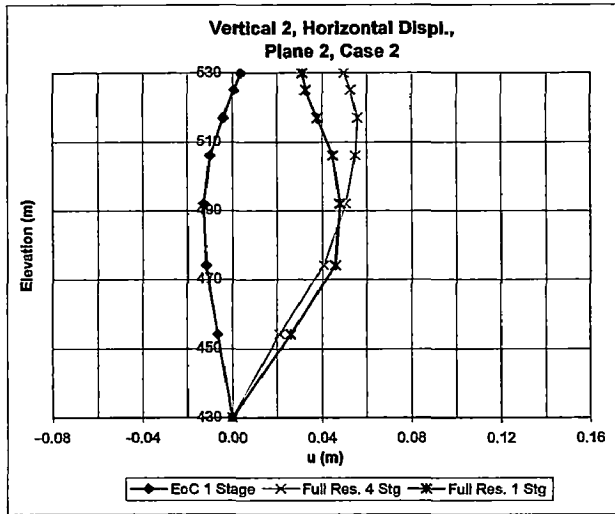
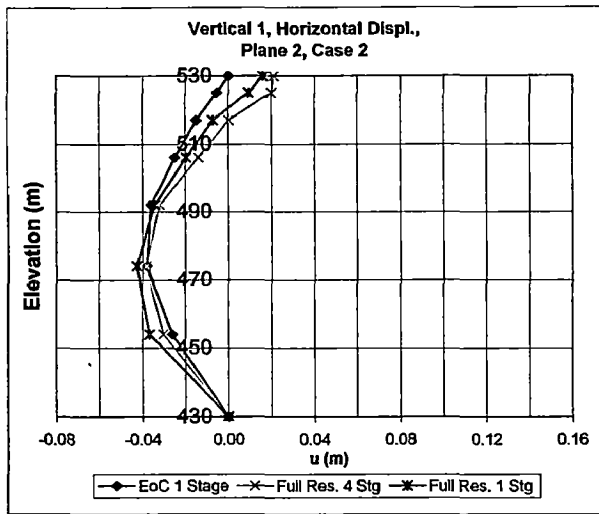


Fig.6.17. Horizontal Displ. u along Height at Different Location over Plane 2, Case 2

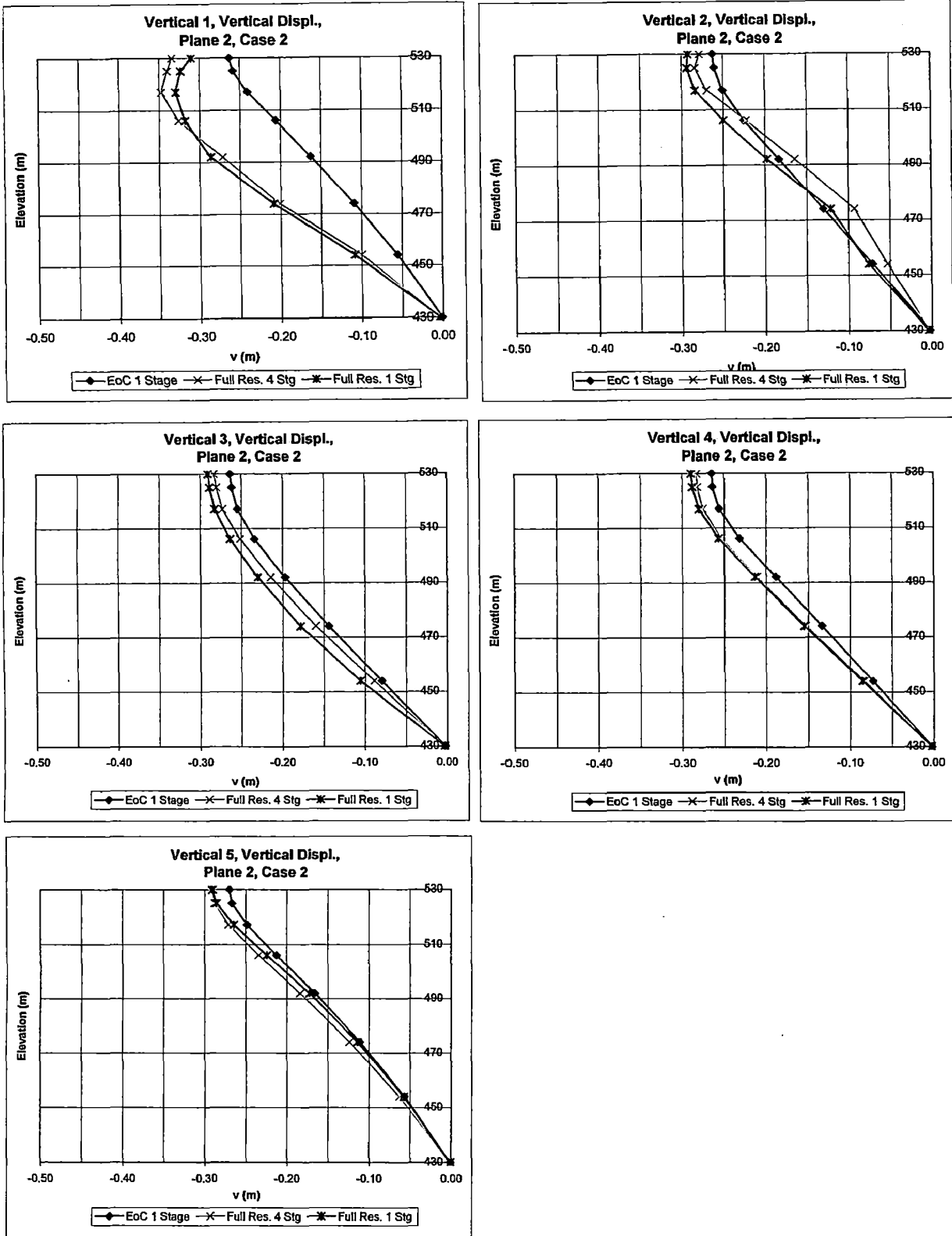


Fig.6.18. Vertical Displ. -  $v$  along Height at Different Location over Plane 2, Case 2

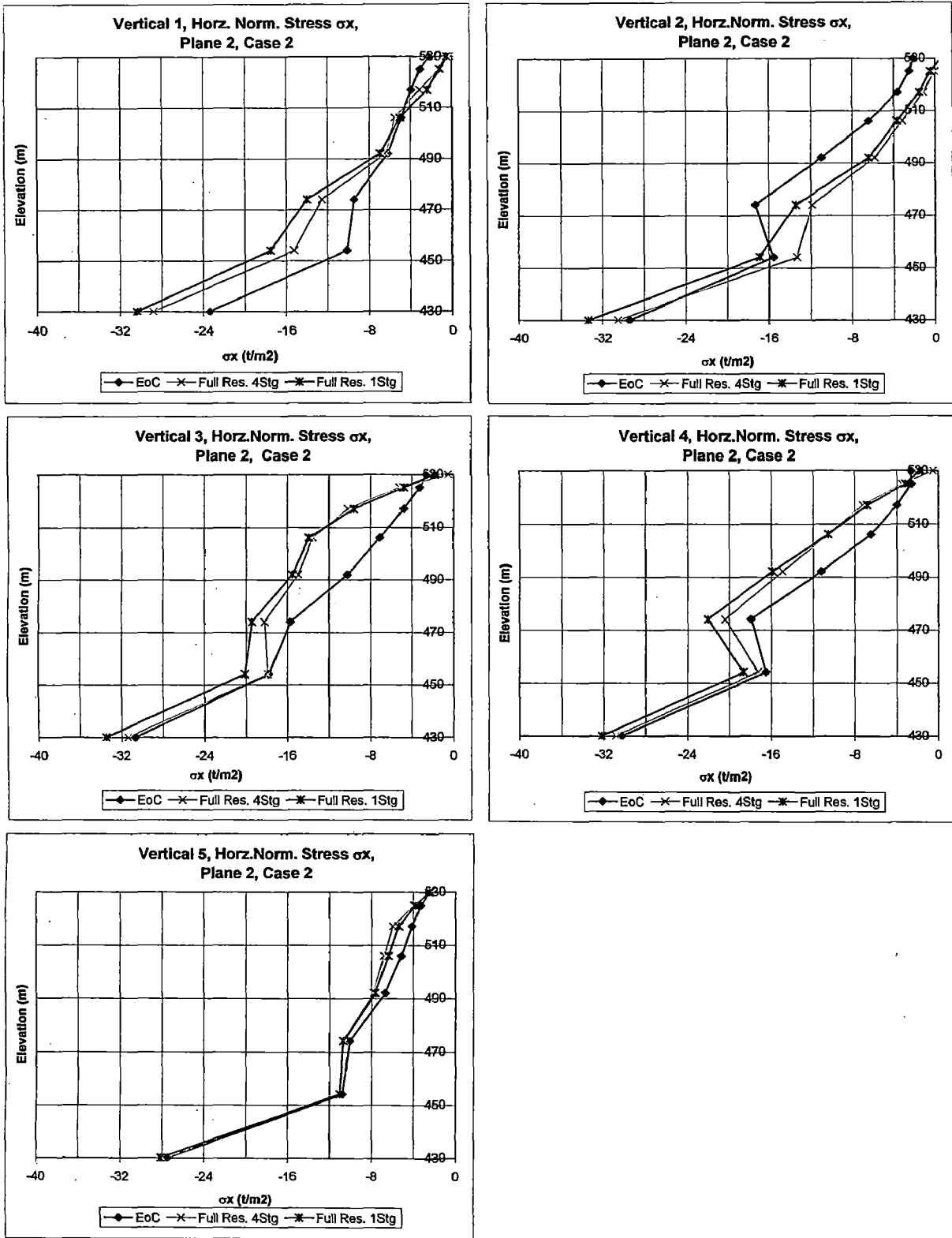


Fig.6.19. Horizontal Normal Stress  $\sigma_x$  along Height at Different Location over Plane 2, Case 2



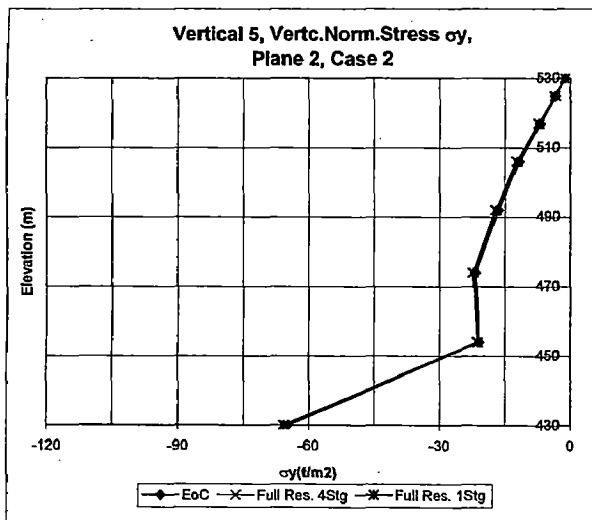
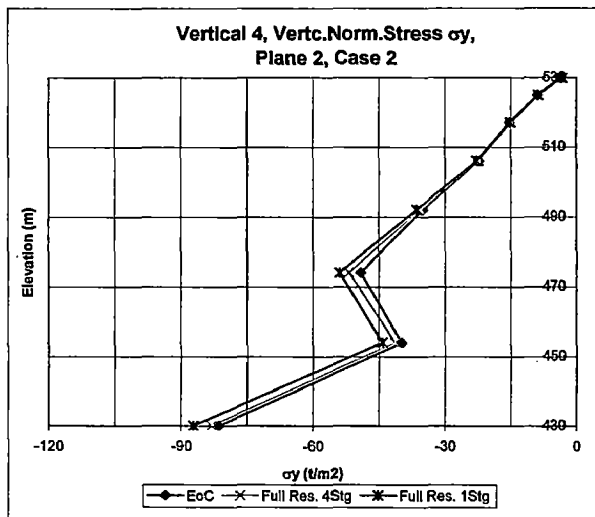
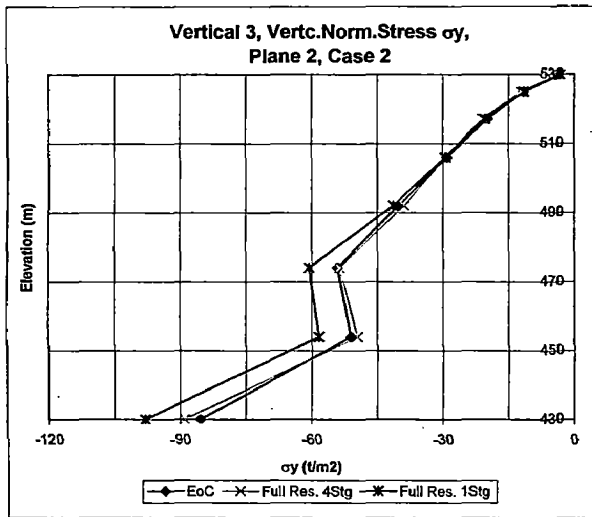
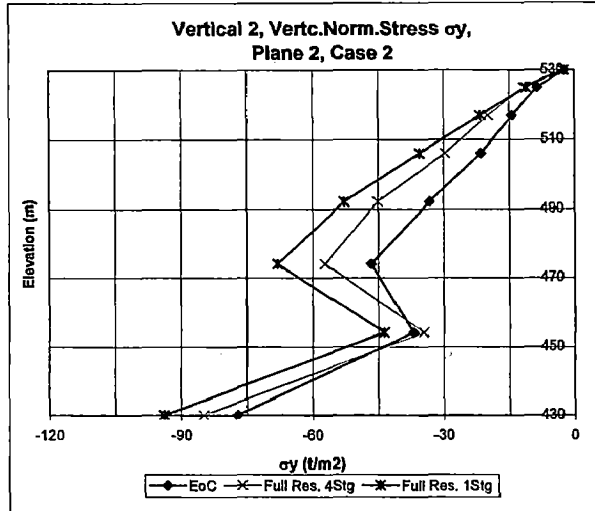
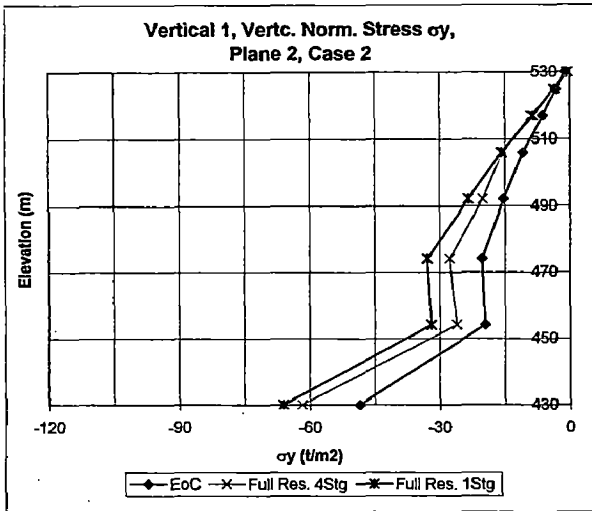


Fig.6.20. Vertical Normal Stress  $\sigma_y$  along Height at Different Location over Plane 2, Case 2

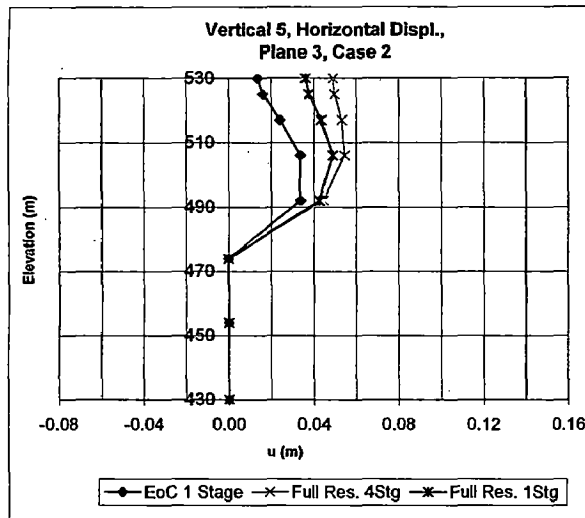
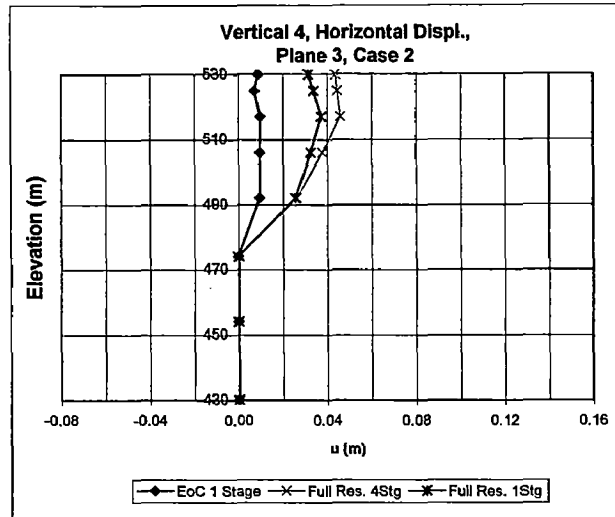
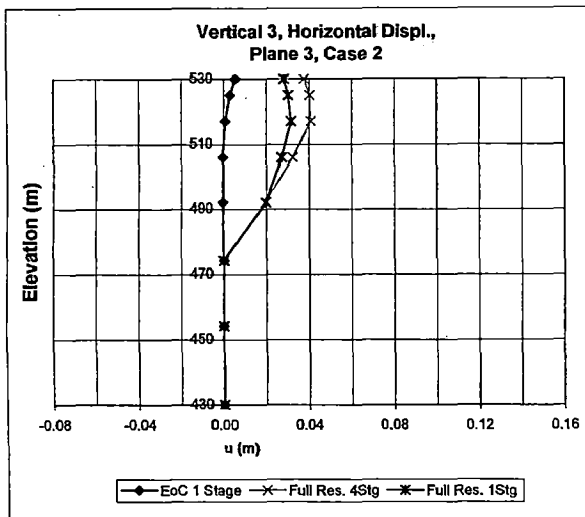
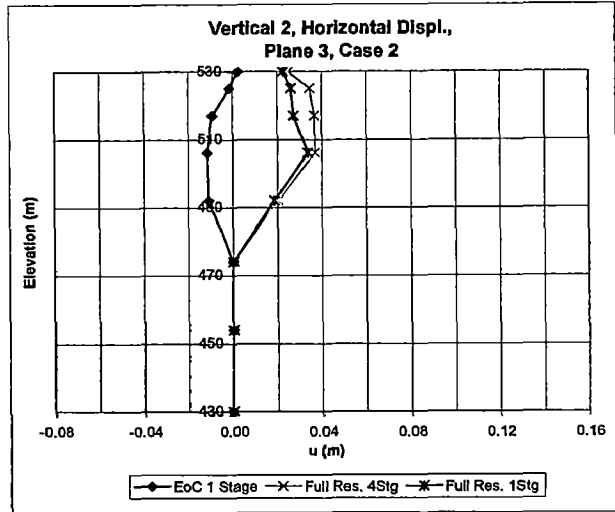
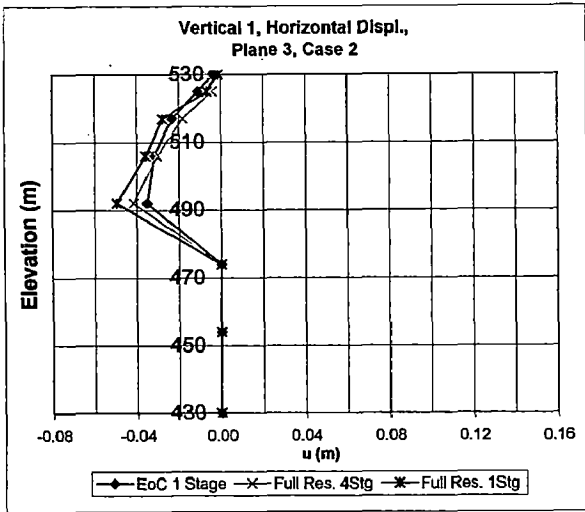


Fig.6.21. Horizontal Displ.  $u$  along Height at Different Location over Plane 3, Case 2

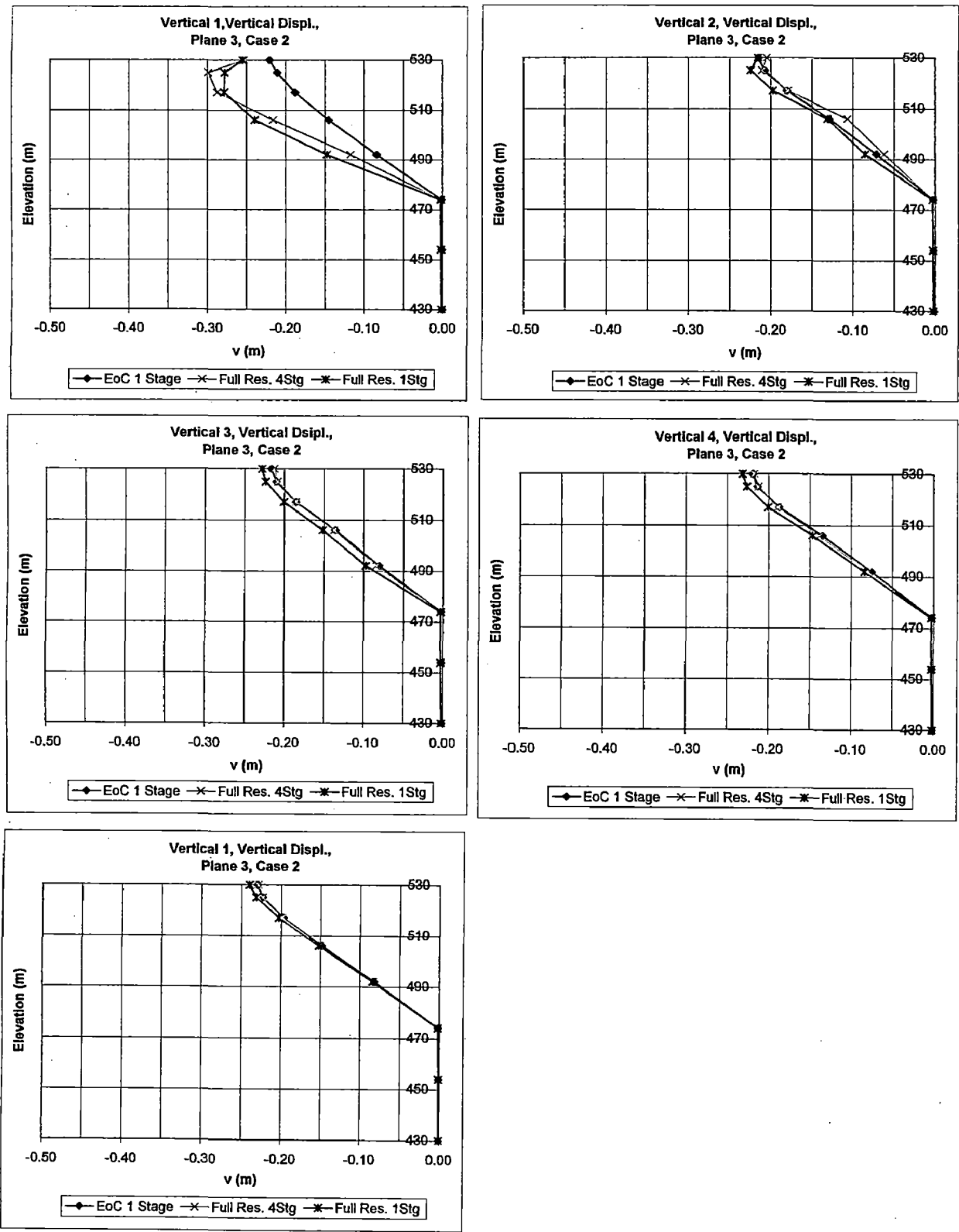
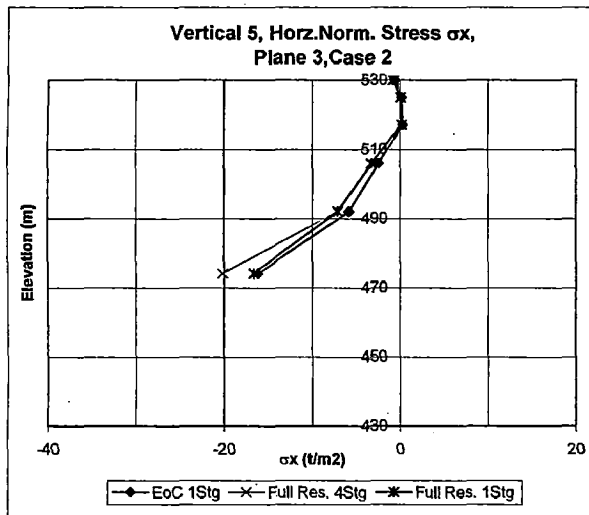
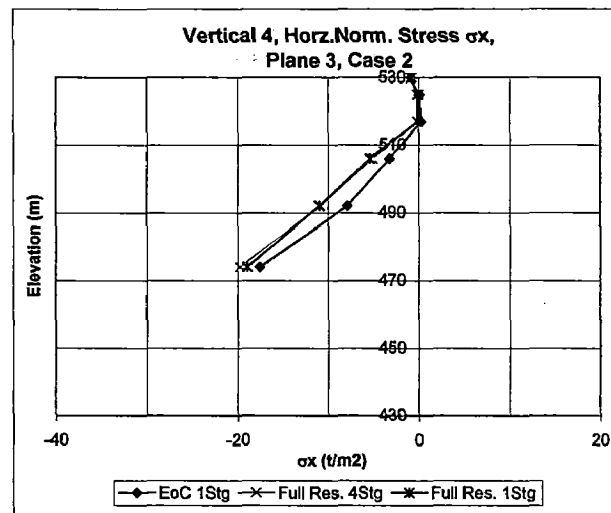
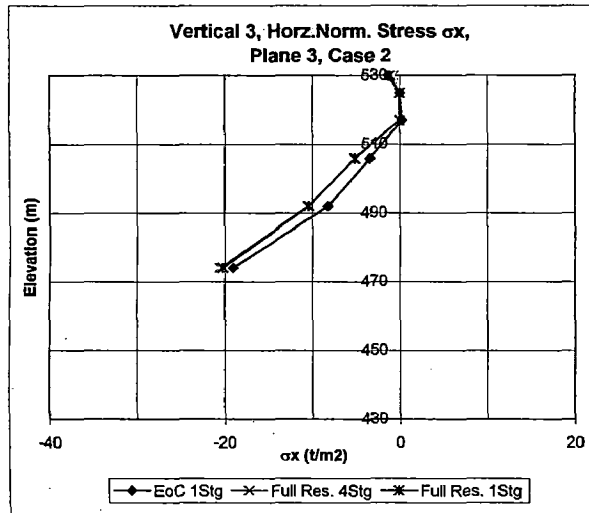
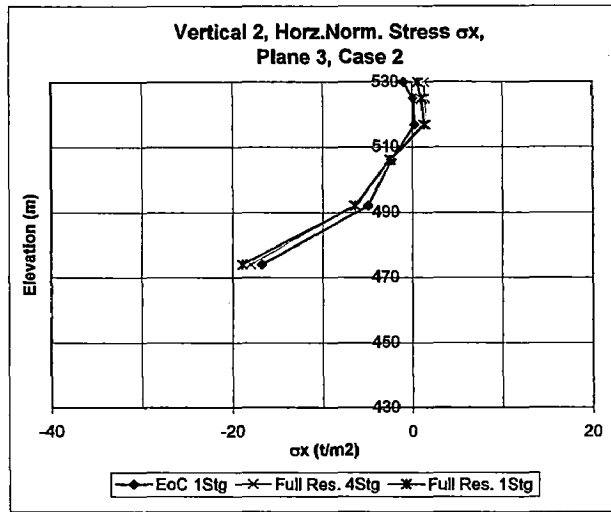
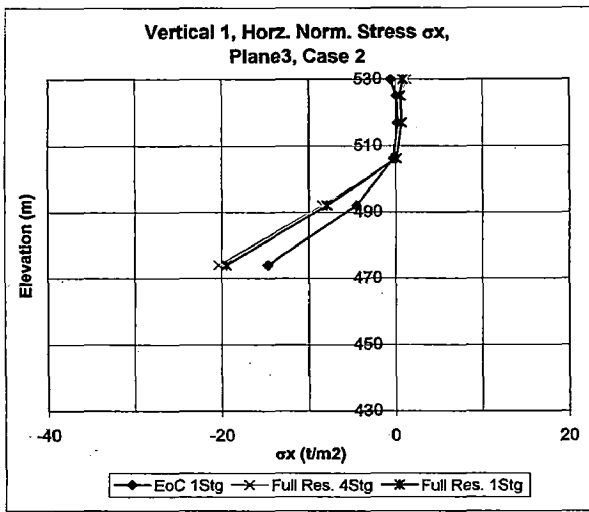


Fig.6.22. Vertical Displ. -  $v$  along Height at Different Location over Plane 3, Case 2



**Fig.6.23. Horizontal Normal Stress  $\sigma_x$  along Height at Different Location over Plane 3, Case 2**

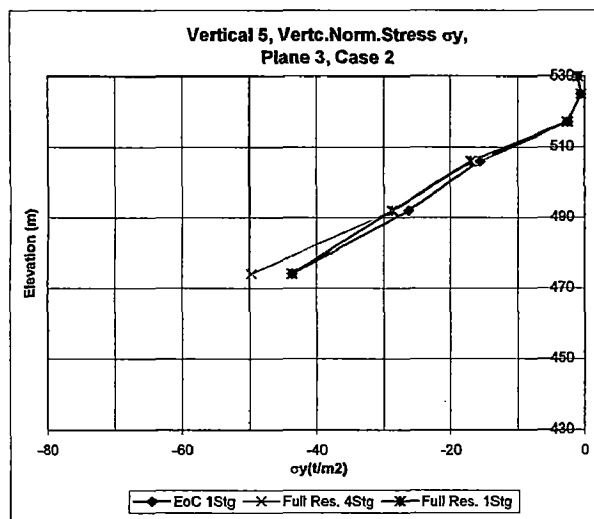
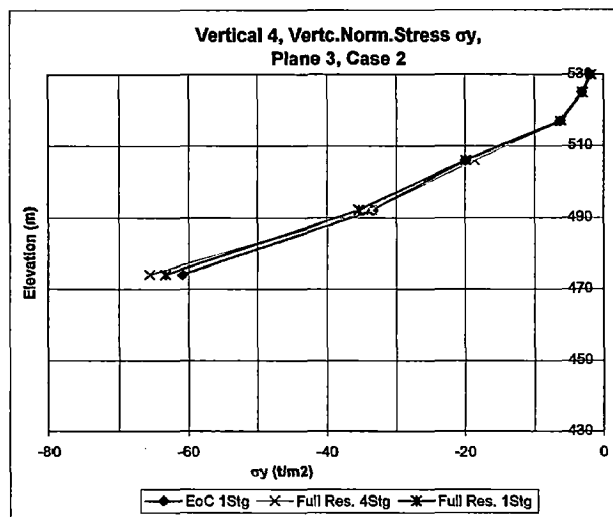
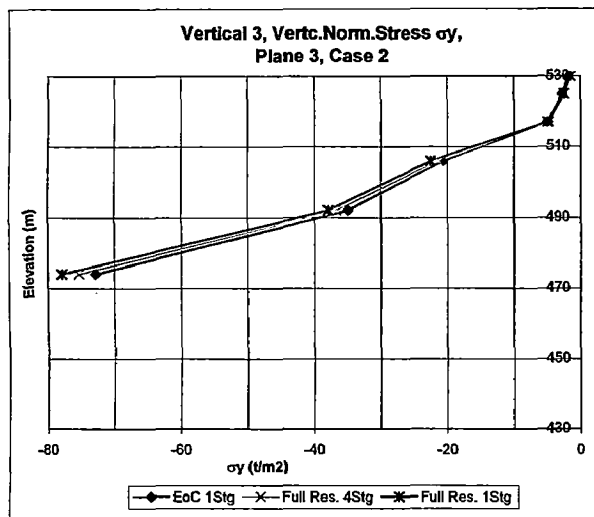
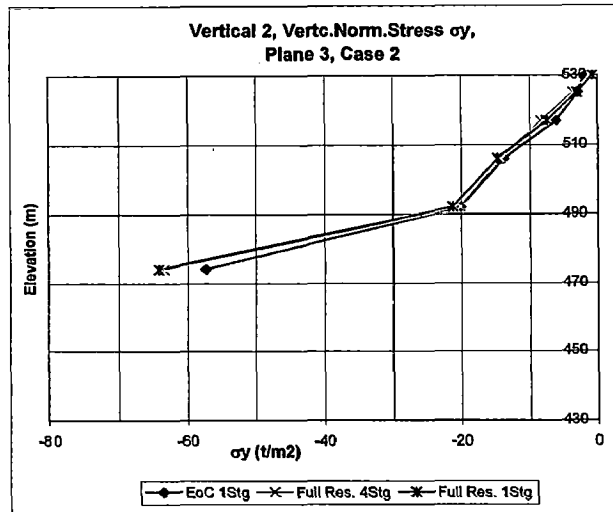
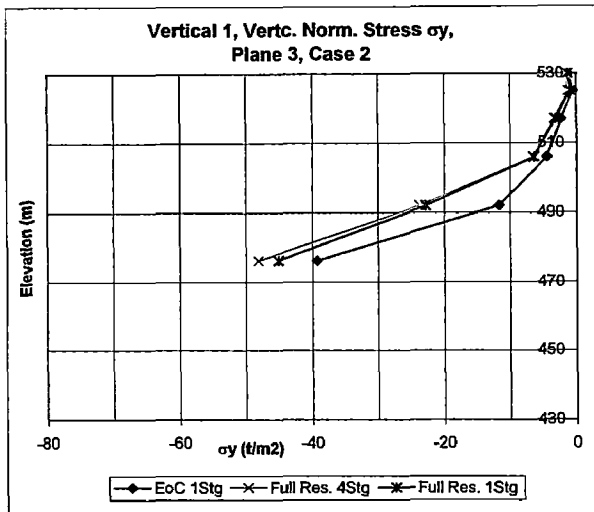


Fig.6.24. Vertical Normal Stress  $\sigma_y$  along Height at Different Location over Plane 3, Case 2

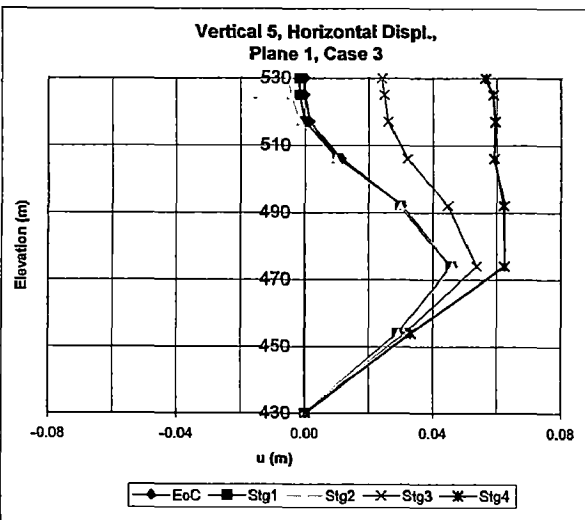
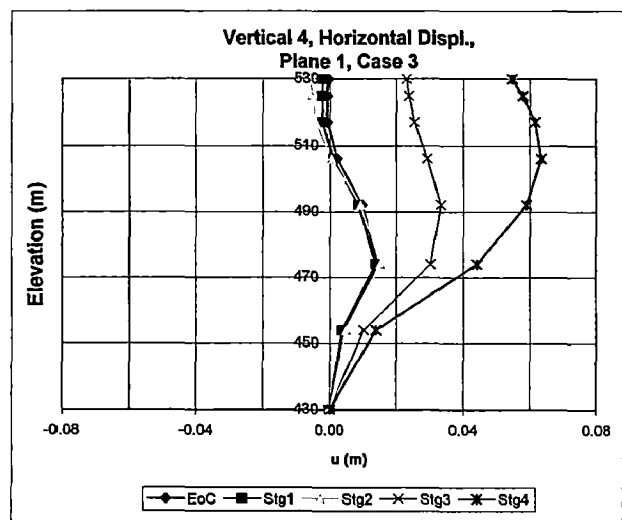
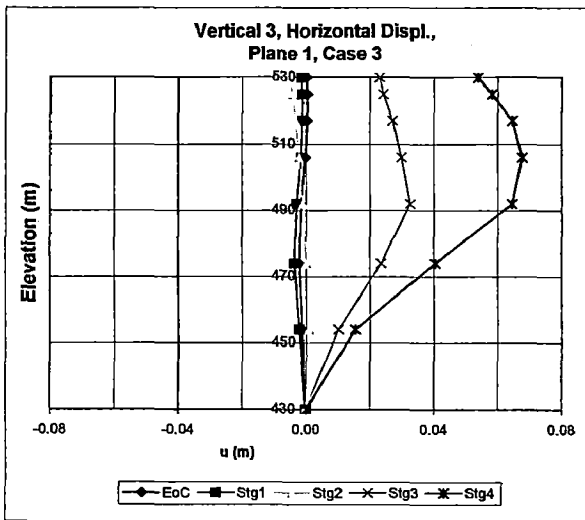
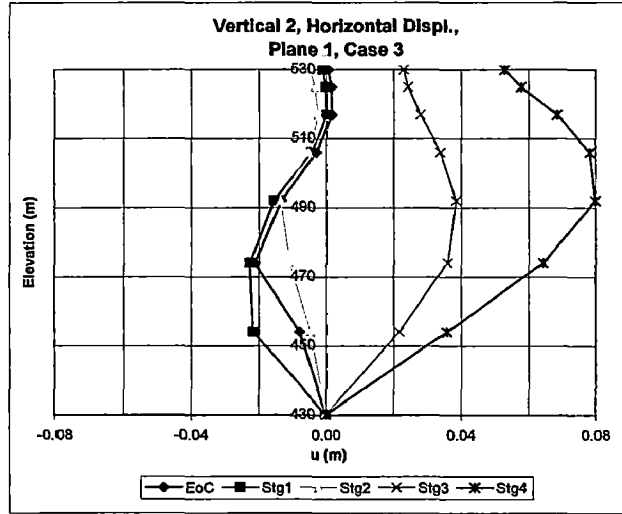
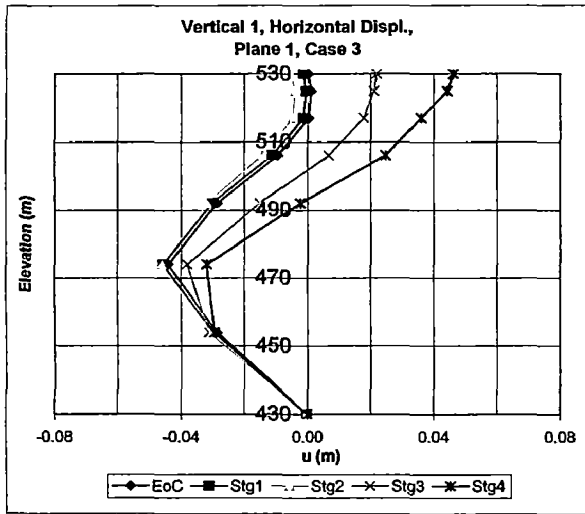


Fig.6.25. Horizontal Displ. u along Height at Different Location over Plane 1, Case 3

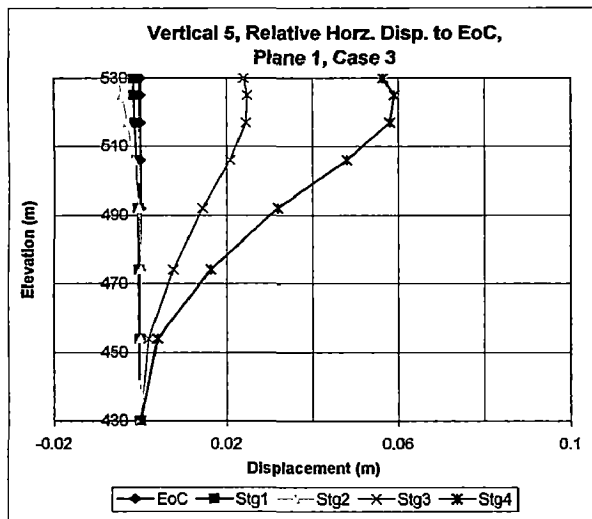
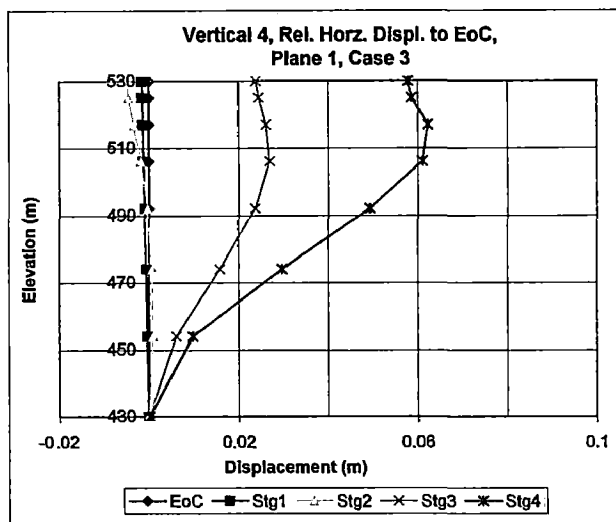
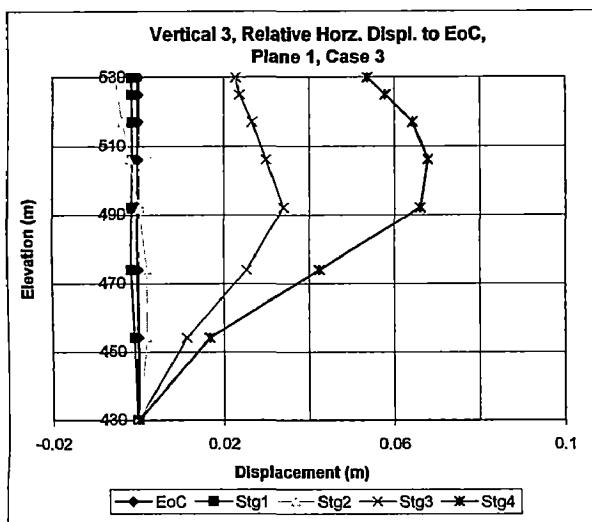
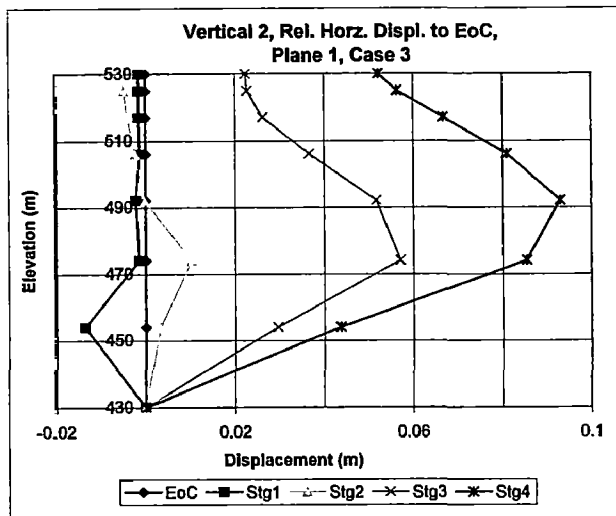
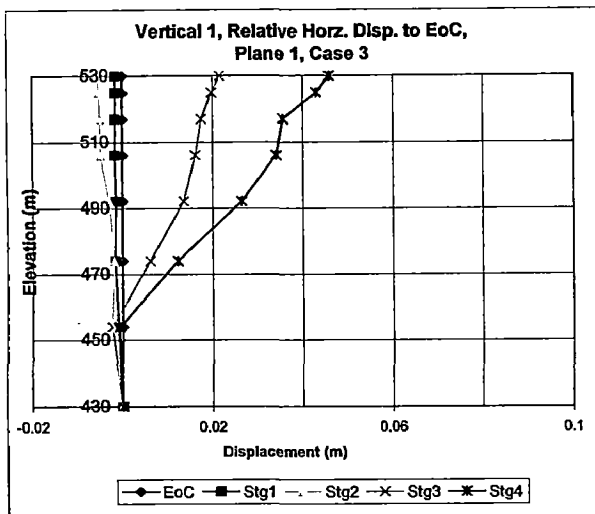


Fig.6.26. Relative Horizontal Displacement to End of Construction over Plane 1, Case 3

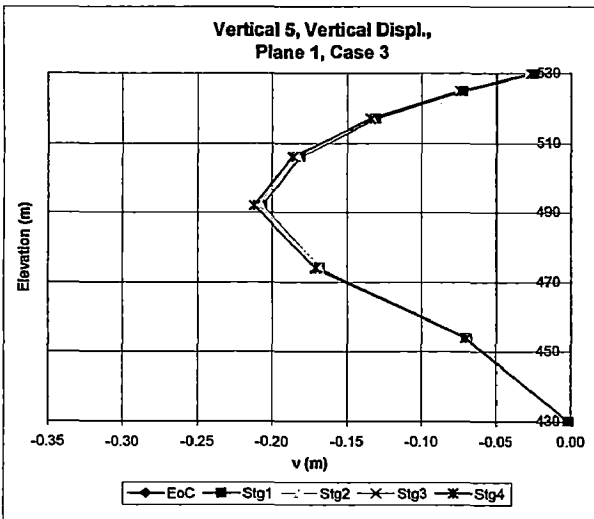
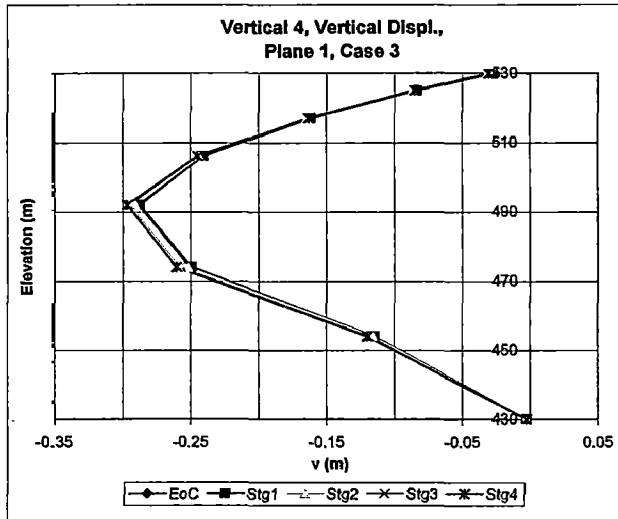
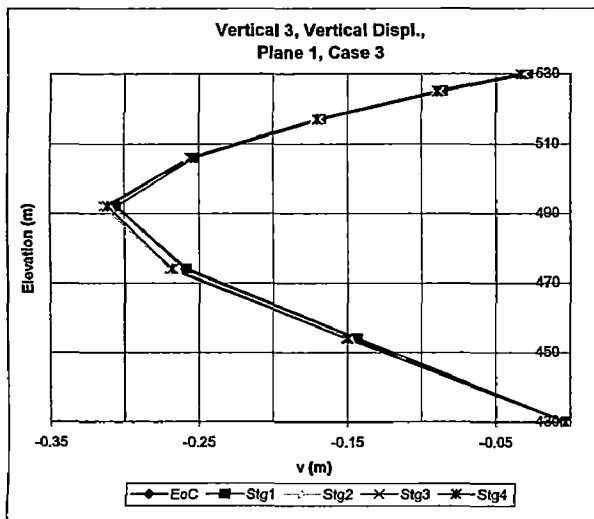
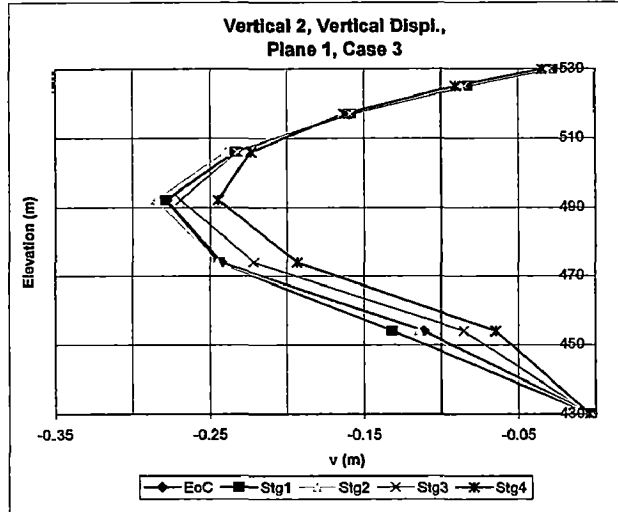
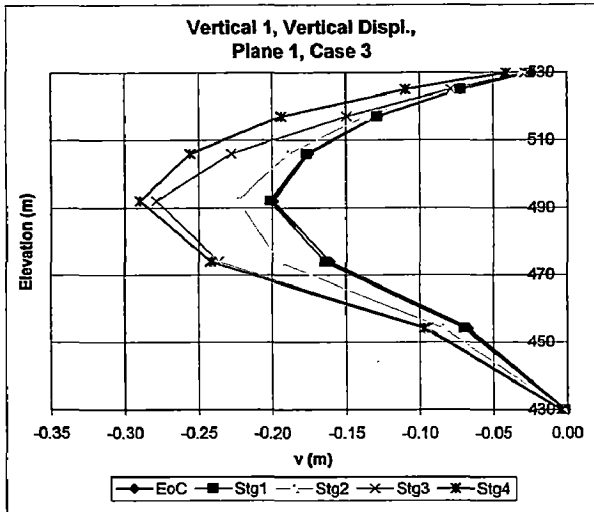


Fig.6.27. Vertical Displ. - v along Height at Different Location over Plane 1, Case 3



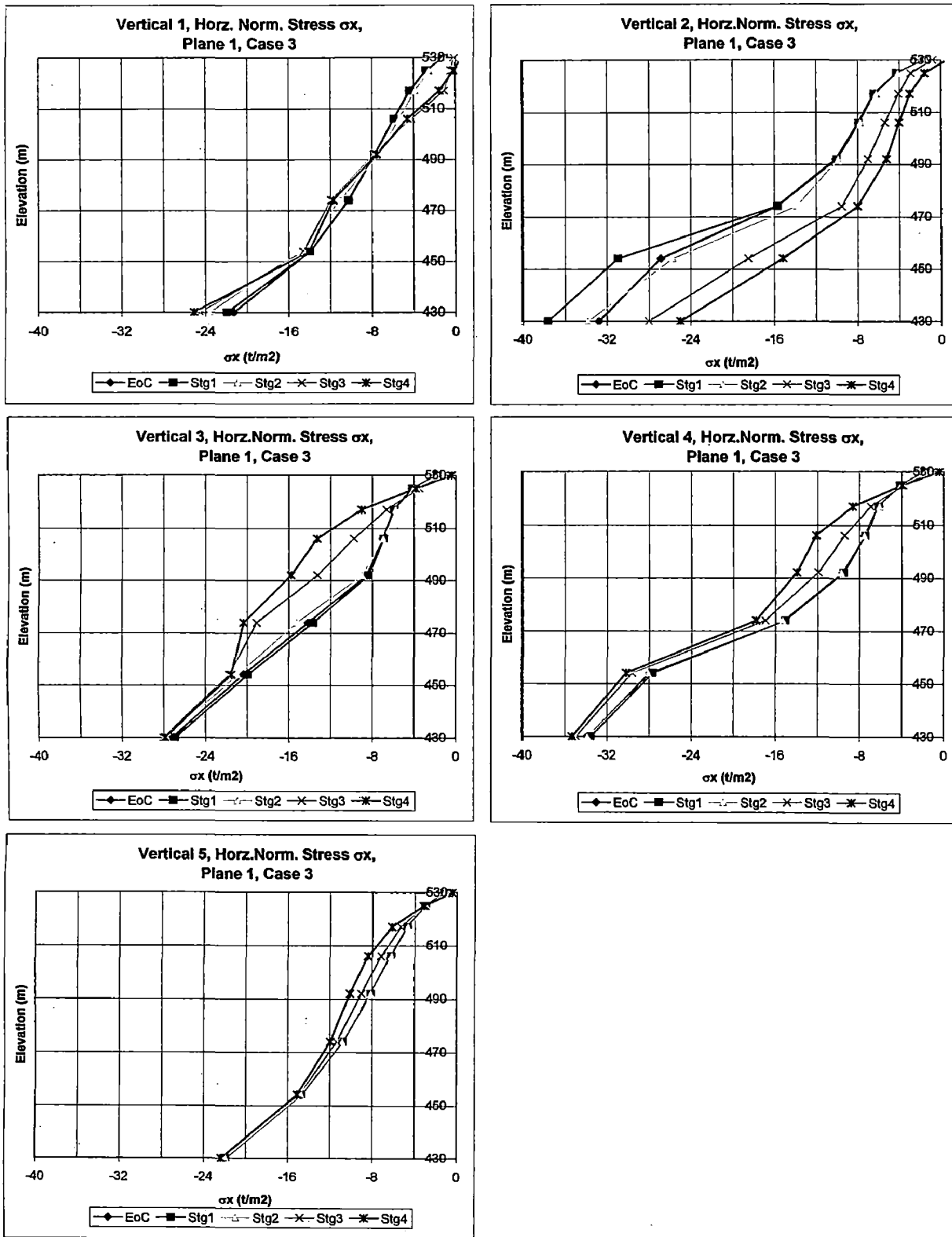


Fig.6.28. Horizontal Normal Stress  $\sigma_x$  along Height at Different Location over Plane 1, Case 3

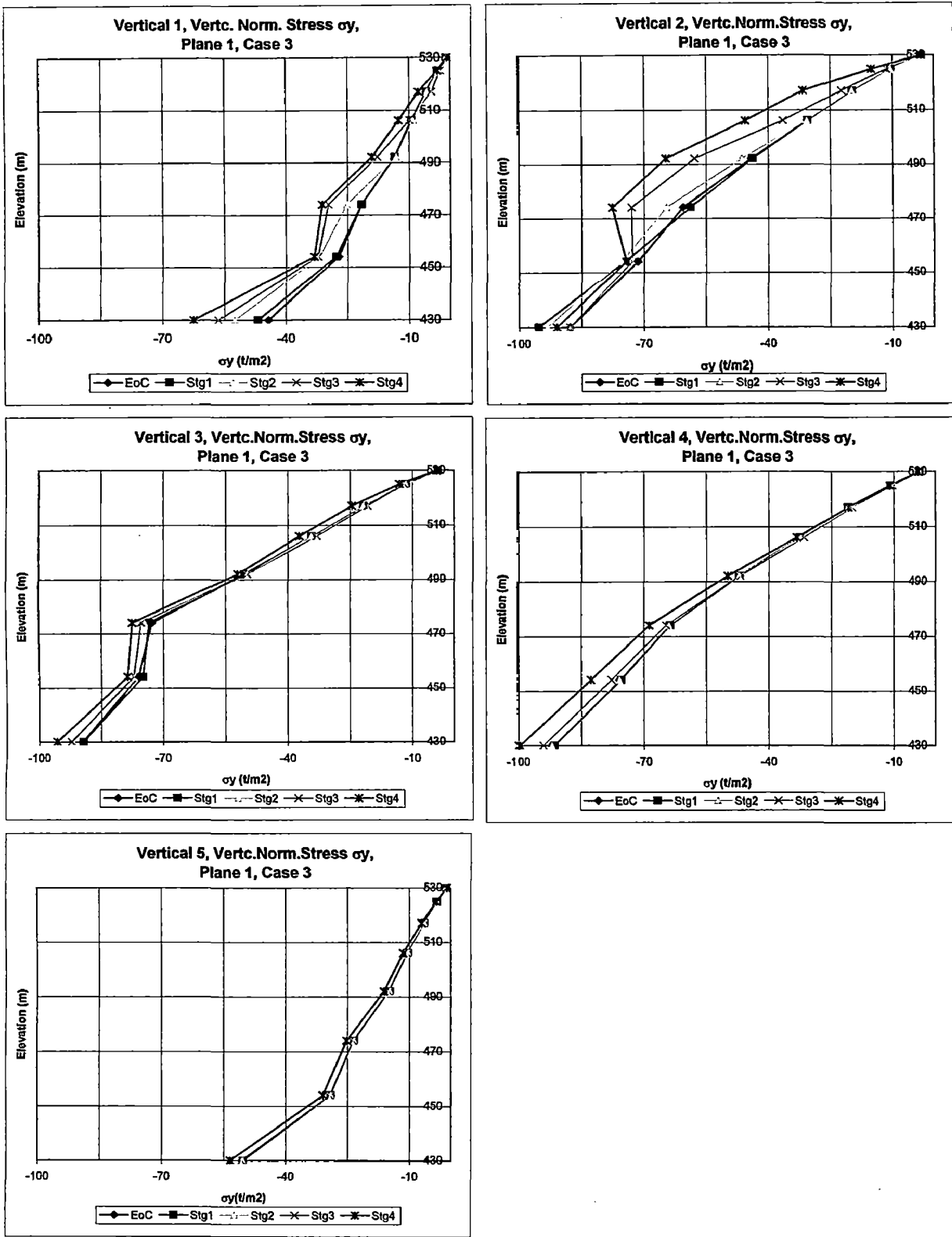


Fig.6.29. Vertical Normal Stress  $\sigma_y$  along Height at Different Location over Plane 1, Case 3

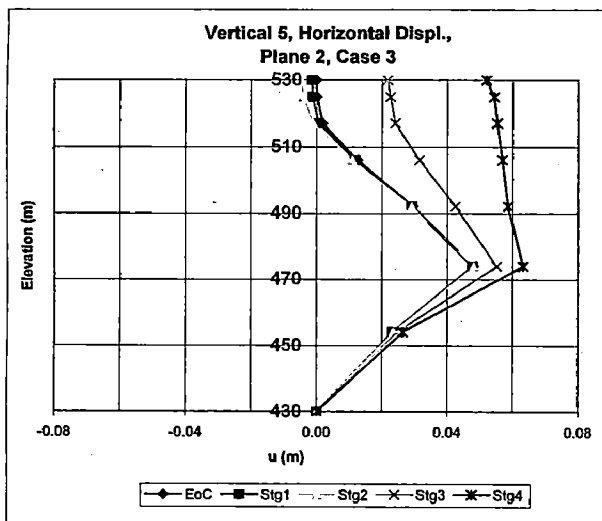
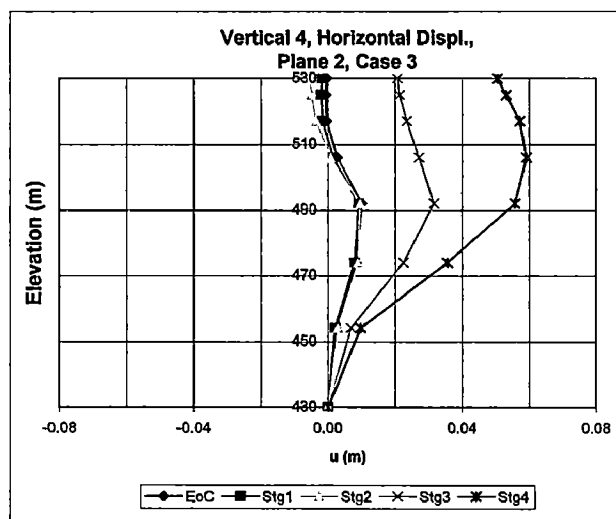
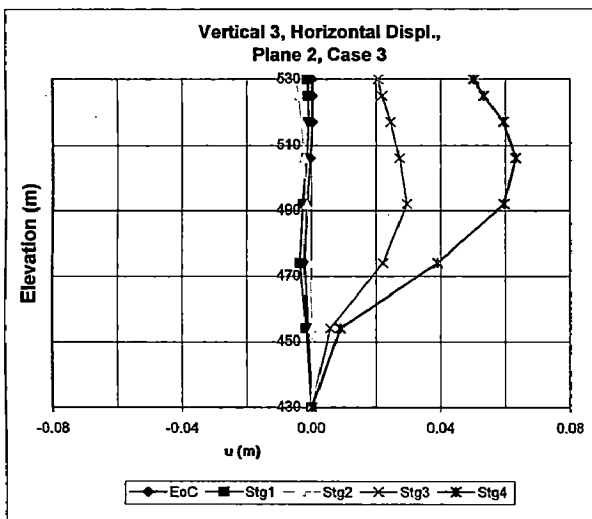
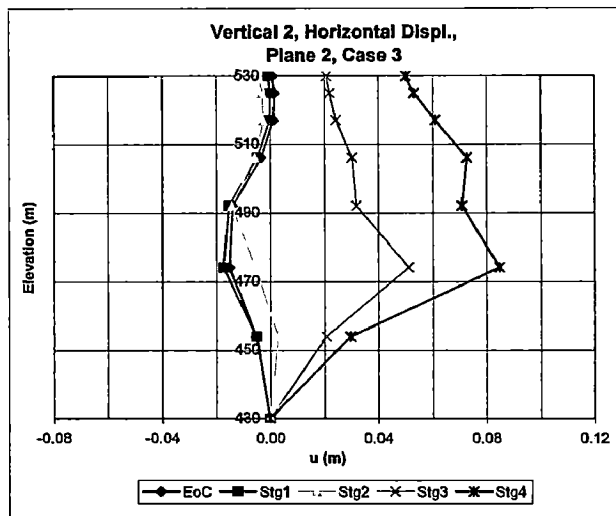
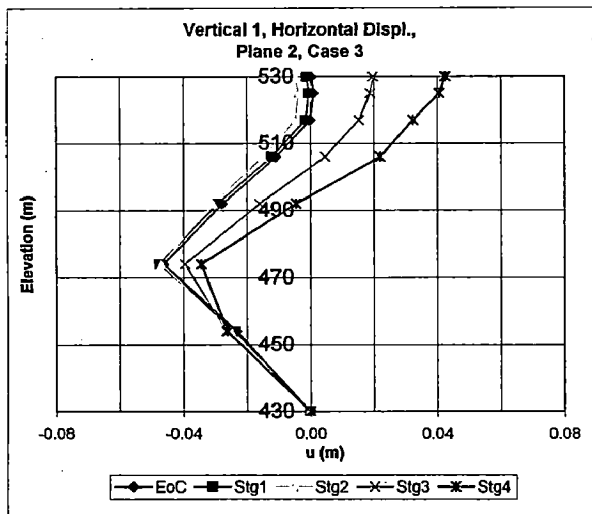


Fig.6.30. Horizontal Movement  $u$  along Height at Different Location over Plane 2, Case 3

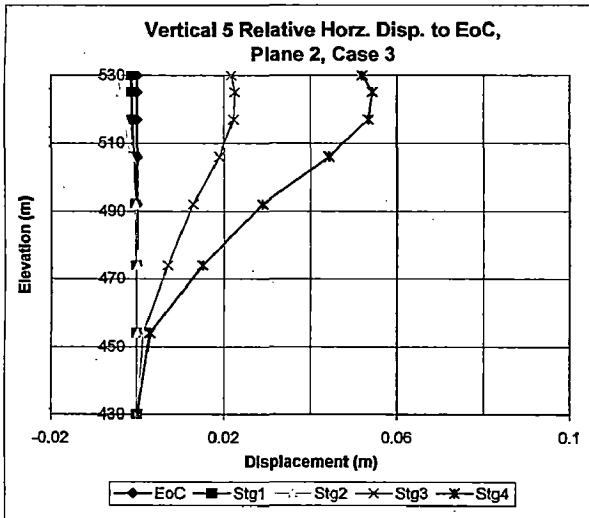
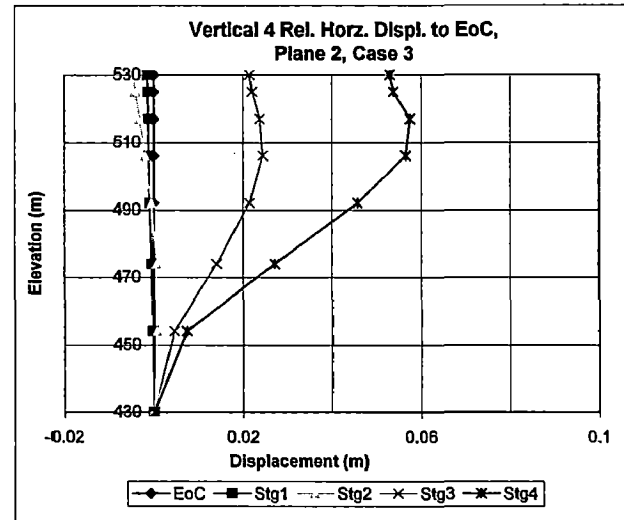
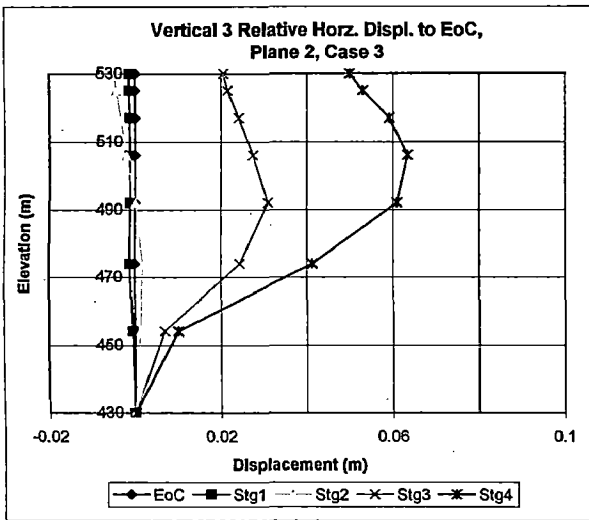
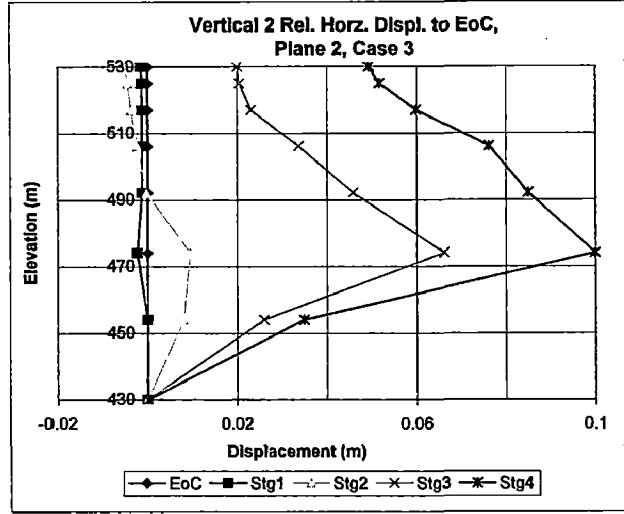
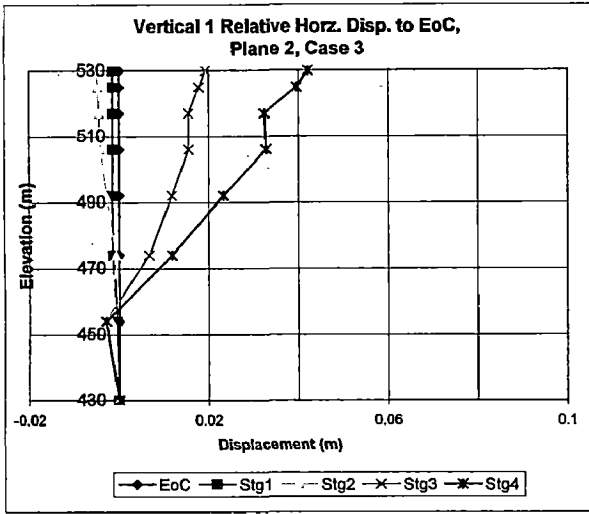


Fig.6.31. Relative Horizontal Displacement to End of Construction over Plane 2, Case 3

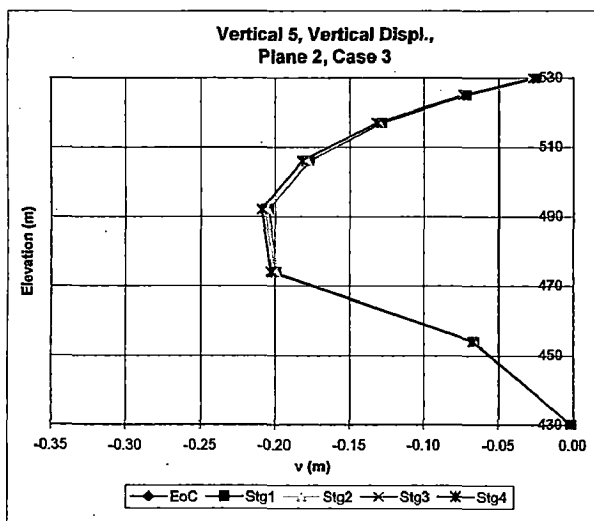
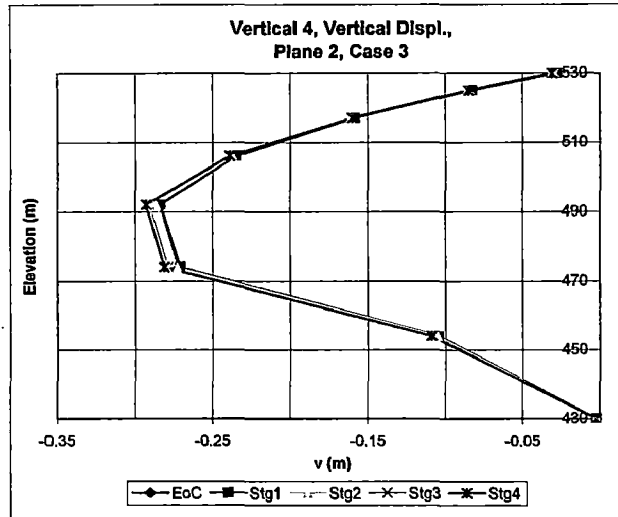
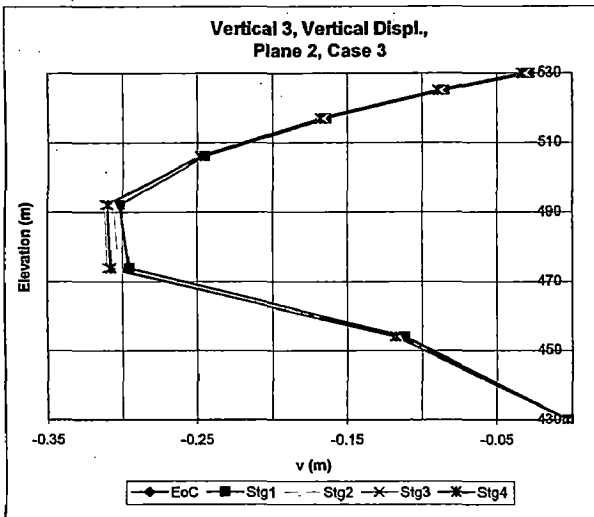
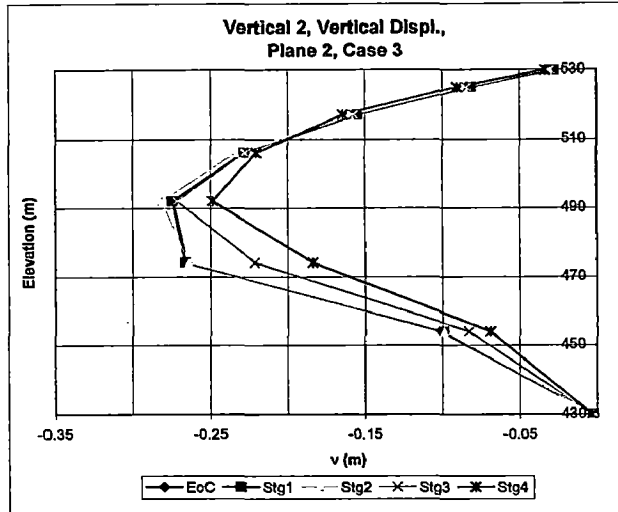
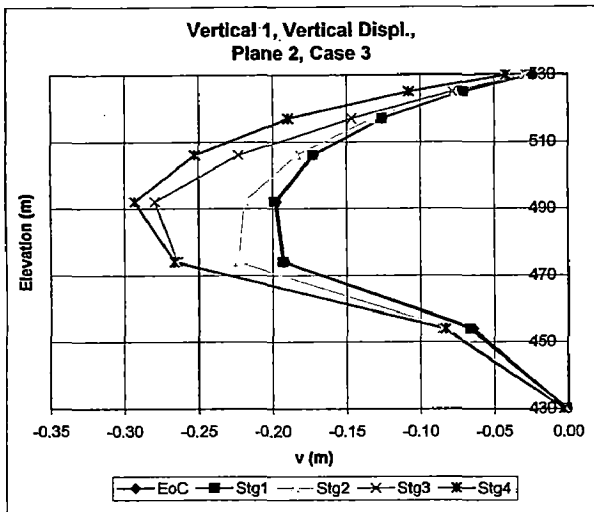


Fig.6.32. Vertical Displ. - v along Height at Different Location over Plane 2, Case 3

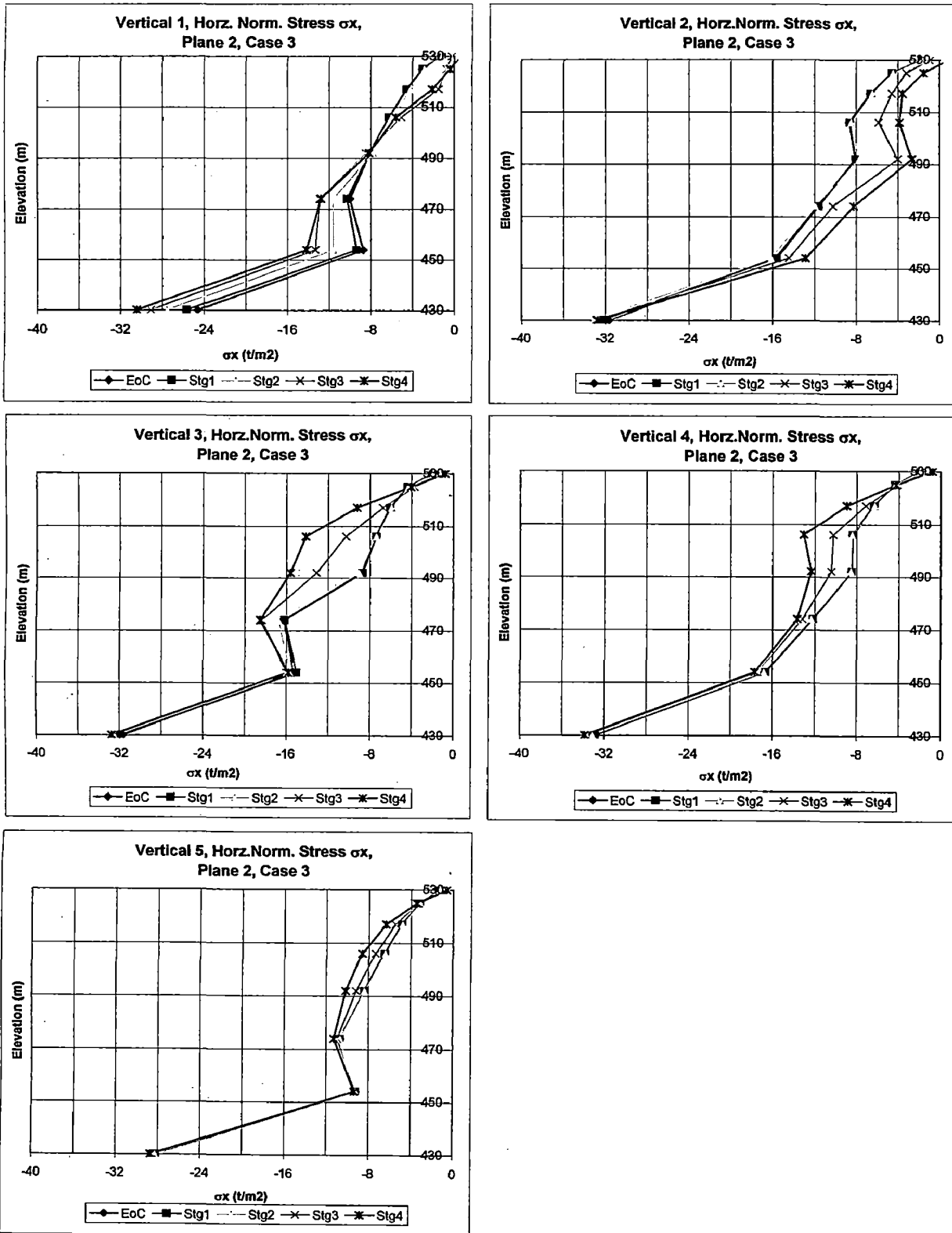
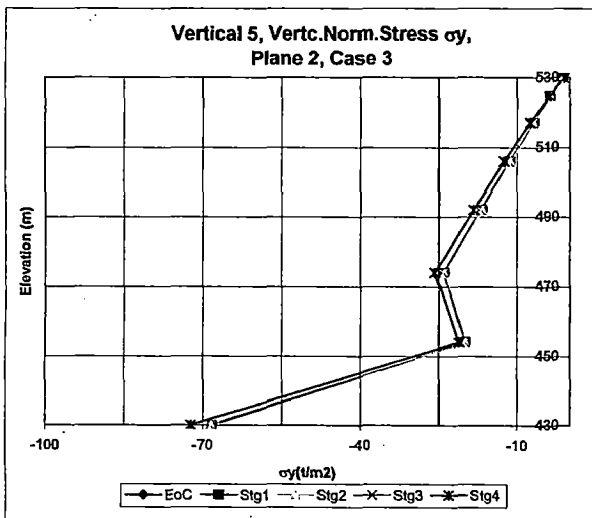
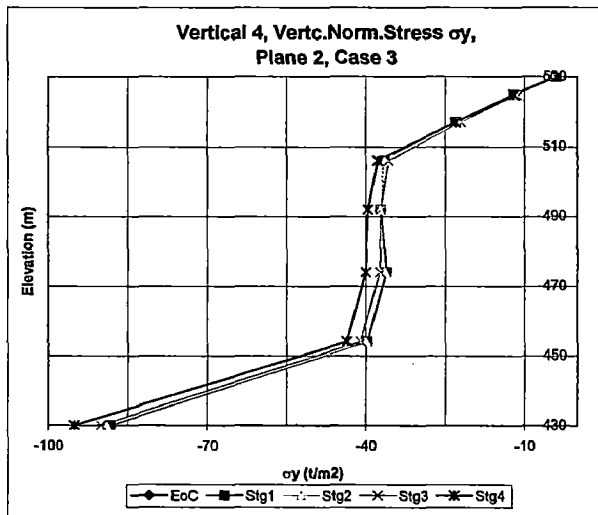
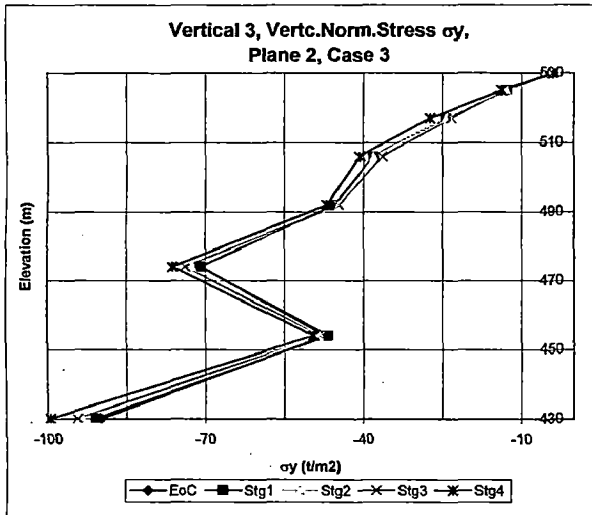
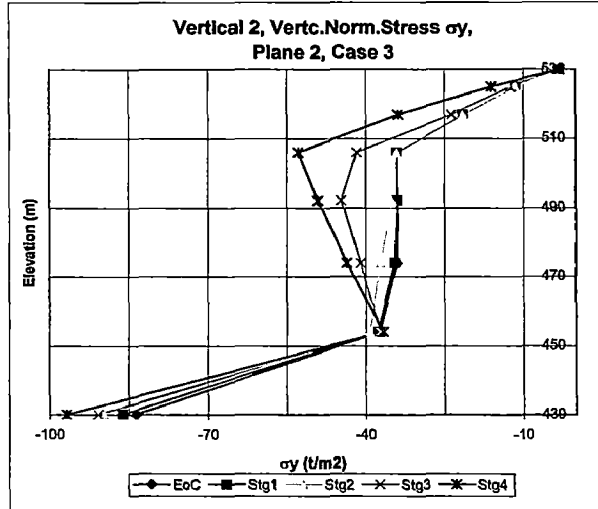
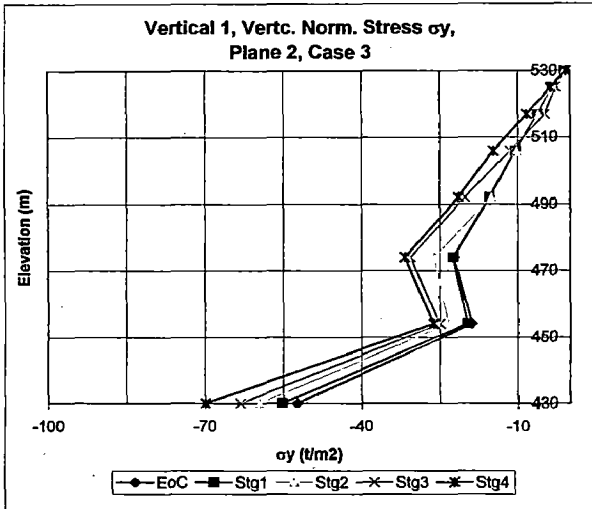


Fig.6.33. Horizontal Normal Stress  $\sigma_x$  along Height at Different Location over Plane 2, Case 3



**Fig.6.34. Vertical Normal Stress  $\sigma_y$  along Height at Different Location over Plane 2, Case 3**

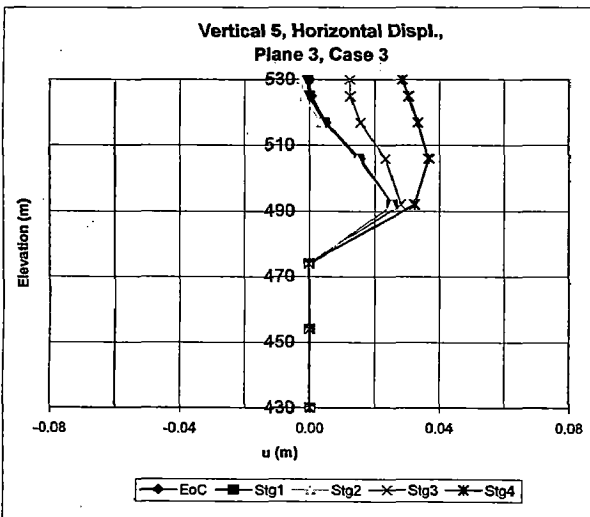
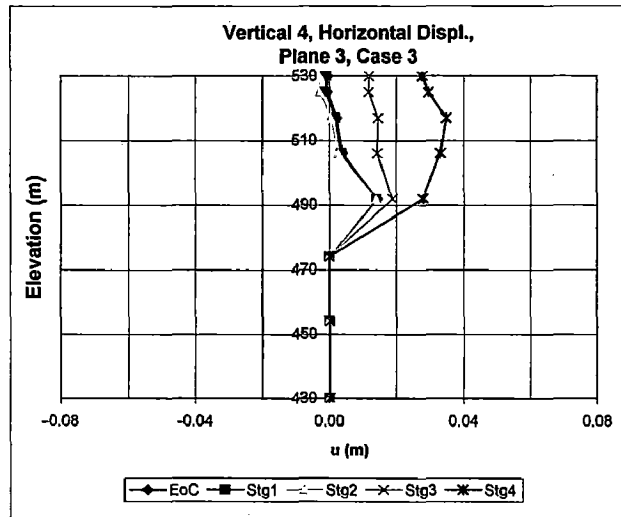
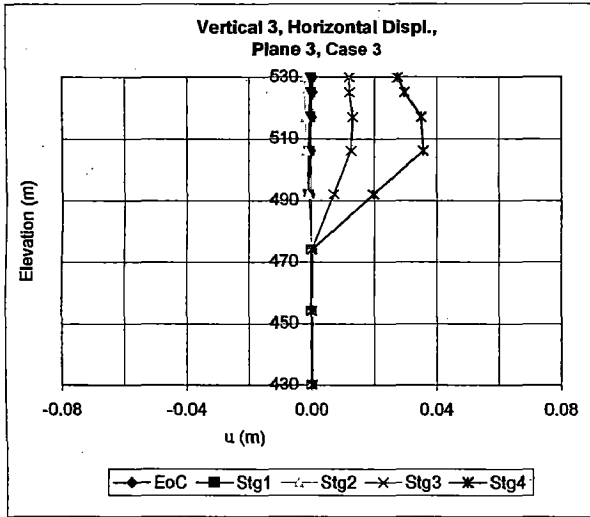
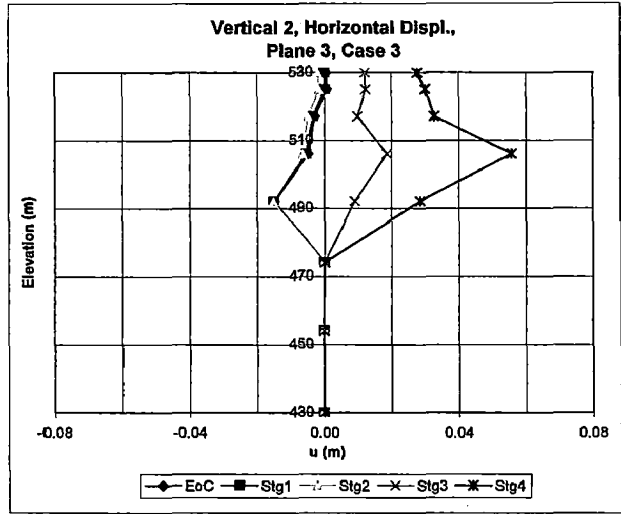
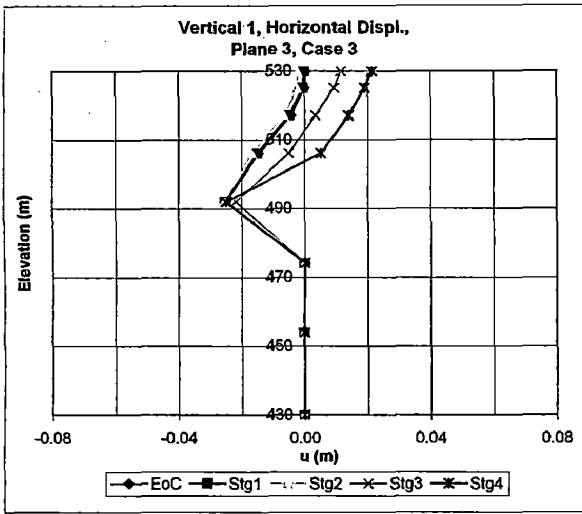


Fig.6.35. Horizontal Displ. u along Height at Different Location over Plane 3, Case 3



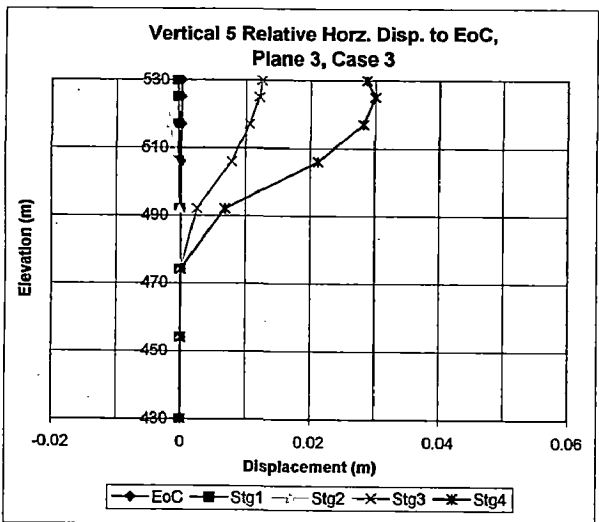
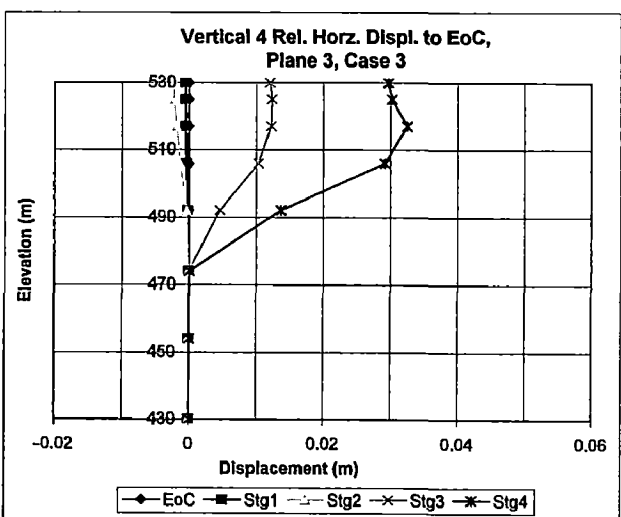
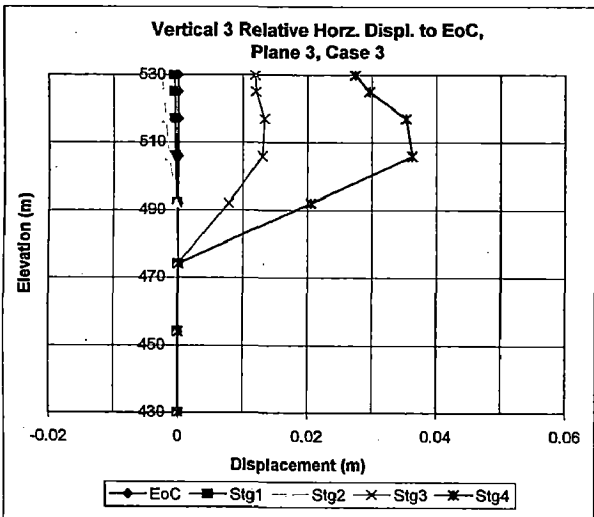
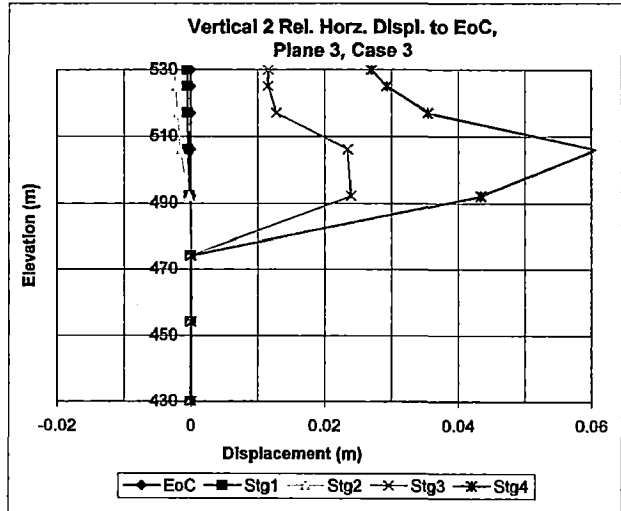
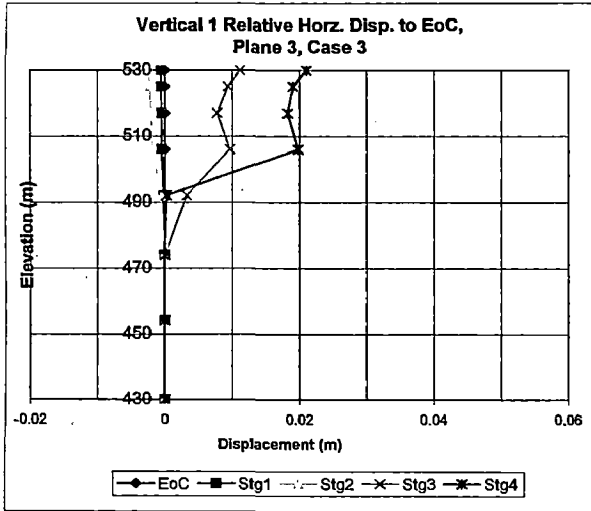


Fig.6.36. Relative Horizontal Displacement to End of Construction over Plane 3, Case 3

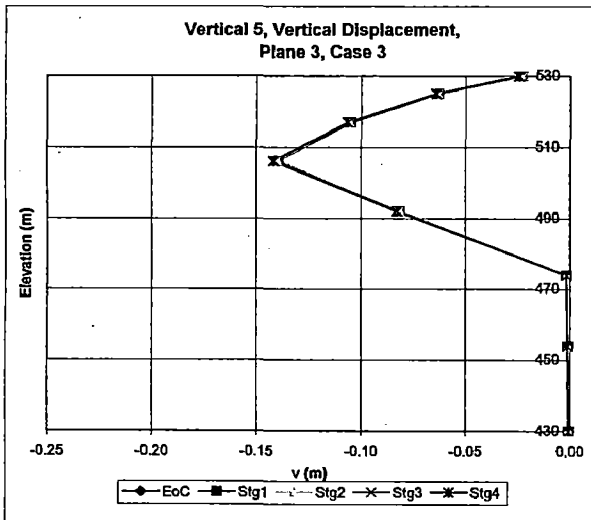
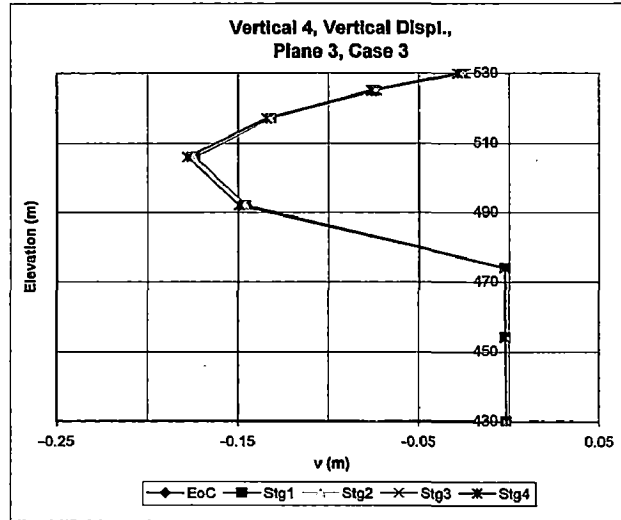
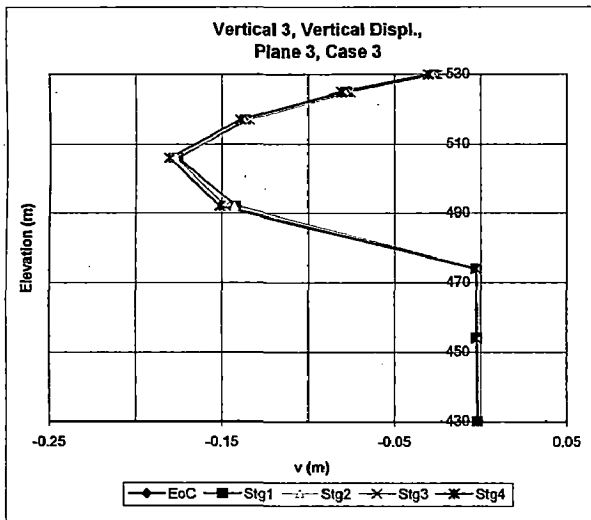
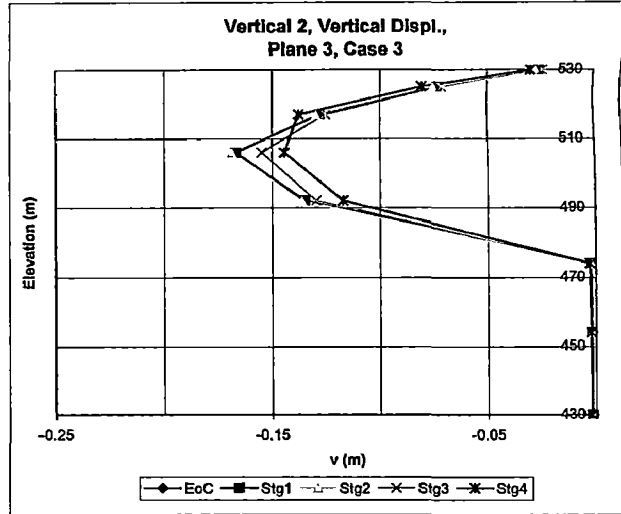
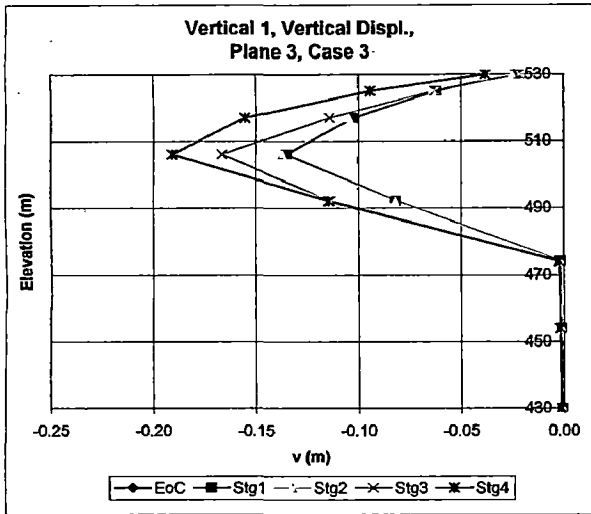
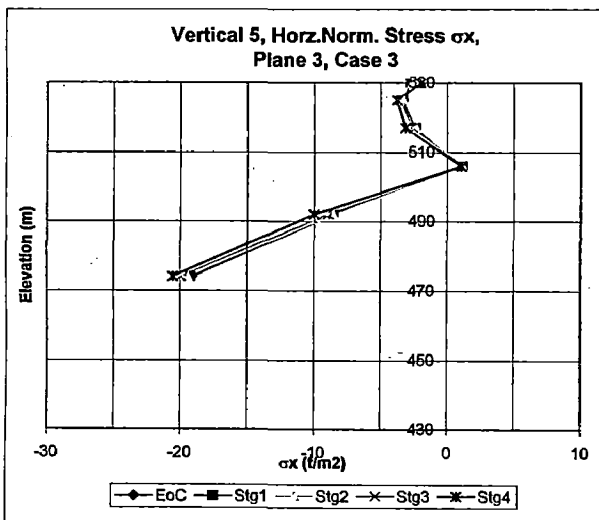
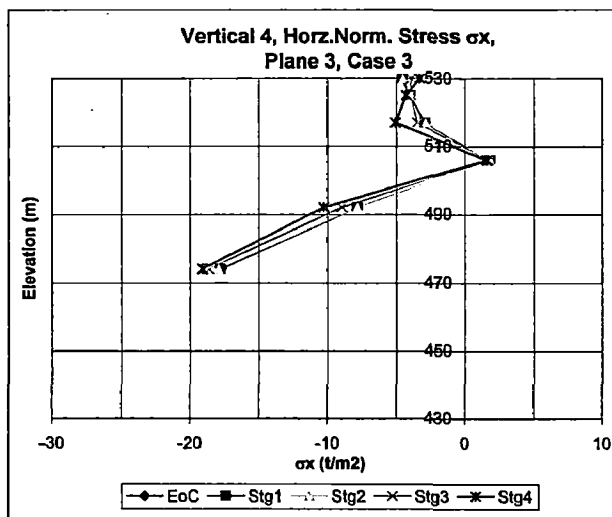
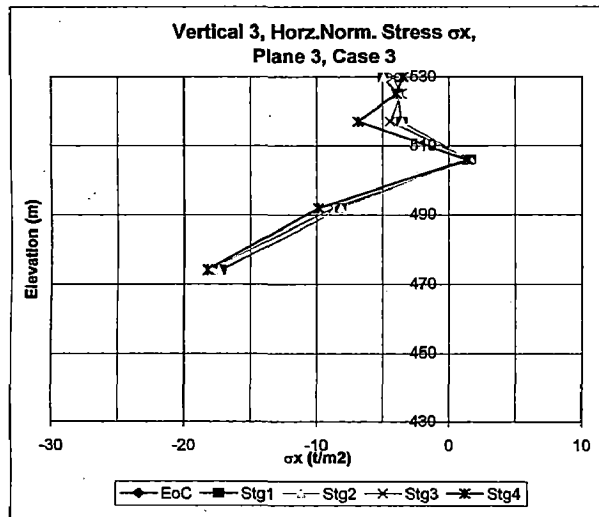
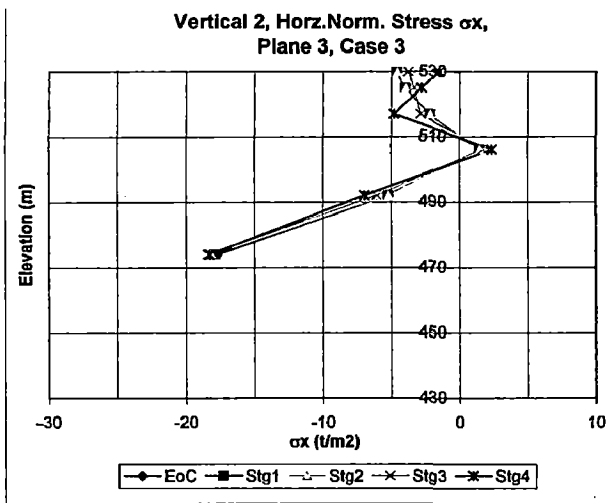
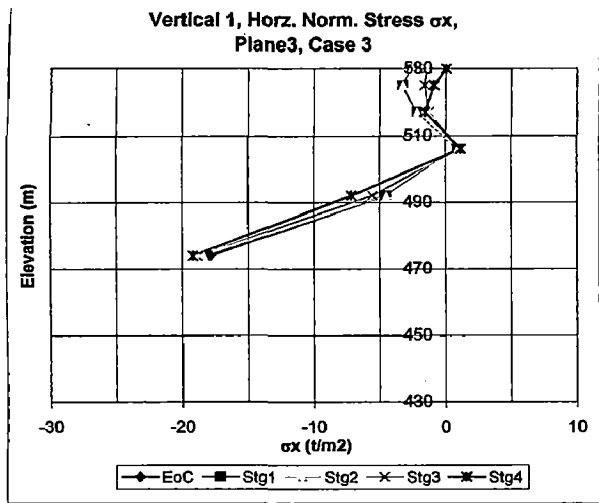


Fig.6.37. Vertical Displ. - v along Height at Different Location over Plane 3, Case 3



**Fig.6.38. Horizontal Normal Stress  $\sigma_x$  along Height at Different Location over Plane 3, Case 3**

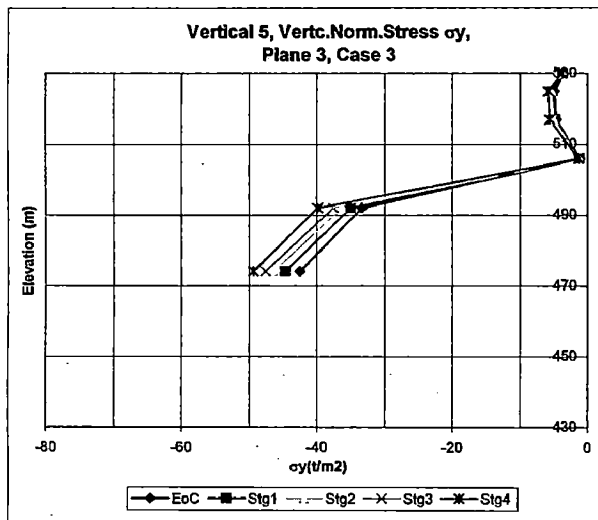
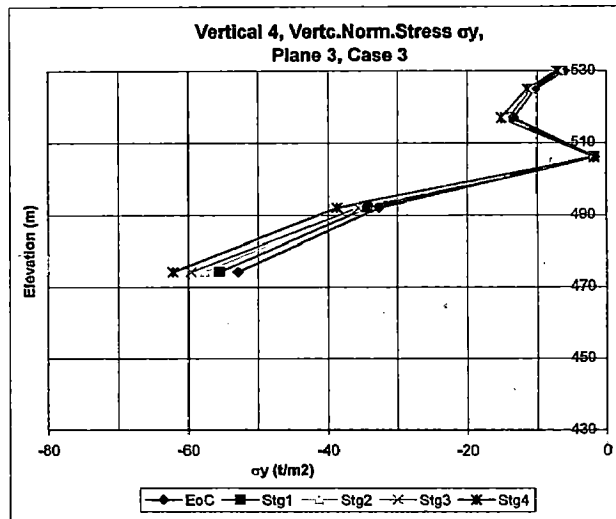
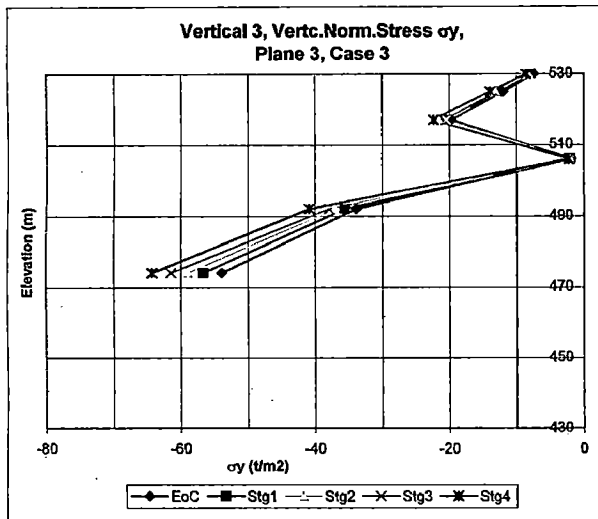
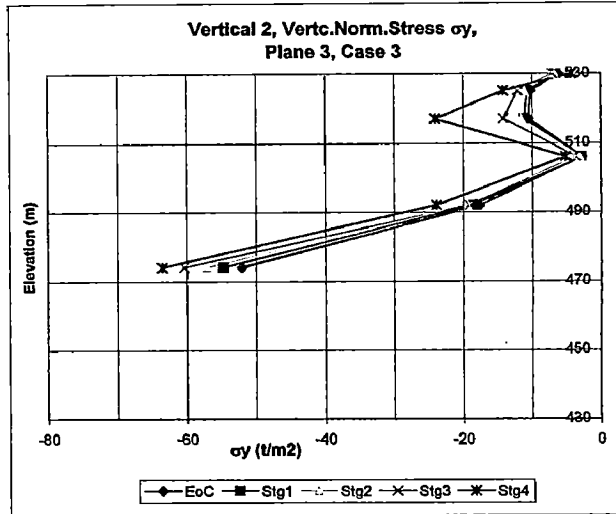
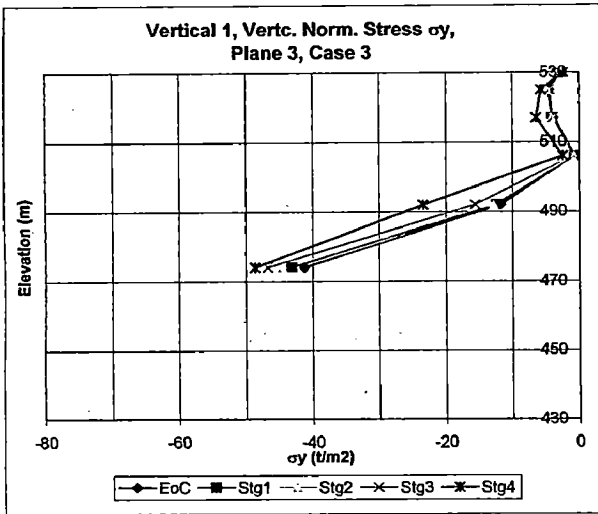


Fig.6.39. Vertical Normal Stress  $\sigma_y$  along Height at Different Location over Plane 3, Case 3

## CHAPTER 7

### CONCLUSIONS

Cognizant to the result obtained for the three cases analysed the following conclusion on the behaviour of the dam under different stages of construction and reservoir filling can be drawn. However these cannot be generalized as only one height and shape of the dam has been analysed on this study.

#### 7.1. CONCLUSION OF CASE I STUDY

Effect of number of lifts for end of construction

1. Horizontal displacements in both cases have shown similar pattern. The upstream shell moves towards upstream direction and the downstream shell moves towards downstream direction. The maximum values are found at mid height in both the upstream and downstream shell. The displacement is negligible in the core. Horizontal displacement in single lift case is found slightly less than seven lifts construction.
2. The location of maximum vertical displacement is found at the mid height of the dam for seven lifts construction while it is at the top of the dam for single lift construction. In seven lifts construction the vertical displacement is more in the core than the shell.
3. The maximum horizontal and vertical stresses for both cases are found at the base of the dam and these gradually decrease towards the top of the dam. The vertical stress distribution shows more stresses in core than in shell for both cases. However, the vertical stresses in seven lifts

- case are more than single lift case. The horizontal stresses are almost similar in the two cases.
4. Single and seven lifts analysis indicate some tension on the crest and top 20% height of the dam near the abutments (Plane 3) extending to some portion of the upstream and downstream faces of the dam (stress contour).
  5. To study the valley effects, it is observed that the values of stress and deformation on Plane 2 are only slightly less than the values on Plane 1. The pattern of stress and deformation distribution also similar with Plane 1 (The height of the two planes is same).
  6. The values of stress and deformation on Plane 3 are reduced to about 21-70% from Plane 1. The deformation on Plane 3 is observed similar to the pattern with Plane 1 while the stress pattern shows some tensile zone in this plane in the top 20% height of dam.

## 7.2. CONCLUSION ON CASE II STUDY

Effects of the reservoir filling have being done in single stage and four stages

1. The reservoir filling is seen to increase the horizontal displacement of end of construction stage at all interfaces except in the upstream shell. The horizontal displacements for single stage of full reservoir filling is found slightly less than four stages reservoir filling. The upstream shell has upstream movement at mid height and downstream movement at top. At all other verticals the movement is in downstream direction at all heights with maximum at the top.

2. The end of construction stage vertical displacement in the upstream shell is observed to increase due to impact of reservoir filling while the other zones do not show any significant impact. The vertical displacement for single stage is found higher than four stages reservoir filling.
3. The stresses due to reservoir filling are affected in the upstream shell and there is only a small impact on the other zones. The stresses distribution due to single stage full reservoir filling is found more than the same obtained by four stages reservoir filling
4. It is observed that the values of stress and deformation on Plane 2 are slightly less than the values on Plane 1. The pattern of stress and deformation distribution is however similar to that of Plane 1.
5. On Plane 3, it is observed that the horizontal normal stress gets close to tension from the crest of the dam to the mid of the height and thereafter increases to the compression at the base of the dam. The deformation and the vertical normal stress pattern is quite similar to Plane 1. The values on Plane 3 are reduced to about 22-56% to that of Plane 1.

### **7.3. CONCLUSION ON CASE III STUDY**

Effect of seven lifts at end of construction with four stages of reservoir filling

1. The horizontal movement of upstream shell in the upstream direction at first and second filling of reservoir is attributed to the effects of softening of the upstream shell material. The horizontal movement in the downstream

direction at later filling stages is the effect of water load on the core.

2. The vertical displacement on the upstream shell due to full reservoir is about 40% more in respect of the end of construction. However, the maximum vertical movement at full reservoir stage is still in the core on Plane 1 at two third the height above base.
3. It is observed from the stresses distribution, that the stress increases with decrease of height from the dam crest down to one third of the dam height and below it the stress increases rapidly to reach the maxima at the base of the dam.
4. At full reservoir filling, it is noted that the increase in stresses in upstream shell was about 18-40% of the end of construction stage but the increase in the core was only about 4-8%.
5. The similar pattern of the stresses and deformations of Plane 1 is found on Plane 2 with the values slightly reduced from Plane 1.
6. The deformations distribution on Plane 3 is similar to Plane 1 with reduced values. For the stress distribution it is observed that there is tension zone at the top of the dam down to the mid height. The values on Plane 3 are reduced to at about 22-66% of Plane 1.

#### **7.4. GENERAL OBSERVATIONS**

1. In single stage construction the horizontal deformation is similar to seven stages construction but vertical deformation is at top in single stage and it is at mid



height in seven stages construction. The stress pattern is similar in the two cases but vertical stresses in core are more in seven stage construction case than the single stage.

2. Reservoir filling largely affects the deformations and stresses in upstream shell as compared to core and downstream shell.
3. Single stage filling has higher values of deformation and stresses as compared to four stages filling.
4. The stresses pattern on Plane 3 (near abutment) show tensile stress on top 20% depth of dam and in upstream and downstream slopes.

#### **7.5. SUGGESTIONS FOR FURTHER STUDY**

1. The study has been done for one height and one slope of the valley wall. Analysis should be carried out for different height and different type of slope.
2. The study was conducted assuming a rigid foundation and may be extended with a flexible foundation to take care of other situations.
3. Further studies with inclined core could also be made considering the creep effects and secondary compression effect into account.
4. The study may be extended with seismic forces.

## REFERENCES

- Adikari, G.S.N., Donald, I.B. and Parkin, A.K. (1982), "Analysis of the Construction Behaviour of Dartmouth Dam", Proc. of the Fourth International Conference on Numerical Methods in Geomechanics, Edmonton, Canada, Vol. 2, pp. 645 - 654
- Clough, R.W. and Woodward, R.J. (1967), "Analysis of Embankment Stresses and Deformations", Journal of the Soil Mechanics and Foundations Division, ASCE, Vol. 93, No. SM4, pp. 529 - 549
- Chrzanowski, Anna S., et.all. (2001), "Use of Geodetic Monitoring Surveys in Verifying Design Parameters of Large Earthen Dams at the Stage of Filling the Reservoir", The 10<sup>th</sup> FIG International Symposium on Deformation Measurements, Orange, California, USA
- Desai, C.S. and Abel, J.F. (1987), "Introduction to the Finite Element Method: A Numerical Method for Engineering Analysis", First Edition, CBS Publisher & Distributors, New Delhi, India
- Duncan, J.M. and Chang, C.Y. (1970), "Nonlinear Analysis of Stresses and Strain in Soils", Journal of the Soil Mechanics and Foundations Division, ASCE, Vol. 96, No. SM5, pp. 1629 - 1653
- Eisenstein, Z., Krishnappa, A.V.G. and Morgenstern, N.R. (1972), "An Analysis of the Cracking at Duncan Dam", Proc. of ASCE Speciality Conference on Performance of Earth and Earth Supported Structures, Purdue University, Lafayette, Indiana, Vol. 1, pp. 765 - 778
- Eisenstein, Z. and Simmons, J.V. (1975), "Three Dimensional Analysis of Mica Dam", Proc. of Symposium on Criteria and Assumption for Numerical Analysis of Dams, Swansea, pp. 1052 - 1069
- Goodman, L.E. and Brown, C.B. (1963), "Dead Load Stress and The Instability of Slopes", Journal of the Soil Mechanics and Foundations Division, ASCE, Vol. 89, No. SM3, pp. 103 - 133
- Inoue, Motoyuki, et.all. (2000), "On the Mechanism of Long Term Settlement of Rockfill Dam After Reservoir Filling", Proc. ICOLD Congress, Beijing, Q.78, R.77, pp. 1261 - 1285
- Justo, Jose L., et.all. (2000), "The Settlement of Yeguas Dam During and After Construction", Proc. ICOLD Congress, Beijing, Q.78, R.49, pp. 759 - 769
- Kulhawy, F.H., Duncan, J.M. and Seed, H. (1969), "Finite Element Analysis of Stress and Movements in Embankment during Construction", Report No. TH-69-4 to W.E.S., Dept. Civil Eng., Univ. of California, Berkeley
- Kulhawy, F.H. and Duncan, J.M. (1972), "Stresses and Movements in Oroville Dam", Journal of the Soil Mechanics and Foundations Division, ASCE, No. SM4, pp. 1629 - 1653
- Kondner, R.L. (1963), "Hyperbolic Stress-Strain Response: Cohesive Soils", Journal of the Soil Mechanics and Foundations Division, ASCE, Vol. 89, No. SM1, pp. 115 - 143

- Mejia, L.H., Seed, H.B., Lysmer, J. (1982), "Dynamic Analysis of Earth Dams in Three Dimensions", Journal of the Geotechnical Engineering Division, ASCE, Vol. 108, No. GT12, pp. 1586 - 1604
- Michels, V.S. and Dickson, R.S. (1979), "Dam-Abutment and Core-Filter Interfaces Dartmouth Dam, Australia", Proc. ICOLD 13<sup>th</sup> Congress, New Delhi, Q.48, R.31, pp. 563 - 590
- Murley, K.A. and Cummins, P.J. (1982), "Design Considerations of Materials during Construction of Dartmouth Dam, Australia", Proc. ICOLD 14<sup>th</sup> Congress, Rio de Janeiro, Q.55, R.37, pp. 627 - 640
- Naylor, D.J. and Mattar, D. Jr. (1988), "Layered Analysis of Embankment Dams", Proc. of the Sixth International Conference on Numerical Methods in Geomechanics, Innsbruck, Rotterdam, Vol. 2, pp. 1199 - 1205
- Nobari, E.S. and Duncan, J.M. (1972), "Movements in Dams due to Reservoir Filling", Proc. of ASCE Speciality Conference on Performance of Earth and Earth Supported Structures, Purdue University, Lafayette, Indiana, Vol. 1, pp. 797 - 815
- Ohmachi, Tatsuo (1991), "A Simplified 3-D FEM and Its Application to Dynamic Analysis of Fill Dams in Narrow Canyons", Proc. ICOLD Congress, Vienna, Q.67, R.9, pp. 165 - 178
- Paul, D.K. (2002), "Seismic Testing of Tehri Dam", Proceeding of 12<sup>th</sup> Symposium on Earthquake Engineering held at IIT Roorkee, Vol.2
- Potts, D.M. and Zdravkovic, L. (2001), "Finite Element Analysis in Geotechnical Engineering: Application", First Edition, Thomas Telford, London, U.K.
- Schober, W. and Hupfauf, B. (1991), "The Bearing Behaviour of Embankment Dams in Narrow Valleys", Proc. ICOLD Congress, Vienna, Q.67, R.5, pp. 77 - 95
- Seed, H.B., Duncan, J.M. and Idriss, J.M. "Criteria and Methods for Static and Dynamic Analysis of Earth Dam", Proc. of Symposium on Criteria and Assumption for Numerical Analysis of Dams, Swansea, pp. 563 - 588
- Sherard, J.L., et.all. (1963), "Earth and Earth Rock Dams", John Willey and Sons Inc., New York
- Singh, R.P., Gupta, S.K. and Saini, S.S. (1985), "Three Dimensional Stress Analysis of Tehri Dam", Proc. Indian Geotechnical Conference, Roorkee, India, Vol. 1, pp.481 - 486
- Singh, R.P. (1991), "Three Dimensional Analysis of Rockfill Dams under Gravity Loading", Ph. D. Thesis, Water Resources Development Training Centre, University of Roorkee, India
- Singh, B. and Varshney, R.S. (1995), "Engineering for Embankment Dams", Oxford & IBH Publishing Co. PVT. Ltd., India
- Zienkiewicz, O.C. and Taylor, R.L. (2000), "The Finite Element Method, Volume 1: The Basis", Fifth Edition, Butterworth Heinmann, Oxford, U.K.